The Handbook of Environmental Chemistry 34
Series Editors: Damià Barceló · Andrey G. Kostianoy

Gilles Lefebvre
Elena Jiménez
Beatriz Cabañas *Editors*

Environment, Energy and Climate Change II

Energies from New Resources and the Climate Change

Springer

The Handbook of Environmental Chemistry

Founded by Otto Hutzinger

Volume 34

More information about this series at
http://www.springer.com/series/698

Environment, Energy and Climate Change II

Energies from New Resources and the Climate Change

Volume Editors: G. Lefebvre · E. Jiménez · B. Cabañas

With contributions by

K. Araus · P. Bonert · P. Cañizares · M.C. Carretón · E. Cerrajero · B. Corona · C. de la Cruz · A.G. del Campo · X. del Toro García · M.P. Domínguez · A.H. Escribano · A. Florence-Sandoval · E. González-Sánchez · F. Gutierrez · M. Karkri · M. Lasheras · E.G. Lázaro · G. Lefebvre · M.B. Lema · J. Lobato · D. López · A. Martín · I. Martín-Rubio · S.M. Martinez · V.G. Mestre · G.S. Miguel · F.J.F. Morales · M. Rodrigo · P. Roncero-Sánchez · L. Royon · F. Sánchez · J. Servert · M. Abdou-Tankari · M. Toledo · J.C.D. Toribio · J.R. Trapero

Springer

Editors
Gilles Lefebvre
CERTES-IUT
The University Paris Est Créteil
Paris Créteil
France

Elena Jiménez
Department of Physical Chemistry
University of Castilla-La Mancha (UCLM)
Ciudad Real
Spain

Beatriz Cabañas
Department of Physical Chemistry
University of Castilla-La Mancha (UCLM)
Ciudad Real
Spain

ISSN 1867-979X ISSN 1616-864X (electronic)
The Handbook of Environmental Chemistry
ISBN 978-3-319-17099-2 ISBN 978-3-319-17100-5 (eBook)
DOI 10.1007/978-3-319-17100-5

Library of Congress Control Number: 2015930134

Springer Cham Heidelberg New York Dordrecht London

Printed on acid-free paper

Springer International Publishing AG Switzerland is part of Springer Science+Business Media (www.springer.com)

The Handbook of Environmental Chemistry Also Available Electronically

The Handbook of Environmental Chemistry is included in Springer's eBook package *Earth and Environmental Science*. If a library does not opt for the whole package, the book series may be bought on a subscription basis.

For all customers who have a standing order to the print version of *The Handbook of Environmental Chemistry,* we offer free access to the electronic volumes of the Series published in the current year via SpringerLink. If you do not have access, you can still view the table of contents of each volume and the abstract of each article on SpringerLink (www.springerlink.com/content/110354/).

You will find information about the

– Editorial Board
– Aims and Scope
– Instructions for Authors
– Sample Contribution

at springer.com (www.springer.com/series/698).

All figures submitted in color are published in full color in the electronic version on SpringerLink.

Aims and Scope

Since 1980, *The Handbook of Environmental Chemistry* has provided sound and solid knowledge about environmental topics from a chemical perspective. Presenting a wide spectrum of viewpoints and approaches, the series now covers topics such as local and global changes of natural environment and climate; anthropogenic impact on the environment; water, air and soil pollution; remediation and waste characterization; environmental contaminants; biogeochemistry; geoecology; chemical reactions and processes; chemical and biological transformations as well as physical transport of chemicals in the environment; or environmental modeling. A particular focus of the series lies on methodological advances in environmental analytical chemistry.

Series Preface

With remarkable vision, Prof. Otto Hutzinger initiated *The Handbook of Environmental Chemistry* in 1980 and became the founding Editor-in-Chief. At that time, environmental chemistry was an emerging field, aiming at a complete description of the Earth's environment, encompassing the physical, chemical, biological, and geological transformations of chemical substances occurring on a local as well as a global scale. Environmental chemistry was intended to provide an account of the impact of man's activities on the natural environment by describing observed changes.

While a considerable amount of knowledge has been accumulated over the last three decades, as reflected in the more than 70 volumes of *The Handbook of Environmental Chemistry,* there are still many scientific and policy challenges ahead due to the complexity and interdisciplinary nature of the field. The series will therefore continue to provide compilations of current knowledge. Contributions are written by leading experts with practical experience in their fields. *The Handbook of Environmental Chemistry* grows with the increases in our scientific understanding, and provides a valuable source not only for scientists but also for environmental managers and decision-makers. Today, the series covers a broad range of environmental topics from a chemical perspective, including methodological advances in environmental analytical chemistry.

In recent years, there has been a growing tendency to include subject matter of societal relevance in the broad view of environmental chemistry. Topics include life cycle analysis, environmental management, sustainable development, and socio-economic, legal and even political problems, among others. While these topics are of great importance for the development and acceptance of *The Handbook of Environmental Chemistry,* the publisher and Editors-in-Chief have decided to keep the handbook essentially a source of information on "hard sciences" with a particular emphasis on chemistry, but also covering biology, geology, hydrology and engineering as applied to environmental sciences.

The volumes of the series are written at an advanced level, addressing the needs of both researchers and graduate students, as well as of people outside the field of

"pure" chemistry, including those in industry, business, government, research establishments, and public interest groups. It would be very satisfying to see these volumes used as a basis for graduate courses in environmental chemistry. With its high standards of scientific quality and clarity, *The Handbook of Environmental Chemistry* provides a solid basis from which scientists can share their knowledge on the different aspects of environmental problems, presenting a wide spectrum of viewpoints and approaches.

The Handbook of Environmental Chemistry is available both in print and online via www.springerlink.com/content/110354/. Articles are published online as soon as they have been approved for publication. Authors, Volume Editors and Editors-in-Chief are rewarded by the broad acceptance of *The Handbook of Environmental Chemistry* by the scientific community, from whom suggestions for new topics to the Editors-in-Chief are always very welcome.

Damià Barceló
Andrey G. Kostianoy
Editors-in-Chief

Volume Preface

This work, which is divided into two volumes, *Environment, Energy and Climate Change I* and *Environment, Energy and Climate Change II*, is a consequence of the *Energy and Environment Knowledge Week* (E2KW) congress that was held in Toledo (Spain) from 20th to 22nd of November 2013 (http//www.congress.e2kw.es). This event offered an exceptional opportunity for presenting cutting-edge research in the field of environmental, energy and climate change and illustrating the wide experience on several interesting topics of the contributing authors. The two volumes aim to address some of the key issues facing the environmental problems through interdisciplinary approaches.

Volume 2, which is dedicated to the *Energies from New Resources and the Climate Change*, collects a selection of 11 chapters that deal with several aspects of (clean) production (*conversion*) and *storage* of (clean) energy. The first chapter (from A. Bret) presents an interesting *Global energy balance* that the humanity has to deal with and the *Climate induced possible changes*. The three following chapters (by A. Martin et al., G. San Miguel et al. and S. Martin Martinez et al.) describe methods and technologies used to improve the efficiency of energy capture from photovoltaic solar radiation and wind. The three following papers (from C. de la Cruz et al., M. Abdou-Tankari et al. and M. Karkri et al.) are dedicated to energy storage which is one of the main not already well-solved problems in heterogeneous energetic hybrid systems. Two of these papers study electrical storage; the first one offers a wide overview of possible electrical storage technologies then focuses on batteries or ultracapacitors as main storage components in hybrid systems; the second paper deals with the sizing of hybrid systems involving heterogeneous electrical production and consumption components. The third paper is a bibliographical critical review of the best-known promising ways for storing thermal energy in phase change materials and encapsulating it in order to be usable in the building industry. Three papers are dedicated to the biomass energy; the first one (from J.-C. Dominguez Toribio et al.) tries a difficult review of the technology of biomass conversion into ethanol, processing schemes, production and the pre-treatment methods of bio-products; the second one (from A. Gonzalez del

Campo et al.) studies the influence of external resistance on microbial fuel cell performance which promisingly produces electricity from wastewater; the last paper (from Maria Paz Domínguez et al.) dedicated to biomass presents how avocado seeds and waste could be used for producing fuel. A last paper (from M. Rubio et al.) describes the main socio-economical barriers to efficiency improvement and proposes to break them through learning strategies.

We sincerely thank all authors for their involvement and efforts in preparing their chapters.

Paris, France — Gilles Lefebvre
Ciudad Real, Spain — Elena Jiménez
Beatriz Cabañas

Contents

Energy and Climate: A Global Perspective

Antoine Bret

Abstract Global warming and energy transition are two of the most important challenges humanity will ever meet. These are complex issues by themselves and by the interconnection they have with each other. The purpose of this chapter is to present an integrated picture of these problems, of their connections, and of a number of scientific and historical facts that should be known before elaborating scenarios for the future.

Keywords Climate, Collapse, Energy, Global warming, History

Contents

A. Bret (✉)
ETSI Industriales, Universidad de Castilla-La Mancha, 13071 Ciudad Real, Spain
e-mail: antoineclaude.bret@uclm.es

G. Lefebvre et al. (eds.), *Environment, Energy and Climate Change II: Energies from New Resources and the Climate Change*, Hdb Env Chem (2016) 34: 1–14,
DOI 10.1007/698_2015_418, © Springer International Publishing Switzerland 2015,
Published online: 8 July 2015

1 Introduction

Climate and energy issues are now routinely making headlines. Expressions like greenhouse gases, peak oil, and global warming, to name a few, have entered our everyday vocabulary. Yet, the abundance of information makes it difficult to get a global picture of the problem. These notions are notoriously interconnected, but it is not always easy to tell how exactly. Like an exhaustive list of the streets of Paris does not easily convey a map of the city, all the climate and energy news in the world do not necessarily show how they fit together.

Instead of a research work, the present chapter is rather a tutorial in which its goal is to supply a global perspective of the climate/energy problem. Section 2 starts emphasizing the world's current energy status. Two observations will be made: First, current energy needs are tremendous, and second, there is no, strictly speaking, short-term fossil fuel shortage. Clearly, these fuels will eventually run out, but the main reason to switch away from them comes from global warming, as will be emphasized in Sect. 3. Section 4 will then review the possible alternatives to oil, coal, and carbon. From a physicist's point of view, it is possible to set up an exhaustive list of energy sources. Some back-of-the-envelope estimates [1] of what it would take them to provide our world the energy it needs will show the magnitude of the challenge that lies ahead of us. This is why the last section will focus on historical examples of past societies who encountered similar challenges.

2 Where Do We Stand?

The historian Ian Morris wrote that greed, fear, and sloth are the motors of history ([2], p. 26). Throughout history, energy is definitely an object of greed. Plant domestication can be viewed as a first attempt to harness solar energy. Mammal domestication, and even slavery, can be considered as the exploitation of extra mechanical energy. Yet, the energy consumption per capita hardly increased before the beginning of the nineteenth century. On average, it was about 15 GJ per capita per year in 1700, versus "at least 10 GJ" per capita at the time of the Roman Empire [3, 4].

How is it then that in spite of being so coveted, energy use did not grow before 1800 or so? The reason is simply that preindustrial energy sources were quite limited in their usage. The main one, biomass burning, was, for example, nearly exclusively restricted to heating. But you cannot plow a field just with heat. Indeed, the key element which triggered the industrial revolution was the steam engine. Suddenly, the steam engine made it possible to use heat for something else than heating. Once it became possible to perform every kind of mechanical work from heat, the thirst for energy grew exponentially.

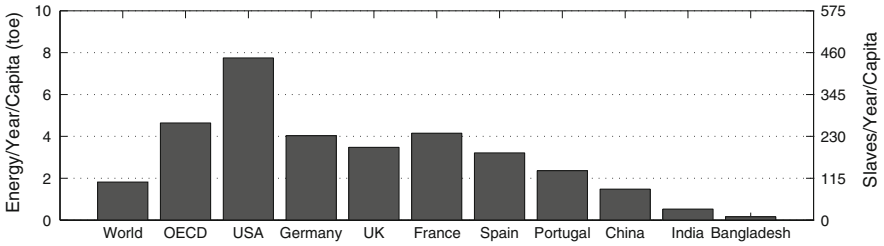

Fig. 1 Yearly energy consumption per capita for various countries or group of countries. *Left scale*: in tons of oil equivalent (toe). *Right scale*: in "energy slaves" equivalent, accounting for 2 MJ/day for a slave ([1], p. 5)

2.1 Energy Slaves

Today, after two centuries of exponential growth, the annual energy consumption per capita in the OECD countries is 4.6 tons of oil equivalent, nearly 200 GJ [5]. The consumption is nearly constant for millennia, before it increases more than tenfold in just two centuries.

An interesting way of grasping how deep our energy dependence has become is to translate joules into "energy slaves." The idea of drawing a parallel between slaves and machines goes back at least to the fourth century BC, where Aristotle noted the latter could replace the former [6]. The term "energy slave" was coined in 1940 by Richard Buckminster Fuller [7] and has been recently picked up by various authors [8–10] to emphasize the depth of our current energy dependence.

Assuming a slave would be given 4,000 calories a day, among which 2,000 should be used for his metabolism, the other 2,000 could be dedicated to mechanical work. Accounting for a muscle efficiency of 25%, he would be left with 500 calories for external work, that is, $500 \times 4.18 \times 10^3 = 2$ MJ/day or 0.7 GJ/year. An OECD citizen, with his 200 GJ/year, uses the work of $200/0.7 = 260$ energy slaves.

Figure 1 features the yearly energy consumption for various countries or group of countries. The left scale gives the consumption in tons of oil equivalent. The right scale translates the result to the equivalent number of "energy slaves."

If, then, a Westerner had to give up every single external energy source, he would need 260 slaves at his service, 24/7. This figure can be compared to the 462 workers registered in the US White House staff.[1] It means that every one of us in the Western world counts on a significant fraction of President Obama's staff. Clearly, we have been living this way for so long that things are irreversible. The world we have built is fundamentally designed to function with far more than our own energy.

[1] See http://www.whitehouse.gov.

2.2 Food Miles

Yet another way of expressing the magnitude of our energy dependence is to look at the amount of transportation implicitly required by our daily life. My laptop was assembled in China, while its hard disk came from Thailand and its memory from Korea. Some of my shirts, pants, and shoes wear a sticker "made in Bangladesh," "made in Vietnam," and "made in the Dominican Republic," respectively. And "made in China" is everywhere. It means that even before I bought these items, they had traveled thousands of kilometers. Their remote manufacturing was made possible by the energy needed to transport them.

Even our food is subsidized by energy. Although conservation techniques are not new [11], people in the past had to eat food that had been produced nearby. Today, the food consumed by a typical household in the USA traveled on average 6,760 km, from the production site to the fridge. This number, accounting for the overall supply chain, varies considerably in terms of the product. Beverages require only 1,200 km, while red meat demands 20,400 km [12].

2.3 Where Is the Problem?

Like the heart pumps blood in our body, energy moves our society. Energy is the heart of our society. Today, about 80% of the world primary energy production comes from fossil fuels [5]. Is that a problem? To start with, there is only a limited amount of these resources on Earth. Therefore, the day will come when the last gram of oil, coal, and gas will have been burnt. This is simply mathematics. But before production drops to zero, it will have to reach a peak. This is also mathematics. The question is not whether fossil fuels will be exhausted or not one day. The question is *when*.

Figure 2 features the forecasted peaks for all three fossil fuels [13]. While the supply of conventional oil is currently peaking, coal and gas peaks are still ahead of us, so that fossil fuels altogether should peak toward 2060. And the figure does not even account for nonconventional oil (tar sands, shale oil, etc.). Therefore, if it were only for the limited amount of fossil fuels, there would be a few decades left to prepare the transition. The reason why the transition should start now is climate change.

3 Climate Science

Fossil fuels are decomposed organic matter. As such, they are overwhelmingly carbon. As a rule of thumb, one can therefore assume that burning 1 ton of those fuels releases 1 ton of carbon in the atmosphere. Indeed, the 2010 world energy

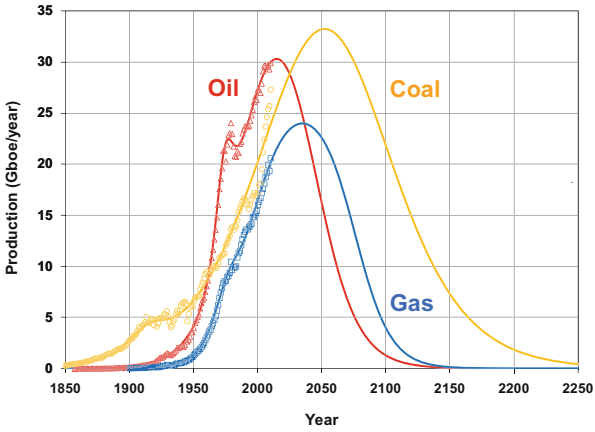

Fig. 2 Forecasted production for oil, coal, and gas [13]. *Plain lines* are the model (Hubbert), and the *symbols* are the historical data

production from fossil fuels was about 10 Gtoe [5], while the measured amount of carbon emitted was 9 Gt.[2]

Carbon is not emitted as such. During combustion, it combines with oxygen to form CO_2. Fossil fuel burning results therefore in carbon dioxide emissions. Are these emissions "important"? In other words, how does the emitted amount relate to the total already in the atmosphere? There are some 720 Gt of carbon in the atmosphere, mostly encapsulated in CO_2 molecules. Releasing 10 Gt more each year is definitely not negligible at all, especially if this is done for more than one century. The total amount of carbon emitted since the beginning of the industrial era is 355 Gt, which is not negligible at all when compared to 720 Gt.

Therefore, if carbon dioxide plays a role in the climate system, then human activity must influence it. And the role it does play is now well recognized: it is a greenhouse gas. The basic rule of climate science is that all the energy the Earth receives from the Sun eventually returns to space [14]. Nothing is stored. The spectrum of the light coming from the Sun is roughly centered on visible light. It is absorbed by the Earth, save a part directly reflected giving rise to the "albedo." Then, the Earth reemits all this energy in the infrared range. Our climate can change either because the incoming amount of energy changes or because the way it is reemitted changes.

The variations of the solar radiation over the last decades are of the order of 0.1%, which is too faint to explain the observed warming. But greenhouse gases tend to block some outgoing wavelengths. More energy must then travel through the non-blocked wavelengths, if the same amount of incoming energy is to be reemitted. The main greenhouse gas is water vapor. But its atmospheric concentration is nearly constant. The next more important greenhouse gases are carbon dioxide and methane (which results from fermentation processes). Carbon dioxide's

[2] See Carbon Dioxide Information Analysis Center, http://cdiac.ornl.gov/.

atmospheric concentration has gone from 280 to 400 ppm since 1800, while methane's concentration has risen from 700 to 1,700 ppb[3] during the same period.

3.1 Mitigating the Warming

The rise of carbon dioxide and methane in the atmosphere perfectly accounts for the current warming. Climate simulations of the last 100 years clearly reproduce the observations if and only if anthropogenic emissions are accounted for ([15], p. 18, 930).

What are then the predictions for the twenty-first century? Since human emissions are difficult to predict, climate scientists resort to various emission scenarios. Figure 3 features two figures of the last report of the International Panel on Climate Change (Workgroup I) [15]. On top, emission scenarios range from the so-called RCP8.5 which peaks toward 2100, to the "RCP2.6" where emissions are cut from 2020. The bottom plot shows the corresponding warming in 2100 with respect to 2000, ranging from +4°C to +1°C.

Since +1°C has already been gained since 1800, burning every single gram of the available fossil fuel is likely to bring an additional +5°C in 2100. Reminding that the global temperature shift between now and the last ice age is about –5°C ([15], p. 400), one can figure out the consequences of a similar warming [16]. Conversely, the RCP2.6 scenario with emissions peaking toward 2020 brings about a more bearable +2°C warming. For us in 2015, 2020 is now. The urgency for alternative energies stems from climate change.

4 Alternative Energies

It is thus clear that avoiding a dramatic warming implies starting to cut fossil fuels now. Which are the alternatives? From the physical point of view, energy can be found in two kinds of vessels: kinetic energy and potential energy. The first one, kinetic energy, is the energy of a moving body. Note that heat is kinetic energy since the heat of an object is nothing but the kinetic energy of its molecules. Potential energy is the energy released when a fundamental force is in action. For example, a falling apple acquires kinetic energy which comes from the gravitational potential energy it had while still hanging on the tree.

Potential energy is therefore always linked to a fundamental force. And there are only four of them: gravity, the electromagnetic force, and the strong and weak nuclear forces. Gravity makes apples fall, electromagnetism makes electrons stick

[3] "ppm" = parts-per-million and "ppb" = parts-per-billion.

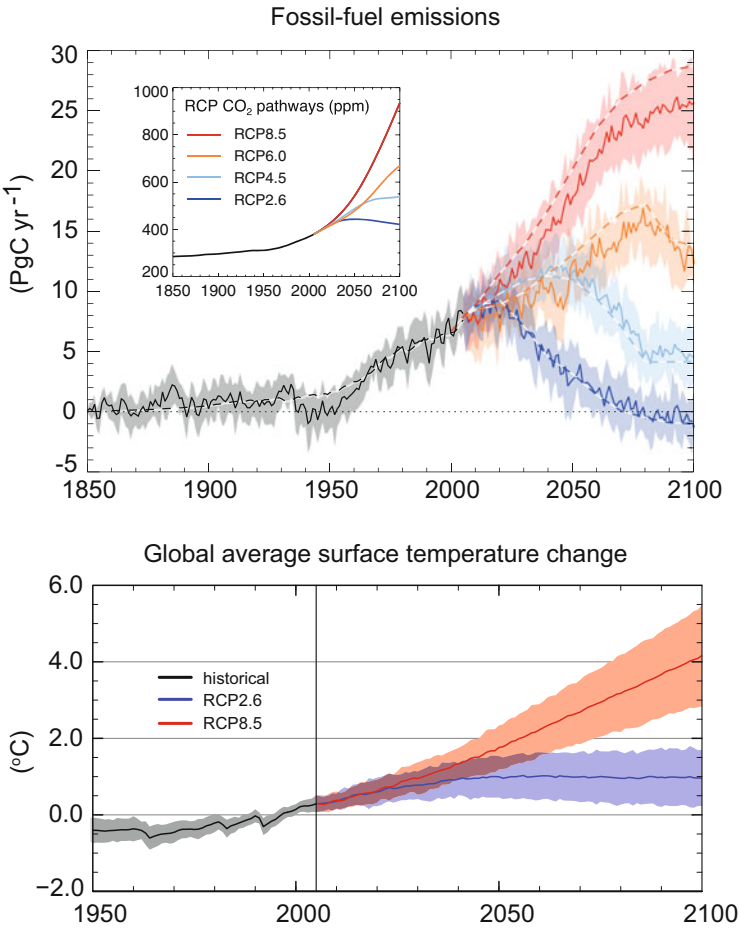

Fig. 3 Emission scenarios considered in the 2013 IPCC report (Workgroup I), together with the corresponding warming. The insert on the top figure shows the projected CO_2 concentration for each scenario. *Source*: Climate Change 2013: The Physical Science Basis. Working Group I Contribution to the Fifth Assessment Report of the Intergovernmental Panel on Climate Change, Figure SPM.7 (a); Figure TS.19 (top). Cambridge University Press [15]

to their atomic nucleus, and the strong nuclear force makes protons stick together inside the nucleus (we leave the weak nuclear force apart).

Figure 4 features the energetic landscape. Whenever one of these reservoirs is found already filled up, there is an energy source. Otherwise, there can still be a storage option. At any rate, any energy source, renewable or not, must fit in one of these categories. There are no other options in this world. Fossil fuels pertain to the realm of potential electromagnetic energy, as any combustion reaction eventually amounts to a release of such energy.

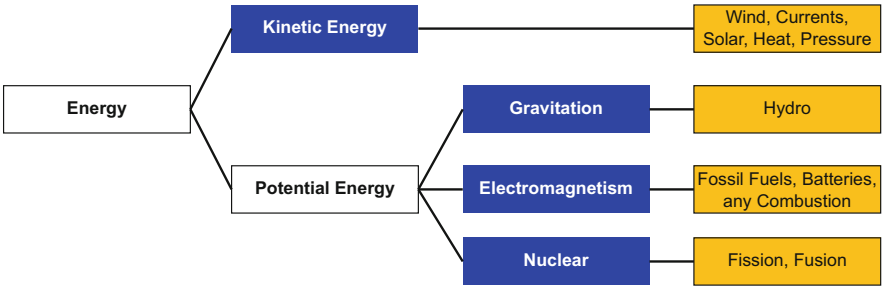

Fig. 4 Energetic bottles where energy can be found. Any energy source, renewable or not, must fit in one of the *blue* categories ([1], p. 21)

As previously said, the 2010 world energy production was 13 Gtoe, that is, 7 billion people burning 1.8 toe each. Let us now review the main renewable energy sources as they appear in Fig. 4 and check what it would take to generate 13 Gtoe. Granted, our energy future is likely to display a mix of solutions, but this exercise will help us figuring things out.

4.1 Kinetic Energy

Starting then with kinetic energy, we need to find something nature is moving for us and extract its kinetic energy. Wind energy comes to mind first. Assuming a windmill can recover some 30% of the kinetic energy of a wind at constant velocity ([17], p. 184), and averaging the result on the typical wind speed distribution (Weibull), a windmill of radius R located in a place where the mean wind speed is V_m can generate in a year

$$E = 22.7R^2V_m^2 \text{ MJ}. \tag{1}$$

When placing the machines in a 2D wind farm, the optimum distance between them in both directions is proportional to their radius. As a consequence, the collected energy density becomes independent of the radius. Considering an optimum spacing of 10 radii,[4] a wind farm of 20 million km^2 is necessary to produce our 13 Gtoe, when setting $V_m = 5$ m/s.

One could think about taking kinetic energy out of ocean currents. The Gulf Stream, for example, is typically 100 km wide, 1 km deep, and flows at 2.5 m/s ([19], p. 249). Yet, the amount of kinetic energy that could be recovered in a year, even assuming a 100% efficiency, is only 4.6% of our 13 Gtoe.

[4] The optimum spacing could be much larger ([18], p. 430).

Geothermal energy also entered the "kinetic energy category." The heat flux from the Earth's interior is 0.087 W/m^2 [20]. Integrating over all the volcanic areas of the globe, namely, ~1% of it [21], yields 0.7% of our target.

Finally, solar energy can be viewed as the capture of the Sun's radiation kinetic energy (it could also fit in the next subsection). Here, the key fact is that each m^2 of the planet receives on average $I = 2.1$ MWh of solar energy per year. Southern Spain has $I = 2$ MWh, while the UK gets only $I = 1$ MWh. Considering the energy can be captured with an efficiency η, the area A needed for the 2010 world energy production is

$$A = \frac{0.14}{\eta I\ [\mathrm{MWh/m^2}]} 10^6\ \mathrm{km^2}. \tag{2}$$

Considering an overall efficiency (captor + portion of the ground covered) of 14% with $I = 2.1$ MWh, gives therefore half a million km^2.

4.2 Potential Energy: Gravity

The next item in Fig. 4 is gravitational potential energy. We thus need to look for substances that nature has put on a height for us and that we could let down. Rain is the obvious choice. If it falls on mountains, dams can be built retaining it. It is thus clear that hydroelectricity needs mountains, plus rain. A direct consequence is that hydro energy production must have a maximum. Once all the dams that could be built have been so, you cannot create more mountains, nor make up more rain. In many European countries like France or Spain, hydroelectricity has nearly reached its full potential. Regarding the whole world, the maximum production could reach 10% of our 13 Gtoe ([22], p. 273).

4.3 Potential Energy: Electromagnetism

All exothermic chemical reactions fall into this category, like fossil fuel burning. Since these fuels are precisely the ones that need to be phased out, they will not be examined any further here.

Solar energy pertains to the present category. Sunlight is composed of electromagnetic radiations, so that solar energy is also electromagnetic energy. Note that a photon of frequency v has the kinetic energy hv, where h is Planck's constant. Therefore, solar energy can equally fit into the "kinetic energy" category.

Biofuels fit here as well. Biofuels are eventually another form of solar energy where the captor is a plant. Which amount of fuel can be generated per year from a 1 hectare field? A good number is 5 tons ([23], p. 34). From this, the area needed for

13 Gtoe is straightforwardly computed with $A = 28 \times 10^6\,\mathrm{km}^2$.

This number is much larger than that obtained for solar energy. It turns out that the mechanism through which plants capture solar energy is photosynthesis. With an efficiency of 5% at best [24], photosynthesis efficiency is the bottleneck.

4.4 Potential Energy: Nuclear

This is the last possible energy reservoir. Because there are only four fundamental forces, there cannot be another reservoir. In order to harness nuclear energy, one has to find exothermic nuclear reactions, in exactly the same way exothermic chemical reactions release energy.

Exothermic chemical reactions release electromagnetic potential energy, and exothermic nuclear reactions release electromagnetic nuclear energy. According to the laws of nuclear physics, there are only two kinds of such nuclear reactions. You can take a big nucleus and split it. This is fission. Or you can take two light nuclei and merge them. This is fusion.

Fission power plants work so far splitting U^{235} nuclei. One single fission event releases 211 MeV so that you need to split 6,310 t of U^{235} to produce 13 Gtoe. Note that U^{235} reserves are running out. But other fission reactions could be used, earning nuclear fission a place among the potential future energies.

Among the existing fusion reactions (some power from the Sun), the one envisioned to produce energy is the fusion of deuterium (^{2}H) and tritium (^{3}H):

$$^2\mathrm{H} + ^3\mathrm{H} \rightarrow \mathrm{He} + n + 17.6\ \mathrm{MeV}. \tag{3}$$

Merging 630 t of deuterium with 880 t of tritium would produce the needed 13 Gtoe. Although this energy source is very promising, none of the strategies adopted to harness it are likely to be operational before 2050. Fusion is therefore definitely a key player in the long-term energy mix, but it cannot help in the energy transition that has to take place within the next few decades.

Table 1 summarizes the numbers gathered in this section. All estimates are optimistic. The energy needed to grow the biofuel fields is not accounted for with biofuels nor is the energy lost when storing large productions of intermittent sources and so on. These numbers show one thing very clearly: switching away from fossil fuels is not an easy task. Past energy transitions typically took place over 50 years [4]. This is the time scale set before us by climate change. But this time, we need to go from an extremely energetically dense, cheap, and convenient source, fossils fuels, to the items listed in the table.

It is therefore clear that humanity faces a tremendous challenge. Did it happen already? Were there in the past civilizations who ran through similar challenges? Historians say “yes,” definitely. Let us now look at the past and see how some past societies overcame their crisis.

Table 1 Requisites to produce 13 Gtoe from each energy sources or percentage of the same amount that could be attained. See details of the calculations in [1]

Source	
Kinetic energy	
Wind energy	20 million km^2 wind farm
Sea currents	Gulf Stream, 4.6%
Geothermal	All volcanic areas, 0.7%
Solar	Half million km^2 field
Gravity	
Hydro	10%
Electromagnetic	
Biofuels	28 million km^2 field
Nuclear	
Fission	6,310 t of U^{235}
Fusion	630 t of D with 880 t of T

5 Historical Precedents, Vikings and Eskimos in Greenland

To start with, it is important to recognize that collapse is nothing exceptional in history. Indeed, it has rather been the inevitable destiny of every single great civilization. Joseph Tainter reports 18 such cases in *The Collapse of Complex Societies* [25]. Jared Diamond studies six more examples in *Collapse: How Societies Choose to Fail or Succeed* [26]. The Great Pyramids and the Roman Coliseum are vivid proofs that collapse did happen.

Going over each case is clearly impossible within this chapter. Instead, we will focus on two societies which shared the same environment at the same time: the Greenland Norse and the Eskimos. One society, the Norse, eventually collapsed, while the other is still around today [26].

By the beginning of the ninth century, the Vikings started to expand from their homeland, Norway. In 874 AD, they settled in Iceland. In 986 AD, they founded a first colony in the south of Greenland. Soon another colony would follow, to the west. Greenland is not too far from Canada, and indeed, there is evidence of Viking visits at the northern tip of Newfoundland island. Maybe due to the bad relationships with the natives, they could not settle there. But the Greenland colony did flourish. By the middle of the thirteenth century, they counted 5,000 souls. Greenland Norse had a bishop and 22 churches, some of them still standing today. This was the pinnacle of the Viking society in Greenland.

Things then changed quickly, for the worse. In 1406 comes the last report of a trip to Iceland. Then, in 1408 is the last mention of the Greenland colonies in Norwegian chronicles. There are no hints of massive return. The Vikings could not maintain their presence in Greenland beyond the middle of the fourteenth century. And it seems they slowly died out, one after another.

But the Vikings were not the only people living in Greenland. There were Eskimos as well, whose presence dates back at least to 2500 BC [27] and who

Table 2 Vikings vs. Eskimos' way of life

	Eskimos	Vikings
Food	Seal, fish, some caribou	Meat (beef, pork), milk (goat)
Houses	Igloo	Wood
Heating	Seal fat	Firewood
Ships	Kayak (skin + bones)	Wood + metal

have been living there until today. Why then could the Eskimos make it while the Norse could not?

Table 2 compares the Vikings and Eskimos' ways of life. It can help understand the fate of both societies. The Vikings imported their culture to Greenland. They came from a land where forests and pastures abound. Wood, firewood, big mammals, and what is needed to maintain them are abundant in Norway. Yet, living in Greenland means living on a strip of land some 50 km wide, squeezed between the sea and the inland glacier. Seafood and ice are abundant in Greenland, not trees, metal, and pastures.

As a consequence, the Vikings had to rely heavily on trade with Iceland and Norway to maintain their way of life. Like our fuel is fossil fuels, the Vikings' fuel was Norway, from where they imported everything they needed and could not find on-site. Two events then occurred which proved fatal for the Greenland Norse.

On the one hand, the Vikings settled in Greenland during the so-called Medieval Climate Anomaly, characterized by a warm climate over Greenland from 950 to 1250.[5] But starting from the thirteenth century, climate got colder, making life and sailing each time more difficult.

On the other hand, the Black Death hit Europe during the fourteenth century and killed half of Norway in 1350 [28]. Given their reliance on Norway, the Greenland Norse could not stand these two challenges and collapsed.

Meanwhile, Table 2 shows that the Eskimos' way of life was completely adapted to the place. They were relying on locally abundant resources, which explains why they could overcome the end of the Medieval Climate Anomaly and did not care about the Black Death ravaging Europe. Could have the Norse learn from the Eskimos? Maybe, but apparently cultural differences were too large and relationships between the two groups too bad.

[5] The Medieval Climate Anomaly had some regions as warm as in the late twentieth century. But these regional warm periods did not occur as coherently as the warming in the late twentieth century ([15], p. 21).

6 Conclusion

On this first part of the twenty-first century, humanity has reached a crossroad. A global civilization has been built, relying on these nonrenewable fossil fuels. Yet, the need to cut them as soon as possible arises from global warming, not from their limited availability. The business-as-usual scenario, consisting in burning them as long as they are available, would most probably result in a dramatic warming by the end of this century.

From the Roman Empire who was fuelled by conquests and collapsed when they stopped [25] to the Greenland Norse's dependence on Norway, a lesson of history seems to be "do not rely on something that can run out." The uniqueness of our situation may lie in the fact that we need to phase fossil fuels out even before we run out of them.

References

1. Bret A (2014) The energy-climate continuum: lessons from basic science and history. Springer, Bücher
2. Morris I (2010) Why the west rules – for now: the patterns of history, and what they reveal about the future. Profile Books, London
3. Smil V (2008) Energy in nature and society: general energetics of complex systems. MIT, Cambridge, MA
4. Smil V (2010) Energy transitions: history, requirements, prospects. Praeger, Santa Barbara, CA
5. International Energy Agency (2012) Key world energy statistics. International Energy Agency, Paris
6. Aristotle (2010) The Politics. University of Chicago Press, Chicago
7. Buckminster Fuller R (1940) Fortune Mag XXI(2):57
8. McNeill J (2001) In: Something new under the Sun: an environmental history of the twentieth-century world (The Global Century Series). The Global Century Series. W. W. Norton
9. Mouhot JF (2011) Past connections and present similarities in slave ownership and fossil fuel usage. Climatic Change 105:329
10. Jancovici J, Grandjean A (2007) Le plein s'il vous plaît !: La solution au problème de l'énergie. Collection Points. Série Sciences (Éd. du Seuil)
11. Shephard S (2006) Pickled, potted, and canned: how the art and science of food preserving changed the world. Simon & Schuster, New York
12. Weber CL, Matthews HS (2008) Environ Sci Technol 42:3508
13. Maggio G, Cacciola G (2012) Fuel 98:111
14. McGuffie K, Henderson-Sellers A (2005) A climate modelling primer. Wiley, Oxford
15. IPCC (2013) Climate change 2013 the physical science basis – working group I contribution to the fifth assessment report of the IPCC. Climate Change 2013. Cambridge University Press, Cambridge
16. Lynas M (2008) Six degrees: our future on a hotter planet. National Geographic Society, Washington
17. Burton T (2001) Wind energy: handbook. Wiley, Oxford
18. Kuerten H (2011) Direct and Large-Eddy Simulation Viii. ERCOFTAC Series. Springer, Netherlands

19. Burton G (2000) Chemical storylines. Salter's Advanced Chemistry Series. Butterworth Heinemann, Oxford
20. Turcotte D, Schubert G (2002) Geodynamics. Cambridge University Press, Cambridge
21. Huddart D, Stott T (2010) Earth environments: past, present and future. Wiley, Oxford
22. Metz B (2007) IPCC Working Group III, Climate change 2007 – mitigation of climate change: working group III contribution to the fourth assessment report of the IPCC. Climate Change 2007. Cambridge University Press, Cambridge
23. Brown L (2006) Plan B 2.0: rescuing a planet under stress and a civilization in trouble. W. W. Norton, Washington
24. Blankenship RE, Tiede DM, Barber J, Brudvig GW, Fleming G, Ghirardi M, Gunner MR, Junge W, Kramer DM, Melis A, Moore TA, Moser CC, Nocera DG, Nozik AJ, Ort DR, Parson WW, Prince RC, Sayre RT (2011) Science 332:805
25. Tainter J (1990) The collapse of complex societies. New studies in archaeology. Cambridge University Press, Cambridge
26. Diamond J (2006) Collapse: how societies choose to fail or succeed. Penguin
27. Gilbert MTP, Kivisild T, Grønnow B, Andersen PK, Metspalu E, Reidla M, Tamm E, Axelsson E, Götherström A, Campos PF, Rasmussen M, Metspalu M, Higham TFG, Schwenninger JL, Nathan R, De Hoog CJ, Koch A, Møller LN, Andreasen C, Meldgaard M, Villems R, Bendixen C, Willerslev E (2008) Science 320:1787
28. Brothen JA (1996) Population decline and plague in late medieval Norway (1350–1550). Annales de démographie historique. pp 137–149

Part I
Solar and Wind Energy

Recursive Estimation Methods to Forecast Short-Term Solar Irradiation

A. Martín and Juan R. Trapero

Abstract Due to modern economies moving towards a more sustainable energy supply, solar power generation is becoming an area of paramount importance. In order to integrate this generated energy into the grid, solar irradiation must be forecasted, where deviations of the forecasted value involve significant costs. Intermittence, high frequency, and nonstationary are common features of solar irradiation data that have attracted the interest of numerous researchers from different disciplines. In fact, complex methods based on artificial intelligence have been typically used to address this problem. Nonetheless, adequate benchmarks have not been employed to justify such utilization. The objective of this work is to analyze the Holt–Winters (HW) method to forecast solar irradiation at short term (from 1 to 6 h). At the best of our knowledge, this methodology, which belongs to the family of the exponential smoothing methods and is widely used in industry applications ranging from supply chain demand forecasting to electricity load energy forecasting, has not been fully exploited in solar irradiation forecasting. Additionally, in case the accuracy achieved by the Holt–Winters method is not enough, still it can be utilized as a competitive benchmark given its feasible implementation. The Holt–Winters method performance is illustrated by forecasting two time series. Firstly, global horizontal irradiation (GHI) data have been chosen since forecasting GHI is a crucial part in systems based on photovoltaic (PV) energy conversion. Fluctuations of GHI due to passing clouds at short timescales (seconds and minutes) lead to high variability of power output from PV plants that can strain the grid due to voltage-flicker and balancing issues. Furthermore, direct normal irradiation (DNI) data are also forecasted given the role of main fuel that DNI plays in solar concentrator technologies such as solar

A. Martín and J.R. Trapero (✉)
Departamento de Administración de Empresas, Universidad de Castilla-La Mancha, Ciudad Real 13071, Spain
e-mail: juanramon.trapero@uclm.es

G. Lefebvre et al. (eds.), *Environment, Energy and Climate Change II: Energies from New Resources and the Climate Change*, Hdb Env Chem (2016) 34: 17–32,
DOI 10.1007/698_2014_304, © Springer International Publishing Switzerland 2014,
Published online: 9 December 2014

thermal (CSP) and concentrated photovoltaic (CPV) power plants. Both solar irradiation data series have been hourly created from 1-minute irradiance measurements that were collected from ground-based weather stations located in Spain.

Keywords Forecasting methods, Recursive estimation methods, Solar irradiation

Contents

1 Introduction

The increasing investment in renewable energy by developing countries is essential to guarantee immediate answers both to the energy supply crisis with high and fluctuating prices of crude and to the diversification of energy supplies, to reduce the external dependence on foreign oil, gas, and coal. This gives a unique possibility for a major move towards no carbon energy sources and at the same time a decrease in external dependency as well as an improvement of efficiency in electricity generation. Thus, solar power generation becomes an area of paramount research, in particular in countries where energy policies are based on fossil fuels, which are increasingly scarce resources. Reliable short-term forecast information of the components of solar radiation is required to achieve an efficient use of fluctuating energy output from photovoltaic (PV), concentrated photovoltaic (CPV), and solar thermal (CSP) power plants. Electricity companies and transmission systems operators need to be adjusted to the expected load profiles, where forecast errors in the fluctuating input from solar systems lead to significant costs [1, 2].

Intermittence, high frequency, and nonstationary are common features of solar irradiation data that have attracted the interest of numerous researchers from different disciplines. Numerical weather prediction models (NWP), which are based on physical laws of motion and conservation of energy that govern the weather, are operationally used to forecast the evolution of the atmosphere up to 15 days ahead. Although NWP models are powerful tools to forecast solar radiation at places where ground data are not available [3], they pose significant limitations. Global NWP models are limited by its coarse spatial resolution. In order to

overcome this limitation, the downscaling by mesoscale models, which are also named Limited Area Models (LAM) or regional models, allows to derive improved site-specific forecasts. LAM models run for the short-range horizon up to 72 h, and although horizontal resolution of mesoscale models has increased rapidly during the last few years, nowadays, details of complex physical processes near the surface cannot be resolved by parameterization equations due to their small-scale features such as cloud cover genesis and variability. Another limitation of NWP models is the temporal resolution. The time step of internal calculations in NWP models (on the order of minutes) is usually higher than the temporal resolution of the output variables, which is normally of 1 h for mesoscale models and from 3 to 6 h for global models. These temporal output intervals are not suitable to assess, for instance, the time-varying cloud cover evolution and solar irradiation at ground level, which are essentials for predicting ramp rates and ranges of variability for solar power plants.

Satellite-derived solar radiation has also become a useful tool for quantifying solar irradiation at ground surface for large areas and over potential emplacements where previous ground-based measurements are not available [4]. Satellite images corresponding to the same area can be superimposed to analyze the time evolution of air mass in an image pixel or in a certain geographical area. The radiance values recorded by the radiometer of the satellite can vary according to the state of the atmosphere, from clear sky to overcast conditions. In this sense, satellite images give information of the cloudiness at a given time and site [4]. Cloud cover and aerosols have the strongest influence on solar irradiation at ground level. Both parameters show a strong variability in time and space, and modeling cloud structure evolution at a given time is an essential task for solar irradiation forecasting. The cloudiness is defined by the radiance measurements of the satellite radiometer as the cloud index, a cloud reflectance-dependent parameter [5, 6]. The spatial resolution depends on the sensitivity of the radiometer, and the time resolution depends on the time interval between two consecutive images. The geostationary satellites can offer a spatial resolution of up to 1 km and a temporal resolution of up to 15 min. The main limitation from the satellite perspective is setting an accurate radiance value under clear sky conditions and under dense cloudiness from every pixel and every image. Another limitation from satellite images comes from algorithms developed for estimating the solar irradiation that are classified as statistical or empirical models [7, 8]. These algorithms do not need accurate information of the parameters that model the solar radiation attenuation through the atmosphere and are based on simple statistical regression between satellite information and surface measurements. Therefore, the satellite statistical approach needs ground-based solar data. The coarser the observed network, the higher the uncertainty of the satellite-derived solar irradiation data.

Ground-based observations as sky imaging techniques fill the intra-hour and sub-kilometer forecasting gap of NWP models regarding cloud cover over solar power plants. Nonetheless, forecast horizons are limited to very short term, ranging from 5 to 25 min ahead [9]. Comparing with satellite-derived solar irradiation data, sky images offer higher spatial and temporal resolution, but only very short

deterministic forecast horizons are feasible using the sky imagery technique due to cloud variability at the fine spatial scale observed.

The aforementioned limitations have placed time series analysis on local weather stations as the dominated methodology in relation to short-term forecasting horizons [1]. The techniques employed range from artificial intelligence algorithms [10] to classical ARIMA modeling [1, 11]. Despite the fact that a high number of publications propose complex algorithms to tackle the solar irradiation forecasting problem from different statistical approaches as stochastic learning methods [12], it is interesting to note that traditional well-known forecasting techniques as the Holt–Winters (HW, [13]) method has remained overlooked. Holt–Winters technique belongs to the family of exponential smoothing methodologies [14, 15]. In particular, HW is indicated when seasonality component is observed in the data, as it is commonly found in solar irradiation variables. Only two recent works were found related to this approach. On the one hand [16], employed the HW in order to improve the control of grid-connected power systems. In this case, the forecasting horizon was both daily and weekly. On the other hand [17], employed an extension of the exponential smoothing family developed in a state space framework for high-resolution (5 min) solar irradiation time series. Unlike those references, this work investigates the HW method to forecast solar irradiation at short term (from 1 to 6 h), where short-term forecasting horizon is defined according to [18].

The main benefits of HW over other sophisticated approaches are: (1) no need of expert hands to identify, interpret, and implement models and (2) no need of expensive software. These reasons have made exponential smoothing methods a forecasting tool widely used in the industry [15].

In order to illustrate the performance of the proposed model, two hourly time series as global horizontal irradiation (GHI) and direct normal irradiation (DNI) have been constructed from 1-minute ground-based irradiance series. GHI has been selected for this study given that fluctuations of GHI due to passing clouds at short timescales (seconds and minutes) lead to high variability of power output from PV plants. This variability may strain the grid as a consequence of voltage-flicker and balancing issues. Additionally, DNI is also a very relevant component of the total solar irradiation for solar concentrators [12], although it is more sensitive to sky disturbances as cloud cover, aerosol content, water vapor, carbon dioxide, and ozone. A comparative performance analysis between both time series will also be provided. Solar irradiation data were collected from weather stations located in Spain.

In summary, the results show that the HW method can on average reduce the forecast errors to about 38% with respect to the persistence technique for the particular case of the GHI series and around 20% for the DNI series.

The article is organized as follows: in Section 2, the case study design is presented. This section includes the description of the study area and the observational data. Section 3 describes the HW model and other typical forecasting benchmarks. Section 4 explores the experimental results. Finally, main conclusions are drawn in the "Conclusion" section.

2 Case Study

2.1 Dataset Description

Various observational datasets were used to highlight the short-term variability of solar radiation observed at the Earth's surface. Hourly time series of solar irradiation data (Whm^{-2}) provided the basis for the Holt–Winters technique in order to validate its reliability as a forecasting tool at short-term periods (from 1 to 6 h).

All data used in this study were provided by the Institute for Concentration Photovoltaics System (ISFOC), located in Puertollano, Ciudad Real (south-middle of Spain). ISFOC is a research center focusing on concentrated photovoltaic technology (CPV) and has installed 1,1 MW of concentrated photovoltaic energy (CPV) and 5 automatic weather stations in Castilla-La Mancha to measure solar radiation.

Solar irradiance measurements (Wm^{-2}) were recorded every 1 min by a set of solar sensors such as thermopile pyranometers and pyrheliometers, which complied with the international standards of Baseline Surface Radiation Network (BSRN, [19]). Solar data were stored by an automatic acquisition system, and solar sensors were cleaned every day at dawn to minimize the solar radiation extinction caused by dust deposition on their glass domes.

Hourly series of solar irradiation data (Whm^{-2}) were constructed for this study from 1-minute ground-based solar irradiance data (Wm^{-2}), which were recorded between January 2009 and December 2011 by the weather station that ISFOC has sited at 38.67°N, 4.15°W, and 687 m (asl).

2.2 Global Horizontal Irradiation Data

Solar irradiance is defined as the solar power per area (Wm^{-2}). Solar irradiation is defined as the solar energy per area resulting from the solar power integrated over a time period, which was defined 1 h for this study (Whm^{-2}). Global horizontal irradiation (GHI) is the solar energy on a horizontal surface and is the sum of the direct normal irradiation (DNI) projected onto the horizontal surface (DHI) and the diffuse horizontal irradiation (DiffHI). Diffuse irradiation refers to all the solar radiation coming from the sky except the DNI.

Global and diffuse irradiances (Wm^{-2}) were measured by a first-class pyranometer according to the international standards of BSRN [19]. It comprises a multi-junction wire-wound thermopile glued to the back of the sensor disc. Mounting the pyranometer on a horizontal plane, the solar radiation flux density (Wm^{-2}) from a field of view of 180° can be measured to obtain the global horizontal irradiance. Diffuse horizontal irradiance was measured shading the pyranometer on a horizontal plane from the direct normal beam and the circumsolar

irradiance using a shade ball. A two-axis sun-tracking system was needed to measure diffuse horizontal and direct normal irradiances.

2.3 Direct Normal Irradiation Data

Direct normal irradiation (DNI) is the solar energy coming directly from the solar disc and the circumsolar irradiation within approximately 2.5° of the sun center. Direct normal irradiance (Wm^{-2}), also called direct normal beam, was measured by a first-class pyrheliometer according to the international standards of BSRN. It comprises a multi-junction wire-wound thermopile at the base of a tube. The full opening field of view is 5°. The inside of the tube is filled with dry air at atmospheric pressure and sealed at the viewing end. Pyrheliometer was mounted on a two-axis tracker for aiming the tube directly at the sun.

2.4 Exploratory Analysis

Our dataset consists of hourly solar irradiation (GHI and DNI) series. These series represent the solar energy integrated over a 1-h period (Whm^{-2}) from 1-minute measured irradiance data (Wm^{-2}) between January 2009 and December 2011. In total, a dataset of 26,280 observations is available. For example, Figure 1 depicts two months of hourly solar irradiation. Upper and lower plot shows the GHI (solid line) and DNI (dashed line) measured in a winter month (January) and a summer month (July) of the same year (2011), respectively. It is interesting to note that a seasonal component can be observed in each month, although the seasonal shape is different in terms of period[1] and amplitude. In this sense, the amplitude of the seasonality in July is almost constant, whereas the amplitude variability in January is more evident. In fact, this variability is more noticeable for the DNI due to its higher sensitivity to atmosphere conditions. In addition, the number of hours where the solar irradiation is different from zero is higher in summer than in winter.

Table 1 shows some descriptive statistics corresponding to the dataset ranging from January 2009 to December 2011. Since the properties of solar irradiation are time-varying, i.e., the solar radiation is greater in summer than in winter, the statistics have been broken down per month. The first and second column represents the mean and standard deviation of the DNI and GHI. It should be pointed out that the DNI mean and standard deviation are higher than its GHI counterpart. Units in Table 1 have been represented in terms of solar irradiation (Whm^{-2}) for the purpose

[1] Although the seasonality period is 24 hours the whole year, we refer to differences of period to the number of hours during a day that solar irradiance is different from zero.

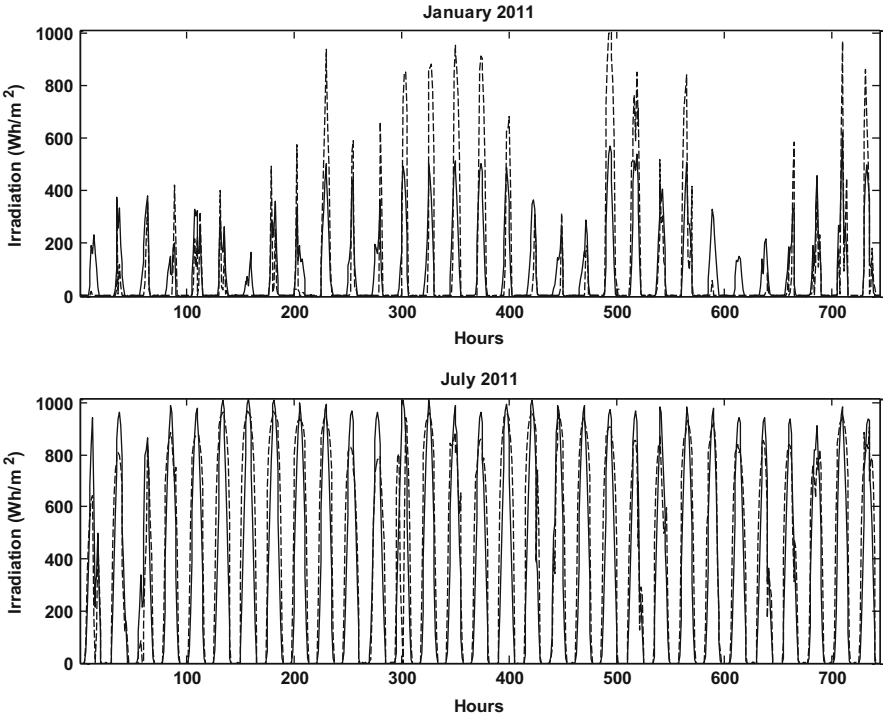

Fig. 1 Hourly solar irradiation (Whm^{-2}) data series corresponding to January 2011 (*upper plot*) and July 2011 (*lower plot*). GHI and DNI are depicted by *solid line* and *dashed line*, respectively

Table 1 Descriptive statistics from January 2009 to December 2011

	Mean (Whm^{-2})		Std (Whm^{-2})	
Month	DNI	GHI	DNI	GHI
Jan	77.58	71.38	209.85	128.58
Feb	163.22	125.55	301.22	195.67
Mar	168.10	165.08	300.90	243.47
Apr	232.22	230.60	331.23	300.37
May	290.35	283.58	351.58	339.38
June	312.43	302.12	356.67	350.35
July	384.28	322.82	382.62	362.30
Aug	317.40	273.33	357.53	330.60
Sept	256.82	209.63	343.40	282.43
Oct	233.67	159.82	339.13	230.73
Nov	133.25	93.82	265.73	159.08
Dec	107.10	72.93	247.38	129.45
Overall	223.03	192.55	315.60	254.37

of making the descriptive statistics related to hourly values of solar radiation easy to read.

3 Models

3.1 Persistence Model and Single Exponential Smoothing

Regarding the problem of solar irradiation forecasting, the most extended technique used to contrast the performance of new models is the persistence model, [20], where the forecast always equals to the last known data point. The persistence model is also known in the forecasting literature as the naïve model or the random walk [21]. Essentially, this model is a particular case of the single exponential smoothing (SES) method [15, 22]. Basically, SES updates the previous forecast by weighting the last forecast error, i.e.:

$$F_{t+1} = F_t + \alpha(y_t - F_t), \tag{1}$$

where α is a constant between 0 and 1. Thus, the persistence model is equivalent to the SES method with $\alpha = 1$.

3.2 Holt–Winters

Typically, time series can be decomposed in different components as trend, seasonality, and irregular term. SES method is adequate when the level is the most important component to explain the time series pattern. Nonetheless, when other typical components as trend or seasonality are present, the previous method should be modified. In the particular case of solar irradiation time series, one of the most important components is the seasonality. Here, the time series has a remarkable periodic behavior every 24 h. A well-known method as the Holt–Winters incorporates those components as follows [21]:

$$L_t = \alpha\frac{Y_t}{S_{t-s}} + (1-\alpha)[L_{t-1} + b_{t-1}], \tag{2}$$

$$b_t = \beta(L_t - L_{t-1}) + (1-\beta)b_{t-1}, \tag{3}$$

$$S_t = \gamma\frac{Y_t}{L_t} + (1-\gamma)S_{t-s}, \tag{4}$$

$$F_{t+1} = (L_t + b_t)S_{t-s+1}, \tag{5}$$

where s is the seasonality period. We assume a daily seasonality ($s = 24$ h). In order to compute the forecasts one step ahead (F_{t+1}) in (5), we need to know the current

underlying level (2), the current underlying trend (3), and the seasonal index (4). Although the model cannot be interpreted in terms of solar radiation physical phenomena, the proposed technique cannot be considered a pure black box model given that each equation stands for a component of the time series in a statistical meaning. The unknown parameters α, β, and γ are positive constants or smoothing constants that vary between 0 and 1. The aforementioned constants weight the previous estimates with respect to the new observations, and so they do not have a physical interpretation in relation to other models based on geometric effects on solar position. These unknown constants can be estimated by minimizing the sum of the one-step-ahead in-sample forecast errors.

Expressions shown in (2)–(5) are the multiplicative version of the HW method. Nonetheless, it cannot be directly used in our application. The problem is the intermittency of the data, i.e., the solar radiation values of GHI and DNI are zero at night and the algorithm in (2)–(5) may have numerical problems. In order to overcome that issue, we propose the additive HW version in (6), where divisions are replaced by subtractions.

More information about the different expressions that exponential smoothing methods can adopt is available in [23]. Note that the forecasting horizon defined by the constant m is included in the last equation in (6). Since this analysis is limited to short-term forecasting horizons, $m = 1, 2, \ldots, 6$.

$$\begin{aligned} L_t &= \alpha(Y_t - S_{t-s}) + (1-\alpha)[L_{t-1} + b_{t-1}], \\ b_t &= \beta(L_t - L_{t-1}) + (1-\beta)b_{t-1}, \\ S_t &= \gamma(Y_t - L_t) + (1-\gamma)S_{t-1}, \\ F_{t+m} &= L_t + mb_t + S_{t+m-s}. \end{aligned} \tag{6}$$

Given the recursive nature of the expressions in (6), the first 24 h is required to initialize the algorithm. Typically, the initialization can be achieved as follows:

$$\begin{aligned} L_s &= \frac{(Y_1 + Y_2 + \ldots + Y_s)}{s}, \\ b_s &= \frac{1}{s}\left[\frac{(Y_{s+1} - Y_1)}{s} + \frac{(Y_{s+2} - Y_2)}{s} + \ldots + \frac{(Y_{s+s} - Y_s)}{s}\right], \\ S_1 &= Y_1 - L_s,\ S_2 = Y_2 - L_s,\ \ldots,\ S_s = Y_s - L_s. \end{aligned} \tag{7}$$

4 Experimental Results

In order to test the aforementioned models, a predictive empirical experiment is carried out. The last week of each month (20% of the data approx.) is reserved as a holdout sample, and it is used for evaluating the different forecasting models. The

experiment design proposed here is exhaustive given that models are tested for each month of a whole year rather than testing the models only for a particular month. That is important because the forecast errors are not expected to be constant throughout the year. In this sense, forecast errors of summer months are lower than winter months as a consequence of a stable weather. The forecasting horizon ranges from 1 to 6 h ahead. A rolling origin evaluation experiment is designed as follows. The three previous months with respect to the week to be forecast are reserved as hold-in sample to optimize the coefficients α, β, and γ. For example, the forecast of the last week of January employs the three previous months to optimize the coefficients. Then, with those coefficients, the algorithm in (6) produces the forecast from 1 h to 6 h ahead. Once the forecast is made, the origin is moved 1 h ahead until the last week of January is exhausted. We proceed analogously to forecast the last week of every month for the rest of the year. Note that the estimation of the coefficients α, β, and γ is re-optimized at every hour as the origin is moved. All models have been implemented in MATLAB®.

The mean absolute error (MAE) is employed to compare the forecasting techniques. The MAE is defined as MAE = mean($|e_t|$), where e_t is the forecast error given by

$$e_t = (y_t - F_t), \quad t = 1, \ldots, T. \tag{8}$$

Here, y_t and F_t stand for the actual value and the forecast, respectively, at time t. Generally, the root mean squared error (RMSE) and the relative root mean squared error (rRMSE) are also used for comparison purposes. The rRMSE is calculated with the following expression:

$$\text{rRMSE} = \frac{\text{RMSE}}{\bar{y}} = \frac{\sqrt{\sum_{t=1}^{T}(y_t - F_t)^2/T}}{\bar{y}}, \tag{9}$$

where $\bar{y}$ is the mean of the observed values. Furthermore, Martín et al. [20] define the improvement over persistence as follows:

$$\text{Improvement} = \left(1 - \frac{\text{rRMSE}_m}{\text{rRMSE}_p}\right) \cdot 100, \tag{10}$$

where rRMSE_m and rRMSE_p stand for the relative root mean squared error for the model proposed and the persistence model, respectively.

Table 2 shows the GHI one-step-ahead forecast errors measured by the previously described metrics on the holdout sample. The errors have been broken down depending on the month of the year. In general terms, the proposed model (HW) outperforms the persistence benchmark in every month. It should be highlighted for its good performance on summer given its low value of rRMSE. In fact, during June, July, August, and September, the improvement over the persistence method is greater than 50%. In winter months, particularly for January

Table 2 Different metrics of one-step-ahead forecast errors per month corresponding to the holdout sample of the GHI data

	MAE (Whm^{-2})		RMSE (Whm^{-2})		rRMSE		
	HW	Persis.	HW	Persis.	HW	Persis.	Improv.
Jan	40.39	43.71	62.39	77.32	87.40	108.30	19.30
Feb	63.27	83.96	97.39	117.87	77.60	93.90	17.40
Mar	65.95	86.26	98.63	117.76	59.70	71.30	16.20
Apr	91.06	107.33	130.74	149.69	56.70	64.90	12.70
May	99.96	123.90	153.65	164.87	54.20	58.10	6.80
June	16.94	119.43	23.47	136.06	7.80	45.00	82.80
July	31.71	121.08	59.28	142.45	18.40	44.10	58.40
Aug	33.68	118.23	58.16	137.14	21.30	50.20	57.60
Sept	31.33	113.13	45.33	132.80	21.60	63.30	65.90
Oct	58.47	77.11	97.60	110.13	61.10	68.90	11.40
Nov	28.13	58.86	45.86	83.75	48.90	89.30	45.20
Dec	13.19	50.78	20.86	76.12	28.60	104.40	72.60
Overall	47.84	91.98	74.45	120.50	45.30	71.80	38.80

and February, the rRMSE is relatively high. This is due to two reasons: (1) higher climate instability and ii) the percentage nature of the error metric provides high values when the solar radiation on average is low, as it is expected in winter months. The last row in Table 2 shows the overall performance of the HW and persistence models along the whole year. In summary, the HW yields an improvement ratio of 38.8% over the persistence model. Units in Table 2 have been represented in terms of the solar energy per area (Whm^{-2}) for the purpose of making the descriptive statistics related to hourly values of solar radiation easy to read.

Analogously, Table 3 shows the DNI one-step-ahead forecast errors on the holdout sample. In general terms, the same conclusions previously found still hold. However, the improvement extent achieved is lower with respect to the GHI results because of the higher data volatility. Again, the overall performance of the HW method is shown in the last row of Table 3. In summary, the HW reduces on average up to 20.8% of the forecast errors provided by the persistence model.

In order to find out whether the HW forecasting accuracy is competitive, a comparison of errors found in the literature should be provided. In that sense, Kraas and collaborators in [2], reviewed the forecasting errors achieved by different techniques in different locations for the variables GHI and DNI. In summary, the rRMSE for GHI forecast was found to be in the range of 30–50%. Meanwhile, the results for the DNI were about 56–77%. If we compare those numbers with the overall rRMSE of the HW, we can corroborate the correct performance of the HW. It should be remarked that, whereas those techniques rely on complex and expensive models, the HW can be implemented straightforwardly in a spreadsheet.

Some examples of the forecasts achieved are shown in Figs. 2 and 3. Figure 2 depicts the one-step-ahead forecasts for the last week of June 2011. Actual values are depicted in a solid line and forecasts are in a dashed line. The upper panel shows

Table 3 Different metrics of one-step-ahead forecast errors per month corresponding to the holdout sample of the DNI data

	MAE (Whm^{-2})		RMSE (Whm^{-2})		rRMSE		
	HW	Persis.	HW	Persis.	HW	Persis.	Improv.
Jan	72.69	62.50	140.42	147.46	181.00	190.10	4.80
Feb	99.66	122.18	166.67	207.30	102.10	127.00	19.60
Mar	103.47	101.85	163.55	174.57	97.30	103.80	6.30
Apr	113.46	116.91	164.79	187.06	71.00	80.60	11.90
May	128.86	131.66	178.55	189.58	61.50	65.30	5.80
June	53.84	103.68	80.76	145.24	25.80	46.50	44.40
July	74.82	122.34	109.21	170.10	28.40	44.30	35.80
Aug	81.08	118.36	105.46	167.26	33.20	52.70	36.90
Sept	86.83	145.03	131.91	193.51	51.40	75.30	31.80
Oct	102.07	117.69	179.12	190.08	76.70	81.30	5.80
Nov	104.67	107.56	162.26	184.55	121.80	138.50	12.10
Dec	71.75	96.54	114.50	175.53	106.90	163.90	34.80
Overall	91.10	112.19	141.43	177.69	79.80	97.40	20.80

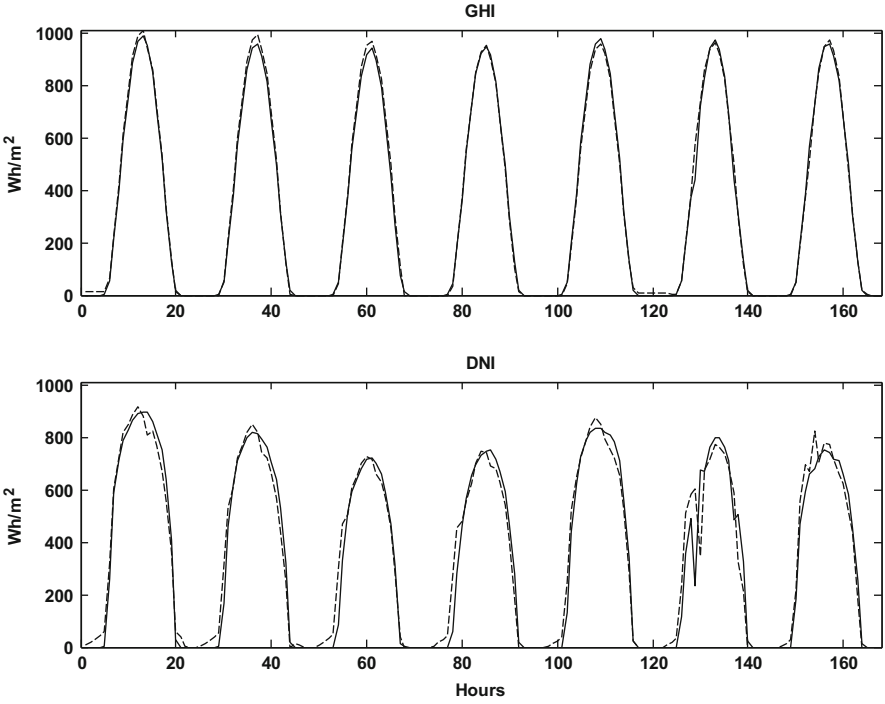

Fig. 2 One-step-ahead hourly forecasts during the last week in June 2011. Actual and forecast values are depicted by *solid* and *dashed line*, respectively. *Upper plot* shows GHI forecasts. *Lower plot* shows DNI forecasts

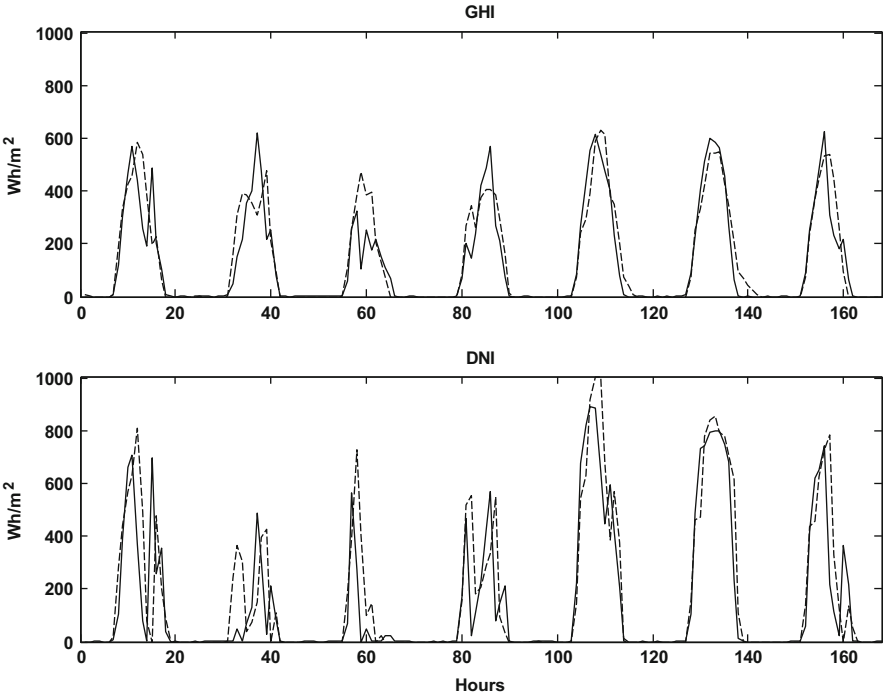

Fig. 3 One-step-ahead hourly forecasts during the last week in October 2011. Actual and forecast values are depicted by *solid* and *dashed line*, respectively. *Upper plot* shows GHI forecasts. *Lower plot* shows DNI forecasts

the results for the GHI variable, whereas the DNI variable is shown in the lower panel. The figures show how the HW method is capable of capturing the clear seasonality of the data and to provide reasonable forecasts. It is also visible how the variable DNI is more difficult to forecast, and the differences between actual and forecasted values are more apparent.

Summers in this area of Spain are typically rather stable, and it makes sense that solar radiation during these days is more feasible to forecast.

Nonetheless, months that belong to spring or autumn are more variable. In order to show the HW performance for those months, Figure 3 shows the results achieved during the last week in October 2011. Again, the solid line represents the actual values and the dashed line the forecasts. Here the forecasts are not as precise as the previous figure, but still they provide competitive forecasts. It should be noted that, although both GHI and DNI depend on cloud cover conditions, DNI is more sensitive than GHI to atmosphere changes as turbidity conditions (atmosphere composition due to the aerosol content and other particulates in the air) and this makes DNI more difficult to forecast, and thus, its forecast errors are also higher than the GHI ones. Note that this discrepancy between forecasting accuracy is in accordance with the literature [2].

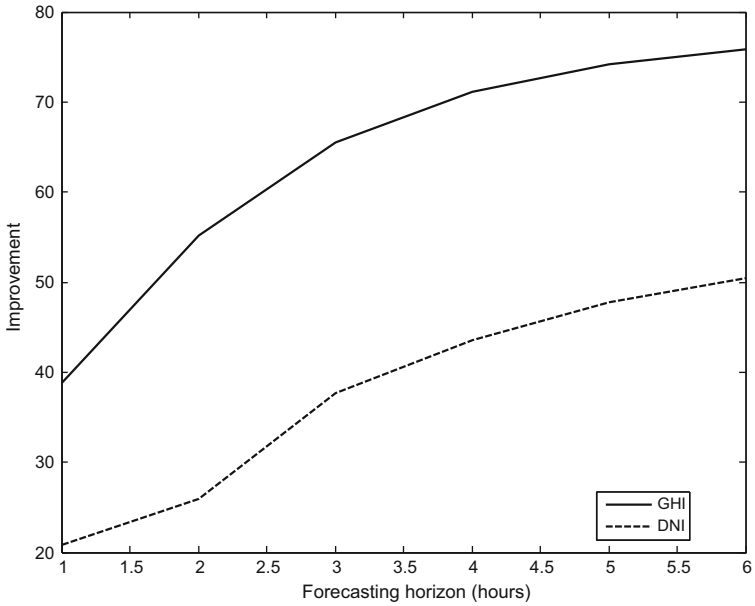

Fig. 4 Improvement of HW on persistence model in the holdout sample vs. forecasting horizon. GHI and DNI are depicted by *solid* and *dashed line*, respectively

So far, the forecasting performance of the proposed models for one-step-ahead forecasting horizon has been analyzed. Figure 4 shows the evolution of the improvement metric with regard to broader forecasting horizons. Since this study is devoted to short-term horizons, the longest horizon is set to 6 h. This picture shows how the improvement of the HW with respect to the persistence raises with the forecasting horizon in a nonlinear fashion. This improvement increase is due to the HW model's capability to capture the seasonality of the data, unlike the persistence model. In addition, the lower improvement ratios achieved by the DNI remark again the difficulties of forecasting the solar radiation measured by DNI instead of GHI.

5 Conclusions

In order to efficiently incorporate renewable energies into the grid, it is very important to provide accurate forecasts. In the particular case of solar energy, the key variable is solar radiation. In recent years, novel methodologies have proliferated to forecast solar radiation with different complexity levels. Nonetheless, there is not unanimity about which technique is the most adequate. In certain extent, this is due to the difficulties found to reproduce the results given the geographical dispersion of each experiment. Nevertheless, another potential reason might be the lack of appropriate benchmarks. Typically, the persistence model is used to test new models.

This article analyzes the Holt–Winters exponential smoothing performance to tackle the problem of solar radiation forecasting. This exponential smoothing version is easy to implement that relaxes the necessity of statistical experts or expensive software. For those reasons, this technique is broadly employed in industry for demand forecasting applications.

The results show that the Holt–Winters method improves significantly the forecast accuracy with regard to the persistence model and it can be considered as a competitive forecasting technique. These conclusions have been validated on the basis of GHI and DNI data measured in weather stations located in Spain. Given the univariate nature of the Holt–Winters that uses only past information to provide forecasts, it seems probable that other techniques that incorporate exogenous variables could improve the Holt–Winters results. In any case, the Holt–Winters approach would be a hard to beat benchmark.

Acknowledgment The authors thank the ISFOC for kindly providing all the data used in this paper.

References

1. Reikard G (2009) Predicting solar radiation at high resolutions: a comparison of time series forecasts. Sol Energy 83:342–349
2. Kraas B, Schroedter-Homscheidt M, Madlener R (2013) Economic merits of a state-of-the-art concentrating solar power forecasting system for participation in the Spanish electricity market. Sol Energy 93:244–255
3. Mathiesen P, Kleissl J (2011) Evaluation of numerical weather prediction for intra-day solar forecasting in the continental United States. Sol Energy 5:967–977
4. Polo J, Zarzalejo L, Ramírez L, Badescu V (ed) (2008) Solar radiation derived from satellite images, vol 18. Modeling Solar Radiation at the Earth's Surface. Springer-Verlag Berlin
5. Cano D, Monget J, Albuisson M, Guillard H, Regas N, Wald L (1986) A method for the determination of the global solar radiation from meteorological satellite data. Sol Energy 37:31–39
6. Diabaté L, Moussu G, Wald L (1989) Description of an operational tool for determining global solar radiation at ground using geostationary satellite images. Sol Energy 42:201–207
7. Noia M, Ratto CF, Festa R (1993) Solar irradiance estimation from geostationary satellite data: I. Statistical models. Sol Energy 51:449–456
8. Noia M, Ratto CF, Festa R (1993) Solar irradiance estimation from geostationary satellite data: II. Physical models. Sol Energy 51:457–465
9. Chow CW, Urquhart B, Lave M, Domínguez A, Kleissl J, Shields J (2011) Intra-hour forecasting with a total sky imager at the UC San Diego solar energy testbed. Sol Energy 85:2881–2893
10. Mellit A, Pavan AM (2010) A 24-h forecast of solar irradiance using artificial neural network: application for performance prediction of a grid-connected PV plant at Trieste, Italy. Sol Energy 84:807–821
11. Pedro HT, Coimbra CF (2012) Assessment of forecasting techniques for solar power production with no exogenous inputs. Sol Energy 86:2017–2028
12. Marquez R, Coimbra CF (2011) Forecasting of global and direct solar irradiance using stochastic learning methods, ground experiments and the NWS database. Sol Energy 85:746–756

13. Winters PR (1960) Forecasting sales by exponentially weighted moving averages. Manag Sci 6:324–342
14. Gardner ES (1985) Exponential smoothing: the state of the art. J Forecast 4:1–28
15. Gardner ES (2006) Exponential smoothing: the state of the art, Part II. Int J Forecast 22:637–666
16. Su Y, Chan LC, Ng SK (2013) A weighted RMSD control model for Holt–Winters forecasting of output power of a grid connected solar photovoltaic system. In: 12th international conference on sustainable energy technologies. Hong Kong
17. Dong Z, Yang D, Reindl T, Walsh WM (2013) Short-term solar irradiance forecasting using exponential smoothing state space model. Energy 55:1104–1113
18. Perez R, Kivalov S, Schlemmer J, Hemker K Jr., Renn D, Hoff TE (2010) Validation of short and medium term operational solar radiation forecasts in the US. Sol Energy 84:2161–2172
19. McArthur LJB (2004) Operations manual. WMO/TD-No, 1274, WCRP/WMO. Baseline Surface Radiation Network (BSRN)
20. Martín L, Zarzalejo LF, Polo J, Navarro A, Marchante R, Cony M (2010) Prediction of global solar irradiance based on time series analysis: application to solar thermal power plants energy production planning. Sol Energy 84:1772–1781
21. Makridakis S, Wheelwright SC, Hyndman RJ (1998) Forecasting: methods and applications, 3rd edn. Wiley, New York
22. Hyndman RJ, Koehler AB, Ord JK, Snyder RD (2008) Forecasting with exponential smoothing: the state space approach. Springer-Verlag Berlin
23. Pegels CC (1969) Exponential forecasting: some new variations. Manage Sci 15(5):311–315

Technical and Environmental Analysis of Parabolic Trough Concentrating Solar Power (CSP) Technologies

Guillermo San Miguel, B. Corona, J. Servert, D. López, E. Cerrajero, F. Gutierrez, and M. Lasheras

Abstract With over 100 commercial projects in operation or under construction worldwide, concentrating solar power (CSP) has the potential to play a key role in the mass production of power. Despite the enormous potential, this technology suffers from a number of weaknesses that are related to the intermittency and variable nature of the solar resource, which results in reduced capacity factors and operation flexibility. The incorporation of energy backup systems provides a solution to these drawbacks, allowing CSP to become more dispatchable, cost effective, and easier to integrate into existing power grids. Backup systems may come in the form of thermal energy storage (TES) or auxiliary fuels (mostly natural gas but also coal, fuel, solid biomass, biogas, biomethane, and syngas). Auxiliary fuels are usually integrated using conventional furnaces or boilers, although higher efficiencies may be achieved when using conventional or aeroderivative gas turbines. The possibility of using heat transfer fluids (HTF) with higher thermal stability (like molten salts) would permit integration of energy backup systems in a more efficient and cost-effective manner. A great deal of research and development is going on at present with the aim of devising CSP plants capable of competing with other energy resources and technologies. This paper provides a critical analysis of CSP technologies based on parabolic trough solar collectors,

G. San Miguel (✉) and B. Corona
Departamento de Ingeniería Energética y Fluido Mecánica, Universidad Politécnica de Madrid, Escuela Técnica Superior de Ingenieros Industriales (ETSII), C/ José Gutiérrez Abascal 2, Madrid E28006, Spain
e-mail: g.sanmiguel@upm.es

J. Servert, D. López, and E. Cerrajero
IDIE. Investigación, Desarrollo e Innovación Energética, S.L. Plaza Manolete 2, Madrid E28020, Spain

F. Gutierrez and M. Lasheras
Cobra Instalaciones y Servicios S.A., C/ Cardenal Marcelo Spínola 10, Madrid E28016, Spain

G. Lefebvre et al. (eds.), *Environment, Energy and Climate Change II: Energies from New Resources and the Climate Change*, Hdb Env Chem (2016) 34: 33–54,
DOI 10.1007/698_2015_334,
Published online: 25 March 2015

describing the pros and cons associated with incorporating backup energy systems. This analysis includes technical and environmental aspects of different CSP configurations.

Keywords Concentrating solar power, CSP, Hybrid, LCA

Contents

1 Introduction to CSP

The nuclear reactions occurring in the Sun's core generate vast amounts of energy that is emitted into the universe in the form of electromagnetic radiation. Some of this energy reaches the Earth's surface and can be utilized to produce electricity using a number of technologies like photovoltaic modules or concentrating solar power (CSP) plants.

In CSP installations, the direct component of the sunlight[1] is concentrated using mirrors or lenses to generate the thermal energy required to drive a conventional thermodynamic cycle (usually Rankine type but also Stirling, Brayton, and combined cycles).[2] The design of the solar collector determines the configuration and operating conditions of the plant. Parabolic trough and linear Fresnel collectors concentrate the solar radiation on a focal line and achieve solar concentration factors typically between 60 and 100. Solar tower and solar dish collectors focus the incoming radiation on a single focal point, resulting in higher concentration factors (up to 1,000) and superior operating temperatures. Most of the installed capacity at present (over 90%) is based on parabolic trough and, to a lesser extent, solar tower (9%) technologies.

[1] Direct Normal Irradiance (DNI)

[2] In conventional power plants, this energy is obtained from the combustion of fuels (coal, oil, natural gas, and biomass) or from nuclear reactions.

The first commercial CSP plants in the world (SEGS-I to SEGS-IX) were built in the Mohave Desert (California, USA) between 1985 and 1991. This solar energy complex, still in operation today, includes nine power stations based on parabolic trough technology with an installed capacity of 354 MWe. No additional capacity was installed between 1991 and 2007, due primarily to reduced interest in renewable energies during that period as a result of reduced fossil fuel prices. The renaissance of CSP commenced in 2007 with the construction of PS10 (power tower) and Andasol-1 (parabolic trough) in Southern Spain. This new upsurge was related to the approval of legislation that supported the production of electricity from renewable energy resources in Spain [1,2]. The regulatory framework secured a feed-in tariff for CSP generation of 26.9 c€/kWh for 25 years.[3]

Spain is currently the largest producer of CSP electricity with 48 plants totaling and installed capacity of 2,204 MWe (March 2014) [3]. The USA has 20 CSP plants in operation totaling 956 MWe [4]. Countries like Algeria, Iran, Egypt, and Morocco have commercial CSP integrated with natural gas combined cycles (integrated solar combined cycle – ISCC). Other countries with good solar resources like United Arab Emirates, Australia, China, India, Iran, Israel, Italy, Jordan, Mexico, and South Africa also have CSP programs and commercial or demonstration projects at different stages of construction and/or operation [4,5]. The International Energy Agency (IEA) estimates that global CSP capacity may grow to 147 GW in 2020 and reach 1,089 GW by 2050 [6].

Despite the obvious benefits of producing electricity from a freely available and renewable energy resource, CSP also has a number of drawbacks inherent to the intermittent and seasonal nature of solar irradiation. In the absence of additional energy inputs, basic CSP plants have a reduced capacity factor[4] and perform badly in terms of power firmness and dispatchability.[5] These aspects have a direct effect on the actual generation capacity of the technology, its economic viability, and its integration into existing power networks. To lessen these weaknesses, modern commercial scale plants typically incorporate energy backup systems in the form of thermal energy storage (TES) and/or integration of auxiliary fuels. The design and configuration of these elements determine to a large extent the power capacity, energy efficiency, economic viability, and environmental performance of the plant.

Any industrial activity has the potential to cause environmental deterioration and CSP is no exception. Life cycle analysis (LCA) is a scientific methodology employed to quantify the environmental performance of processes and products. Various papers have been produced analyzing the sustainability of CSP plants using this methodology, including Burkhardt et al. [7,8], Corona et al. [9], Lechón

[3] Note that support for the generation of electricity from renewable energy resources in Spain was abolished for additional capacity under Real Decreto-ley 1/2012 due to the global financial crisis.

[4] Ratio of the electricity generated during a period of time to the energy that could have been generated if the CSP plant had operated at full-power.

[5] Ability of the plant to provide electricity on demand.

et al. [10], Lovegrove and Pye [11], San Miguel and Corona [12], and Klein and Rubin [13].

Despite the huge potential and technical success of existing CSP plants, the economic viability of this technology has not been proven and relies heavily on public subsidies. A great deal of research and development is taking place at present aimed primarily at investigating novel plant configurations and the integration of advanced energy backup systems that may reduce costs and improve power dispatchability. This paper provides a technical and environmental analysis of existing and novel CSP technologies based on parabolic trough collectors. The paper starts with an evaluation of pros and cons associated with this technology in its basic configuration (no thermal energy storage or auxiliary fuels). The technical challenges and environmental consequences of incorporating energy backup systems based on thermal energy storage (TES) are evaluated. The limitations of existing heat transfer fluids (HTF) and the opportunities arising from novel technologies based on the use of molten salts and direct steam generation (DSG) technologies are discussed. The paper ends with an analysis of alternative strategies and configurations of CSP operating in hybrid mode with backup fuels.

2 CSP Based on Parabolic Trough Collectors

As shown in Fig. 1, parabolic trough collectors are made of curved mirrors forming a linear parabolic shape. The mirrors reflect the solar radiation into a hollow tube (receiver) that runs along its focal point. Individual collectors are grouped into solar collector assemblies (SCA) that incorporate a single-axis tracking mechanism and allow optimum orientation toward the sun. SCAs are arranged into solar loops with total lengths and aperture areas that vary depending on the design and operating conditions of the power block. The solar field is made of many parallel solar loops aligned on a north–south horizontal axis, to track the sun from east to west. The total capacity of the plant is determined primarily by the number of solar loops.

As illustrated in Fig. 2, a set of pumps force the heat transfer fluid (HTF) to circulate inside the hollow receiver, absorbing the solar energy and increasing its temperature as it moves along the solar field. The hot HTF is returned to the power block where a series of heat exchangers are used to generate high-pressure superheated steam that is used to drive a conventional Rankine cycle.

The HTF employed in commercial parabolic trough CSP plants consists of a eutectic mixture of diphenyl and diphenylether (DP/DPO), which is stable at temperatures up to 395°C. This thermal stability determines the operating conditions of the plant[6] and the energy efficiency of the thermodynamic cycle.

Parabolic trough CSP plants like the one described in Fig. 2 incorporate a furnace that operates in series with the solar field. This element is used to avoid

[6] Steam temperature and pressure typically around 370–375°C and 90–100 bar, respectively

Fig. 1 Parabolic trough collector and solar field

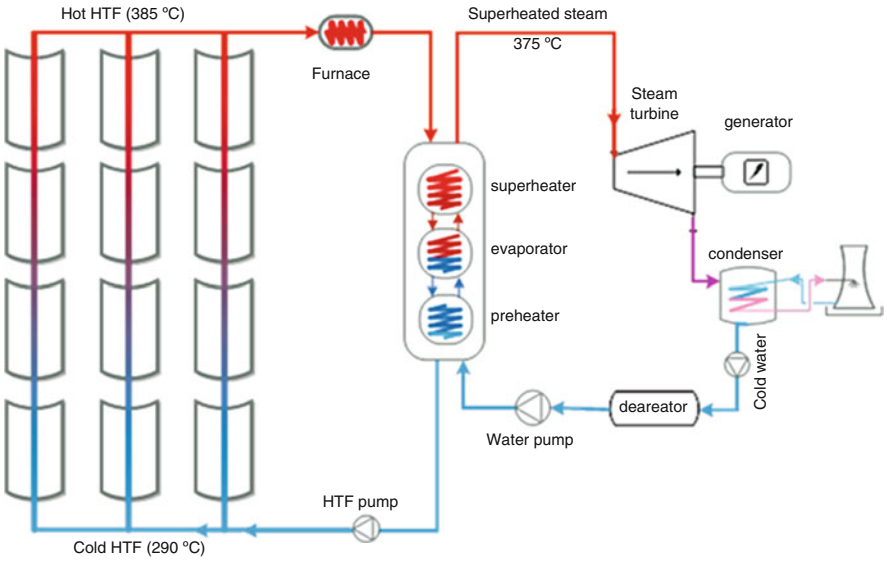

Fig. 2 Process diagram of a simple parabolic trough CSP plant with auxiliary backup furnace installed in series with the solar field

freezing of the HTF during the night, to facilitate daily start-up operations, and also to stabilize the power output during transient periods of low solar radiation. This simple CSP configuration may only generate electricity when solar resource is available, and the plant will stop generating electricity during the night and also whenever solar irradiation is not sufficiently intense.

Table 1 (see basic CSP) describes the main characteristics of a 50-MWe installation based on the configuration described (no energy backup and wet cooling of power block) for solar irradiation values typical of southern Spain (DNI = 2,030 kWh/m^2 years). The data is compared against the same plant incorporating thermal energy storage (TES) and also including energy input from auxiliary fuel (12% of power generation, as permitted under Spanish regulatory

Table 1 Main characteristics of a wet-cooled 50 MWe CSP plant with different configurations: solar only operation, solar only with TES, and solar with TES hybridized with natural gas (12% contribution)

		Basic CSP	CSP with TES	CSP with TES and NG
Installed capacity (MWe)		50		
Thermal efficiency of the cycle (η)		35%		
Net efficiency		16%		
Auxiliary furnace efficiency		95%		
Lifespan (years)		25		
Number of solar collectors		360	624	624
Aperture (m^2)		294,300	510,120	510,120
Occupied area (ha)		135	200	200
Direct normal irradiance ($kWh/m^2 \cdot year$)		2,030		
Full load equivalent hours (h)		1,785	2,800	3,100
Capacity factor (%)		20	32	35
Gross electricity generation (MWh/year)		105,600	165,687	188,281
Auxiliary energy input (MJ/year)	Operation	0	0	2.32E + 08
	Maintenance	4.00E + 06	6.28E + 06	6.28E + 06
Direct water use	m^3/year	458,000	816,598	840,360
	m^3/MWh	5.13	5.07	5.07

system). A simple CSP plant (no TES or auxiliary fuels) would require 360 solar collectors with a total aperture value of 294,300 m^2. The estimated capacity factor would be 20%, equivalent to 1,785 full-load equivalent hours (h) per year, resulting in a gross power output of 105,600 MWh/year and water consumption of 458,000 m^3/year (5.13 m^3/MWh). The consumption of auxiliary fuel for maintenance operations (no power generation) would amount to 4.00E + 06 MJ/year.

Table 2 shows the environmental performance associated with the production of 1 MWh of electricity in this basic CSP configuration, as determined using life cycle analysis (LCA) methodology. The results show total emission values in the climate change category of 26.8 kg CO2 eq./MWh, corresponding primarily to extraction of raw materials and manufacturing (E&M) of the different elements that make the plant (70.2%) and also to operation and maintenance (O&M) activities (20.5%).

Impact values associated with other key environmental categories were calculated as follows: human toxicity (14.3 kg 1,4-DB eq./MWh), particulate matter (69.6 g PM10 eq./MWh), terrestrial acidification (163 g SO2 eq./MWh), freshwater eutrophication (10.6 g P eq./MWh), water depletion 5.35 m^3/MWh), and fossil depletion (9.4 kg oil eq./MWh).

Table 2 Environmental profile of a basic 50 MWe wet-cooled CSP plant determined using life cycle analysis methodology

	Units	Total	E&M	C	O&M	D&D
Climate change	kg CO_2 eq./MWh	26.8	18.8	0.04	5.5	2.5
Human toxicity	kg 1,4-DB eq./MWh	14.3	13.7	0.01	0.51	0.12
Particulate matter	g PM10 eq./MWh	69.6	59.8	0.16	4.5	5.11
Terrestrial acidification	g SO2 eq./MWh	163	135	0.33	12.7	14.9
Freshwater eutrophicat.	g P eq./MWh	10.6	10.2	0.006	0.45	−0.03
Freshwater ecotoxicity	g 1,4-DB eq./MWh	334	319	0.21	10.6	4.22
Marine ecotoxicity	g 1,4-DB eq./MWh	342	325	0.22	11.6	5.37
Urban land occupation	m^2a/MWh	25.8	0.17	25.6	0.01	0.02
Natural land transformat.	m^2/MWh	0.01	0.003	5.82E-05	0.00	1.11E-03
Water depletion	m^3/MWh	5.35	0.18	0.007	5.15	6.503
Metal depletion	kg Fe eq./MWh	7.49	7.79	0.004	0.08	−0.39
Fossil depletion	kg oil eq./MWh	9.4	6.35	0.02	2.1	0.96

E&M extraction of raw materials and manufacturing, *C* construction, *O&M* operation and maintenance, *D&D* dismantling and disposal

3 Thermal Energy Storage in Parabolic Trough CSP

To overcome the limitations associated with simple CSP plants (reduced capacity factor and dispatchability), modern installations incorporate energy backup systems based on the use of thermal energy storage (TES) and/or the combustion of auxiliary fuels. TES allows excess thermal energy produced during the day to be collected for use during the night or during transient periods of reduced solar radiation. Different technologies and thermal storage media are being tested at present. The most efficient and commercially proven TES systems in CSP are based on two-tank indirect technology, like the one illustrated in Fig. 3.

The technology involves two tanks filled with molten salts, which have a high specific heat capacity and relatively low freezing temperature. The salts usually employed in these applications are eutectic binary mixtures of sodium and potassium nitrates with freezing temperatures around 250°C, depending on the specific composition and purity of the salts. Ternary mixtures incorporating calcium nitrates reach lower freezing temperatures (around 150°C), which would improve the efficiency of the plant and reduce energy consumption during the night.

During the day, some of the thermal energy in the synthetic HTF is used to drive the steam cycle and some is used to fill up the TES. The salts leave the cold tank (usually 290°C), pass through the heat exchanger, absorb the energy from the HTF,

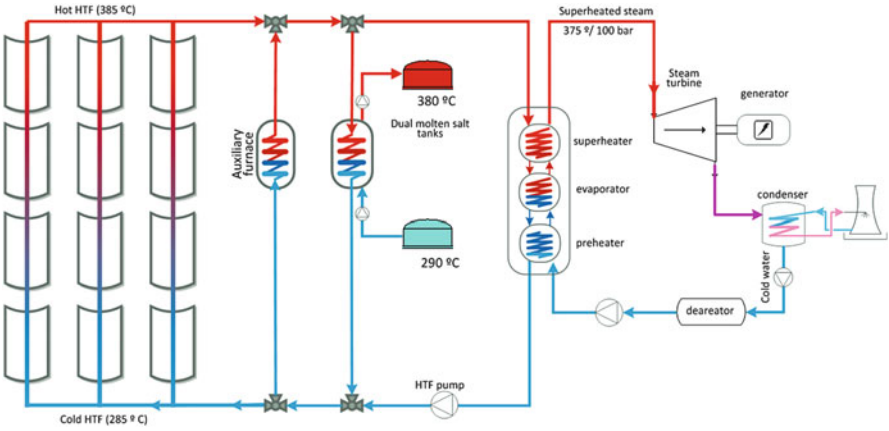

Fig. 3 Process diagram of a conventional CSP plant with integrated TES system and auxiliary backup furnace in series with the solar field

and are stored in the hot tank (380°C). When the solar radiation is not sufficient, the power plant reverses the HTF and molten salt flow direction. In this situation, the hot molten salts heat up the HTF and return to the cold tank, and the hot HTF is directed to the power block for additional power generation.

In commercial CSP plants with TES, an auxiliary furnace is usually connected in parallel to the solar field to stabilize the power block, to avoid freezing of the HTF during the night, and to facilitate daily start-up operations. The minimum amount of auxiliary energy required to operate a commercial parabolic trough CSP installation varies depending on the size of the solar field and the TES, the intensity of solar irradiance, and ambient temperature. For the conditions typically found in southern Spain, this minimum requirement ranges between 100,000 and 130,000 MJ/MW/year, which represents 6.28E + 06 MJ/year for a typical 50 MWe CSP installation or 1.61E + 05 Nm^3/year of natural gas [12].

Table **1** (see CSP with TES) shows the main features and operating characteristics of a wet-cooled 50 MWe CSP plant with 7.5 h TES like the ones installed in southern Spain. The incorporation of TES results in a significant increase in the capacity factor of the plant (32%, compared to 20% in the simple configuration), which results in higher operation capacity (2,800 h, compared to 1,785 h without TES) and yearly gross power generation (165,687 MWh/year, compared to 105,600 MWh/year). The incorporation of a TES involves a significant increase in the capital costs of the plant. This is so because of the investment associated with the TES system itself (mainly tanks and salts) but also due to the enlarged dimensions of the solar field, which needs to generate sufficient thermal energy to

Table 3 Characterized impacts in the life cycle of a CSP plant with TES operating using solar energy only [9,12]

	Units	Total	E&M	C	O&M	D&D
Climate change	kg CO_2 eq./MWh	26.6	21.1	0.03	4.63	0.90
Human toxicity	kg 1.4-D B eq./MWh	13.1	12.9	4.70E-03	0.35	−0.18
Terrestrial acidification	g SO_2 eq.	166	150	0.21	8.96	7.21
Freshwater eutrophication	g P eq.	10.1	10.14	4.05E-03	0.31	−0.36
Marine ecotoxicity	g 1.4-DB eq.	276	271	0.11	6.94	−1.93
Natural land transformation	m^2/MWh	0.005	3.42E-03	3.72E-05	8.30E-04	5.27E-04
Water depletion	m^3/MWh	5.27	0.21	4.34E-03	5.06	1.70E-03
Fossil depletion	kg oil eq./MWh	9.29	7.15	0.01	1.76	0.37

E&M extraction of raw materials and manufacturing, *C* construction, *O&M* operation and maintenance, *D&D* dismantling and disposal

drive the power block and to charge the TES. The solar multiple[7] in a typical CSP plant incorporating 7.5 h of TES usually ranges between 2.0 and 2.2.

The incorporation of the TES systems also involves environmental consequences that need to be considered. Table 3 shows the environmental performance of a parabolic trough CSP plant incorporating a 7.5 h TES system. Environmental impacts in selected categories were estimated as follows: climate change 26.6 kg CO2 eq./MWh, human toxicity 13.1 kg 1,4-DB eq./MWh, marine ecotoxicity 276 g 1,4-DB eq./MWh, terrestrial acidification 166 g SO2 eq./MWh, natural land transformation 0.005 m^2/MWh, eutrophication 10.1 g P eq./MWh, and fossil depletion 9.29 kg oil eq./MWh. Environmental damage in all categories, except water depletion, is attributable primarily to extraction of raw materials and manufacturing (E&M), with a marginal contribution from other life cycle phases (construction, operation and maintenance, dismantling and disposal).

No significant differences were observed in the environmental performance of CSP operating with or without TES. The results show 26.6 kg CO2 eq./MWh with TES compared to 26.8 kg CO2 eq./MWh without. This suggests that the environmental burdens associated with the construction and operation of the TES are compensated by an increased power generation capacity.

[7] The solar multiple represents the actual size of the solar field relative to what would be required to reach the installed capacity of the plant at the time of nominal solar irradiance (typically 850 w/m^2).

Considering the fact that the best solar resources are located in desert areas, a key to the sustainability of CSP technologies relates to direct water consumption during operation and maintenance of the installation. It has been estimated that the 50 MWe CSP plant described in Table 1 (see CSP with TES) consumes 5.27 m^3 of water per MWh generated (considering the life cycle). Most of this derives from direct water use in the power block (80% wet cooling system, 1.2% power cycle water), while a smaller proportion is associated with the cleanup of solar collectors (0.6%). Most of the remaining 18.8% relates to water depleted during extraction of natural resources and manufacturing of materials used in the construction of the plant. Water use is directly related to the electricity generated by the plant, although this consumption may be reduced significantly using dry-cooled condensers. However, the capital and operating cost of dry-cooling systems is comparatively higher and reduces plant efficiency.

4 Advanced HTF in Parabolic Trough CSP

As discussed above, the thermal stability of the HTF imposes a limitation to the technical performance, energy efficiency, and economic viability of parabolic trough CSP. Hence, research and development is being conducted to evaluate the possibility of using other fluids that may transfer the energy collected in the solar field to the power block. Two options, which are not commercially available yet, are discussed in this section: molten salts and direct steam generation.

4.1 Molten Salts as HTF

Molten salts have a much higher thermal stability than synthetic oils, which means that they could operate at significantly higher temperatures (typically between 550 and 650°C). Higher operating temperatures would allow higher energy efficiencies in the thermodynamic cycle. Besides, integration of TES is also more simple and efficient when molten salts are used both as HTF and thermal storage medium. The use of a higher temperature difference between the hot and cold tanks reduces the size (and cost) of the TES, as a smaller storage volume is required for a given amount of energy storage.

Figure 4 shows a process diagram for a parabolic trough CSP plant operating with molten salts. The molten salts are heated in the solar field to temperatures around 550°C. This energy is transferred to the water/steam cycle using a multiple stage heat exchanger. The superheated steam is used to drive the thermal cycle. The cold salts are pumped to the solar field to close the cycle. The temperatures achieved by molten salts are compatible with commercial supercritical steam cycles

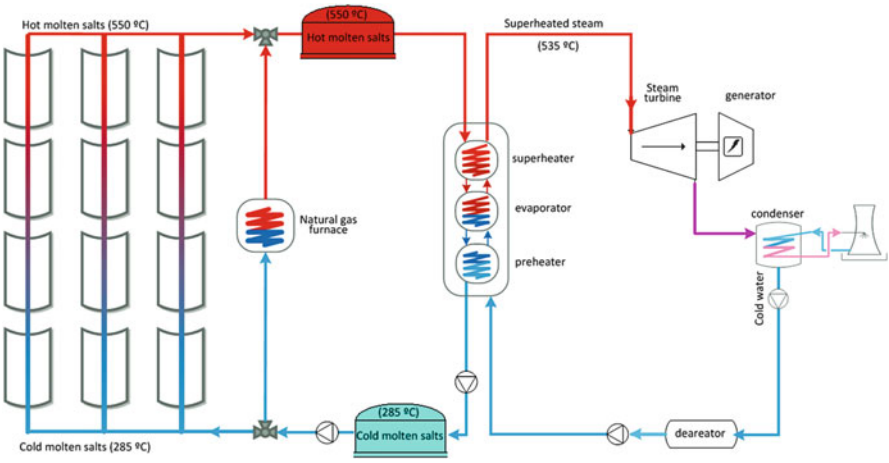

Fig. 4 Process diagram of a CSP plant with thermal energy storage (TES) using molten salts both as HTF and thermal storage medium

that achieve efficiencies in the thermal cycle up to 40–45%, instead of 30–35% in conventional CSP.

The main problem with this technology relates to the relatively high freezing temperatures of the salts, which would require freeze protection and external heating of the solar field during the night. The use of molten salts also involves a number of additional drawbacks and technical challenges: increased maintenance of solar collectors, optimizing start-up and shut-down times, and compatibility of materials (piping, fittings, exchange circuits, etc.).

4.2 Direct Steam Generation

Direct steam generation (DSG) technology employed in CSP plants does not require the use of an intermediate heat transfer fluid. Instead, water/steam is circulated inside the receivers and directly used to drive the steam turbine in the power block. The efficiency of this technology is higher due to the absence of intermediary HTF and heat exchange systems, as shown in Fig. 5. However, thermal energy storage with DSG is more costly and technically complex due to the low density of the fluid.

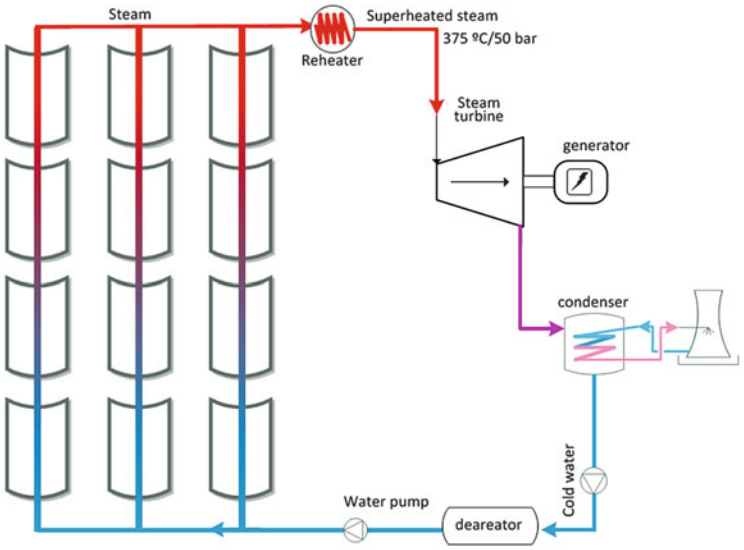

Fig. 5 Process diagram of a CSP plant using direct steam generation

5 Hybridizing CSP with Other Energy Resources

It has been discussed that conventional parabolic trough CSP plants incorporate an auxiliary furnace operating with conventional fuel (usually natural gas) for maintenance activities (to improve stability, avoid freezing of HTF, and facilitate start-up operations). The capacity of this energy input may be increased to extend the operating hours of the plant and, therefore, its overall power output. This strategy where solar radiation is combined with other fuels for power generation is referred to as hybrid operation.

5.1 Hybridization with Auxiliary Fuels in Parallel to the Solar Field

Most CSP plants in Spain operate in hybrid mode. This is so because the Spanish legislation regulating the generation of electricity from renewable resources [2] allowed CSP plants to produce up to 12% of their gross power output from auxiliary fuels. This additional power also benefited from the 26.9 c€/kWh feed-in tariff established for solar thermal power. Table 1 shows the main characteristics of a CSP of this type (TES and auxiliary fuel).

As shown in Fig. 3, the auxiliary furnace is usually integrated in parallel to the solar field and provides supplementary thermal energy to the HTF. Natural gas is

Table 4 Characterized impacts of the CSP technology operating with different NG energy inputs [9]

Impact category	Units	Gross electricity output from natural gas				
		0%	10%	20%	30%	35%
Climate change	kg CO_2 eq./MWh	26.6	108	189	270	311
Human toxicity	kg 1.4-DB eq./MWh	13.1	12.5	11.8	11.1	10.7
Terrestrial acidification	g SO_2 eq.	166	207	247	287	306
Freshwater eutrophicat.	g P eq.	10.1	9.55	8.97	8.39	8.09
Marine ecotoxicity	g 1.4-DB eq.	276	246	231	216	208
Natural land transform.	m^2/MWh	0.005	1.78E-02	3.07E-02	4.36E-02	5.01E-02
Water depletion	m^3/MWh	6.27	6.26	6.25	6.24	6.24
Fossil depletion	kg oil eq./MWh	9.29	41.8	74.3	107	123

used most frequently as auxiliary fuel due to its low cost, clean combustion, and rapid response. For a typical 50 MWe CSP plant like the ones operating in southern Spain, this hybrid operation involves the consumption of 2.32 108 MJ/year of auxiliary fuel and results in the generation of 22,600 MWh/year of additional electricity [9]. Compared to TES, the use of natural gas as energy backup is less capital intensive but involves significantly higher operating costs and technology risks. The greatest weakness to the use of natural gas relates to the reduced efficiencies of the thermal cycle in CSP plants (usually 30–35%), compared to 55% in modern natural gas combined cycle (NGCC) power plants.

Table 4 shows a simulation of the environmental performance of a 50 MWe CSP plant operating with increasing natural gas inputs (up to 35% of power generation). The results evidence a significant increase in the impact associated with certain environmental categories (climate change, terrestrial acidification, fossil depletion, and natural land transformation) but a reduced effect in some others (human toxicity, freshwater eutrophication, and marine ecotoxicity). This is so because the environmental burdens associated with the use of the fossil fuel are compensated with a higher power generation capacity. Despite the reduced impact on certain midpoint categories, a damage-oriented analysis evidences a significant deterioration in the environmental performance of the CSP plant as a result of increasing consumption of natural gas. This is so because of the superior magnitude and significance of the impacts related to the use of this fossil fuel, according to ReCiPe Endpoint Europe (perspective H) normalization and weighting sets [9].

Table 5 shows the environmental performance of CSP when operating with different backup fuels (including biogas, mineral coal, fuel oil, wood pellets, and residual biomass), for a total contribution of 12% of the gross power generation (as it was permitted under Spanish regulatory system) [2]. The use of backup fuels

Table 5 Environmental performance of a wet-cooled 50 MWe with 7.5 h TES parabolic trough CSP plant hybridized with different types of auxiliary fuels, contributing to 12% its power generation [14]

Environmental categories		Hybrid CSP (12% fuel)						Solar Only
		Natural gas	Coal	Fuel oil	Biogas	Wood pellets	Wheat straw	
Climate change	kg CO2 eq./MWh	124	186	159	69.7	37.8	34.3	26.6
Human toxicity	kg 1,4-DB eq./MWh	12.4	64.3	20.7	20.6	30.8	66.1	13.1
Terrestrial acidification	g SO2 eq./MWh	215	1,683	1,022	599	279	288	167
Freshwater eutrophicat.	g P eq./MWh	9.48	84.7	12.7	16.0	15.0	13.3	10.1
Marine ecotoxicity	g 1,4-DB eq./MWh	266	1,426	484	406	396	613	276
Natural land transform.	m^2/MWh	0.020	0.011	0.070	0.008	0.011	0.006	0.005
Water depletion	m^3/MWh	6.26	6.39	6.41	6.41	6.34	6.28	6.27
Fossil depletion	kg oil eq./MWh	48.4	50.7	53.0	9.4	12.5	9.5	9.30

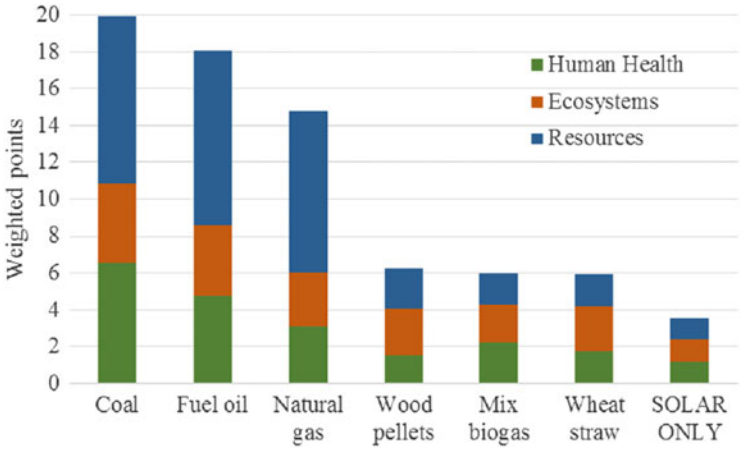

Fig. 6 Weighted profiles of a 50-MWe parabolic trough CSP plant with 7.5 h TES operating in hybrid mode (12% contribution) with different auxiliary fuels [14]

had a detrimental effect on the environmental performance of the CSP plant, which was reflected in all categories (except water depletion).

Hybridizing with natural gas resulted in higher impact values in the climate change category (124 kg CO2 eq./MWh, compared to 26.6 kg CO2 eq./MWh in solar only operation). For comparative purposes, it may be mentioned that greenhouse gas emissions of power generation from natural gas in combined cycle power plants has been reported to range between 474 and 488 kg CO2 eq./MWh [15,16]. Hybridizing with mineral coal was the most impacting alternative in nearly all environmental categories analyzed. Using biomass-derived fuels (biomass, biogas, and biomethane) was less damaging than using fossil fuels in certain categories (climate change and fossil depletion). However, the environmental performance of natural gas was superior to the renewable fuels in certain categories like human toxicity, terrestrial acidification, and freshwater eutrophication.

Figure 6 shows the aggregated environmental profiles of a CSP plant operating in hybrid mode (12% power contribution) with different auxiliary fuels, as determined using ReCiPe (H) endpoint methodology [12]. The results show a 60% increase in the environmental damage associated with the generation of electricity in a CSP plant hybridized with biomass-derived fuels. The environmental performance is worsened significantly when using fossil fuels, mainly coal.

5.2 Steam Integration in Hybrid CSP/Biomass Plants

Another strategy for hybridizing CSP with conventional fuels involves the integration of the steam cycles. In this situation, illustrated in Fig. 7, both the solar and the

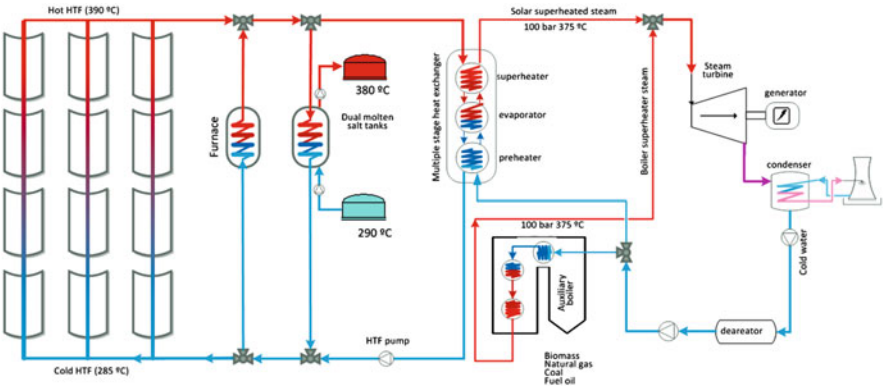

Fig. 7 Process diagram describing the integration of steam cycles in hybrid CSP plant

auxiliary systems would have the capacity to generate superheated steam independently. Hence, the auxiliary furnace operates at different capacities, depending on the solar contribution, to produce a stable steam flow and electricity output.

Despite the low thermal efficiencies of the steam cycle that operates well below nominal values during the night, this hybridization strategy leads to savings due to the shared equipment from the biomass and solar cycles. A 24% saving from the simple addition of the two standard technologies has been estimated for this hybridizing strategy. Biomass combustion plants have the highest operating costs, owing primarily to the cost of the biomass fuel and labor requirements. In contrast, operating costs in CSP plants are one fifth of biomass combustion plants, due to the free nature of the solar resource [17].

5.3 Integrated Solar Combined Cycles (ISCC)

In ISCC plants, a small solar field is associated to a conventional combined cycle (CC) plant in order to supplement power generation. As illustrated in Fig. 8, steam generated in the solar field is fed into the water/steam cycle of the conventional CC plant, thereby increasing the power of the steam turbine and the overall plant efficiency. Five commercial ISCC plants are currently operating in the world including MNG Solar Energy Center (USA) (75 MWe), Hassi R'Mel (Algeria) (25 MWe), Kuraymat (Egypt) (20 MWe), Ain Beni Mathar (Morocco) (20 MWe), and Yazd (Iran) (17 MWe) [4].

The natural gas cycle operates at full capacity continuously, while the solar field supplements the steam cycle only when solar resource is available (during the day). The maximum contribution of the solar field is limited to between 10 and 20% of

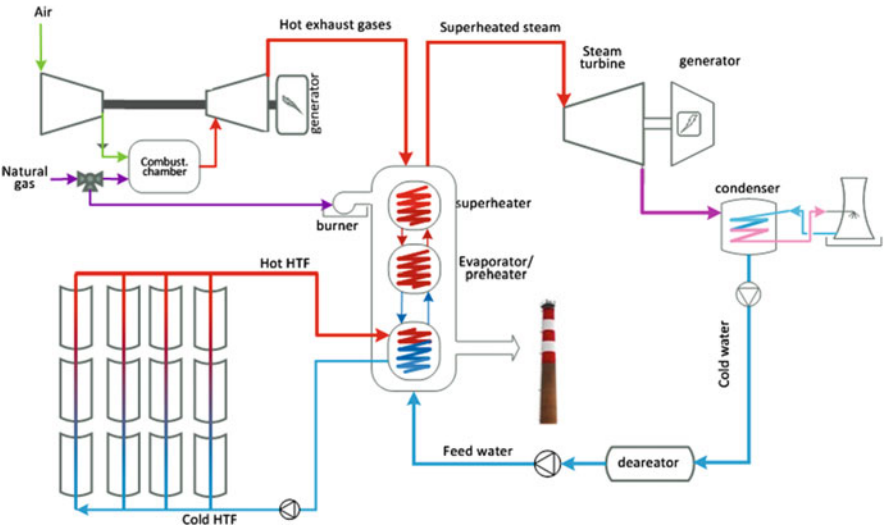

Fig. 8 Process diagram describing a commercial integrated solar combined cycle (ISCC) plant

the total capacity of the plant, as higher inputs result in reduced efficiencies in the steam turbine.[8]

5.4 Integration of Aeroderivative gas Turbines (AGT) in CSP

Hybridizing of auxiliary fuels with CSP faces two limitations: poor fuel utilization efficiency and reduced solar contribution (in the case of ISCC). These drawbacks may be overcome using aeroderivative gas turbines (AGT), instead of conventional furnaces. The gas cycle allows high efficiency in the use of auxiliary fuel, due to the recovery of energy from exhaust gases that may be used to heat the HTF or the TES. A key limitation relates to the physical state of the fuel, which needs to be in gas form.

The flexibility of the AGT allows for multiple hybrid configurations with parabolic trough CSP, some of which have been analyzed by Turchi and Ma [18,19]. AGT have a low mass compared to standard gas turbines, which allows them to heat up to nominal values of operation in a very short time (less than 10 min from cold to full load and less than 4 min from stand by to full load). Exhaust gases are generated at temperatures between 420 and 520°C, and the energy contained may be recovered using a heat exchanger. The capital cost of AGT is relatively low, compared to conventional gas turbines.

[8] Higher steam turbine capacities are not considered because, in that scenario, operation of this element during the night would be below nominal values (hence, resulting in lower efficiencies).

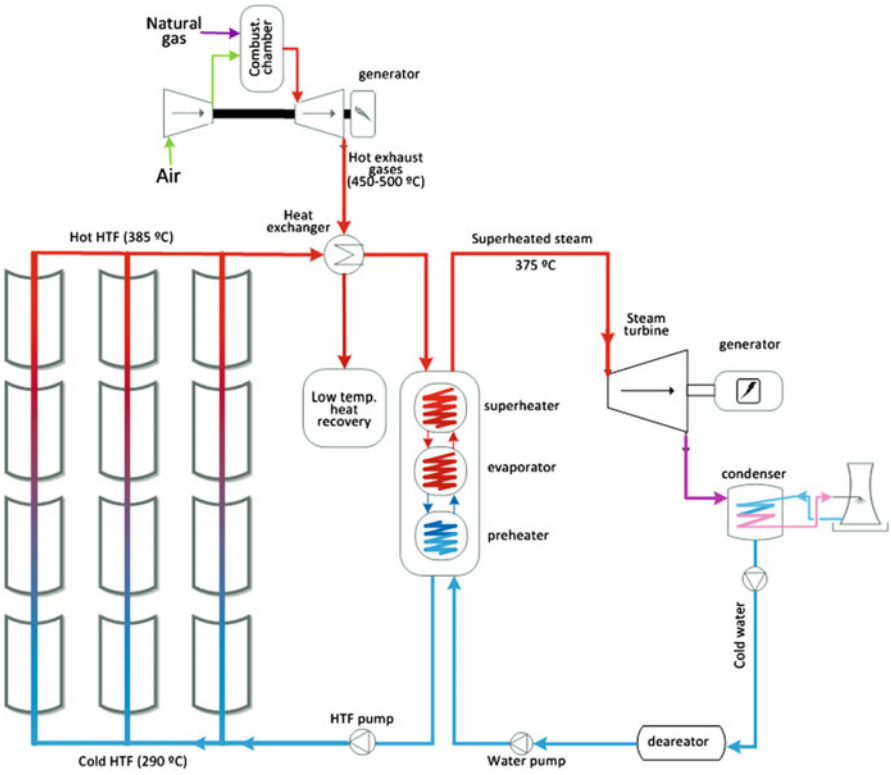

Fig. 9 Hybridization of an AGT with CSP using synthetic HTF

A simple integration of AGT into a conventional parabolic trough CSP without TES is described in Fig. 9. The exhaust gases from the gas turbine are used to heat the synthetic HTF. The gas turbine always runs at full load providing power from its own generator at high efficiency and supplying thermal energy to the solar HTF to support operation of the steam cycle during low irradiation periods. A secondary heat exchanger may be used as a feedwater economizer. Solar contribution in these systems may be greater than 50% and gas to electricity efficiencies comparable to combined cycle plants (>55%).

An advanced configuration for the integration of AGT in CSP is shown in Fig. 10. In this case, the CSP plant uses molten salts as HTF and incorporates a TES. During the day, the solar field will generate thermal energy that is stored in the TES and used for power generation. If additional power is required, the gas turbine may come into operation, producing additional electricity directly and charging storage tanks. The AGT stops when the TES system nears full capacity to maximize the efficiency of the process. This configuration may facilitate the use of molten salts as HTF because the exhaust heat from the gas turbine provides sufficient energy to maintain the salt at a temperature above its freezing point during the night [18].

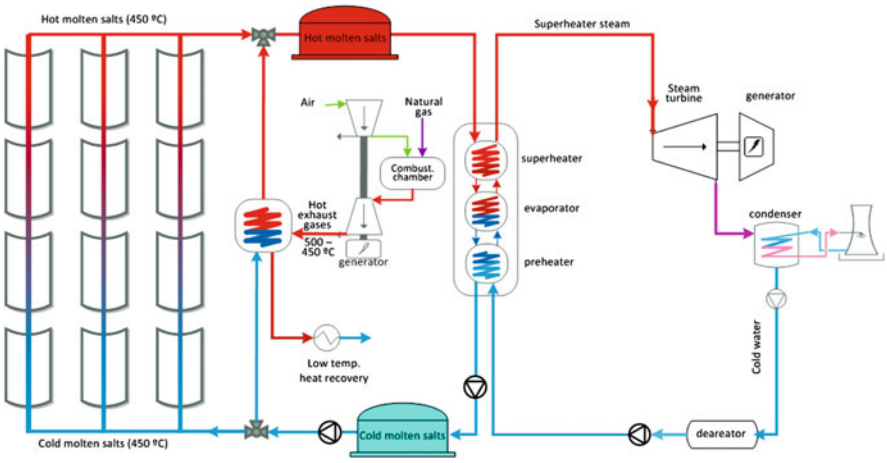

Fig. 10 Hybridization of AGT with CSP using molten salts as HTF

The auxiliary fuel may be of a fossil (natural gas) or renewable nature (biogas, biomethane, or syngas produced from the thermochemical gasification of solid biomass). A research project led by the Spanish company ACS-Cobra and funded by the European Commission (HYSOL) is currently in progress to test the technical, economic, and environmental viability of this technology. A demonstrator will be installed in a commercial CSP plant in Spain in 2014.

6 Conclusions

Concentrating solar power (CSP) has the potential to become a fundamental technology in the generation of electricity in areas of the globe with good solar resource. In its basic configuration (no backup fuels), power generation has virtually zero fuel costs and has a limited incidence on the environment. However, in the absence of public subsidies, CSP cannot compete with commercial power technologies due to the high capital costs involved. CSP technology is at its infancy, and a great deal of research and development is devising alternative configurations and operating strategies that make it more economically viable.

In its simplest form, CSP has a number of drawbacks associated with the intermittency and variable nature of the solar resource. This results in reduced capacity factors and operation flexibility. The incorporation of energy backup systems provides a solution, allowing CSP to become more dispatchable, cost effective, and easier to integrate into existing power grids. Energy backup solutions already in operation in utility-scale CSP plants include thermal energy storage (TES) based on molten salts and the use of auxiliary fuels. The latter typically

involves the incorporation of furnaces where the auxiliary fuel (usually natural gas) is combusted to provide the system with additional stability and extended operating hours. The contribution and the nature of the auxiliary fuels have a significant impact on the environmental performance of the technology, involving an increase of 60% in the environmental impact according to endpoint single score indicator. In general, using fossil fuels for hybridization involves higher environmental impacts (around three times according to the same indicator) than renewable fuels (solid biomass, biogas, or biomethane). Natural gas is notably more benign for the environment than coal or fuel oil.

Despite the benefits achieved, this strategy is criticized because of the low conversion efficiencies achieved in the thermodynamic cycles of conventional CSP plants (37%) compared to modern combined cycle technologies (50–55%). The use of aeroderivative gas turbines (AGT) allows high efficiency in the integration of auxiliary fuels into CSP (around 55% of efficiency). The auxiliary fuel employed, which needs to be in gas form, may be of fossil (natural gas) or renewable nature (biogas, biomethane, or syngas) for improved environmental performance. The use of molten salts both as heat transfer fluid (HTF) and thermal storage medium facilitates the integration and improves the efficiency of energy backup systems.

Acknowledgements Thanks are due to MINECO for funding under Program INNPACTO (IPT-440000-2010-004) and to The European Commission for funding under FP7-ENERGY-2012-1 CP 308912.

References

1. PER (2005) Plan de Energías Renovables de España 2005–2010, Spanish National Plan for Renewable Energies, Ministerio de Industria, Energía y Turismo (MINETUR). http://www.minetur.gob.es/energia/desarrollo/energiarenovable/plan/paginas/planrenovables.aspx
2. RD (2007) Real Decreto 661/2007, de 25 de mayo, por el que se regula la actividad de producción de energía eléctrica en régimen especial, Ministerio de Industria, Turismo y Comercio, BOE-A-2007-10556
3. Protermosolar (2014) Sector en cifras, Asociación Española de la Industria Solar Termoeléctrica. www.protermosolar.com. Accessed Mar 2014
4. NREL (2014) Concentrating Solar Power Projects, National Renewable Energy Laboratory (NREL). www.nrel.gov/csp/solarpaces. Accessed Mar 2014
5. IRENA (2012) Renewable energy technologies: cost analysis series, Concentrating solar power, International Renewable Energy Agency (IRENA), Vol 1. Power Sector Issue 2/5, June 2012
6. IEA (2010) International energy agency, technology road map, concentrating solar power. https://www.iea.org/publications/freepublications/publication/csp_roadmap.pdf
7. Burkhardt JJ III, Heath GA, Turchi CS (2011) Life cycle assessment of a parabolic trough concentrating solar power plant and the impacts of key design alternatives. Environ Sci Technol 45:2457–2464

8. Burkhardt JJ, Heath G, Cohen E (2012) Life cycle greenhouse gas emissions of trough and tower concentrating solar power electricity generation. J Ind Ecol 16:S93–S109
9. Corona B, San Miguel G, Cerrajero E (2014) Life cycle assessment of concentrated solar power (CSP) and the influence of hybridising with natural gas. The International Journal of Life Cycle Assessment, accepted for publication, December 2013
10. Lechon Y, de la Rua C, Saez R (2008) Life cycle environmental impacts of electricity production by solarthermal power plants in Spain. J Sol Energ-T ASME 130:021012
11. Lovegrove KK, Pye J (2012) Fundamental principles of CSP systems. In: Lovegrove K (ed) Concentrating solar power technology: principles, developments and applications. Woodhead, Cambridge
12. San Miguel G, Corona B (2014) Hybridizing concentrated solar power (CSP) with biogas and biomethane as an alternative to natural gas: analysis of environmental performance using LCA. Renew Energy 66:580–587
13. Klein SJW, Rubin ES (2013) Life cycle assessment of greenhouse gas emissions, water and land use for concentrated solar power plants with different energy backup systems. Energy Policy 63:935–950
14. Corona B, San Miguel G (2013). Life cycle assessment of a hybrid concentrated solar power plant: comparison between different fossil and renewable fuels. Proceedings of the Energy and Environment Knowledge Week, Toledo, 20–22 November
15. Odeh NA, Cockerill TT (2008) Life cycle GHG assessment of fossil fuel power plants with carbon capture and storage. Energy Policy 36:367–380
16. Kannan R, Leong KC, Osman R, Ho HK, Tso CP (2005) Gas fired combined cycle plant in Singapore: energy use, GWP and cost – a life cycle approach. Energy Conv Manag 46:2145–2157
17. Servert J, San Miguel G, López D (2011) Hybrid solar – biomass plants for power generation; technical and economic assessment. Global Nest J 13:266–276
18. Turchi CS, Ma Z (2011) Gas turbine/solar parabolic trough hybrid design using molten salt heat transfer fluid, SolarPACES 2011, Granada, Spain, September 20–23, 2011
19. Turchi CS, Ma Z (2011) Gas turbine/solar parabolic trough hybrid designs, ASME Turbo Expo 2011, Vancouver, Canada, June 6–10, 2011

Wind Power Forecast Error Probabilistic Model Using Markov Chains

S. Martín Martinez, A. Honrubia Escribano, M. Cañas Carretón, V. Guerrero Mestre, and E. Gómez Lázaro

Abstract Wind forecast is an important consideration in integrating large amounts of wind power into the electricity grid. The wind power forecast error (WPFE) distribution can have a large impact on the confidence intervals produced in wind power forecasting.

The problem of accurately wind energy forecasting has received a great deal of attention in recent years. There are always some errors associated with any forecasting methodology. It is thus necessary for the transmission system operators (TSOs) and the market participants to understand these errors. WPFE has an important role on system balance reserves calculation. As a result of the former, WPFE has an important economic impact in market costs.

In this work, WPFE statistics are examined for Spanish power system over multiple timescales. Comparisons are made between the experimental data in different years and production ranges. The shape of WPFE probability density function (PDF) is found to change significantly with the length of the forecasting timescale and with wind power production range. Additionally, error sources and magnitudes are analyzed to establish their main characteristics. Finally a Markov chain (MC) probabilistic model is constructed using these WPFE data for validation.

S. Martín Martinez (✉), A. Honrubia Escribano, M. Cañas Carretón, and E. Gómez Lázaro
Renewable Energy Research Institute and DIEEAC-EDII-AB, Universidad de Castilla-La Mancha, Albacete, 02071 Castilla-La Mancha, Spain
e-mail: sergio.martin@uclm.es; andres.honrubia@uclm.es; miguel.canas@uclm.es; emilio.gomez@uclm.es

V. Guerrero Mestre
Escuela Técnica Superior de Ingenieros Industriales, Universidad de Castilla-La Mancha, Ciudad Real, 13071 Castilla-La Mancha, Spain
e-mail: victoria.gmestre@gmail.com

G. Lefebvre et al. (eds.), *Environment, Energy and Climate Change II: Energies from New Resources and the Climate Change*, Hdb Env Chem (2016) 34: 55–70,
DOI 10.1007/698_2014_303,
Published online: 9 December 2014

Keywords Markov chain (MC), Probability distribution functions (PDF), Wind power forecast error (WPFE)

Contents

1 Introduction

Increasing the value of wind generation through the improvement of forecast systems performance, is one of the highest priorities in wind energy research needs for the coming years. The wind power forecast models are becoming a key tool used to facilitate the integration of wind power in power systems with a great amount of wind power capacity. All United States RTOs/ISOs, all European TSOs with significant wind (e.g., Germany, Denmark, Spain, Portugal, Sweden), and most provincial dispatch centers in China forecast wind power production. The use of these forecasts, however, varies considerably from region to region [1].

WPFE has become a very important parameter for reserves estimation in market schedule and power system operation [2, 3]. The biggest influence of WPFE on operational reserves is on running reserves. Running reserves consist on the available generation output capacity to increase or decrease production within a time scope shorter than the time required noticing the connection of an additional thermal unit to the network. Running reserves are allocated in manageable technologies, mainly hydro generation, hydro pumping storage, and available connected thermal units. In large wind power penetration systems, wind intermittency and uncertainty could oblige the system operator to allocate a greater spinning and supplemental energy reserves, in order to balance possible errors between programmed and actually produced wind energy in a certain time period [4]. This would increase total operation costs and, consequently, final energy prices [5]. For example, in the Spanish power system, the developing and continuously improving wind forecast, actualized with wind production in real time, allowing the achievement of more efficient restrictions and reserve markets is one of the current and future challenges associated with wind power integration [6].

Variability and uncertainty in WPF is considered as a critical parameter in large penetration wind energy power systems, and its specifications are strongly dependent on wind power clustering and current scenarios, as described in [7]. According

to these facts, WPFE continues registering high values and generates associated issues in combination with different events [8]. In spite of the fact that wind forecast models have been improved, in both short and long term, a considerable amount of error is still registered in custom conditions, reaching higher values at extreme conditions [9]. Additionally, wind power presents different prevailing dynamics when it is analyzed for a few milliseconds, for several minutes, or for a daily horizon.

Originally, wind power forecast error was assumed to have a near Gaussian distribution. A simple analysis of real data demonstrates that this assumption is not correct in most of the cases. In the scientific literature, several works about wind power forecast error distributions can be found. The errors are often assumed to follow a normal distribution [10–13], though Weibull [14], Beta [15], and Cauchy [16] distributions have also been utilized. In [17], the distribution of wind power forecast errors is studied for different timescales between 6 and 48 h ahead with a particular focus on the additional errors created from converting wind speed forecasts created by numerical weather prediction to wind power output. The study demonstrates that while the numerical weather prediction errors are well represented by a Gaussian curve, the power forecast error distributions exhibit both skewness and excess kurtosis. In [18], the smoothing of forecast errors for multiple wind farms is shown at timescales from 6 to 48 h ahead. In [19], variable kurtosis values between different timescales (with a minimum of 10 min averaged output data) were measured, and the error distributions were modeled using a beta function. This function was then applied to the sizing of an energy storage system that will act to smooth wind power output. In [20], The Cauchy distribution was proposed as a means of representing the forecast error distributions and was compared with some of the other distributions. Additionally, WPFE has been studied using the Pearson system to establish the optimum PDF type for different production ranges [21].

A lot of different methods have been developed for wind speed and power forecast modeling and estimation [22]. Wind power forecast as a dynamic system that involves meteorology is inevitably large and complex, mainly due to their interactions with numerous subsystems. Since exact or closed-form solutions to such large systems are difficult to obtain and they would require extensive measures, one often has to be contented with approximate solutions. Because the precise mathematical models are difficult to establish, near-optimal controls often become a viable and sometimes the only alternative. Such near optimality requires much less computational effort and often results in more robust policy to attenuate unwanted disturbances. Markov chains collect these conditions and have been proposed as an acceptable method to model the stochastic behavior and to reproduce synthetically WPFE, according with its superior theoretical properties for stochastic dynamics [23, 24].

Markov chain concerns about a sequence of random variables. This sequence corresponds to the states of a certain system, in such a way that the state at one period depends only on the previous state period. Based on these characteristics, one of the main advantages of using Markovian models is that they are general

enough to capture the dominant factors of system uncertainty and, in the meantime, it is mathematically tractable [25].

Markov chains have been used in modeling physical, biological, social, and engineering systems such as population dynamics, queuing networks, and manufacturing systems. Traditionally, Markov chains have been applied in electrical engineering for the study of queues and power system reliability given rate of failure and reposition times of its components. In Markov chain Monte Carlo (MCMC) simulations, Markov chains are employed as random number generators with particular characteristics [26].

In meteorology, Markov-switching models are often used to estimate an unobservable climate state which ideally governs other climate variables. For wind energy, Markov chain models have been largely used for generating synthetic wind speed and wind power time series [27, 28], providing simulation results that usually offer excellent fit for both the probability density function and the autocorrelation function of the generated wind power time series.

Considering previous contributions, in the present work, the Spanish power system WPFE data is analyzed to establish their main statistic parameters. WPFE as a function of the power generation range is exhaustively discussed. Then, a probabilistic Markov chain method is developed based on described data. This model is used in order to estimate their ability to reproduce long series of hourly WPFE data.

The structure of the chapter is summarized as follows. In Sect. 2, we introduce the WPFE data used throughout this paper and discuss some general, and particular to the Spanish power system, characteristics relevant to these data. In Sect. 3, we build the Markov chain model, which allows for value considerations for the temporal evolution of the process, remarking and justifying the election of states and associating sequences with the kind of errors described in Sect. 2. Section 4 justifies and explains the results for the first-order Markov chain model implemented for the WPFE, while Sect. 5 considers the conclusions extracted from the model development and results obtained.

2 Wind Power Forecast Error Characteristics and Data Analyzed

In this work, we followed the convention that the error (e_{wpf}) is equal to the actual (P_{wpa}) wind power value minus the forecast (P_{wpf}) value.

$$e_{\mathrm{wpf}} = P_{\mathrm{wpa}} - P_{\mathrm{wpf}}. \tag{1}$$

According to Eq. (1), when actual wind power is higher than the forecasted value, the calculated error is positive, and independently from other system parameters, downward reserves are needed; otherwise, WPFE is calculated as a negative value, and upward reserves are activated.

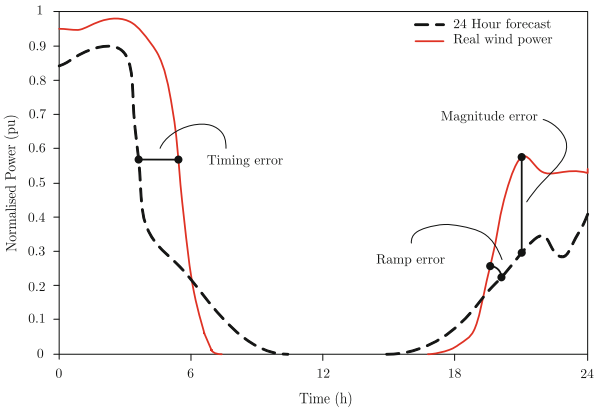

Fig. 1 Comparison between wind power forecast and real production: sources of error

To address the challenges in FE, it is important to understand the three main sources of error in accurately identifying a wind ramp:

- A timing error is defined as an event that it is accurately predicted in magnitude, but occurs at the wrong time. This kind of error can achieve a considerable absolute error even when event magnitude has been correctly forecasted. This type of error is usually corrected for short-term forecast as event is progressively discovered.
- A magnitude error is defined as an event that is forecasted to occur approximately at the right time, but with the wrong magnitude. This can occur in two possible ways: the forecast might be in error about the rate of change or might be in error regarding the overall magnitude of the event.
- A ramp error consists on a ramp event that is forecasted with a different rate of change. This kind of error drives forecast to considerable magnitude errors when wind power reaches maximum values.

Figure 1 shows a comparison between forecasted and real wind power highlighting different examples for the three sources of error previously described. Timing and ramp errors are usually associated with wind power events, like extreme ramps caused by storms or wind power curtailment, while magnitude error is generally a consequence of timing and ramp errors.

2.1 WPFE Data

In this section we describe the database of real data used for the analysis. Data used for the validation of the method selected consist of hourly WPFE measured for the Spanish power system: 1, 6, 12, and 24 h. Additionally, hourly wind power generation values are also used to characterize WPFE in every production range. WPFE values are represented in MW, while production range is represented as per

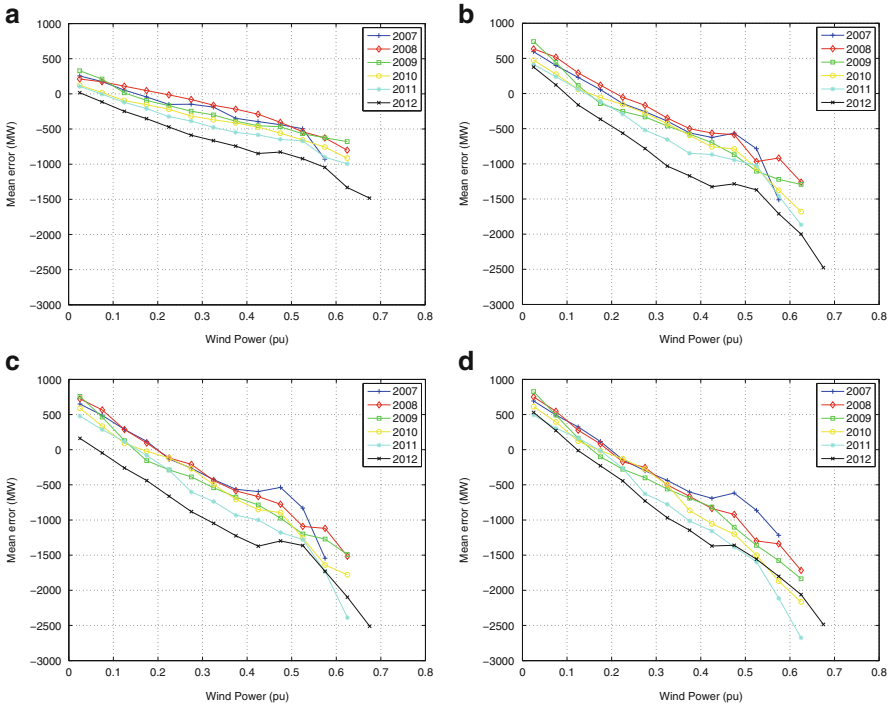

Fig. 2 Mean FE depending on wind power level. (**a**) using 1 h-ahead forecast, (**b**) using 6 h-ahead forecast, (**c**) using 12 h-ahead forecast, (**d**) using 24 h-ahead forecast

unit calculated from total wind power capacity for every year in the Spanish power system. In data filtering, proposed bins with less than 50 data are not shown as it is considered that no relevant information is extracted.

Figure 2 shows mean FE depending on wind power level for the last years using 1 (a), 6 (b), 12 (c), and 24 (d) hour step forecast. Mean error trend decreases almost linearly as wind power increases. Positive mean values are described for low generation bins, reaching zero mean value about 0.1–0.2 pu range. For the rest of the bins, negative means values are shown. The mean error trend is marked by a continuous decrease as production range increases, reaching important negative values around −2,500 MW.

Figure 3 shows the mean and standard deviation for FE depending on wind power level for the last years using 1 (a), 6 (b), 12 (c), and 24 (d) hour step forecast. For standard deviation, there are three ranges to highlight. In the first range, from 0 to 0.2 pu, standard deviation and dispersion are increased in line with wind power increase. These results are very similar independently from the studied year. In the second range, covering medium power bin values, standard deviation values stabilize and are almost constant. Results are similar considering the same time horizon, in a similar way to the first range. Finally standard deviation decreases at high

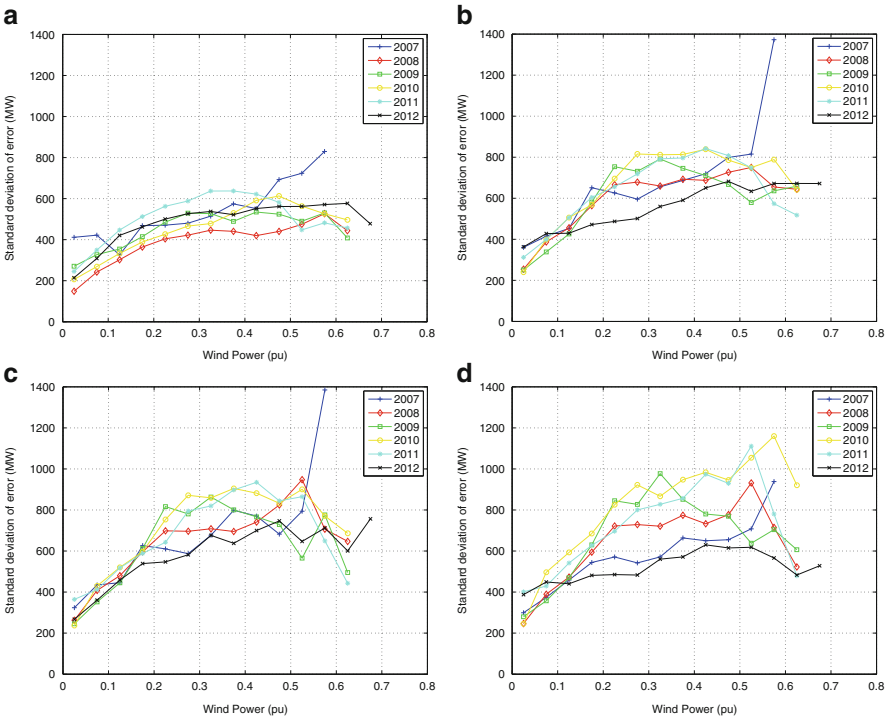

Fig. 3 Standard deviation FE depending on wind power level. (**a**) using 1 h-ahead forecast, (**b**) using 6 h-ahead forecast, (**c**) using 12 h-ahead forecast, (**d**) using 24 h-ahead forecast

power bin values for most of the years. In this range, standard deviation values have important changes between years as extreme events, and bins with few data make condition of these results.

3 Proposed Probabilistic Markov Chain Model

In order to represent the variability of WPFE, a discrete first-order Markov chain has been selected. The use of a first-order chain offers a basic overview of the dominant factors of WPFE without an important complexity increase. In contrast, the use of a second-order Markov chain implies that the number of parameters we need to estimate grows exponentially with the order. Moreover, in Markov chains, the higher the order, the less reliable our parameter estimates are expected.

For this proposed Markov chain model, the sequence of WPFE changes between proposed periods. These series are considered as an observed data sequence$\{X(n)\}$.

The transition frequency F_{ij} in the sequence could be established by counting the number of transitions from state i to state k in one step. Then, the one-step transition matrix can be constructed for the sequence $\{X(n)\}$ as follows:

$$F = \begin{bmatrix} F_{11} & \cdots & F_{1m} \\ \vdots & \ddots & \vdots \\ F_{n1} & \cdots & F_{nm} \end{bmatrix}. \tag{2}$$

This transition frequency offers a vision of the probability of a determined change over the total changes in the whole sequence.

From matrix F, one can get the estimates for P_{ij} as follows:

$$P = \begin{bmatrix} P_{11} & \cdots & P_{1m} \\ \vdots & \ddots & \vdots \\ P_{n1} & \cdots & P_{nm} \end{bmatrix}. \tag{3}$$

The probability P_{ij} represents the probability that the process will make a transition to state i given that currently the process is state j. The probability is calculated in Eq. (4), where

$$P_{ij} = \begin{cases} \dfrac{F_{ij}}{\sum_{i=1}^{m} F_{ij}} \text{ if } \sum_{i=1}^{m} F_{ij} > 0 \\ 0 \text{ if } \sum_{i=1}^{m} F_{ij} = 0 \end{cases}. \tag{4}$$

The matrix containing P_{ij}, the transition probabilities, is called the one-step transition probability matrix of the process.

For an additional analysis for error trend and timing and ramp error identification, $P^{(k)}{}_{ij}$ is defined to be the probability that a process in state j will be in state i after k additional transitions. In particular $P^{(1)}{}_{ij} = P_{ij}$ would be considered the probability of change between state i and state j for an hour ahead. $P^{(k)}{}_{ij}$ is also considered for 4, 6, and 12 h-ahead change to represent the trend of error evolution in different scales.

3.1 State Selection

In this proposed methodology, each Markov state can be seen as a case that characterizes a typical operational mode in power system according with WPFE as an isolated parameter. Full reserves, no reserves, and partial reserves are candidates for Markov states. If partial reserves operation near full reserves is notably different from partial reserves operation near no reserves, they should be considered as distinct Markov states. Furthermore, upward and downward reserves must be considered.

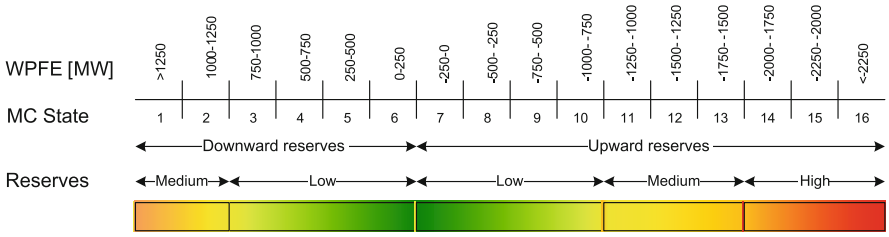

Fig 4 Markov chain states selected for WPFE probabilistic model

According to reserves characteristics, 16 WPFE states have been established. These Markov chain states have been properly classified taking bins for every 250 MW of WPFE scale. Additionally, a state for extreme positive errors (>1,250 MW) and a state for extreme negative errors (<−2,250 MW) are considered. The use of different states allows using a full model of the reserves operation, and the state weighting describes intermediate cases reducing the required number of states. The bins have been configured with the same size to improve the analysis and the interpolation between cases, as the combination of matrix algebra and state probability implies the linear interpolation between the centroids of the states for describing intermediate cases.

In Fig. 4, a discretization with the scheme of selected states arrangement is shown. This discretization of states indicates the possible transitions from a state to another one and the error level in every state. The relationship of these errors with reserves direction and magnitude is also represented, for both, downward and upward. Two reserve levels are included for downward reserves – a low level including 3–6 states and a medium level including 1 and 2 states. Three reserve levels are included for upward reserves – a low level including 7–10 intermediate states, a medium level including 11 to 13 states, and a high level including 14 to 16 states.

Figure 4 is an election of the classifying error including extreme states representing events with a high level of WPFE, both negative and positive. This is crucial when classifying data according with available reserves and power system operation. Because of this, a special attention is focused in these events caused by high WPFE level.

The transition matrix and the probability matrix dimension are 16×16 states according with the number of states. The order of proposed changes between states is established by the order proposed in Fig. 4.

3.2 Results

This section includes the results of the proposed model and their comparison with different timescales and additional transitions. To check the results of proposed Markov chain, several transition matrices and probability matrices representations

are displayed. These figures show a comparison of the behavior of real data performed by WPFE in the Spanish power system. The main tool for the analysis is the heat maps which represent a color tone for every calculated transition number or probability.

To extend the results comparison, a transition matrix $F^{(k)}$ and a probability matrix $P^{(k)}$ have been defined to be the probability that a process in state j will be in state i after k additional transitions. The transition matrix indicates the trends of change from every state i, highlighting the main changes. In contrast, the probability matrix shows the comparison of all transition independently from the initial state. 1, 4, 6, and 12 h-ahead transitions have been considered for change to represent the trend of error evolution in different scales.

The proposed data is used for first-order Markov chain modeling according to the methods and the characteristics previously described.

3.2.1 Transition Matrix

The first step in the analysis includes the transition matrix $F^{(k)}$ study. In Fig. 5, transition matrices using 1 h-ahead forecast for different time-ahead transitions are

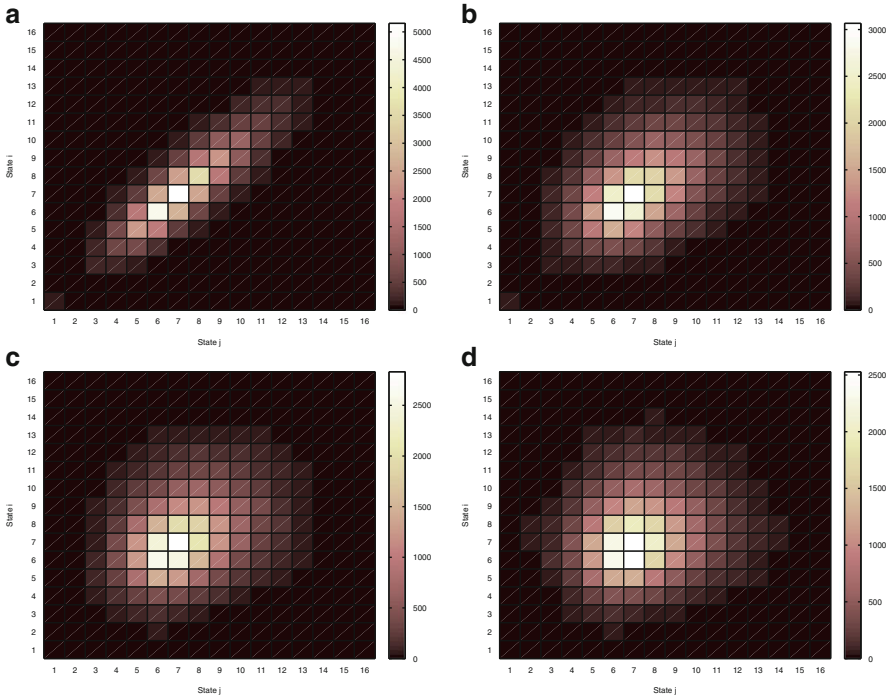

Fig. 5 Transition matrix values for 1 h-ahead forecast error with (**a**) 1 h transition $k = 1$, (**b**) 4 h transition $k = 4$, (**c**) 6 h transition $k = 6$, (**d**) 12 h transition $k = 12$

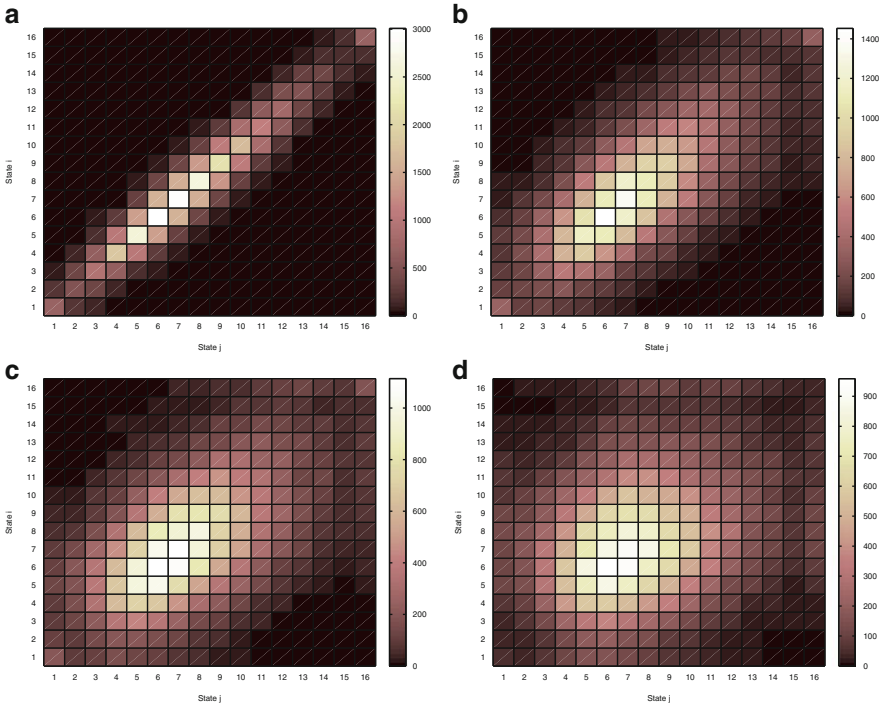

Fig. 6 Transition matrix values for 12 h-ahead forecast error with (**a**) 1 h transition $k = 1$, (**b**) 4 h transition $k = 4$, (**c**) 6 h transition $k = 6$, (**d**) 12 h transition $k = 12$

depicted. When a 1 h-ahead transition is evaluated (Fig. 5a), the majority of changes between states are performed between adjacent states, and the changes are concentrated in medium and especially low WPFE states because of the reduced WPFE for 1 h-ahead forecast. As time-ahead transition is increased, the repeatability of transitions is spread over more distanced states. In Fig. 5b ($F^{(4)}$) an important expansion in state change is observed compared with Fig. 5a, as a sequence of WPFE events are included when 6 h-ahead transitions are considered. This expansion is continued in 6 and 12 h-ahead transitions as shown in Fig. 5c ($F^{(6)}$) and Fig. 5d ($F^{(12)}$).

When the time ahead for the forecast is increased, the WPFE usually rises considerably. This WPFE increase could be appreciated in the transition matrix analysis if 12 h-ahead forecast is considered, as depicted in Fig. 6. For Fig. 6a, the quantified changes to high and extreme WPFE states are considerably higher than in Fig. 5a due to the decrease of forecast accuracy. In contrast, for most of the cases, the changes cover the low and medium states. Furthermore, the level of spreading between state changes is similar as represented with 1 h-ahead forecast.

In the cases of 4, 6, and 12 h-ahead transition (Fig. 6b–d, respectively), there is an important amount of changes with initial, final, or both states situated in high and extreme WPFE states.

3.2.2 Probability Matrix

In a similar way to the previous section for the transition matrix, the probability matrix is studied in this section. In contrast with the transition matrix, the elements of the probability matrix only cover the frequency of change leaving a determined state. For a correct comparison between different time-ahead forecasts, 6 and 24 h-ahead forecast WPFE data have been selected. The results for proposed time-ahead transition lags are shown in Figs. 7 and 8.

In Fig. 7, probability matrices using 6 h-ahead forecast for different 1, 4, 6, and 12 h-ahead changes are depicted. Each time lag transition is related with a matrix ($P^{(1)}$, $P^{(4)}$, $P^{(6)}$, and $P^{(12)}$). The spreading effect shown for the transition matrix is also presented and accentuated in the probability matrix for all the examples proposed.

For $P^{(1)}$ and $P^{(4)}$, there is a persistence in extreme WPFE states as the probability of remain in state 16 and state 1 is very high. This probability is reduced when the time-ahead transition is increased as shown in Fig. 7c and especially in Fig. 7d. To sum up, when the transition time is increased, the trend of WPFE tends to link more distant states.

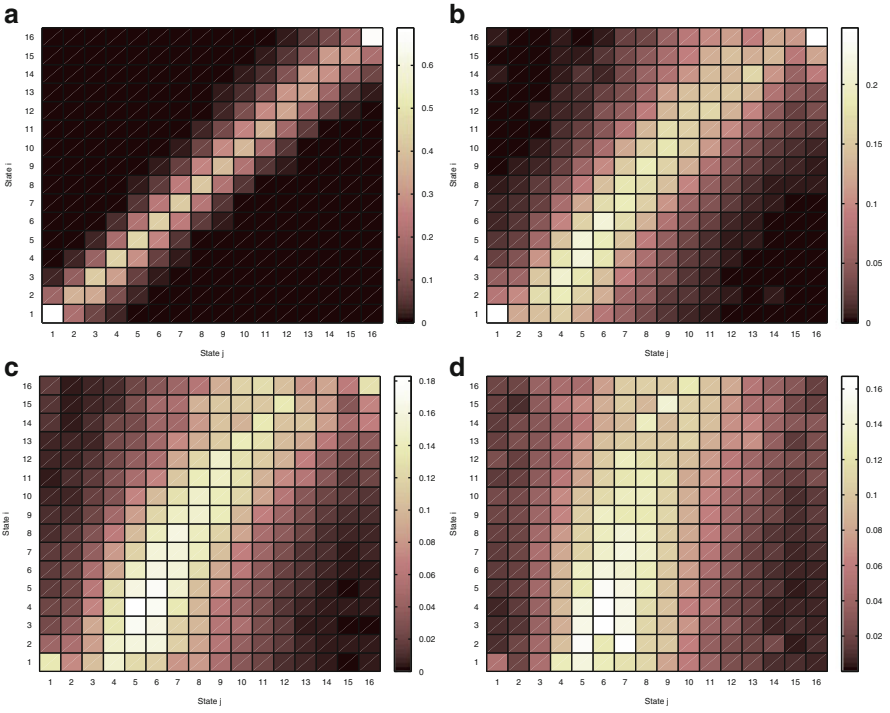

Fig. 7 Probability matrix values for 6 h-ahead forecast error with (**a**) 1 h transition $k = 1$, (**b**) 4 h transition $k = 4$, (**c**) 6 h transition $k = 6$, (**d**) 12 h transition $k = 12$

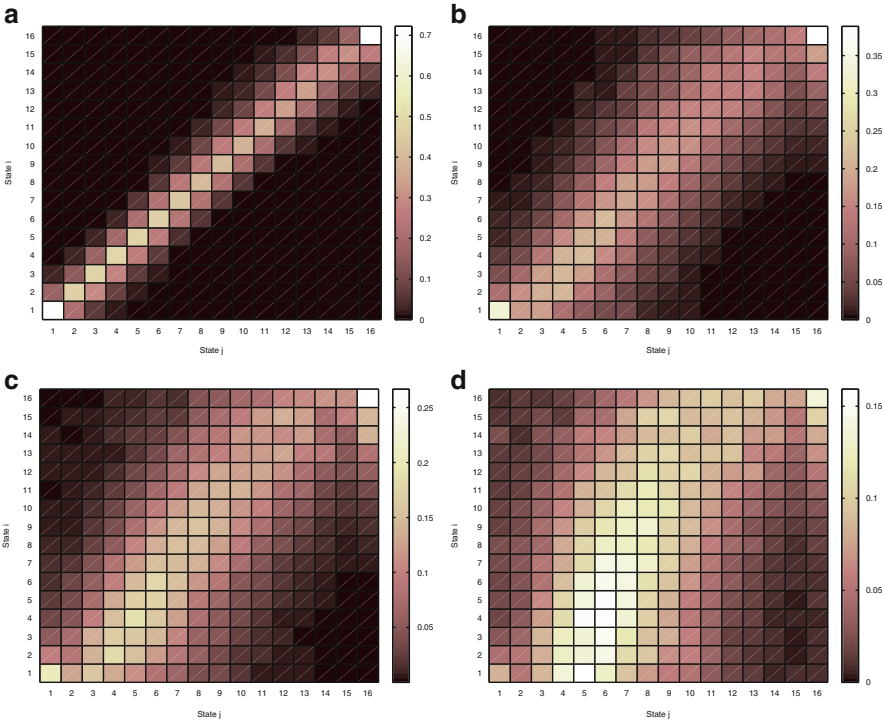

Fig. 8 Probability matrix values for 24 h-ahead forecast error with (**a**) 1 h transition $k = 1$, (**b**) 4 h transition $k = 4$, (**c**) 6 h transition $k = 6$, (**d**) 12 h transition $k = 12$

In Fig. 8, probability matrices using 24 h-ahead forecast for the same, 1, 4, 6, and 12 h-ahead changes are shown in order to be compared with the ones obtained in Fig. 7. As 24 h-ahead forecast implies an important level of error, changes to and from extreme states are more usual. The increment of transition time lag involves the heterogeneity of probability matrix values increasing the values out of the surroundings of the main diagonal. As a clear example, Fig. 8d shows the probability rise between distanced states, when a $P^{(12)}$ for 24 h ahead is considered.

Finally, to complement the previous analysis, an additional representation of types of error in the probability and transition matrices is proposed. Figure 9 indicates an example of sequence transition for a proposed change between states highlighting possible sequences related with the three main sources of error described in Sect. 2. In this example the initial state is state 10. When the next state is a superior state – less WPFE error – a negative ramp error is identified as the error source. In contrast, the error source is a positive ramp error when the next state is a state with more WPFE error – <10. If the sequence remains in the same case, this condition may be caused by two possibilities: a timing error and a constant magnitude error.

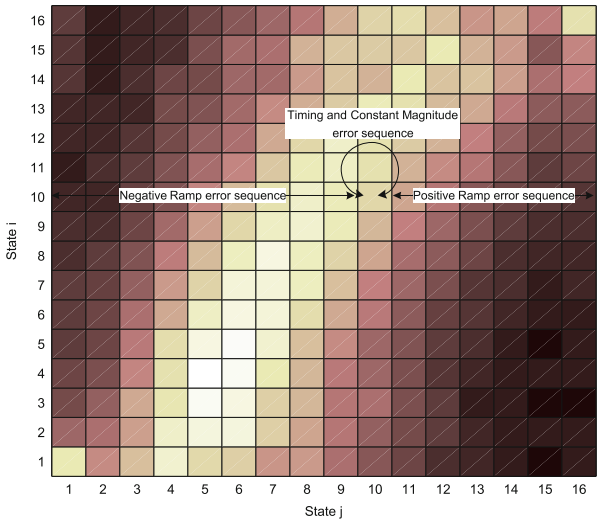

Fig. 9 Example of sequence transition for the three different types of WPFE described in Sect. 2 compared with proposed states and probability matrix

4 Conclusions

This chapter, based on real measurements, contributes to a better knowledge of the probabilistic characteristics of the WPFE, which is the main parameter related to the reserves dispatched in power systems with great amounts of wind power capacity installed.

Wind power FE calculation has been established, and their sources have been identified and characterized. Then, the main statistical parameters of WPFE probability distributions have been analyzed according to the production range when error occurs accounting their parameters for every bin from 0 to 1 pu with a period of 0.05 pu. Relevant results have been found by analyzing the relationships of mean and standard deviation of measured forecast error depending on wind power level. These relationships could be used to establish a model in order to calculate power system reserves to face wind power FE. This analysis is performed using a great amount of real wind power and forecast data measured in the Spanish wind power system during the last years.

Finally, a probabilistic Markov chain model is implemented for FE evaluation, obtaining its trend and residual variability. Different cases have been suggested using several time lag forecasts and time lag transitions. Probability and transition matrices have been calculated for every case. The results obtained indicate some properties of WPFE in different timescales and sequences.

Acknowledgments This work was supported by the Ministerio de Economía y Competitividad (Spain) through the Research Project Ref. ENE2012-34603, a project cofinanced with FEDER funds.

References

1. Cochran J, Miller M, Milligan M, Ela E, Arent D, Bloom A, Futch M, Kiviluoma J, Holtinnen H, Orths A, Gómez-Lázaro E, Martín-Martínez S, Kukoda S, Garcia G, Mikkelsen KM, Yongqiang Z, Sandholt K (2013) Market evolution: wholesale electricity market design for 21st century power systems. National Renewable Energy Laboratory, IBM, VTT Technical Research Centre of Finland, Energinet.dk, Universidad de Castilla La Mancha, International Copper Association, Global Green Growth Institute, China National Renewable Energy Center, pp 1–57
2. Gil A, de la Torre M, Domínguez T, Rivas R (2010) Influence of wind energy forecast in deterministic and probabilistic sizing of reserves. In: Ninth international workshop on large-scale integration of wind power into power systems as well as on transmission networks for offshore wind plants. Quebec
3. Holtinnen H, Milligan M, Ela E, Menemenlis N, Dobschinski J, Rawn B, Bessa RJ, Flynn D, Gómez-Lázaro E, Detlefsen N (2012) Methodologies to determine operating reserves due to increased wind power. IEEE Trans Sustainable Energy 3(4):713–723
4. Martin-Martinez S, Vigueras-Rodriguez A, Gómez-Lázaro E, Molina-Garcia A, Muljadi E, Milligan M (2012) Operation of power systems with large amounts of wind power: a view from the Spanish case. Advances in wind power. Intech, Croatia
5. Fabbri A, Gomez San Roman T, Rivier Abbad J, Mendez Quezada V (2005) Assessment of the cost associated with wind generation prediction errors in a liberalized electricity market. IEEE Trans Power Syst 20
6. Rodríguez García JM, Alonso García O, de la Torre Rodríguez M (2008) Wind power integration experience in spain. In: Wind power in power systems, 2nd edn. Wiley, Chichester, pp 595–622
7. Zhang J, Hodge BM, Gomez-Lázaro E, Lovholm AL, Berge E, Miettinen J, Holttinen H, Cutululis N, Litong-Palima M, Sorensen P, Dobschinski J (2013) Analysis of variability and uncertainty in wind power forecasting: an international comparison. In 12th international workshop on large-scale integration of wind power into power systems as well as on transmission networks for offshore wind power plants, Energynautics. London, England
8. Martin-Martinez S, Gómez-Lázaro E, Molina-Garcia A, Vigueras-Rodriguez A, Milligan M, Muljadi E (2012) Participation of wind power plants in the Spanish power system during events. In: Power and energy society general meeting, 2012 IEEE. IEEE, pp 1–8
9. Costa A, Crespo A, Navarro J, Lizcano G, Madsen H, Feitosa E (2008) A review on the young history of the wind power short-term prediction. Renew Sust Energ Rev 12(6):1725–1744
10. Methaprayoon K, Lee WJ, Yingvivatanapong C, Liao J (2005) An integration of ANN wind power estimation into UC considering the forecasting uncertainty. In: IEEE industrial and commercial power systems technical conference. Saratoga Springs, New York
11. Pappala V, Erlich I, Rohrig K, Dobschinski J (2009) A stochastic model for the optimal operation of a wind-thermal power system. IEEE Trans Power Syst 24:940–950
12. Castronuovo E, Lopes J (2004) On the optimization of the daily operation of a wind-hydro power plant. IEEE Trans Power Syst 19:1599–1606
13. Doherty R, O'Malley M (2005) A new approach to quantify reserve demand in systems with significant installed wind capacity. IEEE Trans Power Syst 20:587–595
14. Dietrich K, Latorre J, Olmos L, Ramos A, Perez-Arriaga I (2009) Stochastic unit commitment considering uncertain wind production in an isolated system. In: 4th conference on energy economics and technology. Technische Universität of Dresden, Dresden, Germany
15. Bludzuweit H, Dominguez-Navarro JA, Llombart A (2008) Statistical analysis of wind power forecast error. IEEE Trans Power Syst 23:983–991
16. Lange M (2005) On the uncertainty of wind power predictions - analysis of the forecast accuracy and statistical distribution of errors. J Sol Energy Eng 127:177–184

17. Focken U, Lange M, Monnich K, Waldl HP, Beyer H, Luig A (2002) Short-term prediction of the aggregated power output of wind farms - a statistical analysis of the reduction of the prediction error by spatial smoothing effects. J Wind Eng Ind Aerodyn 90:231–246
18. Hodge BM, Milligan M (2011) Wind power forecasting error distributions over multiple timescales, power and energy society general meeting. IEEE
19. Soman SS, Zareipour H, Malik O, Mandal P (2010) A review of wind power and wind speed forecasting methods with different time horizons. In: North American power symposium (NAPS), 2010. IEEE, pp 1–8
20. Trombe PJ, Pinson P, Madsen H (2012) A general probabilistic forecasting framework for offshore wind power fluctuations. Energies 5(3):621–657
21. Martin-Martinez S, Honrubia-Escribano A, Cañas-Carretón M, Gómez-Lázaro E, Molina-Garcia A (2014) Wind power forecast error probability distribution function using Pearson system for different timescales. EWEA Annual Event, Barcelona, Spain
22. Mur-Amada J, Bayod-Rújula AA (2007) Wind power variability model part I-foundations. In: 9th international conference on electrical power quality and utilisation, 2007 (EPQU 2007). IEEE. Barcelona, Spain, pp 1–6
23. Ching WK, Huang X, Ng MK, Siu TK (2013) Markov chains: models, algorithms and applications, vol 189. Springer, New York
24. Carpinone A, Langella R, Testa A, Giorgio M (2010) Very short-term probabilistic wind power forecasting based on Markov chain models. In: IEEE 11th international conference on probabilistic methods applied to power systems (PMAPS). IEEE, pp 107–112
25. Ross SM (2009) Introduction to probability and statistics for engineers and scientists. Academic, Oxford, UK
26. Shamshad A, Bawadi MA, Wan Hussin WMA, Majid TA, Sanusi SAM (2005) First and second order Markov chain models for synthetic generation of wind speed time series. Energy 30(5):693–708
27. Nfaoui H, Essiarab H, Sayigh AAM (2004) A stochastic Markov chain model for simulating wind speed time series at Tangiers. Renew Energy 29:1407–1418
28. Sahin AD, Sen Z (2001) First-order Markov chain approach to wind speed modelling. J Wind Eng Ind Aerodyn 89(3–4):263–269

Part II
Energy Storage

Energy Storage Integration with Renewable Energies: The Case of Concentration Photovoltaic Systems

Carlos de la Cruz, Mónica Baptista Lema, Xavier del Toro García, and Pedro Roncero-Sánchez

Abstract The integration of energy storage in electrical transmission and distribution grids is seen as the solution to secure the continuous supply of energy and increase stability and efficiency. The increasing presence of renewable energy sources with an intermittent and unpredictable behavior is threatening the balance between generation and demand that allows the stable operation of electrical power systems. Energy storage is the enabling technology to achieve the decoupling of generation and demand required to increase the share of renewable energies in the generation mix. The first part of this chapter presents the existing energy storage technologies, describing their main features and fields of application. In a second part, the particular case of concentration photovoltaic generation systems and their combination with a hybrid storage solution based on the integration of lead–acid batteries and ultracapacitors is presented.

Keywords Battery • Concentration photovoltaic (CPV) system • DC–DC converter • Energy storage system • Ultracapacitor

Contents

C. de la Cruz, M. Baptista Lema, X. del Toro García, and P. Roncero-Sánchez (✉)
School of Industrial Engineering, University of Castilla-La Mancha. Campus universitario s/n, 13071 Ciudad Real, Spain
e-mail: cdelacruzr85@gmail.com; mbaptistalema@gmail.com; Xavier.deltoro@uclm.es; Pedro.Roncero@uclm.es

G. Lefebvre et al. (eds.), *Environment, Energy and Climate Change II: Energies from New Resources and the Climate Change*, Hdb Env Chem (2016) 34: 73–94,
DOI 10.1007/698_2014_289,
Published online: 18 December 2014

1 Introduction

There is a wide variety of energy storage systems, some of them have been used for more than two centuries, as in the first electric cars dated from 1830, which already used non-rechargeable batteries. However, it can be said that in the overall, the high cost of storage, higher in several orders of magnitude in €/kWh than the cost of generation, has so far deprived further development of these technologies.

Energy storage systems differ from each other in several aspects such as their physical operating principle, geographical restrictions, power level, amount of stored energy, modularity, portability, efficiency, etc., but a certain set of features is sought in any technological solution, comprising:

- High energy density (energy stored per volume or mass unit)
- High power density (power that can be delivered per unit volume or mass)
- Highly efficient charge–discharge cycle (round-trip efficiency)
- Low internal losses (self-discharge)
- Long life (often expressed as charge–discharge cycles)
- Low cost (associated with the availability of materials and manufacturing process)
- Simple integration (especially those with an electrical nature, since they have no moving parts and the converting steps are reduced, leading to a decrease in losses)
- No geographic restrictions
- High reliability
- Environmentally friendly materials and manufacturing processes

The main role of the energy storage systems in electrical power systems is to decouple power generation from the consumption of energy with the aim that its operation becomes as independent as possible, balancing energy flows and providing ancillary services.

The balancing of energy flows allows variations in the consumption profile independently of the electrical power generation. In the consumption off-peak periods of time, storage systems can store the excess of generated energy that can then be released during peak times. This often allows a better use of transport and distribution infrastructures which tend to be oversized to respond at the instants of maximum consumption. In a similar way, storage systems can support generation systems responding to fast increases in consumption (peak shaving) or transients in which large generation systems are connected and disconnected (bridging power). For this kind of operation, storage systems with high power and the capability to

store large amounts of energy are required, such as in the case of pumped-storage hydropower or large facilities of stationary batteries.

These features are also of great interest in the field of renewable energies, due to its intermittent nature that leads to poor dispatchability. Furthermore, energy storage could provide the necessary energy reserves to avoid incurring in penalties for not reaching energy levels established by predictions [1].

The provision of ancillary services refers to the requirements and functionalities demanded by the network operator to maintain the stability, reliability, and power quality in electrical power systems. The increasing use of renewable energy sources, such as wind and photovoltaics in the energy mix, will gradually lead to extra requirements and services to be provided by these types of generation through the definition of more demanding grid codes. The term ancillary services comprises the regulation of active and reactive power; power factor compensation; voltage and frequency control; fault ride-through, as in the cases of voltage dips; and improving power quality. In contrast to the balancing function of energy flows, ancillary services only require that the storage system deliver energy for very short periods of time, hence reducing the required energy. On the other hand, the ability to deliver high power with very low response time becomes essential. These characteristics make it particularly suitable to use certain emerging technologies such as flywheels or ultracapacitors. Finally, it is important to note that the economic viability of these solutions largely depends on the added value provided, which is closely related to the existing network operation requirements defined in the grid codes.

This chapter is divided into two main sections. The first section is a review of the existing energy storage solutions in use nowadays, including the most mature and widely spread solutions and new emerging technologies. The various technologies are classified according to their principle of operation, and their main features and fields of application are discussed. In the second section of the chapter, the particular case of a concentration photovoltaic (CPV) generation systems is analyzed, and a storage solution adapted to this type of generation system is proposed.

2 Energy Storage Technologies in Use

The use of energy storage technologies for renewable energies arises from the need of matching generation and consumption in order to ensure the stability of the electrical power supply, as previously explained. This section provides a brief description of the state of the art in energy storage technologies. The existing solutions are classified according to their operating principle, as shown in Fig. 1.

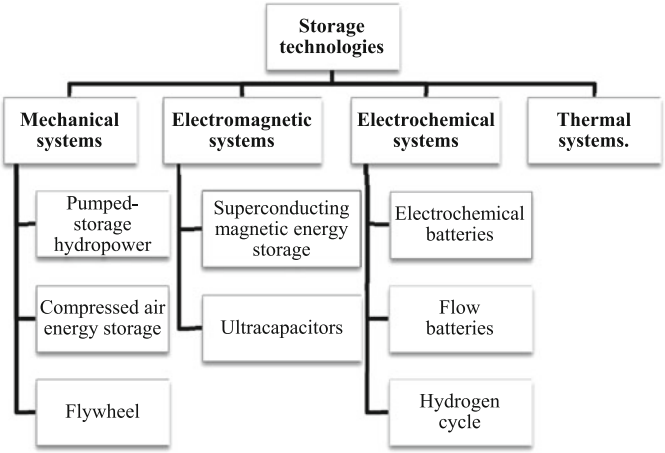

Fig. 1 Energy storage technologies

2.1 Mechanical Systems

2.1.1 Pumped-Storage Hydropower (PSH)

A pumped-storage hydropower plant is a kind of hydroelectric plant with two water reservoirs located at different height levels. During off-peak hours, in which lower consumption of energy is registered, the water located in the lower reservoir is pumped to the upper reservoir, increasing the potential energy of a vast mass of water. The energy consumed in the pumps is paid at a low off-peak price. Hence when energy is demanded during peak hours of consumption, this plant operates like a conventional hydropower plant releasing the water and using it to produce electricity by means of turbines.

These pumped-storage plants can be classified into two groups, conventional pumping stations and hybrid pumping stations, in which the lower reservoir has a natural source of water, such as a river, a lake, or even seawater. Furthermore, this lower reservoir can be placed below the ground level, using existing excavations or making an underground excavation. With this strategy, there is only one reservoir on the surface, reducing in this way the environmental impact [2, 3].

High levels of power and stored energy are achieved with an efficiency of about 70%, which is limited by the efficiency of the pump and the turbine used [4]. These systems provide large storage capacity, energy balancing, stability, and ancillary grid services such as network frequency control and reserves due to the ability of PSH to respond to potentially large electrical load changes within seconds [5]. They are used in very-long-term and long-term applications with a time response of minutes [6].

However, they require unique geographical locations and constructions, as well as having a high cost and in general a strong environmental impact. In many countries, the potential locations for new facilities are rather limited.

2.1.2 Compressed Air Energy Storage (CAES)

This storage technology is based on the use of compressors to store heat in the compressed air located in large reservoirs, such as underground cavities or above storage tanks, during low-demand periods. This stored heat is released through gas turbines to generate electricity along the discharge cycle.

CAES systems have lower efficiency in comparison to PHS: about 55–60% [7]. Nowadays, this technology comprises two different types of systems [3, 8]:

- *Diabatic CAES cycle*. The heat stored is reheated by the combustion of other fuel, usually natural gas, and is expanded through a turbine to produce electricity and reusable heat. This process involves certain losses in efficiency due to the heat dissipation and the use of fuel in the reheating process but is easier to implement than adiabatic CAES.
- *Adiabatic CAES cycle*. The stored compressed air is reheated by the heat extracted in the compression stage, reducing almost completely the need for fuel consumption. This type of system has only been implemented as a pilot plant for research purposes so far.

Although this is a technology used since the nineteenth century for different industrial applications, it has failed to become widely used due to the need of unique geological sites. Furthermore, it requires a large consumption of energy due to the compression stage and produces CO2 emissions if the recovery stage is not adiabatic. It is also important to mention the huge cost of this type of facility, although cheaper systems that use prefabricated containers instead of geological formations are developing in recent years.

The main benefits from this technology include the large amount of electric power generated (tens of kW) and the fast start-up achievable.

CAES systems are normally used in long-term and very-long-term applications with powers in the range of megawatts [6].

2.1.3 Flywheel Energy Storage (FES)

A flywheel is a rotating mass with high inertia which can store kinetic energy E, according to Eq. (1). Their principle of operation is based on the opposition to accelerations and decelerations presented due to their high inertia [9]:

$$E = \frac{1}{2} I \omega^2, \tag{1}$$

where I is the inertia momentum of the flywheel (kg m^2) and ω is the angular speed (rad/s).

The maximum stored energy is ultimately limited by the tensile strength of the flywheel material. The maximum specific energy density E_{sp} that can be stored in a flywheel is given by Eq. (2):

$$E_{sp} = k_s \frac{\sigma_m}{\rho}, \tag{2}$$

where σ_m is the maximum tensile strength of the flywheel material (N m^2), the parameter ρ is the density of the flywheel material (kg m^3), and k_s is the shape factor.

This technology has been traditionally used to stabilize the output voltage of synchronous generators. Flywheels stand out for their high power rating and quick response time playing a relevant role in primary frequency regulation [9]. The amount of number of cycles is considered almost unlimited, having a lifetime greater than 20 years [10]. Disadvantages included its high self-discharge due to friction [11], and therefore they cannot be used to maintain the energy stored for long periods of time. Modern systems are also composed of a large rotating cylinder with magnetically levitated bearings that eliminate wear and extend the lifetime of the system. These systems are used in low-pressure environments to reduce the air friction with the aim of increasing efficiency, which is typically close to 90% [10].

Flywheel systems are highly indicated for short-term applications requiring fast response [6].

2.2 *Electromagnetic Systems*

2.2.1 Superconducting Magnetic Energy Storage (SMES)

In SMES systems, a DC current is circulating through an inductance in order to store energy into its magnetic field. These systems, based on superconducting coils, are composed of a superconductor unit, a cryogenic refrigeration system, and a power conversion stage. The energy stored in the inductance E is given by Eq. (3), where L is the value of the inductance and I_L is the current [11]:

$$E = \frac{1}{2} L I_L^2. \tag{3}$$

This technology has been traditionally limited by the use of conventional conductive materials, but nowadays its development has been promoted due to the upgrade of these materials. New materials have virtually no Joule losses, such as

the niobium–titanium case, and few intermediate energy conversions. Only losses produced by the electronic converters must be taken into account. Besides, this type of storage stands out for its fast response time, around milliseconds, delivering high power peaks [7].

However, one of its main limitations is the refrigeration process at very low temperatures with helium or liquid nitrogen. This process entails a high extra cost, and, furthermore, many problems associated with the electromagnetic emissions result from the huge magnetic field that can be created in the superconducting coils.

2.2.2 Ultracapacitors

Ultracapacitors, also known as supercapacitors or electrochemical double-layer capacitors, are becoming a very attractive solution for storing energy due to the technological development produced in recent years. The operating principle is mainly electrostatic, as in conventional capacitors. However, part of the so-called pseudocapacitance responds to electrochemical principles. Their capacity has been greatly increased in several orders of magnitude by enlarging the effective area of its electrodes and bringing charges of opposite sign at near distances of a molecular size.

The accumulation of electric charges into the capacitors is produced between the plates and the dielectric insulation. However, in ultracapacitors this accumulation occurs along the interaction of metal ions with a porous medium, which is usually carbon. Therefore, pseudocapacity is discussed instead of capacity; thus this phenomenon makes that the capacity of an ultracapacitor dependent on the voltage, unlike in the case of conventional capacitors where capacity is always constant in spite of their state of charge [12].

Ultracapacitors are systems with very high efficiency (about 90% [9]), characterized by delivering or absorbing large amounts of energy in very short periods of time. Besides, they are compact, rugged, reliable, and capable of handling many charge–discharge cycles. The main problem with ultracapacitors is that the period of time in which they can store energy is not very long due to the self-discharge, as it happens with the flywheels. Another issue is that the operating voltage is low, and the connection of several ultracapacitors in series is necessary to build higher-voltage modules that can suit a wider range of applications. This series connection implies the need of some mechanism for balancing the voltages between cells.

In many applications, ultracapacitors can be a complement or even replace the use of batteries, as in the case of regenerative braking for electric vehicles, uninterruptible power supplies, lighting systems, etc. Another emerging field of application is their use for power quality improvement and their integration with renewable energy sources. Like in the case of flywheels, ultracapacitors and SMES systems are recommended for short-term applications [6].

2.3 Electrochemical Systems

2.3.1 Electrochemical Batteries

Batteries are devices that convert chemical energy into electrical energy through oxidation and reduction reactions. They are built in a modular way based on a base unit, called cell or element, which is subsequently attached to other cells, in series or in parallel, to obtain specific levels of capacity and voltage.

In spite of being the oldest and most widely used storage system due to their modularity, ease of use, and energy densities, it has some restrictions such as the negative effect of high power peaks and deep discharges on their life, the self-discharge, and the reduction in performance due to aging effects. In addition it is important to take into account the high toxicity of heavy metals employed in some types of batteries.

According to their application, different types of elements are used in batteries such as: lithium-ion (Li–ion), sodium–sulfide (Na–S), nickel-cadmium (NiCd), nickel–metal hydride (Ni–MH), and lead–acid (Pb–acid).

Due to their low cost and the level of technological maturity, the lead acid batteries are still the most commonly used in stationary applications where there are severe restrictions in terms of weight and volume, such as uninterrupted power supply (UPS). On the other hand, lithium-ion batteries provide the best energy density, being the best choice for mobile applications intended for consumer electronics and electric vehicles. However, complex electronic management systems are required to avoid risks, and their high cost reduces their suitability for stationary applications.

Regarding sodium sulfide batteries, there are already large-scale demonstrators that stand out due to their great potential in applications of mass storage connected to the grid. The main advantages over lead–acid batteries are their high energy density, low cost, and the safety of operation. Nevertheless, they require high temperatures for an optimum operation.

2.3.2 Flow Batteries (Redox)

These types of batteries are still at an early stage of development although the first commercial models are already available. Flow batteries are electrochemical systems with two electrodes and one electrolyte, as in a conventional battery, but in this case the electrolyte is stored in a separate tank, achieving an energy storage capacity which depends on the size of the reservoir and that is independent of the power [9].

Different compositions have been proposed for flow batteries, but so far the three that have achieved greater development are polysulfide bromide, vanadium redox, and zinc bromine [8].

The main advantages of this storage solution are their high output power capability, in the order of tens of kW, and that the recharge time is very fast because the replacement of the electrolyte can be done quickly and easily. The main disadvantages are their high cost and environmental problems presented by some of the materials employed.

Batteries are widely used in almost any storage application.

2.3.3 Hydrogen Cycle

Hydrogen reacts with oxygen to form water, releasing a huge amount of energy. The calorific value of this element is very large, over three times the values of gasoline or natural gas, making it one of the best fuels. Furthermore, this reaction does not emit CO_2 or other products except the water. Hydrogen is therefore considered an energy vector and the hydrogen cycle one of the energy storage methods with a brightest future.

The main difficulty is that hydrogen is not available in nature, so it must be generated by means of several methods that require the consumption of energy, such as the electrolysis of water.

One of the most interesting applications for the hydrogen cycle is to store renewable energy. Hydrogen is stored in pressurized tanks and cryogenic tanks or chemically fixed in metal hydrides, so when the energy demanded is greater than the generated energy, the electricity can be obtained from a fuel cell using the stored hydrogen. This process can reach an overall efficiency of 30–50% [8].

A further advantage of the hydrogen cycle is that it can take advantage of the residual heat coming from thermal loads in domestic or industrial facilities.

Some of the main disadvantages are:

- High cost, due in part to the platinum used in fuel cells.
- Low level of maturity of this technology, there are still few companies in this sector.
- The transport of hydrogen requires tanks with a large volume or very high pressure.
- Special safety measures are required due to the high fugacity of hydrogen.

Like in the case of batteries, hydrogen can be employed in a wide variety of storage applications [6].

2.4 Thermal Systems

Thermal storage systems can be subdivided into different technologies: storage of sensible heat, storage of latent heat, and thermochemical and absorption storage. In the context of energy storage systems, the most relevant technologies are based on the use of the sensible and/or latent heat coming from some kind of materials.

In general terms, this heat is stored to be released later as thermal energy when necessary.

These systems are usually implemented in environments where fluids are used at high temperatures, as in the case of solar thermal power plants where energy can also be produced during night due to the heat released by those fluids.

Although different oils or even air can be used, one of the most advanced methods of thermal storage is the employment of molten salts. It is a system based on two tanks in which a fluid composed of inorganic salts is stored.

The composition of these salts is not fixed being the most commonly used mixture of potassium or sodium nitrate and more recently calcium nitrate. They are stored in liquid form in a cold tank; when the sun is radiating, these salts are pumped to the heat exchanger in which heat is absorbed reaching high temperatures, and subsequently they circulate to a hot tank. When there is no solar radiation, the process is inverted: the content of the hot tank is transferred to the cold tank, and the hot salt transfers energy to the fluid and synthetic oil which produces steam [13].

3 Solutions for Renewable Energies: The Case of CPV Systems

The remarkable cost reduction and increase in efficiency of photovoltaic (PV) panels is making the cost of energy production in PV installations converge toward the costs in conventional generation systems. The so-called grid parity (i.e., equal cost of production) has already been achieved in certain countries. Moreover, the considerable increase of installed PV power is raising the requirements demanded by grid operators and national regulations. An example is the Royal Decree 1565/2010 of 19 November 2010 in Spain, which establishes regulations and modifies certain aspects of the activity. This implies that the PV systems of more than 2 MW are required to comply with the terms of the operation procedure 12.3 "Requirements for response to voltage dips in wind farms." Besides, the requirements for reactive power injection are also established by the aforementioned document. This indicates a clear trend toward higher technical requirements for PV systems, related to ancillary services.

In this context, energy storage becomes the solution to overcome the uncertainty and intermittency of PV generation. The storage system has to operate providing a fast response to power fluctuations in the PV system and bridging the gap before alternative power sources of the backup capacity can be started (i.e., the so-called bridging power functionality). Therefore, energy storage is mainly needed for the short term, from seconds to few hours, being the dynamic behavior of the storage solution even more important than its long-term capacity [14].

Regarding the particularities of concentration photovoltaic systems CPV, its on–off operation, in terms of power delivery, must be emphasized. Only direct radiation is converted into electricity in this technology, due to the small acceptance

angle of the optic system that is incorporated to concentrate solar radiation on high-efficiency cells. CPV panels are consequently mounted on high-precision two-axis trackers. Energy storage can therefore bring numerous benefits to CPV technology as listed below:

- Smoothing the power profile avoiding the characteristic on–off operation and large voltage gradients
- Avoiding the need for connection and disconnection, fast maneuvers aimed to not allow the absorption of energy from the grid when the DC bus is discharged
- Avoiding the need to oversize the grid inverter rating in concentrator photovoltaic systems which have been estimated at 110% of the power of the CPV modules for an optimum efficiency
- Eliminating the need of supplying energy to the power electronics control from the grid side to avoid the shutdown of the equipment due to shadows
- Compensating the variations according to the production forecasts, reducing the uncertainty from the grid operator point of view
- Better provision of ancillary services such as support to the damping of frequency fluctuations and voltage control

Considering the most appropriate storage technologies for CPV systems and taking into account the short-term fast-dynamic requirements, it is apparent that the use of batteries and ultracapacitors can be one of the best solutions due to their electrical nature, efficiency, and modularity. Their sizing can be optimally adjusted to match the requirements of a CPV generator, which leads to cost reduction. Furthermore their integration by means of power electronics is easy and does not significantly differ from the equipment already used in PV systems. Finally, there is the possibility of building hybrid storages systems combining both technologies, because their characteristics are complementary: the high power density of ultracapacitors is combined with the higher energy density of batteries.

The following sections describe the main characteristics of batteries and ultracapacitors, concentrating on their electrical behavior and modeling. Finally a hybrid storage solution integrating both technologies with a CPV system is proposed and simulation results are provided.

3.1 Batteries and Ultracapacitors: Main Features, Models, and Parameter Identification

In this section, batteries and ultracapacitors technologies will be described for a better understanding of their operating principles. However, the design process of a hybrid energy storage system (HESS) also requires the selection of the most appropriate models based on the equivalent electrical circuits for each component. These models should represent with reliability the physical phenomena that occur inside these devices. Nevertheless, simplicity is also sought to provide a practical

tool for design. After the selection, these models can be implemented using simulation software, and the electrical behavior of the whole system can be predicted and controlled.

3.1.1 Batteries

The use of electrochemical batteries is widespread, and it is nowadays the most frequently used solutions for the energy storage of PV systems, particularly in isolated (off-grid) installations.

There are many kinds of batteries, such as Pb–acid, NiCd, Li-ion, Na–S, and Ni–MH. Although they work by means of different internal chemical reactions, all of them consist of:

- A negative or reducing electrode (anode), which gives up electrons to the external circuit and is oxidized during the electrochemical reaction.
- A positive or oxidizing electrode (cathode), which accepts electrons from the external circuit and is reduced during the electrochemical reaction.
- An electrolyte, inside the cell and between the anode and the cathode, which provides ions as the medium for transfer of electrons. The electrolyte is typically a liquid, such as water or other solvents, with dissolved salts, acids, or alkalis to increase ionic conductivity.

The electrical circuit can be externally connected to either a load or a power supply to discharge or charge, respectively, the battery. In order to describe this electrical behavior, batteries can be modeled through a wide variety of equivalent electrical circuit models, but all of them can be considered as modifications of the following main models:

The simplest model is shown in Fig. 2. It consists of a voltage source V_{oc}, which represents the electromotive force and an internal series resistance R_{bs}. They can be considered as constant values, but their values have some dependency on the state of charge (*SOC*), the operating temperature, and aging. Taking this fact into account, the model is accurate for long-time simulations. Transients and high-frequency behavior are not well modeled, however.

The Thévenin model, shown in Fig. 3a, offers a good balance between low complexity and high precision in short-time periods and during transients. In this

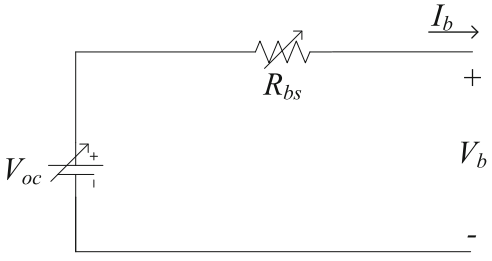

Fig. 2 Resistive model of the battery

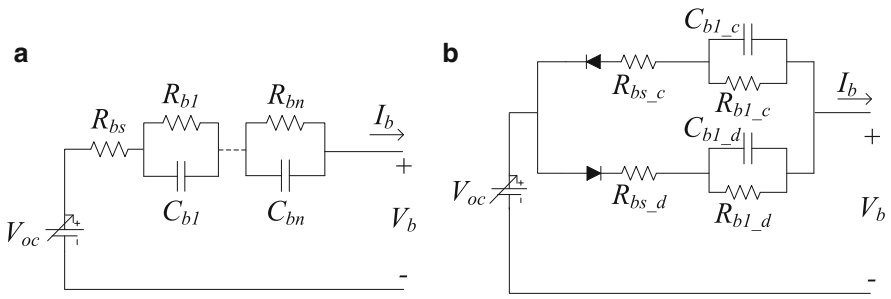

Fig. 3 Battery models: (**a**) Thévenin model and (**b**) Salameh model

model, C_{b1} to C_{bn} represent the capacity, and R_{b1} to R_{bn} stand for the contact resistance of the plate and the electrolyte 1. These values also have some dependency on the SOC, the temperature, and the aging.

Several combinations of resistances and capacitors (RC) could be considered; nevertheless, a single RC branch is accurate enough as has been demonstrated in previous works [15].

Apart from the described dependencies, the values of resistances and capacitors in charging cycles are different than in discharging ones. The Salameh model [16], shown in Fig. 3b, includes two branches with ideal diodes connected in opposite directions in order to activate the corresponding branch depending on the direction of the current.

After the selection of the most appropriate model, its parameters should be identified in order to match the simulations with the behavior of the real storage devices by means of experimental tests. Time and frequency domain tests are the two main kinds of identification methods. Time domain tests consist in measuring the output voltage when several current steps are applied to the battery. Then, the parameters can be obtained by adjusting the test results with the transfer function of the battery impedance, using, for instance, nonlinear least-square optimization techniques. The tests in the frequency domain are made by means of an electrical impedance spectroscopy, which also requires adjusting the current and voltage behavior with the model transfer function, performing a frequency sweep of the frequency range of interest.

The estimation of the SOC is a major issue due to the complex relation between the capacity level and V_{oc}, besides the complexity of measuring this voltage when the battery is operating. For this purpose, the most used method is the Coulomb counting technique [17], based on the integration of the output current during the time for estimating the changes in the total energy stored.

3.1.2 Ultracapacitors

In a traditional electrostatic capacitor, the electrodes consist of a thin surface on which the charges are accumulated. In an ultracapacitor, the electrodes consist of a

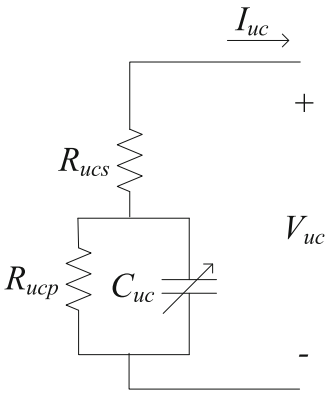

Fig. 4 First-order RC model of an ultracapacitor

porous microstructure that can be made of carbon material, and around it the electrolyte is deposited. This structure gives a significantly larger specific surface area than the conventional capacitors have. To separate anode and cathode, a thin isolation membrane is located between the electrodes with a small separation, which allows a high energy density in ultracapacitors.

When compared to batteries, the modeling of ultracapacitors has not yet been investigated so thoroughly due to their more recent development, but there are several different circuit models that have been proposed in the literature.

The simplest ultracapacitor equivalent circuit is the first-order RC model, which has only one RC branch, as shown in Fig. 4. This model is composed of a resistor R_{ucs}, which models the ultracapacitor ohmic losses, usually called equivalent series resistor (ESR), and a capacitor C_{uc}, which simulates the ultracapacitor capacitance during charging and discharging stages. R_{ucs} is a parameter that is usually given by the manufacturer. C_{uc} varies almost linearly with the voltage level or SOC of the ultracapacitor. This relationship is a significant characteristic of ultracapacitors in contrast to conventional capacitors. Additionally the resistance, R_{ucp}, which is the energy leakage due to the self-discharge, can be considered. For very short simulation periods, R_{ucs} can be considered infinite since the self-discharge is negligible [18].

An improvement to the previous model is the RC parallel-branch model [19]. It can be composed of several RC branches, each one with a different time constant. For simplicity, many authors consider a three-branch model accurate enough, as shown in Fig. 5a.: the first branch dominates the charge and discharge behavior in the order of a few seconds. $C_{\mathrm{uc\_f1}}$ is the capacitor that models the dependency on the output voltage. The second branch has a time scale of minutes. And the third branch usually governs the long-term (minutes) charge and discharge behavior.

The RC transmission-line model is the most similar to the physical structure of double-layer capacitors [20]. As they have porous electrodes, each pore can be modeled as a transmission line. The result is an equivalent circuit with many RC elements. A simplification as shown in Fig. 5b is therefore needed for a less complex parameter identification process.

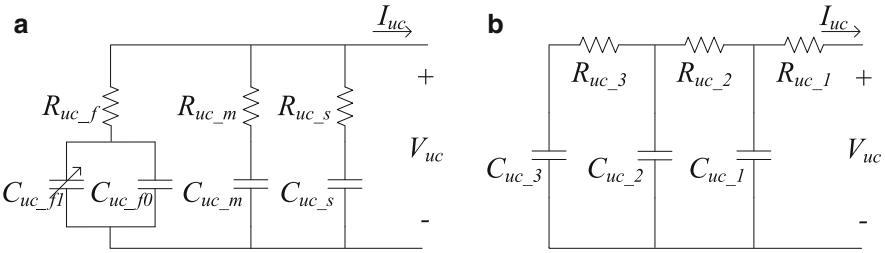

Fig. 5 Ultracapacitor models: (**a**) RC parallel-branch and (**b**) RC transmission-line models

Table 1 Comparison between batteries and ultracapacitors

Feature	Batteries	Ultracapacitors
Energy density (Wh/kg)	10–100	1–10
Power density (kW/kg)	0.2	1–10
Efficiency (charge/discharge)	70–80%	95%
Charge/discharge cycles	1,000	1,000,000
Temperature range (°C)	>−10	−40–70
Lifetime (years)	7–8	30
Discharge time	Hours	Seconds
Cost (with respect to a Pb–acid battery with the same capacity)	Li-ion x7	x20
	Ni–MH x2	

By adapting the tests to the ultracapacitor models, the methods for the parameters identification either in the time or in the frequency domain are similar as detailed for batteries.

The most important features of batteries and ultracapacitors are summarized in Table 1. It shows the main differences in their behavior that should be taken into account in the development process and control design of a HESS, as it is detailed in Sect. 3.2.

3.2 Hybrid Energy Storage System with Batteries and Ultracapacitors

The integration of the different components comprised in a HESS requires the use of power electronic DC–DC converters that allow a precise control of the energy flows and the state of charge of the storage devices.

The purpose of the DC–DC converters is supplying electric power in a regulated way, and, therefore, the output voltage and/or the output current will be controlled and independent of the input or load magnitudes. They are known as switched-mode power converters because their operation is based on one or more switches which commute at high frequencies performing the regulation of the system [21].

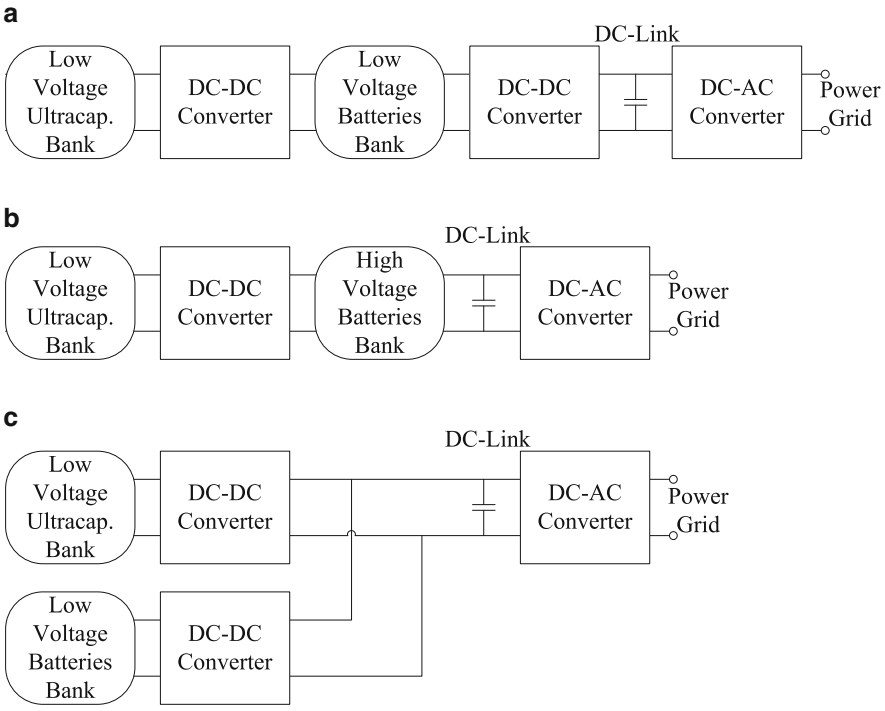

Fig. 6 HESS topologies

The nonisolated DC–DC converters are usually based on three elementary topologies: buck (step-down) converter, boost (step-up) converter, and buck–boost (step-down/step-up) converter. These basic models are technologically mature and reliable solutions, which enable high modularity and, with additional device replacement, may become bidirectional converters, allowing the connection of some elements that either deliver or absorb energy according to the requirements. This is the case of the energy storage devices [22].

Various kinds of topologies can be used for the interconnection of the batteries and ultracapacitor banks with the power grid or within a microgrid [23]. Most of them include a DC–AC converter that shares its DC side with the other devices by means of a common bank of capacitors, called DC link, in order to ensure an appropriate voltage level. The main configurations used in literature are shown in Fig. 6 or consist in a variation of them. DC–DC converters can be series connected as in Fig. 6a. If the batteries bank has a voltage level as high as required by the DC link, it is possible to remove the batteries converter as in Fig. 6b. DC–DC converters can also be paralleled and connected as Fig. 6c shows, where the voltage levels at the low side of the batteries and ultracapacitors banks can be independently controlled.

Based on Fig. 6c, the proposed configuration for a CPV plant with a HESS is depicted in Fig. 7. For this application, this parallel topology is the most

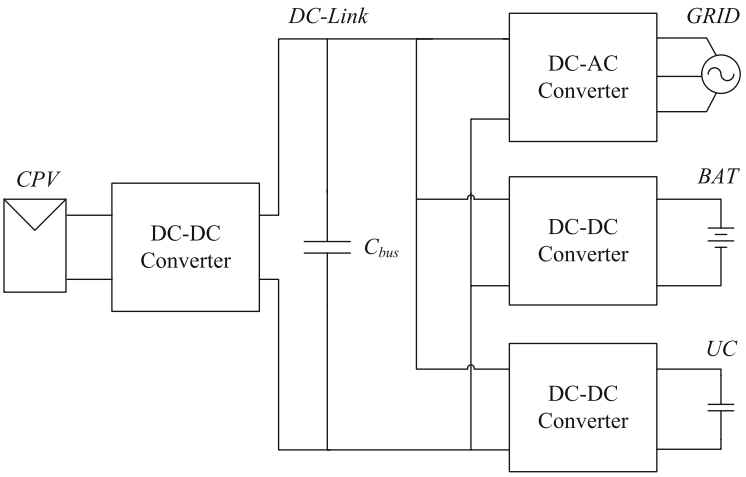

Fig. 7 Proposed HESS for a CPV plant

comprehensive and versatile and can be modified for different technical and economic requirements.

The objective of the batteries and ultracapacitor converters is controlling the current using a proportional-integral (PI) control law and applying a pulse-width modulation (PWM) technique.

Besides that, most of HESS needs an upper system for the energy flows management, which means a central system which receives all the information of the plant and decides the operating modes and the reference values to properly control each converter.

In order to split the instantaneous power to be supplied or absorbed by the batteries and ultracapacitors, one possible solution is based on the use of a low-pass filter [24]. This scheme obtains a smoother power profile from the batteries, maximizing in this way their performance and duration and reducing their utilization during short interruptions of the CPV output power (i.e., cloud passing).

In order to illustrate the performance of the components in conjunction with the control systems described, a 3 kW HESS for a CPV plant with the scheme shown in Fig. 7 has been implemented by means of the simulation software PSCAD/EMTDC. All the converters use a switching frequency of 20 kHz. The total simulation time is 100 s. The time constant of the low-pass filter in charge of distributing the demanded power between the ultracapacitors bank and the batteries bank is set to 2 s. It should be noticed that although this time constant can be increased in real applications according to the available capacity of the ultracapacitors bank, its value has been chosen to properly illustrate the performance of the system during the simulated time duration.

Figure 8 shows the dynamic behavior of the HESS during sudden variations of the power generated by the CPV modules. It should be noticed that, according to the

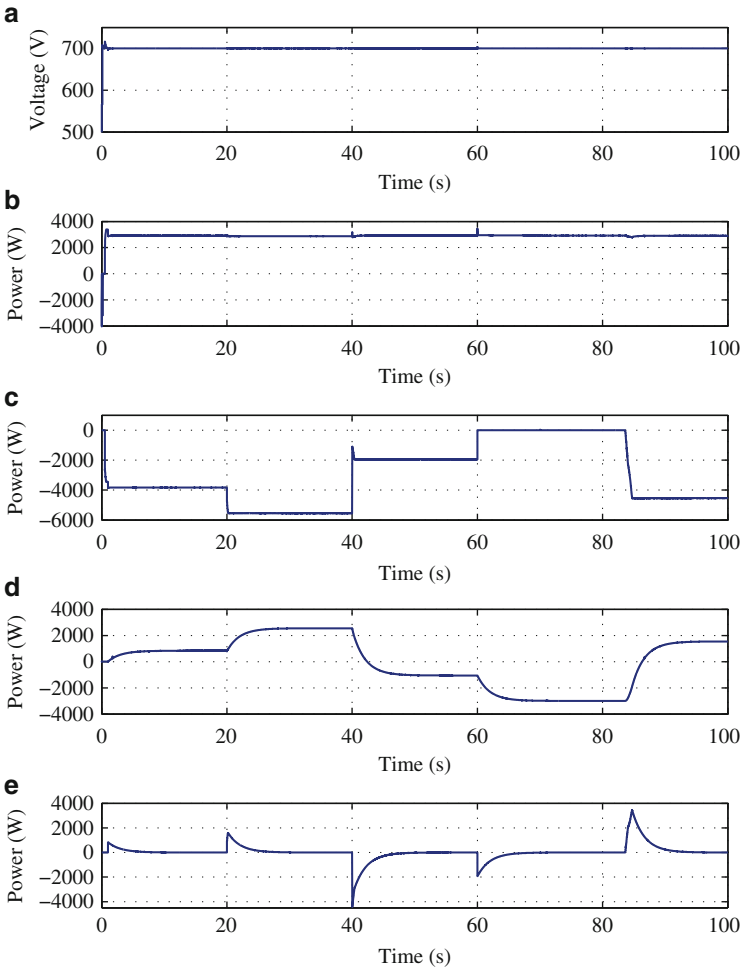

Fig. 8 Simulation results: (**a**) voltage at the DC link, (**b**) active power injected into the grid, (**c**) power generated by the CPV plant, (**d**) power flow of the batteries bank, and (**e**) power flow of the ultracapacitors bank

passive sign convention, the generated power is negative, e.g., the power of the CPV system, while the power injected into an element is positive, e.g., the grid.

The simulation has been carried out as follows: initially, the voltage of the ultracapacitors bank is 140 V, whereas the voltage of the batteries bank is 153.1 V. In addition, the capacitors of the DC link are charged from 0 to 700 V. During this time interval, the DC-link capacitors absorb power from the grid as shown in Fig. 9, which plots the main wave forms in the initial time interval between 0 and 1.6 s. The controller of this voltage includes an anti-windup mechanism to stop the integration when the controller reaches either the lower or the upper limit [25]. After that, at instant $t = 0.5\,\mathrm{s}$, the CPV modules initiate their

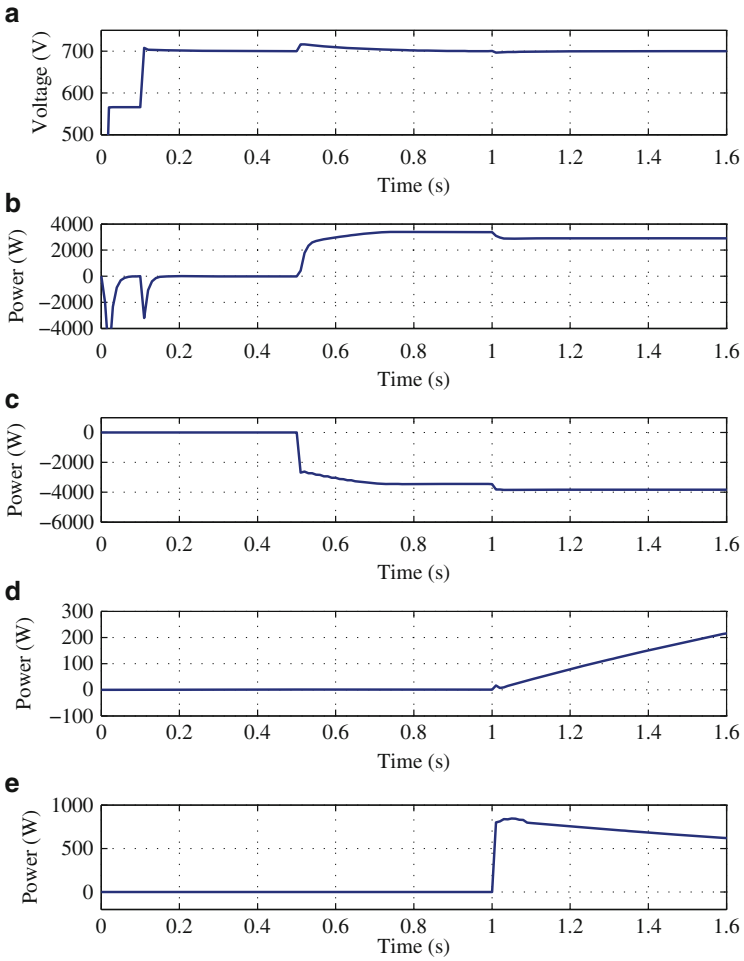

Fig. 9 Detail of the wave forms of Fig. 8 ($0\,\text{s} \leq t \leq 1.6\,\text{s}$): (**a**) voltage at the DC link, (**b**) active power injected into the grid, (**c**) power generated by the CPV plant, (**d**) power flow of the batteries bank, and (**e**) power flow of the ultracapacitors bank

operation without the intervention of the HESS. Therefore, all the power generated by the CPV system is injected into the grid as Figs. 8 and 9 show. Since the power generated by the CPV system is higher than 3 kW at this time, the HESS is connected at $t = 1\,\text{s}$, limiting the power injected into the grid to 3 kW and storing the excess of generated power. At instant $t = 20\,\text{s}$, the CPV system generates 5.5 kW, and the HESS must absorb 2.5 kW to keep the power injected into the grid constant at 3 kW as Fig. 8 shows. At instant $t = 40\,\text{s}$, the power generated by the CPV system decreases to 2 kW, and, consequently, the HESS must inject 1 kW in order to maintain at 3 kW the power injected into the grid. The solar energy production is reduced to zero from $t = 60\,\text{s}$ to $t = 84\,\text{s}$: during this time interval, the

HESS must be able to inject all the power demanded by the grid. This would be the case of a cloud passing over the panels avoiding the absorption of any solar direct radiation. Finally, an increase of 4.5 kW in the power generated by the CPV system takes place at $t = 84$ s: once again the HESS is able to absorb the extra amount of power generated by the CPV system. It should be noticed that the voltage of the DC-link capacitors remains constant at 700 V during the operation of the CPV system, as illustrated in Fig. 8a, which implies that the profile of the power injected into the grid is also constant.

Figure 10 shows the voltage and current profiles of the ultracapacitors and batteries banks. It can be seen that the voltages of the batteries and ultracapacitors

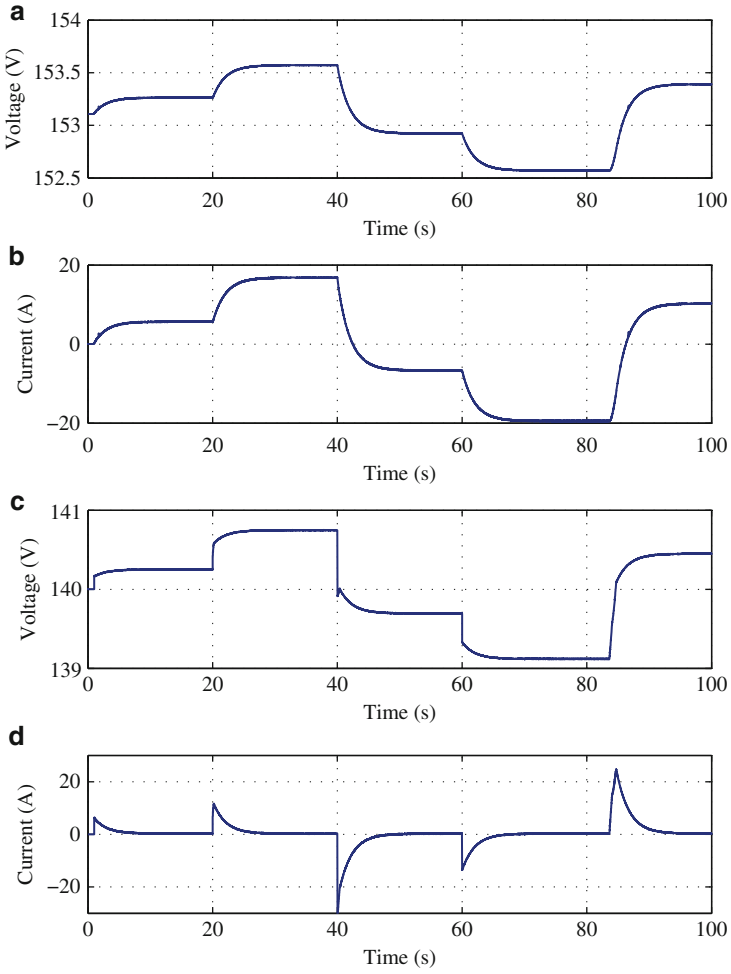

Fig. 10 Simulation results: (**a**) voltage of the batteries bank, (**b**) current absorbed by the batteries bank, (**c**) voltage of the ultracapacitors bank, and (**d**) current absorbed by the ultracapacitors bank

increase when they absorb power and decrease when the HESS must inject power into the grid (see Fig. 10a, c, respectively). Moreover, Fig. 10d shows that the ultracapacitors are able to absorb/inject peaks of current of high amplitude in a short period of time, while the time response of the current absorbed/injected by the batteries corresponds to the smoothed power demand obtained with the low-pass filter with the constant time of 2 s as Fig. 10b shows.

4 Conclusions

Energy storage systems can bring many benefits to the management and security of supply in electrical transmission and distribution systems, in which the impact of renewable energy sources is growing. These storage solutions are not only intended to compensate the uncertainty and intermittency of renewable energy sources, such as PV systems, but also to provide ancillary services and advanced functionalities to support a safe and stable operation of the grid.

Many different storage technologies with different degrees of maturity are available nowadays. The best solutions for particular applications must respond to certain requirements and constraints such as capacity, dynamic response, power density, weight, volume, and cost. The case of CPV systems, with their inherent fast power fluctuations, has been analyzed in this chapter. A hybrid energy storage solution combining batteries and ultracapacitors has been proposed to provide a short-term fast-dynamic solution. The high power density of ultracapacitors matches the higher energy density of batteries, to provide a modular and easy-to-integrate solution. The proposed system has been implemented in simulation using the software PSCAD/EMTDC, and some results are provided to illustrate the performance of the combined CPV hybrid energy storage solution.

Acknowledgments This work has been partially supported in part by the Ministry of Economy and Competitiveness of Spain under the research project ENE2012-33541, in part by the Ministry of Economy and Competitiveness of Spain in the framework of the National Program of Scientific Research, Development, and Technological Innovation (2008–2011), and in part by the European Regional Development Fund under the Research Project IPT-2011-1468-920000. Xavier del Toro Garcia has been supported by the "Juan de la Cierva" program (JCI-2011-10371) of the Ministry of Economy and Competitiveness of Spain.

References

1. Márquez Angarita J, Garcia Usaola J (2007) Combining hydro-generation and wind energy: biddings and operation on electricity spot markets. Electr Power Syst Res 77(5–6):393–400
2. ESA Energy Storage Association (2014) http://energystorage.org/
3. Bradbury K (2010) Energy storage technology review. Tech. rep., Duke University, Durham
4. Whittingham MS (2012) History, evolution, and future status of energy storage. Proc IEEE 100:1518–1534

5. Miller R, Winters M (2009) Opportunities in pumped storage hydropower: supporting attainment of our renewable energy goals. In: Proceedings of the Waterpower XVI conference, pp 27–30
6. Regional Government of Madrid Energy Foundation (2011) Energy storage guide. Tech. rep., Council of Madrid
7. Hausheer R, Heinze K, Katai S, Kaufman K, Litten J, Madaiah G (2010) Evaluating energy storage options: a case study at Los Angeles harbor college. Tech. rep., Donald Bren School of Environmental Science & Management. University of California, Santa Barbara
8. Swierczynski M, Teodorescu R, Rasmussen CN, Rodriguez P, Vikelgaard H (2010) Overview of the energy storage systems for wind power integration enhancement. In: Proceedings of the IEEE international symposium on industrial electronics, ISIE, pp 3749–3756
9. San Martín JI, Zamora I, San Martín JJ, Aperribay V, Eguía P (2011) Energy storage technologies for electrical applications. In: Proceedings of the international conference on renewable energies and power quality (ICREPQ'11), pp 1–6
10. Chen H, Cong TN, Yang W, Tan C, Li Y, Ding Y (2009) Progress in electrical energy storage system: a critical review. Prog Nat Sci 19(3):291–312
11. Verma H, Gambhir J, Goyal S (2013) Progress in electrical energy storage system: a critical review. Int J Innov Technol Explor Eng 3(1):63–69
12. Burke A (2000) Ultracapacitors: why, how, and where is the technology. J Power Sources 91 (1):37–50
13. Kempener R, Simbolotti G, Tosato G (2013) Thermal energy storage. Technology brief. Tech. rep., EA-ETSAP and International Renewable Energy Agency IRENA Technology Brief E17
14. DG ENER Working Paper (2013) The future role and challenges of energy storage. Tech. rep., European Commission Directorate-General for Energy
15. Einhorn M, Valerio Conte F, Kral C, Fleig J (2013) Comparison, selection, and parameterization of electrical battery models for automotive applications. IEEE Trans Ind Electron 28 (3):1429–1437
16. Salameh ZM, Casacca MA, Lynch WA (1992) A mathematical model for lead-acid batteries. IEEE Trans Energy Convers 7(1):93–98
17. Tremblay O, Dessaint LA (2009) Experimental validation of a battery dynamic model for ev applications. World Electr Veh J 3:1–10
18. Spyker RL, Nelms RM (2000) Classical equivalent circuit parameters for a double-layer. IEEE Trans Aerosp Electron Syst 36(3):829–836
19. Zubieta L, Bonert R (2000) Characterization of double-layer capacitors for power electronics applications. IEEE Trans Ind Appl 36(1):199–205
20. de Levie R (1963) On porous electrodes in electrolyte solutions: I. capacitance effects. Electrochim Acta 8(10):751–780
21. Hart DW (2011) Power electronics, International edn. McGraw-Hill, New York
22. Himmelstoss FA (1994) Analysis and comparison of half-bridge bidirectional DC-DC converters. In: Proceedings of the 25th annual IEEE power electronics specialists conference, PESC'94, vol 2, pp 922–928
23. Choi DK, Lee BK, Choi SW, Won CY, Yoo DW (2005) A novel power conversion circuit for cost-effective battery-fuel cell hybrid systems. J Power Sources 152:245–255
24. Lu D, François B (2009) Strategic framework of an energy management of a microgrid with a photovoltaic-based active generator. In: Proceedings of the 8th international symposium on advanced electromechanical motion systems & electric drives joint symposium. ELECTROMOTION 2009, pp 1–6
25. Roncero-Sánchez P, Acha E (2014) Design of a control scheme for distribution static synchronous compensators with power-quality improvement capability. Energies 7(4):2476–2497

Battery- and Ultracapacitor-Based Energy Storage in Renewable Multisource Systems

Mahamadou Abdou-Tankari and Gilles Lefebvre

Abstract In this paper, wind generator and photovoltaic systems are associated to the diesel generator to supply energy to the DC-bus. The maximum power point tracking methods are applied to the wind generator and photovoltaic systems to increase the renewable energy contributions and to reduce the fuel consumption. Interactions between sources are studied, and the storage device characteristics are analyzed in aims to make a choice of the appropriate storage technologies. The interest of combining the ultracapacitors with the battery, as storage devices, is prospected, and the number of cycles is estimated by using the rainflow counting method. The experimental tests bench is designed in a reduced scale, and some simulations and experimental results are presented and analyzed.

Keywords Battery, DC/DC converter, Diesel generator, Photovoltaic power storage devices, Ultracapacitors, Wind power generation

Contents

M. Abdou-Tankari (✉) and G. Lefebvre
CERTES Laboratory, Créteil University, 61, Avenue du Général De Gaulle, 94010 Créteil Cedex, France
e-mail: mahamadou.abdou-tankari@u-pec.fr; lefebvre@u-pec.fr

G. Lefebvre et al. (eds.), *Environment, Energy and Climate Change II: Energies from New Resources and the Climate Change*, Hdb Env Chem (2016) 34: 95–122,
DOI 10.1007/698_2014_292,
Published online: 9 December 2014

1 Introduction

High pollution and global warning are the big results of the human activities in energy production and consumption [1]. This situation is exacerbated by the growing of the population inducing a great need of energy. In general cases, electricity is produced from fossil fuels. But, their scarcity leads to a gradual increase of the energy costs and requires the use of alternative energy sources. In this context, the diversification of energy sources is presented as an interesting alternative to achieve energy savings, to reduce the energy costs and to reduce the air pollution [2]. This can be led by increasing the ratio of renewable energy in the electricity production. But, the electricity generated by the renewable energy sources is subject to several constraints that are as follows: high funding costs, intermittencies of climatic resources, and the need of the energetic autonomy for the islanded sites. They are very fluctuating and not predictable. Also, the correlation between the power need and the renewable energy production is not frequent, especially for off-grid systems. So to optimize the using of renewable energy, it can be interesting to insert the storage devices in the system.

Particularly, the power fluctuations are very large in the small wind generator system. The wind variations are less attenuated by the generator inertia than in the big wind generator system. So, ultracapacitors and batteries are recently combined in complementary modes to ensure the system stability [3–6]. The wind energy variations are not predictive, as well as the periodicity of storage units. So, the storage sizing is a big challenge for designers of the wind power applications.

Generally, the sizing of such a system is based on hourly average data. The proposed methods are formulated as an optimization problem (minimizing of the energy cost and maximizing of the wind power) [7–9]. In most of these studies, the short-term fluctuations and the detailed characteristics of sources are not taken into account. By neglecting these parameters, the system life cost and performances can be different (or worse) than estimated behaviors [10–12]. As example, by considering only the hourly average data, someone cannot show the interest of using the ultracapacitors (or flywheel) to mitigate the short-term fluctuations [13]. The control strategies of the power converters can also have impacts on the system performances and life cost.

In this paper, the coupling of the wind-PV-diesel hybrid system is studied, and the interactions of sources are analyzed. The storage devices are used to absorb disturbances due to the wind speed variations. An interesting method of storage sizing is introduced. This method takes into account the actual conditions of the system operation, the sources dynamics, the storage lifetime in actual conditions and the control strategies of power converters.

The wind energy fluctuations are shared between ultracapacitors (UC) and batteries according to the dynamics of each device. Using UC in the hybrid system reduces the number of batteries' cycles and can improve their lifetime. UC have capacity to support a larger number of cycles contrary to the batteries [14, 15]. So, batteries are the weak link of the system. For this reason, it becomes important to estimate their lifetime by taking into account the application conditions. To do this, the rainflow counting method is used to estimate the number of cycles and the lifetime. The synoptic of the considered hybrid is presented in Fig. 1. The components' missions and characteristics are also reported in the figure.

In this paper, sources and storage devices models are not presented. In first time, a principle of the renewable and conventional optimal power generation is treated. The major parameters that determine the optimal operation are presented. In the second time, the interactions of the system components on the DC-bus are analyzed before to introduce the sizing method of the storage devices in third time. After this, the converters control and energy management methods are presented.

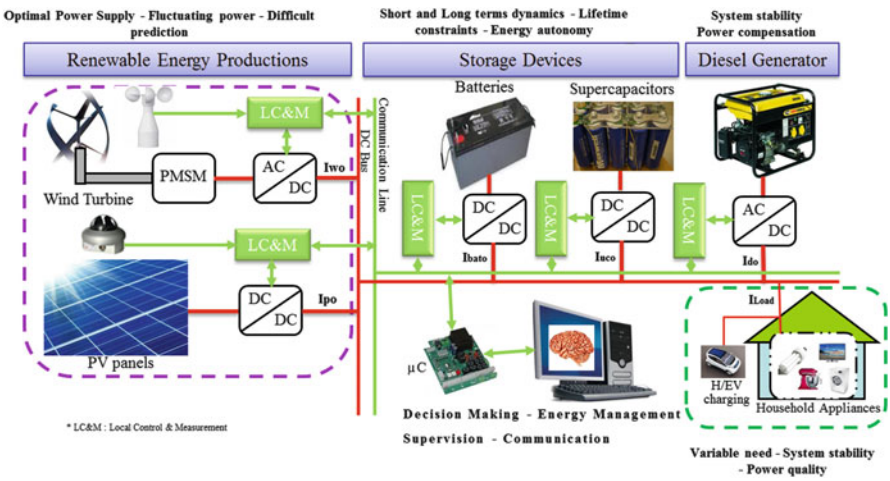

Fig. 1 Synoptic of the renewable-based hybrid system

2 Power Generation

Power is generated by renewable energy sources (wind and PV) and by a diesel generator. The wind and photovoltaic productions are optimized, and their fluctuations are mitigated by the energy storage devices. The power deficit is compensated by the diesel generator to realize the power balance. All energetic chains are coupled on a DC-bus common coupled point as shown by Fig. 2. The principle of the power sharing and the converters' control laws is presented in Fig. 3. In this figure, the blocks Q1, Q2, Q4, and Q5 correspond to Eqs. (9), (11), (10), and (12), respectively. Q3 is determined according to Eq. (12) to control the converter in unidirectional mode.

The control and supervision system is based on different levels defined as follows:

Level 1 is dedicated to the measurement of the climatic conditions, wind speed, and solar radiations.

In *Level* 2, the power generation principle is presented, and the energy sharing strategies are developed. The controller reference values are also determined in this section and used in *Level* 4.

Level 3 is dedicated to the decision laws implementation in the supervision system. It can decide when all (or part) of the system would be started or stopped by realizing the power balance and by ensuring a good lifetime of the components.

Level 4 is dedicated to the implementation of the polynomial controllers that switch the power converters of wind generator, PV generator, and storage devices. For each dynamic variation of the system parameters, corresponding duty cycles are generated in this level.

Level 5 is dedicated to the duty cycles estimation for PWM generation. These last are conditioned by the converter drivers.

2.1 Wind Energy Generation

The wind speed is generally considered as a sum of low frequencies and turbulent components. So, energy provided by the wind generator *WG* is very fluctuating according to the wind condition variations. The significant part of this energy is located in the frequency domain below 1 Hz according to the Van Der Hoven diagram [16]. Most of high-frequency fluctuations (above 1 Hz) are effectively damped out by the large inertia of wind generator; their magnitudes are not significant. In Fig. 1, a permanent magnet synchronous generator (PMSM) is driven by the wind turbine to generate the wind power. A diode rectifier bridge is associated to a buck converter to operate the system at its maximum power. Some maximum power point tracking methods are developed in the literature [17–19]. But, in this paper, a method based on the current control is used to estimate the reference value (I_{wo_ref}) of the DC converter controller [20]. A polynomial

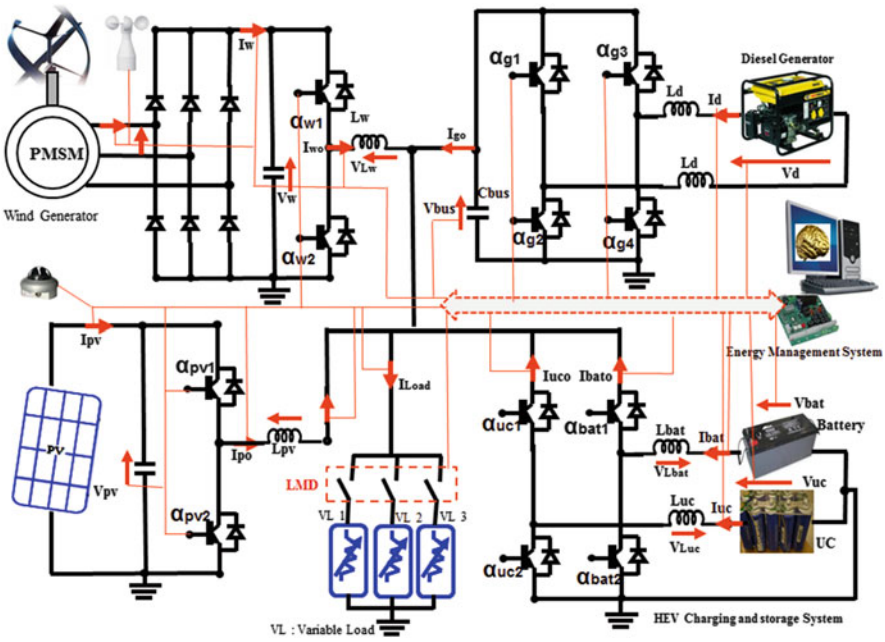

Fig. 2 Power converter architectures in the hybrid system. LMD is the load management system

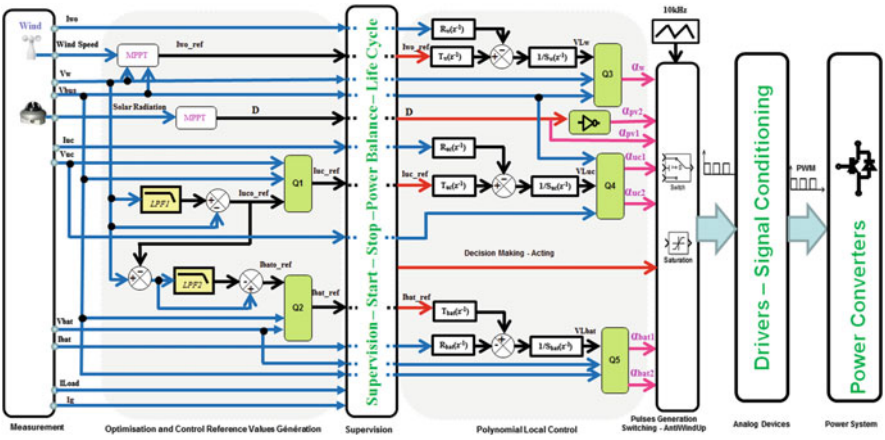

Fig. 3 Energy management and converter control strategy (EMACS)

controller is applied to this reference value (I_{wo_ref}) to transfer the wind maximum power to the voltage bus through a dc converter.

2.2 PV Generator

A buck converter is interfaced between the *PV* panel and the *DC-bus* to transfer the *PV* maximum power. The *MPPT* strategy used in this paper is based on the *PV* current measurement to track the maximum power [20]. The *PV* current is measured for each variation of the solar radiation for the duty cycle *D* estimation. The DC converter is directly switched by the estimated duty cycle *D*, without using the polynomial controller. In this study, it is considered that the PV panels generate a smoothed power.

2.3 Diesel Generator

The diesel generator *DG* is used to stabilize the DC-bus and to realize the power balance. The diesel engine model includes combustion delay and dependant phenomenon [21]. The value of the delay depends upon the number of cylinders, the engine capacity, and the rotating speed. To satisfy the requested power, the diesel engine is operated at variable speed in a limited (optimal) variation band. It assumes that the diesel generator compensates only the low variation component of the deficit. In these conditions, it is expected that the fuel consumption and the system cost (power, dimensions, and weight) can be reduced significantly [22–24].

3 Interactions on the DC-Bus of a No-Storage Wind-PV-Diesel System

Disturbances induced by the wind generator on the DC-bus can reduce the system performance. So, analysis of these disturbances is required to ensure compatibility between the diesel generator (*DG*) missions with its dynamics. In such a hybrid system, the *DG* system mission is to ensure the *DC-bus* voltage stability by compensating the power deficit that can be very fluctuating according to the wind speed variations. But, in aims to operate efficiently, the diesel speed variations can be limited in a defined band, called "diesel engine efficiency band," and its operating dynamics have to be low.

Taking into account these constraints and to realize proper system performance, faster compensation of fluctuations must be ensured by using high dynamics sources, such as storage units. The storage devices are able to absorb high dynamic

disturbances to improve the hybrid system performance. According to each unit dynamics, ultracapacitors and batteries can be used in a complementary mode to mitigate the high and middle components of the power fluctuations. An iterative method of storage units sizing (IMSUS) is introduced, in this paper, to design the appropriate storage capacities.

4 Dedicated Sizing of Storage Devices in the Hybrid System

Sometimes, when the storage units are used, the renewable energy system is designed by considering only the storage devices lifetime estimated by the manufacturer and by using the hourly data. The impacts of actual conditions (intermittencies of wind or solar energies) in the storage devices lifetime are not taken into account. But, knowledge of renewable energy system shows that the batteries' lifetime is drastically reduced by intermittencies of the *WG* power in such a system [4, 25]. So, it becomes important to size the storage devices by taking into account the turbulent part (short-term variations) of the renewable resources.

To do this, an iterative method of storage units sizing (IMSUS) is proposed in this paper. The principle of this strategy is shown in Fig. 4 and explained as follows:

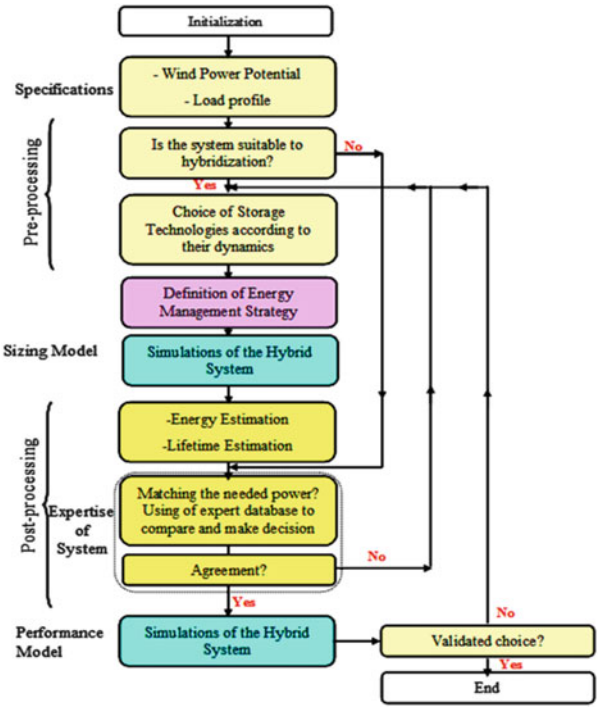

Fig. 4 Flowchart of storage devices sizing method (IMSUS)

1. Hybridization factors are applied to the specifications (wind energy potential of the location and load power) to determine whether or not storage units are necessary.
2. Various storage configurations are then studied. Three cases are possible: using only batteries, using only ultracapacitors, or using of batteries and ultracapacitors in a complementary mode.
3. Depending on the system configuration, a strategy for energy management is defined and applied to the system.
4. Simulations are then performed with Simulink software model by considering that the storage units can effectively ensure their predefined mission.
5. The storage capacity is estimated from the simulations results. The database of manufacturers is used to select the characteristics of the storage devices. Then, the lifetime of the storage units is estimated.
6. If the determined parameters are acceptable (better than for other configurations), then the system is simulated again with more refined models of the selected storage units.
7. After this, if the system is considered as efficient (disturbances effectively absorbed by storage devices), the storage devices choice is validated; otherwise, the sizing loop is computed again.

4.1 Hybridization Factors

The storage devices are integrated in the hybrid system in an aim to optimize the system performance. Their choice must therefore meet a real need of power in the operation conditions. To do this, it is necessary to provide criteria for decision support that can give the designer an idea about the potential reduction of fluctuations when storage units are used.

The required characteristics (capacity, dynamics) of the storage devices technologies depend mainly on the variations' profile of the power to be compensated by the diesel generator. The relative variation of power, defined as the power hybridization factor *PHF* (Eq. 1), reflects the magnitude of the fluctuating power compared to the average value of the diesel generator mission.

In this equation, $P_{\max}$ and P_{mean} are, respectively, the maximum and average values of the *DG* power. The system is very favorable to hybridization if PHF is equal to 1 and very unfavorable for *PHF* equal to 0.

$$\text{PHF} = \begin{cases} \dfrac{P_{\max} - P_{\text{mean}}}{P_{\max}} & \text{if} \quad P_{\text{mean}} \geq 0 \ \text{ and } \ P_{\max} > 0 \\ 1 & \text{else} \end{cases} \tag{1}$$

Nevertheless, it appears that two profiles of same maximum power and same average power, with same *PHF*, may contain fluctuations with different nature. Thus, for the same *PHF*, the capacity of storage units may be more or less large

depending on the fluctuations speed (frequency) and their amplitudes related to the mean power. A second factor is therefore necessary in an aim to take into account the nature of the disturbances contained in the mission profile of the *DG*.

The energy hybridization factor (*EHF*) is used to express the nature (frequency and regularity) of the energy variability (Eq. 2). Its value indicates the degree of difficulty to integrate the storage units in the system. A more regular profile (the largest *EHF*) contains less energy to store and therefore a greater potential of hybridization. It is therefore more appropriated to the energetic hybridization of the system.

$$\mathrm{EHF} = \begin{cases} \dfrac{P_{\max}}{\Delta E_{\mathrm{s}}} & \text{if} \quad P_{\max} \geq 0 \ \text{ and } \ \Delta E_{\mathrm{s}} \neq 0 \\ +\infty & \text{else} \end{cases} \tag{2}$$

The component ΔE_{s} is estimated as presented in Eq. (3).

$$\begin{cases} E_{\mathrm{s}} = \displaystyle\int_0^{\tau} (p(t) - p_{\mathrm{mean}})\mathrm{d}t \\ \Delta E_{\mathrm{s}} = \max(E_{\mathrm{s}}(t)) - \min(E_{\mathrm{s}}(t)) \end{cases} \tag{3}$$

4.2 Application of the PHF and EHF Factors

To illustrate this method, a wind-diesel system is considered, without using storage devices and by assuming that there are no short-term fluctuations in the PV power. The potential wind current and the load profile of the considered system are presented in Fig. 5. The difference between these two signals is to be compensated by the diesel generator (Fig. 6) if the storage devices are not used. This is called the *DG* primary mission profile.

Application of the *PHF* and *EHF* factors equations to this profile of mission provides a PHF = 47% and an EHF = 1.55 mHz. Thus, the magnitudes of the fluctuations and their regularity are relatively significant compared to the average

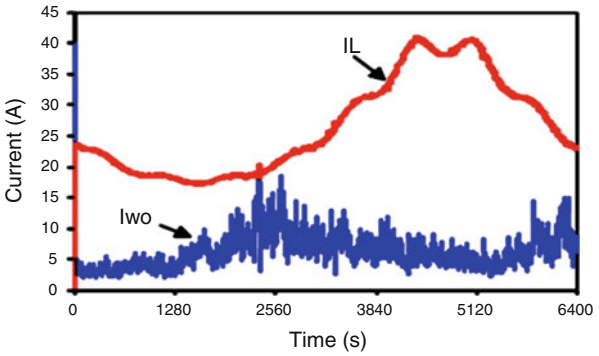

Fig. 5 Wind current and load profile I_{L} of the considered site

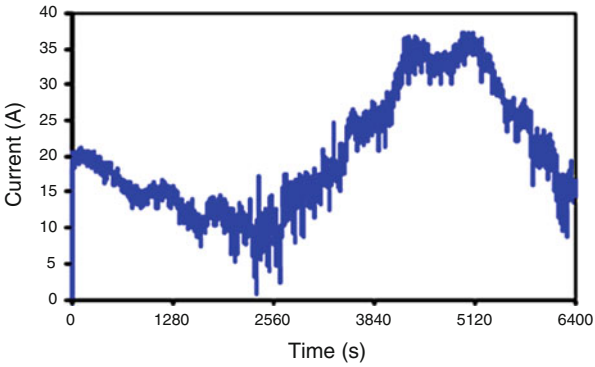

Fig. 6 Current to be compensated by the diesel generator

power. This allows the integration of storage devices in the wind-diesel system. The choice of the appropriate storage technologies can be done from the analysis of the storage devices characteristics and their lifetime.

4.3 Ultracapacitor and Battery Lifetime Analysis

4.3.1 Ultracapacitors' Lifetime Analysis

The lifetime of the ultracapacitors (*UC*) is mainly affected by the combined effects of the voltage and the operating temperature [26, 27]. The performance of *UC* decreases with the capacity decreasing or with the increasing of the internal resistor. Thus, the end of lifetime is reached when the capacity decreases by 20% of its nominal value and/or when the internal resistor increases by 200%, according to industry standards [26]. The lifetime of *UC* is less affected by the number of cycles compared to battery ones. In a wind-diesel system, the batteries' lifetime is reduced by the large number of micro-cycles contained in wind power. For this reason, it is important to take into account the effects of operation conditions on the batteries' lifetime in the wind-diesel hybrid system design.

4.3.2 Battery Lifetime Estimation

The battery lifetime is strongly affected by the number of charge and discharge cycles [28–30]. Thus, they are the weak link of the system when they are used in a wind energy system.

The method for estimating the battery lifetime is illustrated in Fig. 7. The rainflow counting method is applied to the battery energy, estimated from simulations or experimental results, to quantify the number of cycles applied to the batteries. This method is illustrated through an example (Figs. 8 and 9).

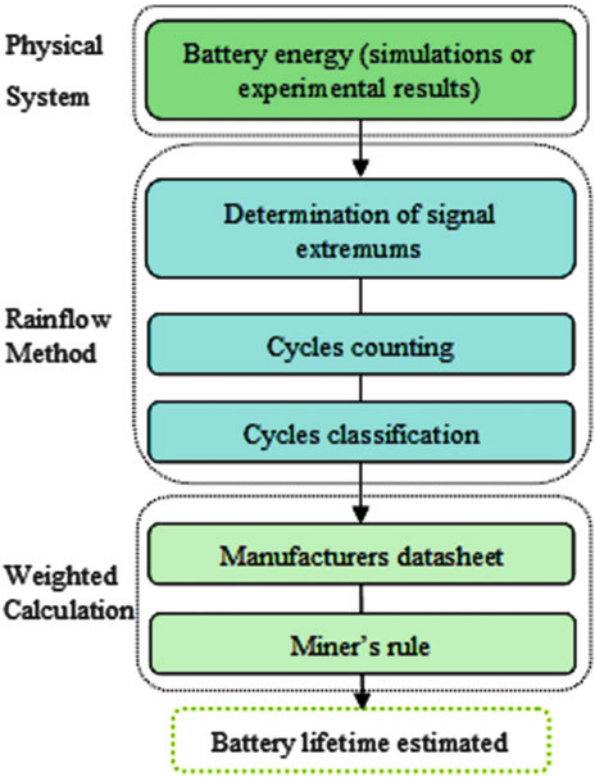

Fig. 7 Battery lifetime estimation process

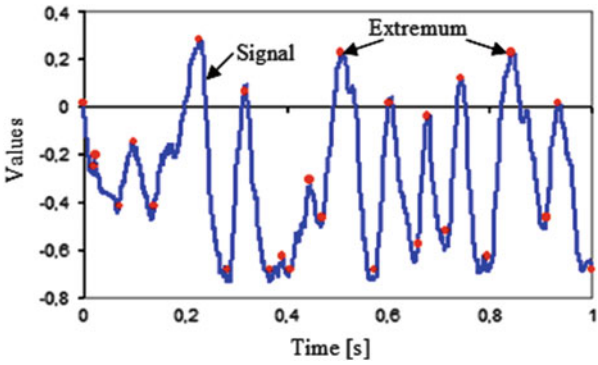

Fig. 8 Extremums extraction from the considered signal

1. Extremums are extracted from the considered signal as shown in Fig. 8.

   Then, these extremums are classified into two column matrices. The first column is dedicated to the corresponding number of each extremum. The second column contains the extremums values.

   In this study, three points rainflow method is used. It consists in tests based on three consecutive points E_i, E_{i+1}, E_{i+2} as presented in Eq. (4). If $\Delta E_i \leq \Delta E_{i+1}$,

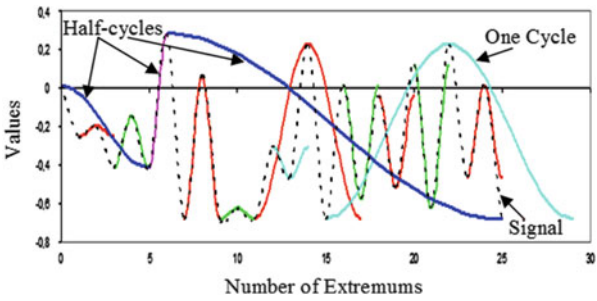

Fig. 9 Cycles counting

one cycle is counted, else zero cycle is counted. This strategy is illustrated in Fig. 9.

$$\begin{cases} \Delta E_{\mathrm{i}} = |E_{\mathrm{i}} - E_{\mathrm{i+1}}| \\ \Delta E_{\mathrm{i+1}} = |E_{\mathrm{i+1}} - E_{\mathrm{i+2}}| \end{cases} \tag{4}$$

2. The individual charge and discharge cycles are then stored into classes (usually 20 classes are used) of equal size. These classes correspond to different depths of discharge, and the last class corresponds to the complete discharge and recharge cycle of a fully battery [30, 31].
3. Then, the weight of each depth of battery charge is determined from the batteries' data provided by the manufacturers. From these data, the cycle's numbers versus the magnitude of the discharge current is determined as Eq. (5). The parameters a_1, a_2, a_3, and a_4 are obtained by using the method of least mean squares. C_{F} is defined as cycles to failure.

$$C_{\mathrm{F}} = a_1 + a_2 \mathrm{e}^{-a_3 \cdot \mathrm{DoD}} + a_4 \mathrm{e}^{-a_5 \cdot \mathrm{DoD}} \tag{5}$$

The lifetime is then calculated from the *Palmgren-Miner* rule by considering that the fraction of lifetime consumed during a given cycle is $1/C_{\mathrm{F}}$. The total damage D of the batteries over a given time is expressed in Eq. (6) by considering N_i cycles of 20 fractions of discharge depths that are classified from 0.05 to 1 (i.e., 5–100%). The end of the battery lifetime is reached when $D = 1$, and the battery must be replaced. $C_{\mathrm{F},i}$ is the number of cycles to failure according to class i.

$$D = \sum_{i=1}^{20} N_i \frac{1}{C_{\mathrm{F},i}} \tag{6}$$

In the case of this study, it is assumed that one charge and discharge cycle of the battery is equal to 6,400 s. This period of charge is chosen arbitrarily in aims to illustrate the sizing method. In this condition, the simulation results can be extrapolated to obtain a yearly data in an aim to determine the batteries' lifetime.

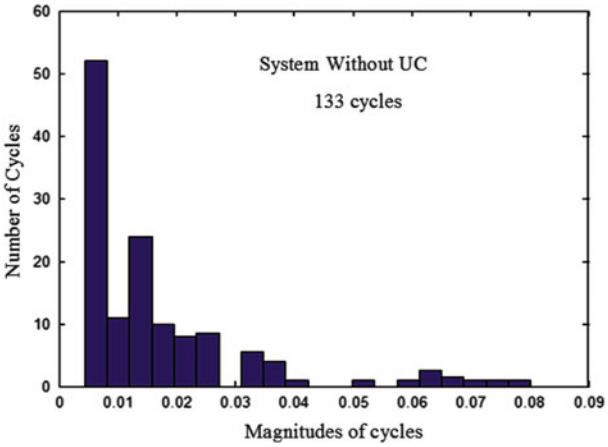

Fig. 10 Number of cycles of the battery in the system without UC

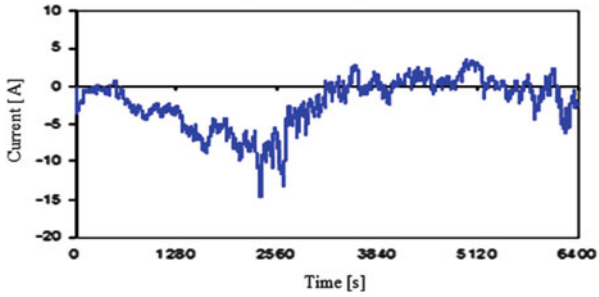

Fig. 11 Battery instantaneous current

4.3.3 Simulation Results for Lifetime Estimation

In first time, the simulations are doing with wind generator, diesel generator, and the batteries' bank to satisfy the load need. The number of cycles for different magnitudes contained in the battery state of charge is illustrated in Fig. 10 in this context.

In second time, *UC* are added to the hybrid system. Batteries and *UC* currents are presented, respectively, in Figs. 11 and 12 in an aim to show the density of the *UC* current. It can be observed that the big part of the fluctuations is effectively absorbed by the *UC*. The resulting number of the batteries' cycles is presented in Fig. 13. In a system without *UC*, 123 cycles and 10 half-cycles are counted. After adding the *UC* in the system, five cycles and ten half-cycles are counted. Thus, the battery's number of cycles is greatly reduced when *UC* are used and its lifetime is improved.

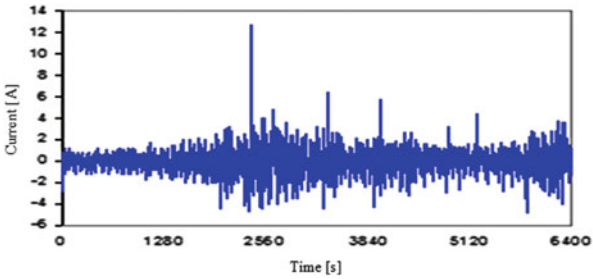

Fig. 12 UC instantaneous current

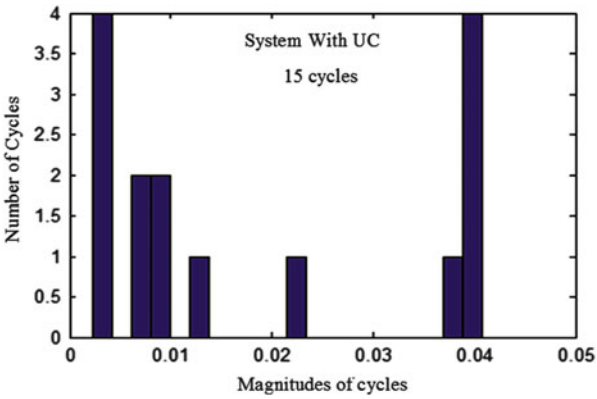

Fig. 13 Number of cycles of the battery in the system with UC

5 Energy Management and Converter Control Strategies in the Hybrid System

The control levels of the energy production and transfer in the hybrid system are detailed in this section. The first level (global supervisory) integrates the global control laws. The wind energy frequencies are distributed, and the control references are generated for local controllers. The second level (local control) is dedicated to each converter to be controlled.

5.1 Wind Energy Fluctuation Distribution

Qualitatively, each storage device has a proper reaction time according to Ragone theory [32]. Thus, in the time horizon of the wind energy, it is possible to assign a storage device suitable for each segment corresponding to its dynamics.

In this approach of storage devices using the wind power can be divided into three components. The current supplied by the wind generator to the DC-bus voltage is assumed to be a sum of low-frequency component (I_{BF}), middle-frequency component (I_{MF}), and high-frequency component (I_{HF}) as shown in

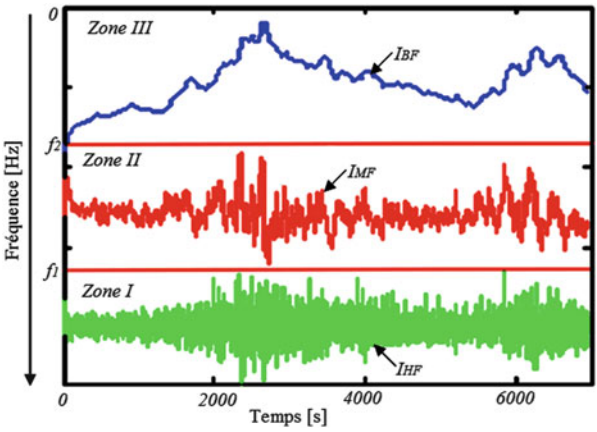

Fig. 14 Wind generator current distribution in three components

Fig. 14. The high-frequency currents (*zone I*) are allocated to *UC*, and the medium-frequency currents (*Zone II*) are mitigated by the batteries.

In this context, the DG and the PV provide the difference between the load demand and the mean value of wind power (*zone III*). These components are expressed in Eq. (7).

$$\begin{cases} I_{\text{wo}} = I_{\text{BF}} + I_{\text{MF}} + I_{\text{HF}} \\ I_{\text{bato}} = I_{\text{MF}} \\ I_{\text{uco}} = I_{\text{HF}} \\ I_{\text{do}} + I_{\text{pvo}} = I_{\text{L}} - I_{\text{BF}} \end{cases} \tag{7}$$

Two low-pass filters are used to obtain the three components of the wind power. The filter frequencies are f_1 and f_2, with $f_1 > f_2$. The *UC* and battery reference currents are given in Eq. (8).

The choice of the filter frequencies is related to the power and energy densities of the considered storage device. These frequency values can be estimated from the Ragone theory, according to Eq. (9).

$$\begin{cases} I_{\text{uco-ref}} = I_{\text{wo}} - I_{\text{wo}} \cdot \left\{ 1/\left(1 + s \cdot \tau_1/Q + (s \cdot \tau_1)^2\right) \right\} \\ I_{\text{bato-ref}} = \Delta I - \Delta I \cdot \left\{ 1/\left(1 + s \cdot \tau_2/Q + (s \cdot \tau_2)^2\right) \right\} \\ \tau_{1,2} = 1/\left(2 \cdot \pi \cdot f_{1,2}\right), \qquad \Delta I = I_{\text{wo}} - I_{\text{uco}} \end{cases} \tag{8}$$

In this equation, ρ_{p} and ρ_{e} are, respectively, power and energy densities.

$$f = \frac{\rho_{\text{p}}}{\rho_{\text{e}}} \tag{9}$$

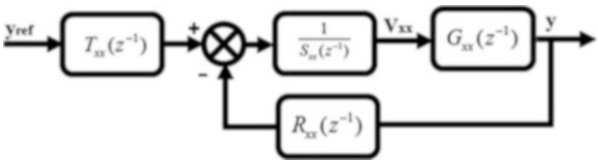

Fig. 15 Closed loop used for parameter estimation of the current and voltage controllers

Table 1 Closed-loop parameter design

Parameters	Batteries current controller	Wind current controller	UC current controller
Process	L_{bat}	L_{w}	L_{uc}
G_{xx}	$G_{i_{\text{bat}}}$	$G_{i_{\text{wo}}}$	$G_{i_{\text{uc}}}$
y_{ref}	$I_{\text{bat\_ref}}$	$I_{i_{\text{wo\_ref}}}$	$I_{\text{uco-ref}}$
y	I_{bat}	$I_{i_{\text{wo}}}$	I_{uc}
V_{xx}	$V_{L_{\text{bat}}}$	$V_{L_{\text{w}}}$	$V_{L_{\text{uc}}}$
R_{xx}	$R_{i_{\text{bat}}}$	$R_{i_{\text{w}}}$	$R_{i_{\text{uc}}}$
S_{xx}	$S_{i_{\text{bat}}}$	$S_{i_{\text{w}}}$	$S_{i_{\text{uc}}}$
$R_{0\text{xx}}$	$R_{0i_{\text{bat}}}$	$R_{0i_{\text{w}}}$	$R_{0i_{\text{uc}}}$
$R_{1\text{xx}}$	$R_{1i_{\text{bat}}}$	$R_{1i_{\text{w}}}$	$R_{1i_{\text{uc}}}$
ω_{xx}	$\omega_{i_{\text{bat}}}$	$\omega_{i_{\text{w}}}$	$\omega_{i_{\text{uc}}}$
β_{xx}	$\beta_{i_{\text{bat}}}$	$\beta_{i_{\text{w}}}$	$\beta_{i_{\text{uc}}}$

5.2 Polynomial Controller Design Method

The control strategy is based on a closed loop of current control, while the DC-bus voltage is stabilized by the *DG*. The series inductance L_{xx} is considered as the process of the current loop. The corresponding differential equation is expressed by Eq. (10). Note that the index "xx" is used because the same method is applied to control the wind generator, battery, and ultracapacitor currents. $V_{L_{\text{xx}}}$ is the voltage drop in L_{xx} inductor estimated from the controller for the corresponding energetic chain.

$$V_{L_{\text{xx}}} = L_{\text{xx}} \cdot \frac{d}{\text{d}t}(I_{\text{xx}}) \tag{10}$$

The resulting transfer function is Eq. (11)

$$G_{\text{xx}}\left(z^{-1}\right) = \frac{I_{\text{xx}}(z^{-1})}{V_{\text{xx}}(z^{-1})} = \frac{T_{\text{e}}}{L_{\text{xx}}} \cdot \frac{z^{-1}}{1 - z^{-1}} = \frac{B_{\text{xx}}(z^{-1})}{A_{\text{xx}}(z^{-1})} \tag{11}$$

The polynomial controller is defined by three components $R_{\text{xx}}(z^{-1})$, $S_{\text{xx}}(z^{-1})$, and $T_{\text{xx}}(z^{-1})$. The basic control loop used for estimating the parameters is shown in Fig. 15. The same scheme is applied to the wind and supercapacitors current control according to Table 1. So, the polynomial controller equations can be used for each case (wind generator, batteries, or ultracapacitors) by changing only the variable names and values.

The controller parameters are estimated from the Bezout's identity (Diophantine equation). The characteristics polynomial, expressed by Eq. (12), is a second-order equation. So, the closed loop can be a second-order equation [6]. $G_{xx}(z^{-1})$ is a first-order system. Consequently, $R_{xx}(z^{-1})$ and $S_{xx}(z^{-1})$ can be first-order equations.

$$P_{xx}\left(z^{-1}\right) = 1 + p_{1xx} \cdot z^{-1} + p_{2xx} \cdot z^{-2} \tag{12}$$

The minimal static error, with a perturbation rejection, is obtained by choosing $R_{xx}(z^{-1})$ and $S_{xx}(z^{-1})$ according to Eq. (13).

$$\begin{cases} S_{xx}(z^{-1}) = 1 - z^{-1} \\ R_{xx}(z^{-1}) = r_{0xx} + r_{1xx} \cdot z^{-1} \end{cases} \tag{13}$$

The transfer function of the closed loop is expressed as Eq. (14)

$$F_{xx}\left(z^{-1}\right) = \frac{T_{xx}(z^{-1}) \cdot B_{xx}(z^{-1})}{A_{xx}(z^{-1}) \cdot S_{xx}(z^{-1}) + B_{xx}(z^{-1}) \cdot R_{xx}(z^{-1})} \tag{14}$$

In a particular case, it can be considered an equality between $R(z^{-1})$ and $T(z^{-1})$ (Eq. 11) in aims to reduce the number of the parameters to be identified.

$$T_{xx}\left(z^{-1}\right) = R_{xx}\left(z^{-1}\right) \tag{15}$$

The desired polynomial $P_{xx}(z^{-1})$ corresponds to the denominator of the closed-loop transfer function (F_{xx}) (Eq. 16).

$$\begin{cases} P_{xx}(z^{-1}) = A_{xx}(z^{-1}) \cdot S_{xx}(z^{-1}) + B_{xx}(z^{-1}) \cdot R_{xx}(z^{-1}) \\ P_{xx}(z^{-1}) = \left(1 - z^{-1} \cdot \exp(-\omega_{xx} \cdot T_e)\right)^2 \end{cases} \tag{16}$$

The coefficients (P_{1xx}) and (P_{2xx}) are identified by developing and by comparing the polynomial $P_{xx}(z^{-1})$ to Eq. (12), using Eq. (13). The pulsation ω_{xx} is function of the converter switching frequency F_{dec}. Same value (10 kHz) is used for all converters used in the system. For current control, it can be considered that $\omega_{xx} \leq \frac{2 \cdot \pi \cdot f_{dec}}{10}$.

The coefficients of the current loop controller are identified as Eqs. (17) and (18). T_e is the sampling period.

$$\begin{cases} r_{0xx} = (p_{1xx} + 2) \cdot \frac{L_{xx}}{T_e} \\ \quad\quad = 2 \cdot \{1 - \exp(-\omega_{ixx} \cdot T_e)\} \cdot \frac{L_{xx}}{T_e} \\ \quad\quad \approx 2 \cdot \left(1 - \frac{1}{1 + \omega_{xx} \cdot T_e}\right) \cdot \frac{L_{xx}}{T_e} \end{cases} \tag{17}$$

$$\begin{cases} r_{1xx} = (p_{2xx} - 1) \cdot \dfrac{L_{xx}}{T_e} \\ \quad = \{\exp(-2 \cdot \omega_{xx} \cdot T_e) - 1\} \cdot \dfrac{L_{xx}}{T_e} \\ \quad \approx \left(\dfrac{1}{1 + 2 \cdot \omega_{xx} \cdot T_e} - 1\right) \cdot \dfrac{L_{xx}}{T_e} \end{cases} \tag{18}$$

The coefficients determined previously are obtained by considering a lossless system and by using some approximations. So, in actual operation, it can be interesting to adjust these values by adding the parameter β_{xx}, according to Eq. (19):

$$\omega_{xx} \leq \frac{2 \cdot \pi \cdot f_{dec} \cdot \beta_{xx}}{10} \tag{19}$$

The estimated parameters of the controller are implemented in a microchip microcontroller PIC18F4431. β_{xx} is changed online to track, and adjust, the good value of the polynomial controller parameters that ensure an efficient operation. The current control algorithm is defined as Eq. (20).

$$\begin{cases} \Delta y_{xx}(n) = y_{ref}(n) - y(n) \\ V_{xx}(n+1) = V_{xx}(n) + r_{0xx} \cdot \Delta y_{xx}(n+1) + r_{1xx} \cdot \Delta y_{xx}(n) \\ \Delta y_{xx}(n+1) = y_{ref}(n+1) - y(n+1) \end{cases} \tag{20}$$

5.3 *Ultracapacitor Energy Conversion System*

Ultracapacitors are used to mitigate the short-term fluctuations of the *WG* current. A characterization method of *UC* is presented in [33]. The *UC* energy is managed by using a bidirectional buck-boost converter. A polynomial controller is implemented to control the *UC* charge and discharge current I_{uc}, according to the method presented previously. The reference current I_{uc_ref} is estimated by using the converter's efficiency Eq. (21). $I_{uco\text{-}ref}$ is generated according to Eq. (8) with $f_1 = 20$ MHz. η_{uc}, η_w, η_{bat} are the converters' theoretical efficiencies, respectively, for UC, wind generator, and battery systems. α_{1uc}, α_{2uc} are the *UC* converter duty cycles in buck and boost modes, respectively.

$$I_{uc\_ref} = \frac{V_{bus}}{V_{uc}} \cdot \eta_{uc} \cdot I_{uco\_ref} \tag{21}$$

The duty cycles (buck and boost modes) are expressed in Eq. (22). These control laws are used to control the *UC* converters.

$$\alpha_{uc1} = \frac{V_{L_{uc}} + V_{uc}}{V_{bus}},\ \alpha_{uc2} = 1 - \frac{V_{uc} - V_{L_{uc}}}{V_{bus}} \tag{22}$$

The best method to improve the batteries' lifetime is to prevent them from fast dynamic currents and from high number of charge and discharge cycles [28, 34]. In this paper, the batteries' module is interfaced by a bidirectional buck-boost

converter (Fig. 23). The converter's efficiency is used to estimate the batteries' reference current I_{bat_ref} as expressed in Eq. (23). α_{1bat}, α_{2bat} are the batteries' converter duty cycles (buck and boost modes). In this equation, the converter output reference current I_{bato_ref} is generated according to Eq. (8). The wind generator output current I_{wo} is measured and filtered by a second-order low-pass filter, with $f_2 = 1.3$ mHz.

$$I_{bat\_ref} = \frac{V_{bus}}{V_{bat}} \cdot \eta_{bat} \cdot I_{bato\_ref} \tag{23}$$

The duty cycles for buck and boost modes are estimated from Eq. (24).

$$\alpha_{bat1} = \frac{V_{L_{bat}} + V_{bat}}{V_{bus}}, \quad \alpha_{bat2} = 1 - \frac{V_{bat} - V_{L_{bat}}}{V_{bus}} \tag{24}$$

The use of two complementary storage devices (*UC* and batteries) enables a match between the dynamics of the interconnected sources and their missions. But, the coupling between these components is not sufficient to guarantee the system performance. It is necessary to design storage units by taking into account the actual operating conditions, the strategies for energy management, and the converters control methods.

Simulations are conducted by using Matlab/Simulink software to illustrate the proposed strategies.

6 Simulation Results

The hybridization criteria are applied to the *DG* mission in the no-storage hybrid system. The following values are obtained: PHF = 57% and EHF = 20 MHz. These results show that the *DG* mission is favorable to the use of storage devices.

Simulations are performed to illustrate the efficiency of the proposed strategy for energy management in a wind-PV-DG-UC-battery system. A fluctuating power is provided by the *WG* as presented in Fig. 16. The *WG* system operates at the maximum power as shown by Fig. 17.

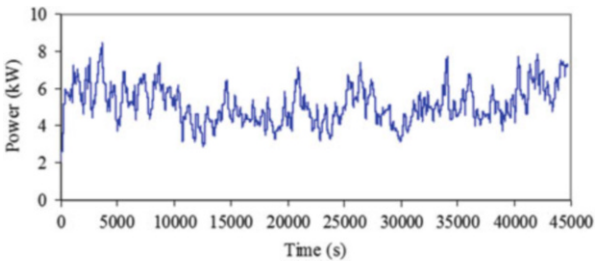

Fig. 16 Power provided by the WG

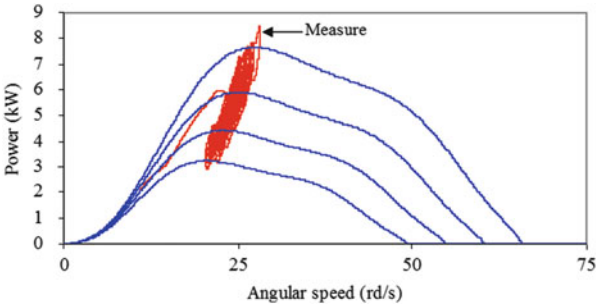

Fig. 17 WG power as function of rotating speed

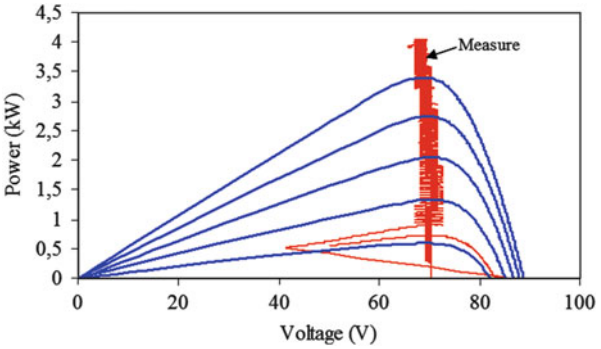

Fig. 18 PV power as function of PV voltage

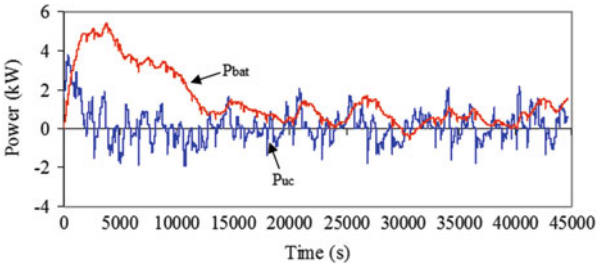

Fig. 19 Stored power by *UC* and batteries

In Fig. 18, it can be observed that the *PV* system operates at its maximum power for each value of solar radiation. The disturbances induced by the *WG* power on the DC-bus are effectively absorbed by the storage units as shown in Fig. 19. It can be observed that the major part of the micro-cycles is smoothed by the *UC*. Doing this, the batteries' cycles are greatly reduced and their lifetime improved.

In Fig. 20, it can be observed that the *DG* power is smoothed and varies according to the variations of load (P_{Load}), PV (P_{PV}), and *WG* mean power ($P_{\text{wo\_mean}}$). Figure 21 presents the *DC-bus* voltage control result, which is well regulated around 110 V from the *DG*. This confirms the good efficiency of the energy management and of the power converters' control method.

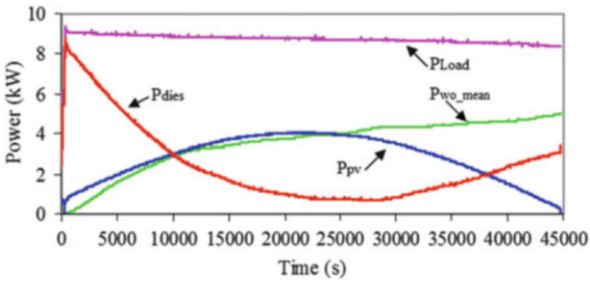

Fig. 20 Load, DG, and PV powers

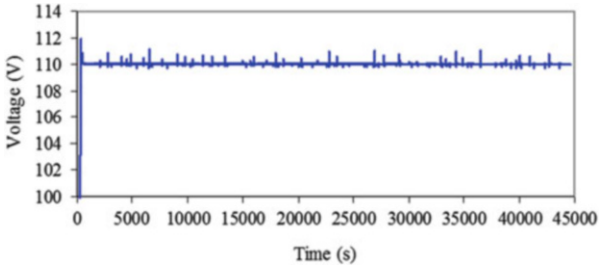

Fig. 21 *DC-bus* voltage regulated around 110 V by the *DG*

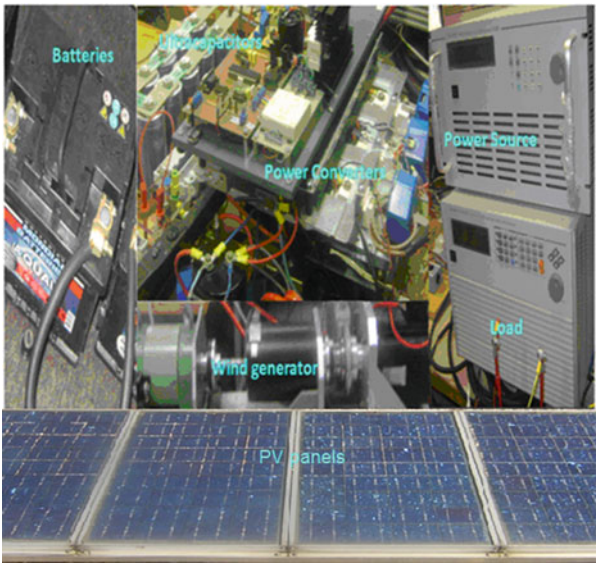

Fig. 22 Hybrid system experimental test bench

7 Experimental Setup and Results

An experimental setup (Fig. 22) including wind generator emulator, PV panels, and programmable power source (*PPS*), *UC*, batteries, and variable electric load is realized in laboratory. A hardware-in-the-loop (HIL) system is used to emulate the wind generator. The wind turbine model is implemented in a Matlab/Simulink

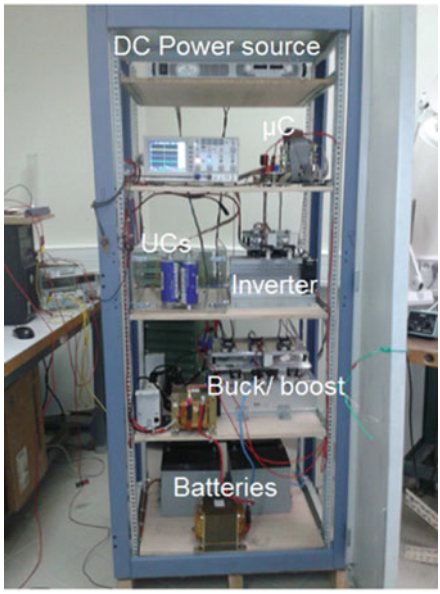

Fig. 23 Batteries and ultracapacitors characterization bench (BUCBench)

software, and information exchange between the software and the hardware is ensured by a Dspace card. Two coupled machines are associated to the electronics converters as hardware system. One machine is used as a motor which operates according to the wind turbine speed, provided by the Simulink model, and drives the second machine (generator). The diesel generator is emulated by the programmable power source (*PPS*) that ensures the DC-bus stability and the smoothed power compensation.

The characterization of the storage devices is realized for the simulation models' development by means of the test bench (BUCBench) designed in the laboratory (Fig. 23). The control and energy management algorithms are implemented in a microchip's microcontroller (PIC18F4431). LabVIEW software and PXI station are used for data monitoring.

The experimental results of the wind generator current I_w are presented in Fig. 24. A zoom of this current compared to its reference is plotted in Fig. 25. These curves show that the proposed control strategy is satisfactory and performing. Figure 26 presents the UC controller reference value compared to the measured current. A zoom of these curves is illustrated in Fig. 27. It can be observed that the reference values are well tracked, and the implemented control law is very interesting. These results enable to conclude that the major part of the fluctuating current provided by the wind generator is absorbed by ultracapacitors. Figure 28 shows the battery's measured current compared to its controller reference current estimated from Eq. (16). The load current and the currents provided to the DC-bus by the DGE and by the PV panels are illustrated in Fig. 29.

Comparing the all measured currents in DC-bus (I_w, I_{uco}, I_{bato}, I_d, I_{pvo}, and I_{Load}), it can be observed that the PPS current (I_d) is smoothed, and the major part of the

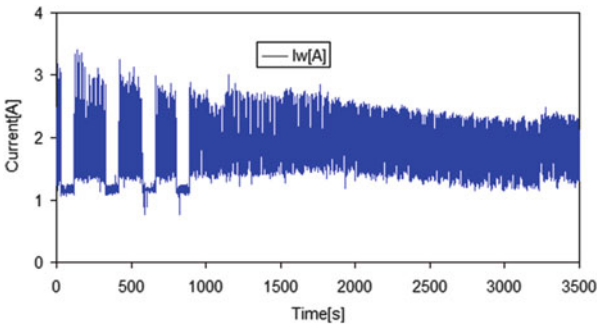

Fig. 24 Wind generator current I_w

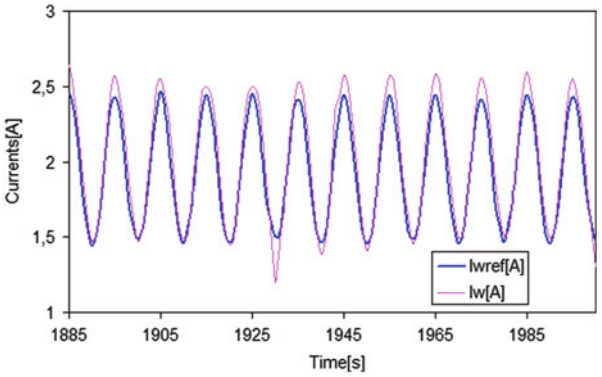

Fig. 25 Zoom of the WGE's current compared to its reference value

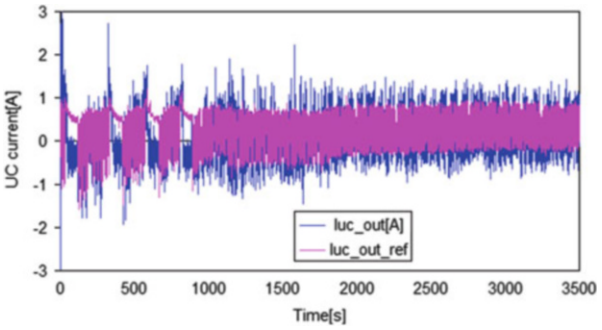

Fig. 26 UC current I_{uc_out} compared to its reference value $I_{uc\_out\_ref}$

wind current fluctuations is absorbed by the *UC* and batteries. So, as expected, the resulting current from the interaction between the WGE and the storage devices has slow variations and corresponds to the mean value of the I_w.

Figure 30 presents the DC-bus and the PV panel's voltages. It can be observed that the DC-bus voltage is well maintained around a constant value (48 V) by the *PPS*. The storage device (batteries and *UC*) voltages are plotted in Fig. 31. These voltages vary according to the system evolutions.

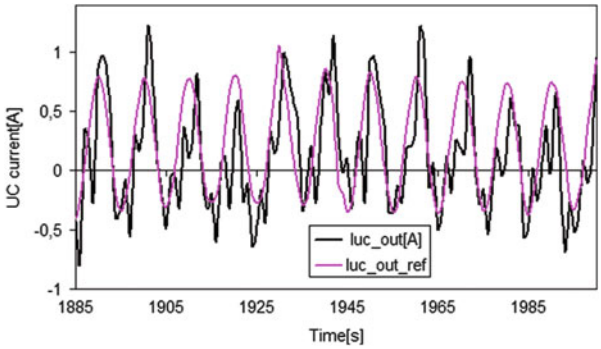

Fig. 27 Zoom of the UC's current compared to its reference value

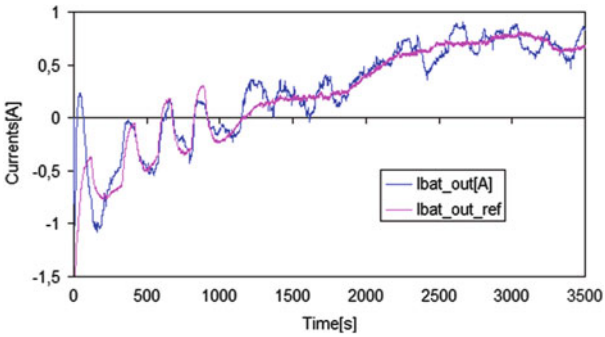

Fig. 28 Battery current $I_{\text{bat\_out}}$ compared to its reference value $I_{\text{bat\_out\_ref}}$

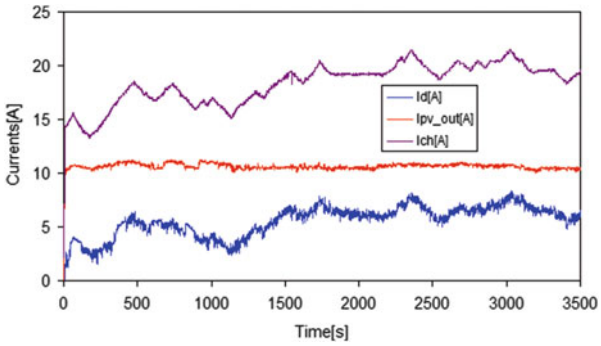

Fig. 29 Electric load, PPS, and the PV currents

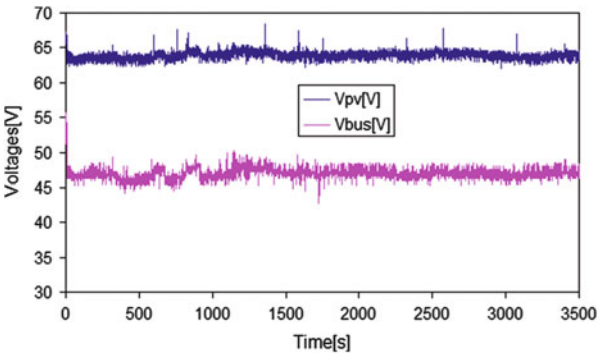

Fig. 30 PV panels and DC-bus voltages

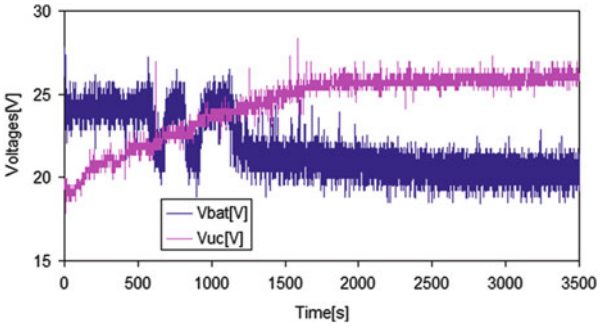

Fig. 31 Battery and UC voltages

Conclusion

In this paper, strategies of energy transfer and fluctuation smoothing, applied to a wind-PV-diesel hybrid system, are proposed. Batteries and ultracapacitors are used in a complementary mode to mitigate the fluctuating currents induced by the wind speed stochastic variations. The renewable sources (PV and wind generator) operate at their maximum power point. The use of the PV power can reduce the diesel generator contribution and the fuel consumption. The diesel generator provides a smoothed current and maintains the voltage at a constant value. Efficiency of the implemented control strategies is shown through some experimental results analysis.

Simulation results show the need of the storage devices for fluctuation mitigation, in aims to ensure optimal conditions of the diesel generator operation. The choice of the storage device technologies is performed from the analysis of the device characteristics and by using the hybridization factors. It is shown that the combination of the ultracapacitors and batteries is an interesting solution. This can improve the batteries' lifetime according to the rainflow cycles counting method used in this study.

(continued)

The experimental results show that the use of ultracapacitors can effectively mitigate the short-term variations. Thus, the batteries' storage cycles can be controlled safely with a total lifetime increase benefit. In this context, the diesel generator compensates the deficit of energy while stabilizing the DC-bus.

References

1. Randolph J, Masters GM (2008) Energy for sustainability, technology, planning, policy. Island Press, Washington DC
2. Kabouris J, Kanellos FD (2010) Impacts of large-scale wind penetration on designing and operation of electric power systems. IEEE T Sust Energy 1(2):107–114
3. Li W, Joos G, Bélanger J (2010) Real-time simulation of a wind turbine generator coupled with a battery supercapacitor energy storage system. IEEE T Ind Electron 57(4):1137–1145
4. Tankari MA, Camara MB, Dakyo B, Nichita C (2011) Wind power integration in hybrid power system with active energy management. Int J Comput Math Elect Electron Eng 30(1):245–263
5. Tankari MA, Camara MB, Dakyo B, Nichita C (2010) Ultracapacitors and batteries integration in wind energy hybrid system - using the frequencies distribution method. Int Rev Elect Eng IREE 5(2):521–529, ISSN 1827–6679
6. Guoju Z, Xisheng T, Zhiping Q (2010) Research on battery supercapacitor hybrid storage and its application in microgrid. In: Proceedings of IEEE Asia-Pacific power and energy engineering conference (APPEEC), pp 1–4
7. Atwa YM, El-Saadany EF (2010) Optimal allocation of ESS in distribution systems with a high penetration of wind energy. IEEE T Power Syst 25(4):1815–1822
8. Saha TK, Kastha D (2010) Design optimization and dynamic performance analysis of a standalone hybrid wind–diesel electrical power generation system. IEEE T Energy Conver 25 (4):1209–1217
9. Brekken TKA, Yokochi A, Jouanne AV, Yen ZZ, Hapke HM, Halamay DA (2011) Optimal energy storage sizing and control for wind power applications. IEEE T Sust Energy 2(1):69–77
10. John K, Kanellos FD (2010) Impacts of large-scale wind penetration on designing and operation of electric power systems. IEEE T Sust Energy 1(2):107–114
11. Bragard M, Soltau N, Thomas S, De Doncker RW (2010) The balance of renewable sources and user demands in grids: power electronics for modular battery energy storage systems. IEEE T Power Electr 25(12):3049–3056
12. Abbey C, Li W, Joós G (2010) An online control algorithm for application of a hybrid ess to a wind–diesel system. IEEE T Ind Electron 57(12):3896
13. Teleke S, Baran ME, Bhattacharya S, Huang AQ (2010) Optimal control of battery energy storage for wind farm dispatching. IEEE T Energy Conver 25(3):787–794
14. Khaligh A, Li Z (2010) Battery, ultracapacitor, fuel cell, and hybrid energy storage systems for electric, hybrid electric, fuel cell, and plug-in hybrid electric vehicles: state of the art. IEEE T Veh Technol 59(6):2806–2814
15. Thounthong P, Chunkag V, Panarit S (2009) Comparative study of fuel-cell vehicle hybridization with battery or supercapacitor storage device. IEEE T Veh Technol 58(8):3892–3904
16. Burton T, Sharpe D, Bossanyi E (2001) Wind energy handbook. Wiley, New York
17. Seul-Ki K, Jin-Hong J, Chang-Hee C, Jong-Bo A, Sae-Hyuk K (2008) Dynamic modeling and control of a grid-connected hybrid generation system with versatile power transfer. IEEE T Ind Appl 55(4):1677–1688
18. Eisenhut C, Krug F, Schram C, Klockl B (2007) Wind-turbine model for system simulations near cut-in wind speed. IEEE T Energy Conver 22(2):414–420

19. Bleijs JAM (2007) Wind turbine dynamic response–difference between connection to large utility network and isolated diesel micro-grid. IET Renew Power Gen 1(2):95–106
20. Tankari MA, Camara MB, Dakyo B, Nichita C (2010) Ultracapacitors and batteries integration in wind energy hybrid system - using the frequencies distribution method. Int Rev Electr Eng 5 (5)
21. Stavrakakis GS, Kariniotakis GN (1995) A general simulation algorithm for the accurate assessment of isolated diesel-wind turbines systems interaction. IEEE T Energy Conver 10(3):577–590
22. Koczara W, Chlodnicki Z, Al-Khayat N, Brown NL (2008) Energy management and power flow of decoupled generation system for power conditioning of renewable energy sources. In: 13th International Power Electronics and Motion Control Conference (EPE-PEMC)
23. Leuchter J, Bauer P, Zobaa AF, Bojda P (2010) An interface converter of hybrid power sources with supercapacitors. In: Proceedings of 36th annual conference of the IEEE industrial electronics society (IECON'10), pp 3244–3251
24. Lee JH, Lee SH, Sul S-K (2009) Variable speed engine generator with supercapacitor, isolated power generation system and fuel efficiency. Int Conf IEEE Ind Appl Soc 45(6):2130–2135
25. Li W, Joos G (2008) A power electronic interface for a battery supercapacitors hybrid energy storage system for wind applications. In: Proceedings of IEEE annual power electronics specialists conference (PESC), pp 1762–1768
26. MAXWELL Technologies (2009) Product guide-maxwell technologies boostcap ultracapacitors. http://www.maxwell.com/pdf/1014627BOOSTCAPProductGuide.pdf. Doc. No. 1014627
27. Hammar A, Venet P, Lallemand R, Coquery G, Rojat G (2010) Study of accelerated aging of supercapacitors for transport applications. IEEE T Ind Electron 57(12):3972–3979
28. Jossen A (2006) Fundamentals of battery dynamics. Power Sources J 154:530–538
29. Wenzl H et al (2005) Life prediction of batteries for selecting the technically most suitable and cost effective battery. Power Sources J 144:373–384
30. Bindner H, Cronin T, Lundsager P, Manwell JF, Abdulwahid U, Baring-Gould I (2005) Benchmarking - lifetime modelling. enk6-ct-2001-80576. Riso National Laboratory, Denmark
31. Hansen AD, Sorensen P, Hansen LH, Bindner H (2000) Models for a stand-alone pv system. Riso National Laboratory, Roskilde. http://www.solenergi.dk/rapporter/sec-r-12.pdf
32. Christen T, Carlen MW (2000) Theory of Ragone plots. Int J Power Sources 91(2):210–216
33. Camara MB, Gualous H, Gustin F, Berthon A, Dakyo B (2010) DC/DC converters design for supercapacitors and battery power management in hybrid vehicle applications-polynomial control strategy. IEEE T Ind Electron 57(2):587–597
34. Chen LR, Wu SL, Chen TR, Yang WR (2010) Study of lead-acid battery charging by using sinusoidal current. Int Rev Electr Eng (IREE) 5(1)

Different Phase Change Material Implementations for Thermal Energy Storage

Mustapha Karkri, Gilles Lefebvre, and Laurent Royon

Abstract This paper presents the principal methods available for phase change material (PCM) implementation in different storage applications. The first part is devoted to a non-exhaustive overview of the various chemical processes used to develop stable PCM (such as microencapsulation, emulsion polymerization or suspension polycondensation, polyaddition, etc.) based on the available literature. The second part deals with shape-stabilized PCM, developed from an intimate combination of a polymer matrix and a phase change element. Materials able to include more thermal energy as usual ones are interesting as they increase the thermal inertia of the system that presents by this way advantages. The energy efficiency of buildings may be improved including PCMs that store and provide enthalpy from one hand and without any significant temperature modification during the phase change process on the other hand. If the solid phase of the PCM does not present any problem, it is not the same for the liquid phase which must be maintained mechanically at its assigned location. Furthermore, the PCM in the solid (and furthermore in the liquid phase) does not have mechanical properties which allow to use it as a structural material able to support charge loads. This paper presents different methods to distribute and maintain the PCM in the thermal solid matrix.

Keywords Phase change material (PCM), Energy storage, Heat storage, Energy efficiency

M. Karkri and G. Lefebvre (✉)
Université Paris Est, CERTES 61 Av. du Général de Gaulle 94010, Créteil Cedex., France
e-mail: mustapha.karkri@u-pec.fr; gilles.lefebvre@u-pec.fr

L. Royon
Laboratoire MSC, Université Paris-Denis Diderot, 10 rue Alice Domon et Léonie Duquet CC 7056, Paris cedex 13, France

G. Lefebvre et al. (eds.), *Environment, Energy and Climate Change II: Energies from New Resources and the Climate Change*, Hdb Env Chem (2016) 34: 123–150,
DOI 10.1007/698_2015_332, © Springer-Verlag Berlin Heidelberg 2015,
Published online: 9 June 2015

Contents

1 PCM Encapsulation

PCMs (phase change materials) have become an efficient way for thermal energy storage since they can absorb, store, or release large latent heat when the material changes phase or state [1–3]. The sizes of PCMs play important roles in determining their melting behaviors. It has been shown that if the size of PCM is reduced by a factor of 10, the time required for complete melting will reduce by a factor of 100 [4, 5]. In order to fully exploit the latent heats of fusion, it is desired to have the PCM as small as possible so that it can melt almost instantaneously. In many cases, the PCM should be encapsulated to prevent leakage upon melting, which can lead to the agglomeration of PCMs and the temperature delay in the following melting cycle [6].

Microencapsulation techniques provide opportunities to fabricate advanced PCMs with a greater heat transfer area, reduced reactivity with the outside environment, and controlled volume changes during the phase transition [7]. For these reasons, microencapsulated phase change materials (MEPCMs) have attracted considerable attention for over 20 years [8–11].

Microcapsules can be described as particles that contain core material surrounded by a coating or shell [12] and have diameters in the 1–1,000 μm range. Microencapsulation is widely used in commercial applications including carbonless copying paper, functional textiles, adhesives, cosmetics, pharmaceuticals, and other medical applications [13–19]. MEPCMs have also been used in solar energy installations and advanced building materials [20–22].

Coating materials used in the encapsulation of PCMs should meet the following characteristics:

- Have high strength, flexibility, and thermal stability
- Stable to UV exposure, barrier to moisture, air, etc.
- Stable to environmental conditions
- Capable of being used safely

- High thermal conductivity
- Not corrosive to container materials
- No migration of PCMs into coating materials
- No reaction between PCMs and coating materials

A literature survey on MEPCMs indicates that urea–formaldehyde (UF) resin, melamine–formaldehyde (MF) resin, and polyurethanes (PU) are usually selected as the microcapsule shell materials for the protection of PCMs [23].

The advantages of heat storage with encapsulated PCM, some of them not exclusive of PCM encapsulation, are the following:

- The PCM does not absorb the heat energy directly, the shape of storage may then be arbitrary, and the temperature gradient is generally more favorable.
- The PCM boundaries are always "dry," and liquid handling is consequently eliminated as the phase change occurs within the coating material.
- The effective heat transfer area is increased and provides larger heat transfers.
- Large quantities of thermal energy can be stored and released at a relatively constant temperature without significant volume changes. Sufficient free space exists within the supporting structure and size remains constant.
- Various needs for energy storage and suitable containment systems may be designed.
- No expansion system is needed as the PCMs propagate and contract directly in the microcapsules.
- The microcapsule embedment in heat storage is simple.
- PCM with different melting temperature could be used.
- The phase separation is avoided or at least hidden in the microcapsule.

Different encapsulation techniques may be applied to prepare microcapsules with a polymer cover and a PCM core. The strategies employed involve complex coacervation, suspension, emulsion, condensation, or polyaddition polymerization. The characteristics of different MEPCMs are given in Table 1.

Despite of its real advantages, two main drawbacks must be indicated.

The cost; for PCM encapsulation, MEPCMs need appropriate properties such as desired morphology, proper diameter distribution, thermal stability, shell mechanical strength, and penetration abilities [20]. One must pay attention to the variation (non-stability) of useful properties when many freezing-thawing phase changes occur.

1.1 Coacervation

The term coacervation was originated from the Latin word "acervus," meaning "heap" [37]. Coacervation is an encapsulation technique that involves the use of more than one colloid [6, 38]. Coacervation results from the mutual neutralization of two or more oppositely charged colloids in an aqueous solution. As a result of the reduction, the coacervated particles separate out to form two new phases with rich

Table 1 Representative property and stability studies of MEPCM in literature

Encapsulation method	PCM	Shell material	Microcapsules size (μm)	Temperature of phase transition (°C)	Heat of phase transition (kJ/kg)	References
Complex coacervation	*n*-Tetradecane (with tetradecanol as nucleating agents)	Gelatin	90–125; average: 100	Melting: 5.5°C; cooling:5.0°C (with 2 % tetradecanol)	182 (with 2% tetradecanol)	[24]
Polymerization	*n*-Octadecane (with different nucleating agents)	Melamine–formaldehyde		Depends on the kind and amount of nucleating agents	Generally 160–170	[25]
Polymerization	Hexadecane (C16H34)	Amino plastics		18°C melting	234	[26]
Ultrasonic assistant miniemulsion in situ polymerization	*n*-Octadecane	Styrene	50–200 nm; average: 124 nm	Close to that of *n*-octadecane	124.4	[27]
Two step coacervation	*n*-Octadecane	Melamine–formaldehyde	2	–	–	[28]
Coacervation	Paraffin wax	Gelatin and acacia	–	–	86	[6]
	Paraffin wax	Gelatin and acacia	–	–	193–221	[13]
	Coco fatty acid	Melamine–formaldehyde	1–1,000	29–31°C	-	[14]
Emulsion polymerization	*n*-Octacosane	PMMA	0.15–0.33	50.6°C	86	[29]
	Docosane	PMMA	0.14–0.47	41°C	55	[23]
Polyaddition	Paraffin mixture	Epoxy resin	-	45 ± 0.5°C and -58 ± 0.5°C	189	[30]

Polymerization	Docosane	PMMA	0.14–0.466	41°C	54.6	[31]
Polycondensation	Hexadecane	Melamine–formaldehyde resin	5–20	23°C	210	[15]
	Octadecane	Melamine–formaldehyde resin	5–20	28°C	150	[15]
	Lauryl alcohol	Melamine–formaldehyde resin	5–10		110	[32]
	Butyl stearate	Polyurea	20–35	29°C	80	[16]
	n-Dodecanol	Melamine–formaldehyde resin	Mean diameter of 30.6	21.5°C	87–187.5	[17]
	n-Tetradecane	Urea–formaldehyde resin	Ca. 100 nm	5–9°C	100–130	[18]
	n-Octadecane	Polyurea	3–25	26–28	153–189	[33]
Emulsion polycondensation	*n*-Heptadecane	Polystyrene (PS) (1: 2)	1–20	21.75	128.27	[23]
In situ polymerization	Tetradecane	PVAc, PS, PMMA, PEMA	5–40	2.06–5.68°C	66.26	[28]
	Paraffin	Urea–formaldehyde	5–20	54°C	157.5	[34]
	DPNT06-0182 (Ciba specialty chemicals)	–	10–100	35°C	8.074–96.968	[35]
	Lauryl alcohol	Melamine–formaldehyde	5–10	24°C	80.62 kJ/kg	[28]

(continued)

Table 1 (continued)

Encapsulation method	PCM	Shell material	Microcapsules size (μm)	Temperature of phase transition (°C)	Heat of phase transition (kJ/kg)	References
	n-Octadecane	Urea–melamine–formaldehyde	0.2–5.6	–	–	[30]
Interfacial polymerization	*n*-Octadecane; *n*-nonadecane; *n*-eicosane	Urea–melamine–formaldehyde			160	[36]

and poor colloid concentrations [39]. Hawlader et al. [13, 38] prepared microencapsulated wax by complex coacervation technique and studied the influence of core-to-coating mass ratio on its characteristics and performance such as hydrophilicity, energy storage capacity, and size distribution. They used gelatin/gum acacia as a shell material, and the processing conditions were optimized based on the response surface method (RSM). In different studies, Hawlader et al. [6] performed both experiments and simulation to investigate the characteristics of MEPCMs prepared by complex coacervation method. Also microencapsulation of Rubitherm RT 27, a paraffin wax-based material, was successfully done by Bayés-García et al. [40] via complex coacervation method. They used two different coacervates as shell composition (sterilized gelatin/acacia gum and agar-agar/acacia gum), and the SEM results show an average diameter of 12 μm for the SG/AG shell and smaller capsules for the AA/AG shell, where nanocapsules were also observed. They obtained encapsulation ratios of 49% and 48% for the SG/AG and AA/AG shells, respectively.

Microcapsules of natural coco fatty acid mixture were prepared using coacervation methods by Ozonur et al. [14]. The microscopic results showed that microcapsules produced by the coacervation process attain a geometrically spherical shape, and FTIR spectra revealed that chemical stability of the mixture was not affected by microencapsulation. Bayes-Garcıa et al. [41] studied novel phase change microcapsules obtained by using two different bio-based coacervates: sterilized gelatin/arabic gum (SG/AG) and agar-agar/arabic gum (AA/AG).

1.2 Suspension Polymerization

Microcapsules with a polymer cover and a PCM core can be obtained by a process based on suspension polymerization. This process generally involves the dispersion of a monomer, mainly as small droplets of liquid, into an appropriate medium with the polymerization initiator being dissolved in the monomer. For PCM microencapsulation, the site for the generation of free radicals will be the interface between water and the oil droplet with the paraffin inside the forming polymer covering layer. This method can be seen as an "inside-out" approach for PCM microencapsulation [39]. Sánchez at al. [39] successfully encapsulated different nonpolar PCMs such as PRSs wax, tetradecane, Rubitherm RT27, Rubitherm RT20, and nonadecane with a polymer shell of polystyrene by suspension polymerization method. They concluded that it is not possible to encapsulate polar PCMs (polyglycols) because of their hydrophilic nature. They also studied the influence of operating conditions such as reaction temperature, stirring rate, and mass ration of PRSs wax to styrene on the properties of MEPCMs (thermal storage capacity, particle size distribution, and morphology) [42]. In another study, Sánchez at al. [43] used the Shirasu porous glass (SPG) membrane with a pore size of 5.5 μm to produce a narrow microcapsule size distribution. They investigated the effect of different parameters such as the ratios of PRSs wax/styrene,

polyvinylpyrrolidone (stabilizer)/styrene, and water/styrene on the particle size distribution and thermal energy storage of microcapsules prepared via suspension polymerization method. Afterwards, Sánchez-Silva et al. [44] successfully designed a pilot plant for MEPCM production via suspension polymerization technique with a similar particle size and PCM content to those obtained in the laboratory. Recently, Li et al. [45] fabricated a series of MEPCMs by suspension-like polymerization with *n*-octadecane as the core and styrene–1,4-butylene glycol diacrylate copolymer (PSB), styrene–divinylbenzene copolymer (PSD), styrene–divinylbenzene–1,4-butylene glycol diacrylate copolymer (PSDB), or polydivinylbenzene (PDVB) as the shell. In another study, *n*-octadecane that contained homodispersed polypyrrole (PPy) particles was encapsulated with a PMMA/PAMA copolymer shell [46]. They succeeded in eliminating the supercooling from the MEPCM by adding 4–14 wt% PPy in the core, while PPy had no influence on the morphology and particle distribution of the microcapsules. A new hybrid shell of polymer/SiO2 was used by Yin et al. [47] to encapsulate dodecanol as a core material. They successfully eliminated the surfactant or dispersant material by using the organically modified SiO2 particles.

1.3 Emulsion Polymerization

Emulsion polymerization is a scientifically, technologically, and commercially important reaction. It was developed during the Second World War because of the need to replace the latex of natural rubber. The synthetic rubbers were produced through radical copolymerization of styrene and butadiene [48]. Today, emulsion polymerization is the large part of a massive global industry. It produces high molecular weight colloidal polymers and no or negligible volatile organic compounds. The reaction medium is usually water; this facilitates agitation and mass transfer and provides an inherently safe process. Moreover, the process is environmentally friendly. In emulsion polymerization, unlike suspension polymerization, the initiator is soluble in the aqueous phase, and the monomer is emulsified in the polymerization medium by the aid of a surfactant. As illustrated in Fig. 1, the monomer is distributed between droplets emulsion, surfactant micelles, and scarcely the water phase. Since the initiator is present only in the aqueous phase, the starting point for the polymerization reaction is in this phase (i.e., outside the droplets and micelles) and subsequently extends to the micelles. The average diameter of the resulting particles is mainly affected by the fraction of the monomer molecularly dissolved in the aqueous phase. Besides, it is influenced by the emulsifier concentration, initiator concentration, and polymerization temperature.

PMMA microcapsules with a controlled narrow particle size distribution and containing docosane were successfully prepared by emulsion polymerization [23]. SEM analyses revealed that the MEPCMs had a compact surface and an average capsule diameter of 160 μm. The authors concluded that PMMA/docosane microcapsules were reliable as a Thermal Energy Storage Materials (TESM) based on

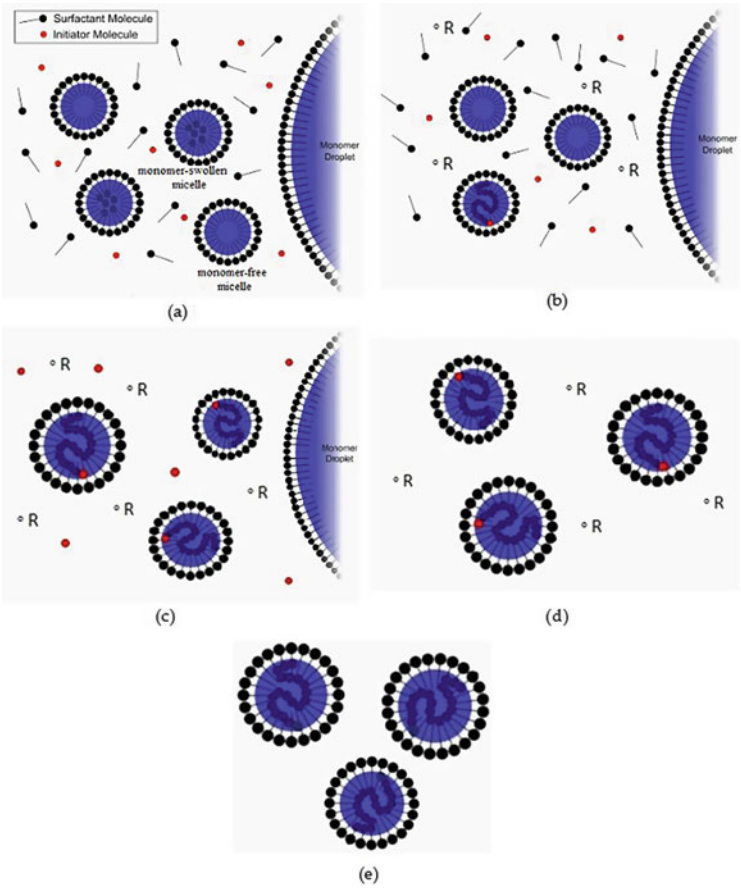

Fig. 1 Schematic representation for the mechanism of emulsion polymerization [49]

thermal cycling tests and the high temperature resistance [23]. In other studies, PMMA microcapsules containing *n*-octacosane or *n*-eicosane were investigated [29, 40]. The best PCM properties were exhibited by the PMMA microcapsules containing 43 wt.% of *n*-octacosane as a core.

Baek et al. [50] successfully prepared PCM (*n*-octadecane) nanocapsules by emulsion polymerization of styrene. They used alkali-soluble resin (ASR) of poly (ethylene-co-acrylic acid) (EAA) and poly(styrene-co-acrylic acid) (SAA) as surfactant and water-soluble potassium persulfate as initiator. The maximum encapsulation ratio of 66.7% was achieved through the use of SAA surfactant. Alkan and their colleagues carried out a number of studies in the preparation of microencapsulated PCM by emulsion polymerization using docosane [51], *n*-octacosane [23], *n*-hexadecane [40, 52], and *n*-heptadecane [53] as core material and PMMA resin as shell material. They characterized their properties such as particle size distribution, chemical characterization, latent heat, and thermal

stability using SEM, FTIR, DSC, and TGA. Based on all results, they concluded that the PMMA/PCM microcapsules have good energy storage potential. They also indicated that the type of alkane and cross-linker agent (e.g., glycidyl methacrylate, allyl methacrylate, and ethylene glycol dimethacrylate) has a great influence on the encapsulation ratio, the particle size, and the structure of the microcapsules.

The particles prepared using n-hexadecane as a core material and glycidyl methacrylate or ethylene glycol dimethacrylate as a cross-linker agent had higher encapsulation ratio (i.e., 62% compared to 28–43%), more spherical surface, and smaller size. The ultraviolet (UV) light is a useful tool for initiating polymerization. One of the most important advantages of the UV-initiated polymerizations is the temperature independency of the radical flux, whereas a high temperature is necessary in chemical initiation [54]. Ma et al. [55] successfully prepared wax microcapsules with PMMA shell through an emulsion polymerization, which were initiated by UV irradiation in the presence of a water-soluble photoinitiator of photocure 2959. Alay et al. [56] produced microencapsulated *n*-hexadecane with poly(butyl acrylate) (PBA) by using allyl methacrylate, ethylene glycol dimethacrylate, and glycidyl methacrylate as cross-linkers. The results indicated that the microcapsules prepared using ethylene glycol dimethacrylate cross-linker had the highest heat capacity.

1.4 Polycondensation

An in situ polycondensation process was applied by Su et al. to prepare a series of melamine–formaldehyde (MF) microcapsules with a PCM core [20]. The study demonstrated that the shell structures of MEPCMs can be controlled by the formation process using an optimum dropping rate of shell material of 0.5 ml/min and a temperature increase of 2°C/10 min. DSC revealed that the melting point of the PCM in shells remained virtually unchanged to that of an uncapsulated PCM [20]. In a subsequent development, double-shell-structured microcapsules with melamine–formaldehyde resin as the coating material of PCM were fabricated [32]. Compression tests on the single- and double-shell-structured MEPCMs showed that the latter structure had greater mechanical stability than the former one [32]. Lee and coworkers [15] prepared MEPCMs by in situ polycondensation of melamine and formaldehyde for the shell with hexadecane or octadecane as the core. They found that particle size decreased and its uniformity was enhanced if the mixing intensity during emulsification was increased. Additionally, MEPCMs were incorporated in gypsum, and it was established that the thermal fluctuations in such PCM-building materials were smoother and smaller than these in building materials without PCMs. To evaluate the heat storage characteristics of the material, gypsum wallboards containing MEPCMs were produced as shown in Fig. 2.

More recently, Yu et al. [17] studied the effects of the polarity of the PCM and the types and amounts of emulsifier on the properties of microencapsulated PCMs. They synthesized microcapsules containing polar PCM (*n*-dodecanol) by in situ

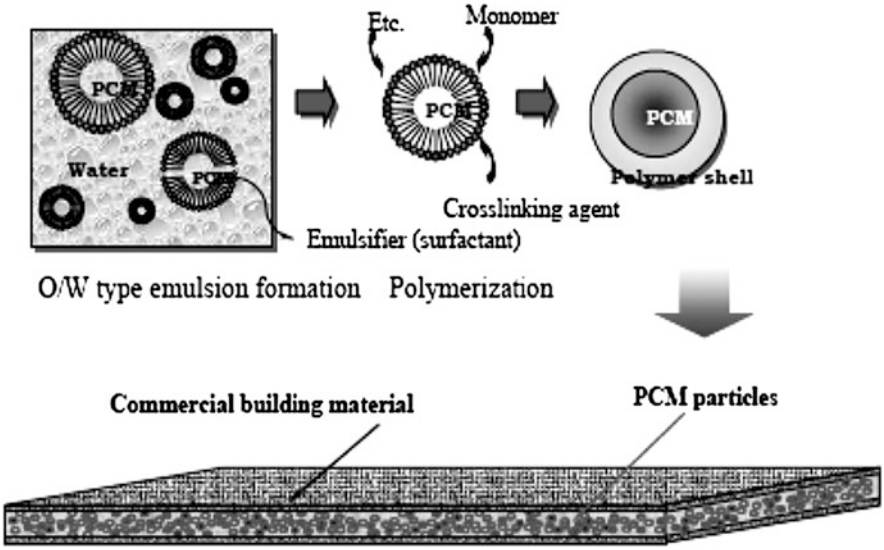

Fig. 2 Conceptual diagram of building materials containing MEPCM. Reprinted from [15] with permission from Springer

polycondensation using melamine–formaldehyde resin as the shell and styrene–maleic anhydride copolymer (SMA) as an emulsifier. The results showed that the type and amount of SMA emulsifier had a major influence on the properties and morphology of the MEPCMs. SMA was suitable for the encapsulation of *n*-dodecanol, and an increase in the amount of emulsifier initially caused the phase change latent heat and encapsulation efficiency to increase, but then to decrease [17].

Capsules containing wax as phase change core were synthesized in situ by Jin et al. [57] by the absorption and condensation polymerization of urea–formaldehyde prepolymer onto the core using hydrolyzed styrene–maleic anhydride copolymer in an aqueous phase as the emulsifier. This approach can be extended to other paraffins having tunable melt/crystallization temperatures. Fang et al. [18] obtained PCM nanocapsules containing *n*-tetradecane by in situ polycondensation of urea and formaldehyde. SEM analysis indicated that the nanocapsules size was ca. 100 nm and that the core material was well encapsulated. Moreover, the thermal stability of the nanocapsules could be improved by a NaCl addition during the polymerization process. Peng et al. [30] encapsulated low melting temperature paraffin wax PCMs in cured epoxy resin or styrene–ethylene–butylenes (SEB) terpolymer. It was found that the thermal conductivity of the composites increased when the PCM was liquid, partly because of better wetting of the epoxy by the liquid paraffin. Oxidized hard Fischer–Tropsch paraffin waxes as PCMs in an epoxy resin matrix were prepared by Luyt and Krupa by mechanically mixing wax powder and a liquid resin at room temperature and then curing by UV [31]. The results indicated that the PCM distribution in the polymer matrix improved with an increasing wax content and its presence influences the mechanical properties of the PCMs, especially above the melting point of the wax.

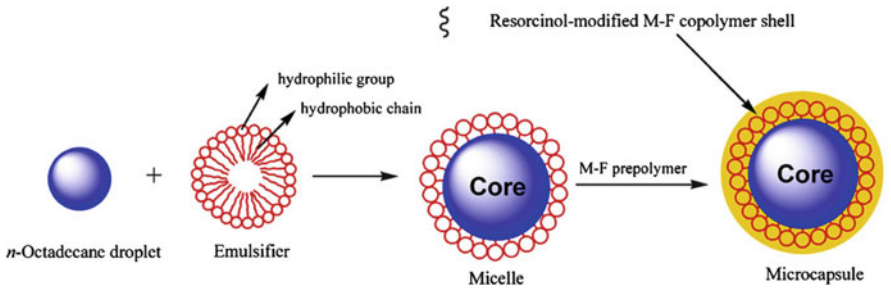

Fig. 3 Schematic formation of the Micro encapsule PCM (MEPCM) based on *n*-octadecane core and resorcinol-modified melamine–formaldehyde shell through in situ polymerization [33]

1.5 Polyaddition

Chen et al. [16] prepared polyurea microcapsules containing PCMs using toluene-2,4-diisocyanate (TDI) and ethylenediamine (EDA) as monomers and butyl stearate as the core material. MEPCMs based on a core of *n*-octadecane and polyurea shells, synthesized by polyaddition of TDI as an oil-soluble monomer and various amines, e.g., EDA, diethylenetriamine, or polyetheramine, as the water-soluble monomers, were prepared by Zhang and Wang [33] as displayed in Fig. 3. It was revealed that the microcapsules synthesized by using polyetheramine had a smoother and more coherent surface and larger mean particle size with a narrow size distribution than those using EDA or diethylenetriamine. Furthermore, the microcapsules synthesized with a core/shell weight ratio of 70/30 possessed the optimum properties for TES applications [33].

1.6 Other Methods

Microencapsulation of *n*-tetradecane with different shell materials such as acrylonitrile–styrene copolymer (AS), acrylonitrile–butadiene–styrene terpolymer (ABS), and polycarbonate (PC) was carried out by phase separation method [34] (see Fig. 4).

AS was the most suitable shell material as it gave the highest encapsulation efficiency and the greatest transformation enthalpy. The molecular weight of the shell material also influenced the microencapsulation – a lower molecular weight gave greater encapsulation efficiency because of the higher mobility of the shell molecules, but it reduced the shell's strength [34]. Recently, Jin et al. [59] have produced microcapsules of PCM using silica as the shell in a one-step procedure without surfactants or dispersants. This allowed fabrication of capsules with controlled size and dispersity incorporating various core materials. The benefits of the method include an easy scale-up and no necessity for a stabilizing agent as the amine groups self-stabilize. Macro-capsules containing SSPCM consisting of

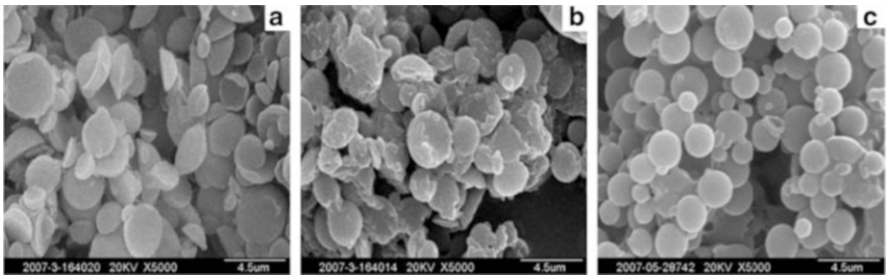

Fig. 4 SEM images of (**a**) AS/*n*-tetradecane, (**b**) ABS/*n*-tetradecane, and (**c**) PC/*n*-tetradecane microcapsules. Reprinted from [58] with permission from Elsevier

50 wt.% of *n*-octadecane and 50 wt.% of HDPE were prepared using calcium alginate (CaAlg) as the shell material [60]. The MEPCM based on *n*-octadecane core and a silica shell was designed and synthesized via a sol–gel process by Zhang et al. targeting an enhancement of the thermal conductivity and phase change performance [61]. The MEPCMs were spherical with a well-defined core–shell microstructure giving a single endothermic peak on the DSC profile, quite similar to that of the bulk material. The thermal conductivity of the studied MEPCMs was significantly superior to that of the nonstructured materials.

2 Form-Stable (Shape-Stabilized) PCMs (SSPCMs)

This kind of PCM, called shape-stabilized PCM, does not require any encapsulation, because of the presence of a polymeric matrix. This compound can keep its shape stabilized even when the PCM state changes from solid to liquid. The mass percentage of phase change element can reach more than 85 wt% without any obvious modification of its melting point, suggesting excellent energy storage capacity. Compared with conventional PCM, shape-stabilized PCM reduces the liquid PCM leakage danger, the additional thermal resistance, and the container cost. This material can be shaped into different forms as spheres, cylinders, and plates. In recent years, some researchers have studied the preparation method and the thermal properties of several shape-stabilized PCMs [62–74]. Various polymers are applied as matrices in shape-stabilized PCMs, and they are described in the following subchapters.

2.1 SSPCMs with a Polymer Matrix

2.1.1 Polyethylene

Polyethylene (PE), due to its properties and chemical affinity to paraffins, is widely used in form-stable PCMs as a supporting material [75]. Sari [76] prepared paraffin/HDPE composites as SSPCMs by melt mixing. The maximum amount for two

different types of paraffin in the PCM composites was 77%, and it was observed that the paraffin was well dispersed in the solid HDPE matrix. In addition, to improve the thermal conductivity of the SSPCMs, graphite, expanded and exfoliated by heat treatment, was added and increased the thermal conductivity by 14–24% [77, 86]. Form-stable composites, based on low-density polyethylene (LDPE) mixed with soft and hard Fischer–Tropsch paraffin waxes, were studied by Krupa et al. [78]. They found that the two waxes behaved totally differently. The Fischer–Tropsch paraffin wax co-crystallized with the LDPE crystals to form a more compact blend than the soft paraffin wax. The blends were found to be efficient SSPCMs with the LDPE matrix keeping the material in a compact shape at the macroscopic level. In other work, Cai et al. [79] investigated shape-stabilized phase change nanocomposite materials based on HDPE–ethylene–vinyl acetate (EVA) alloy, organically modified montmorillonite (OMT), paraffin, and intumescent flame retardant (IFR), processed in a twin-screw extruder. The results indicate that the HDPE–EVA/OMT nanocomposites acted as the supporting material and formed a three-dimensional network structure, while the paraffin PCM is kept in the network. SEM and DSC showed that the IFR additives hardly have effect on the network structure or on the latent heat of the shape-stabilized nanocomposites. However, incorporating a suitable amount of OMT into the form-stable PCM increased its thermal stability as revealed by TGA data.

2.1.2 Acrylics

Acrylic-based matrixes are easily processed, possess end-use properties, and are cost effective. In this field, Alkan et al. [80] studied PEG blends with acrylic polymers such as PMMA, Eudragit S (Eud S, copolymer of methacrylic acid and methyl methacrylate), and Eudragit E (Eud E, copolymer based on dimethylaminoethyl methacrylate, butyl methacrylate, and methyl methacrylate) as form-stable PCMs. The PEG acted as a phase change LHTES material with the acrylic polymers as supporting materials. The maximum percentage of PEG without leakage was found to be ca. 80 wt.%. In their later work [81], blends of Eudragit S with SA, PA, and MA were prepared and characterized.

The maximum mass percentage of fatty acids in the blends to avoid their seepage in the molten state was found to be 70%. These results were confirmed by Kaygusuz et al. for blends of Eudragit E and fatty acids [82]. Later, a series of fatty acid/poly (methyl methacrylate) (PMMA) blends such as SA/PMMA, PA/PMMA, MA/PMMA, and LA/PMMA was tested as SSPCMs. The blends were prepared by a solution casting method with different mass fractions of fatty acids to determine the maximum blending ratio with no leakage above the melting temperature [83]. Recently, Zhang et al. [84] investigated PEG/PMMA and PEG/PMMA/aluminum nitride (AlN) composites as form-stable PCMs. It was found that for a PEG mass fraction less than 70%, the SSPCMs remained solid without leakage above the PEG melting point. With the increase in the mass fraction of PEG, the latent heat capacity of the composite PCMs increased accordingly, which effectively is in

agreement with the theory of mixtures. Thermal analysis showed that the prepared PCMs possessed desirable latent heat capacities and thermal stability, and AlN additive effectively enhanced the heat transfer properties of the organic PCM.

2.1.3 Poly(vinyl chloride)

The structure of poly(vinyl chloride) (PVC) gives rise to a relatively tough and rigid material able to accept a wide range of additives, including PCMs. In this context, blends of PVC/PA and PVA/PA were investigated by Sari et al. [85]. They established that there was no leakage of PA even in the molten state and that the maximum miscibility ratio of PA with both polymers was found at the level of 50% while maintaining the shape-stabilization effect. Blends of PVC, the supporting material, with fatty acids as PCMs, were studied. The maximum PVC/fatty acid ratio for which no leakage of fatty acid was observed above their melting temperatures for several heating cycles of the SSPCMs was 50 wt.% [86].

2.1.4 Polyurethanes

Polyurethane (PU) foams are lightweight materials with a high strength/weight ratio, superior insulating properties, and high-energy absorbency. The mechanical properties of PU foams are an important consideration for structural and semi-structural applications, such as composite foam cores and mold patterns. Unlike thermoplastic foams, PU foams are formed by reactive processing in which polyaddition and foam blowing occur simultaneously – the network structure must build up rapidly to support the brittle foam, but not too rapidly to prevent bubble growth.

For energy storage purposes, PU foams were modified by *n*-hexadecane or *n*-octadecane during polymerization process by Sarier and Onder [87]. An FTIR analysis showed that the chemical compositions of the PU samples were significantly different from that of the PU control sample, and it was verified that they displayed the functional groups which indicated the presence of linear chain hydrocarbons. SEM showed that the PCM micelles were located in the cells of a perfect honeycomb structure – see Fig. 5.

Polyurethane foams containing PCMs can be assumed to be leakage protected, and this gives the prospect for PU-PCM production on an industrial scale [87]. Composites obtained by impregnation of rigid PU foams with PEG have also been tested [88]. DSC analysis shows that PU–PEG materials yielded high enthalpies over certain temperature intervals suggesting that the heat absorption/release capacities of PU foams may be improved by the incorporation of PEG. You et al. [89] studied PU composite foams containing microencapsulated PCMs produced by in situ polycondensation process of melamine and formaldehyde, for the shell, and *n*-octadecane as the core. PU composites were fabricated by adding heat-treated microencapsulated PCMs during the synthesis which resulted in them being evenly

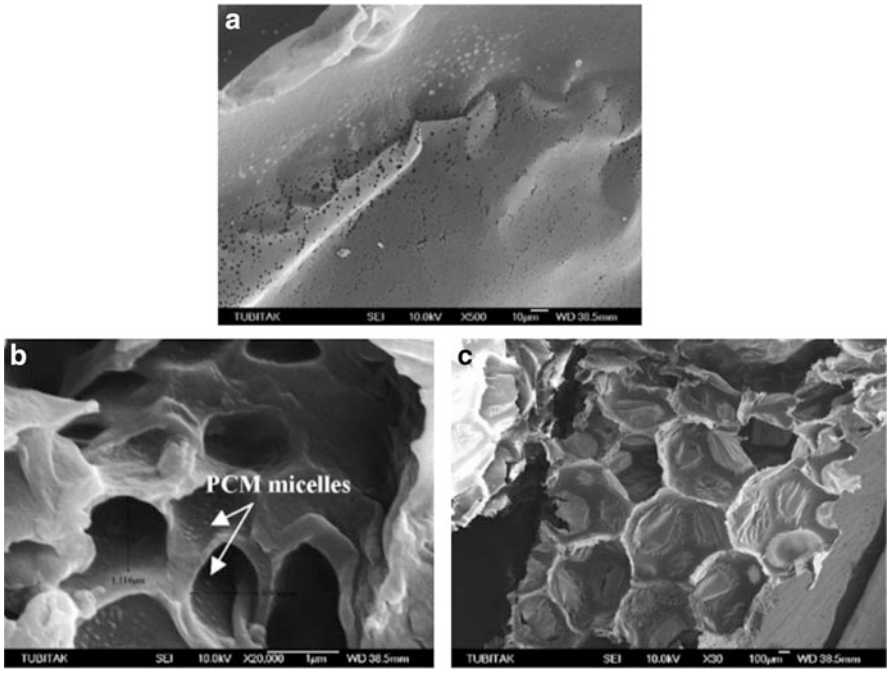

Fig. 5 PU containing *n*-hexadecane: (**a**) magnification 500, (**b**) magnification 20,000, and (**c**) magnification 30,000. Reprinted from [87] with permission from Elsevier

distributed inside the foam. It was not possible to produce qualified MEPCMs/PU composite foams containing more than ca. 12 wt.% PCM. The limitation was probably caused by the existence of reactive hydroxymethyl groups in the polymerized melamine–formaldehyde shell. In a recent development, Ke et al. [90] prepared porous membranes based on PU and PEG. The results showed that the PU–PEG membranes had a highly porous structure and suitable transition temperatures and enthalpy changes.

2.1.5 Other Polymers

In an effort to search for novel shape-stabilized PCMs, blends of poly(vinyl alcohol) (PVA) with LA, MA, PA, or SA were studied by Sari and Kaygusuz [91]. The maximum mixture ratio for all the fatty acids in the shape-stabilized form was found to be 50 wt.%. In their later work, fatty acids were introduced to a maleic anhydride copolymer matrix by the solution casting method. As much as 85 wt.% of fatty acids were incorporated successfully, and no leakage above the melting point was detected [92]. Mengjin et al. [93] prepared fibers of PVA and paraffin using a wet-spinning technique. The thermal regulating fiber had an acceptable thermal stability when the content of paraffin in fiber was below 30%. An interesting

approach was adopted by Chen et al. [94] who obtained ultrafine composite fibers of stearyl stearate/poly(ethylene terephthalate) (SS/PET) by electrospinning. Depending on the SS/PET mass ratio, the morphology and thermal properties of the composite fibers changed considerably.

In other work, they prepared ultrafine fibers based on the composites of PET and a series of fatty acids – LA, MA, PA, and SA by electrospinning [95]. Cai et al. [96] also prepared by electrospinning ultrafine composite fibers consisting of LA/PET/nano-SiO2 as a form-stable PCM. DSC indicated that the amount of nano-SiO2 in the fibers had an influence on the crystallization of LA and played a significant role on the heat enthalpies of the material. The morphology and thermal and thermo-mechanical properties of polyamide (PA) 12/maleic anhydride-grafted wax blends and the possible interactions between PA12 and the functionalized wax were studied by Luyt et al. [97]. Results showed that it was practically impossible to prepare homogeneous blends containing more than 30 wt.% of wax, and a low heat of phase transition was observed. At lower wax contents, the wax crystals were homogeneously distributed through the PA12 matrix, and there was no leakage of the wax from the matrix during processing. The novel form-stable phase change composite materials of PEG/epoxy resin (EP) were prepared by Fang et al. [98]. As the epoxy resin was the supporting material for the PEG PCM, the mechanical deformation of PEG/EP composites was very small, and the composites retained their shape even when the phase change from solid to liquid took place. It was demonstrated that the overall transition was a solid–solid phase change. Zhang et al. [99] produced a series of polyol acetal derivatives by condensation reactions of aromatic aldehyde with polyols. Three-dimensional structural PCMs were obtained using paraffin doped with different gelation agents, which proved to be thermally stable and showed no leakage of paraffin above the melting point of the saturated hydrocarbon.

3 SSPCMs with Expandable Graphite Matrix

Paraffin (*n*-docosane)/expanded graphite (EG) composites prepared by absorbing liquid paraffin into the EG, as a form-stable PCM, were studied by Sari et al. [100]. A composite PCM with a 10% mass fraction of EG was found to be form stable. Because of the capillary and surface tension forces of EG, no leakage of liquid paraffin was observed during the phase transition. The enhancement of thermal conductivity and the latent heat capacities of the PCM materials were roughly equivalent to the theoretical values calculated based on the mass ratios of the paraffin and EG in the composites [24]. Fatty acid/expanded graphite (EG) composites prepared by a vacuum impregnation method were investigated too. It was found that the maximum fatty acid absorption of EG was 80 wt.% without molten fatty acid oozing from the composites. DSC results indicated that the melting and solidification temperatures of the composite PCMs were almost identical to those of the fatty acids, but the latent heats of the composites were

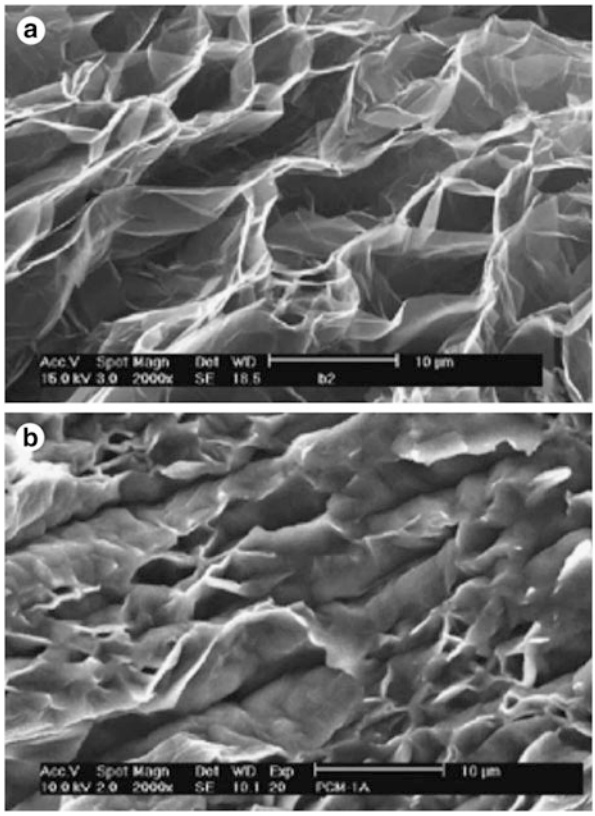

Fig. 6 SEM photomicrographs of the expanded graphite and paraffin/expanded graphite composite PCM: (**a**) expanded graphite, (**b**) paraffin/expanded graphite composite PCM. Reprinted from [103] with permission from Elsevier

slightly lower than those of the pure fatty acids [101, 102]. A paraffin/expanded graphite phase change TES material was investigated by Zhang and Fang [25]. The composites were prepared by absorbing the paraffin into EG – a material which, because of its layered microporous morphology, has excellent absorbability (see Fig. 6).

In such a composite, the expanded graphite acts as the supporting material. The capillary and surface tension forces prevent leakage of the molten paraffin from the porous structure [104]. Wang et al. [105] investigated the composite made by blending PEG with expandable graphite. The maximum mass percentage of PEG dispersed in PCM composites without any leaking of the polymer was found to be as high as 90 wt.%. It is of interest that the thermal conductivity was considerably increased because of the thermally conductive network formed by the EG's porous structure. Zhang et al. [106] investigated EG/paraffin composite PCMs with an EG mass fraction varying 0–10 wt.%. Thermal characterization of the composite PCMs by DSC revealed shifts in the phase change temperatures. Initially, the latent heat of the paraffin in the composite PCMs increased but then decreased with an increase in the fraction of EG. An SSPCM composed of PEG and mesoporous active carbon

(AC) was prepared by a blending and impregnating method [103]. Lower phase change temperatures and enthalpies were observed, as the content and molecular weight of PEG were decreased. The authors concluded that the phase change properties of the PEG/AC PCMs were influenced by the adsorption confinement of the PEG segments in the porous structure of AC and by the role of the AC during PEG crystallization.

3.1 Other SSPCMs

Xing et al. [107] employed silica gel to encapsulate form-stable paraffin PCMs, in which the paraffin served as the Latent Heat Storage (LHS) material and HDPE as the supporting material. It was found that keeping a high mass percentage of paraffin, it was possible to encapsulate form-stable paraffin with random ratios of the mass of the core materials to that of the coating materials. The results also indicate that there are more advantages to use PE form-stable paraffin as the core material rather than using paraffin directly because of the lower cost of producing the PCMs, the higher mass percentages of paraffin encapsulated, better hydrophilicity, and better fire resistance [108]. PEG/SiO2 composites were investigated by Wang et al. [108] with PEG as the PCM and SiO2 as the supporting material. They were prepared by dissolving PEG in water and adding silicon dioxide which enables composites containing between 5 and 95 wt.% of SiO2 to be obtained. It was found that up to 85% PEG could be dispersed in the PCM composite without any leakage of the molten PEG. It was established that the thermal conductivity was improved because of the thermal conductive network formed by the porous structure of the SiO2. Recently, Tang et al. [109] obtained PEG/SiO2 hybrid form-stable PCM with improved thermal conductivity by in situ Cu doping via the chemical reduction of CuSO4 using an ultrasound-assisted sol–gel process. Zhang et al. [110] produced granular phase change composites for TES by means of a vacuum impregnation method, using organic PCMs, including fatty acids, their derivatives, and paraffins, with inorganic porous materials, including expanded clay, expanded fly ash, and expanded perlite.

This method enabled a volume of up to 65% PCMs to be loaded into porous materials [111]. Vacuum impregnation was also used by Karaipekli and Sari [53, 111–114] to incorporate a eutectic mixture of CA and MA into expanded perlite (EP) and pure CA or LA in EP. The maximum fatty acid absorption of EP was found to be 55–60 wt.% without molten PCM seepage from the composite, and therefore, this mixture was described as a form-stable composite. Thermal cycling tests of the form-stable composite PCM indicated good thermal reliability up to 5,000 thermal cycles. Moreover, the addition of 10 wt.% of EG improved the thermal conductivity of the form-stable CA–MA/EP composite PCM by about 58%. Subsequently, CA–MA eutectic mixture/vermiculite (VMT) composites were obtained by vacuum impregnation [114]. The CA–MA eutectic mixture was restricted to a maximum percentage of 20 wt.% without seepage of molten PCM

from the porous structure of the VMT. The introduction of 2 wt.% of EG into the composite increased the thermal conductivity of the form-stable CA–MA/VMT composite PCM by about 85%. Li et al. [115] prepared CA–PA binary blends impregnated into attapulgite. The pore structure of the CA–PA/attapulgite composite PCM was found to be an open-ended tubular capillary type, which was beneficial for the adsorption processes. The same group of researchers also investigated binary fatty acid/diatomite shape-stabilized PCMs. Taking account of the phase diagrams, a series of binary fatty acids composed of CA, LA, PA, and SA was prepared. The binary fatty acids were absorbed into four types of diatomites having different specific areas, which then acted as the supporting material. The results showed that there is an optimum absorption ratio between the binary fatty acids and the diatomite [115]. Karaman et al. [116] incorporated PEG into the pores of diatomite and characterized the resulting PEG/diatomite composite as a novel form-stable composite PCM. It was found that up to 50 wt.% PEG could be retained in the pores of the diatomite without the leakage of molten PEG from the composite. The effects of the porosity and thermal properties of a porous medium infiltrated with PCM were investigated by Mesalhy et al. [117]. They employed carbon foam matrices with various porosities and different thermal properties as the porous medium, and paraffin wax was introduced into the matrix pores as the PCM. The matrix composite was located in a cylindrical enclosure while it experienced heat from a heat source set on the top of the enclosure. The results showed that the porosity and thermal conductivity of the matrix composite played important roles in the thermal performance of the device. In another study, a form-stable PCM prepared by impregnating SA into a silica fume matrix using a solution impregnation technique was investigated [118]. The results show that the form-stable composite PCM has the optimal effect, preventing the leakage of SA from the composite, which emerged when the SA and silica fume mass ratio is 1:0.9. Experimental investigations on the thermal performance of paraffin/bentonite composite PCMs, prepared by a solution intercalation process, were conducted by Li et al. [119]. The results showed that the interlayer distance of bentonite was increased from 1.492 nm to 1.962 nm through organic modification – paraffin can be thus intercalated into the layers of bentonite to form SSPCM.

The presence of bentonite enhanced the heat transfer rate of the composite material. Mei et al. [120] investigated the CA/halloysite nanotube (CA/HNT) composite as form-stable composite PCM.

The composite can contain up to 60 wt.% CA without any leakage after 50 melt–freeze cycles. A graphite addition improved the performance of the composite with the thermal storage and release rates increased by 1.8 and 1.7 times, respectively. Recently, Zhou et al. [121] have prepared highly conductive 3D porous graphene/Al2O3 composites using ambient pressure chemical vapor deposition. The formation mechanism of graphene was attributed to the carbothermic reduction occurring at the Al2O3 surface to initiate the nucleation and growth of the graphene. It was shown that such a porous composite is attractive as a highly thermally conductive reservoir for PCMs (SA) for TES (see Fig. 7).

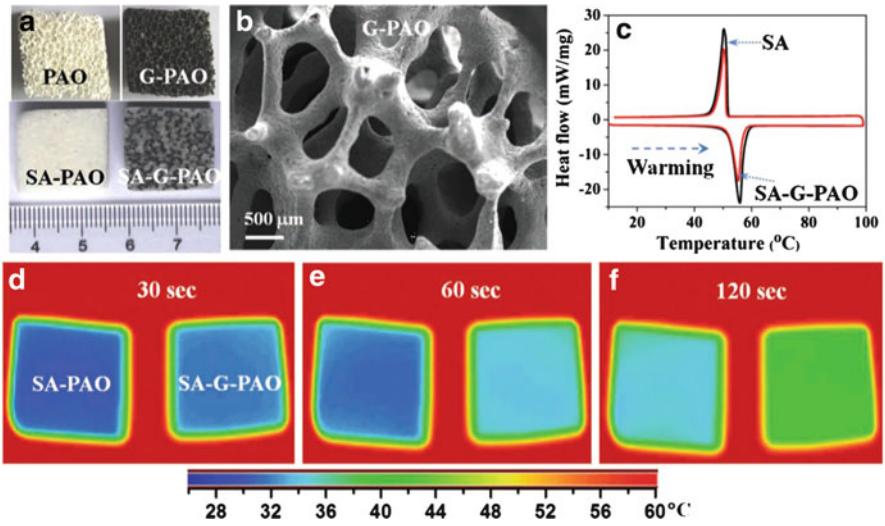

Fig. 7 (**a**) Photographs of large porous alumina (PAO), graphene-coated porous alumina (G-PAO), SA-filled porous alumina (SA-PAO), and SA-G-PAO. (**b**) SEM image of G-PAO. (**c**) DSC curves of SA and SA-G-PAO composite. (**d**–**f**) Thermal transport evolution of SA-PAO and SA-G-PAO. The thermal images visually illustrate the excellent thermal characteristics of the G-PAO. Reprinted from [121] with permission from Wiley

4 Conclusion

Phase change materials (PCMs) used for the storage of thermal energy as sensible and latent heat are an important class of modern materials which substantially contribute to the efficient use and conservation of waste heat. The storage of latent heat provides a greater density of energy storage with a smaller temperature difference between storing and releasing heat than the sensible heat storage method. In order to fully exploit the latent heats of fusion, it is desired to have the PCM as small as possible so that it can melt instantaneously. In many cases, the PCM should be encapsulated to improve their thermal conductivity and prevent possible interaction with the surrounding and leakage during the melting process, where there is no complete overview of the several methods and techniques for microencapsulation of different kinds of PCMs that leads to microcapsules with different morphology, structure, and thermal properties. This paper presents a non-exhaustive overview of the various chemical processes used to develop stable PCM (such as microencapsulation, emulsion polymerization or suspension polycondensation, polyaddition, etc.) and the shape-stabilized PCM, developed from an intimate combination of a polymer matrix and a phase change element.

References

1. Agyenim F, Hewitt N, Eames P, Smyth M (2010) A review of materials, heat transfer and phase change problem formulation for latent heat thermal energy storage systems (LHTESS). Renew Sustain Energy Rev 14:615–628
2. Jeon J, Lee J-H, Seo J, Jeong S-G, Kim S (2013) Application of PCM thermal energy storage system to reduce building energy consumption. J Therm Anal Calorim 111:279–288
3. Li G, Hwang Y, Radermacher R, Chun HH (2013) Review of cold storage materials for subzero applications. Energy 51:1–17
4. Tyagi VV, Kaushik SC, Tyagi SK, Akiyam T (2011) Development of phase change materials based microencapsulated technology for buildings: a review. Renew Sustain Energy Rev 15:1373–1391
5. Yokota T, Murayama M, Howe JM (2003) In situ transmission-electron-microscopy investigation of melting in submicron Al-Si alloy particles under electron-beam irradiation. Phys Rev Lett 91:265504
6. Hawlader MNA, Uddin MS, Zhu HJ (2002) Encapsulated phase change materials for thermal energy storage. Int J Energy Res 26:159–171
7. Farid MM, Khudhair AM, Razack SAK, Al-Hallaj S (2004) A review on phase change energy storage: materials and applications. Energy Convers Manag 45(9):1597–1615
8. Cho JS, Kwon A, Cho C-G (2002) Microencapsulation of octadecane as a phase-change material by interfacial polymerization in an emulsion system. Colloid Polym Sci 280:260–266
9. Delgado M, Lazaro A, Mazo J, Zalba B (2012) Review on phase change material emulsions and microencapsulated phase change material slurries: materials, heat transfer studies and applications. Renew Sust Energ Rev 16:253–273
10. Wei J, Li Z, Liu L, Liu X (2013) Preparation and characterization of novel polyamide paraffin MEPCM by interfacial polymerization technique. J Appl Polym Sci 127:4588–4593
11. Hu W, Yu X (2014) Thermal and mechanical properties of bio-based PCMs encapsulated with nanofibrous structure. Renew Energy 62:454–458
12. Benita S (1996) Microencapsulation: methods and industrial applications. Marcel Dekker, New York
13. Hawlader MNA, Uddin MS, Khin MM (2003) Microencapsulated PCM thermal-energy storage system. Appl Energy 74:195–202
14. Ozonur Y, Mazman M, Paksoy HO, Evliya H (2006) Microencapsulation of coco fatty acid mixture for thermal energy storage with phase change material. Int J Energy Res 30:741–749
15. Lee SH, Yoon SJ, Kim YG, Choi YC, Kim JH, Lee JG (2007) Development of building materials by using micro-encapsulated phase change material. Korean J Chem Eng 24:332–335
16. Chen L, Xu L, Shang H, Zhang Z (2009) Microencapsulation of butyl stearate as a phase change material by interfacial polycondensation in a polyurea system. Energy Convers Manag 50:723–729
17. Yu F, Chen ZH, Zeng XR (2009) Preparation, characterization, and thermal properties of microPCMs containing n-dodecanol by using different types of styrene–maleic anhydride as emulsifier. Colloid Polym Sci 287:549–560
18. Fang G, Li H, Yang F, Liua X, Wu S (2009) Preparation and characterization of nano-encapsulated n-tetradecane as phase change material for thermal energy storage. Chem Eng J 153:217–221
19. Su J, Ren L, Wang L (2003) China material report: p. 141.
20. Su J, Wang L, Ren L (2006) Fabrication and thermal properties of microPCMs: used melamine–formaldehyde resin as shell material. J Appl Polym Sci 101:1522–1528
21. Mulligan JC, Colvin DP, Bryant YG (1996) Microencapsulated phase-change material suspensions for heat transfer in spacecraft thermal systems. J Spacecr Rocket 33:278–284

22. Zalba B, Marın JM, Cabeza LF, Mehling H (2003) Review on thermal energy storage with phase change: materials, heat transfer analysis and applications. Appl Therm Eng 23:251–283
23. Alkan C, Sari A, Karaipekli A, Uzun O (2009) Preparation, characterization, and thermal properties of microencapsulated phase change material for thermal energy storage. Sol Energy Mater Sol Cells 93:143–147
24. Alvarado JL, Marsh C, Sohn C, Vilceus M, Hock V, Phetteplace G et al (2006) Characterization of supercooling suppression of microencapsulated phase change material by using DSC. J Therm Anal Calorim 86(2):505–509
25. Fan YF, Zhang XX, Wang XC, Li J, Zhu QB (2004) Super-cooling prevention of microencapsulated phase change material. Thermochim Acta 413:1–6
26. Zhang S, Niu JL (2010) Experimental investigation of effects of supercooling on microencapsulated phase-change material (MPCM) slurry thermal storage capacities. Sol Energy Mater Sol Cells 94:1038–1048
27. Fang YT, Kuang SY, Gao XN, Zhang ZG (2008) Preparation and characterization of novel nanoencapsulated phase change materials. Energy Convers Manag 49:3704–3707
28. Yang R, Xu H, Zhang YP (2003) Preparation, physical property and thermal physical property of phase change microcapsule slurry and phase change emulsion. Sol Energy Mater Sol Cells 80:405–416
29. Hoffman F, Delbrück K (1909) German Patent. 250,690, 12 Sept 1909
30. Jin Z, Wang Y, Liu J, Yang Z (2008) Synthesis and properties of paraffin capsules as phase change materials. Polymer 49:2903–2910
31. Peng S, Fuchs A, Wirtz RA (2004) Polymeric phase change composites for thermal energy storage. J Appl Polym Sci 93:1240–1251
32. Alay S, Göde F, Alkan C (2011) Synthesis and thermal properties of poly(n-butylacrylate)/n-hexadecane microcapsules using different cross-linkers and their application to textile fabrics. J Appl Polym Sci 120:2821–2829
33. Luyt AS, Krupa I (2009) Phase change materials formed by uv curable epoxy matrix and Fischer–Tropsch paraffin wax. Energy Convers Manag 50:57–61
34. Zhang H, Wang X (2009) Synthesis and properties of microencapsulated n-octadecane with polyurea shell containing different soft segments for heat energy storage and thermal regulation. Sol Energy Mater Sol Cells 93:1366–1376
35. Sarı A, Alkan C, Döğüşcü DK, Bicer A (2014) Micro/nano-encapsulated n-heptadecane with polystyrene shell for latent heat thermal energy storage. Sol Energy Mater Sol Cells 126:42–50
36. Zhang GH, Zhao CY (2011) Thermal and rheological properties of microencapsulated phase change materials. Renew Energy 36:2959–2966
37. Jyothi NVN, Prasanna PM, Sakarkar SN, Prabha KS, Ramaiah PS, Srawan G (2010) Microencapsulation techniques, factors influencing encapsulation efficiency. J Microencapsul 27:187–197
38. Hawlader MNA, Uddin MS, Zhu HJ (2000) Preparation and evaluation of a novel solar storage material: microencapsulated paraffin. Int J Sol Energy 22:227–238
39. Su JF, Wang LX, Ren L, Huang Z (2007) Mechanical properties and thermal stability of double-shell thermal-energy-storage microcapsules. J Appl Polym Sci 103:1295–1302
40. Sari A, Alkan C, Karaipekli A, Uzun O (2009) Microencapsulated n-octacosane as phase change material for thermal energy storage. Sol Energy 83:1757–1763
41. Bayés-García L, Ventolà L, Cordobilla R, Benages R, Calvet T, Cuevas-Diarte MA (2010) Phase change materials(PCM) microcapsules with different shell compositions: preparation, characterization and thermal stability. Sol Energy Mater Sol Cells 94:1235–1240
42. Sanchez L, Sanchez P, de Lucas A, Carmona M, Rodriguez JF (2007) Microencapsulation of PCMs with a polystyrene shell. Colloid Polym Sci 285:1377–1385

43. Sánchez L, Sánchez P, Carmona M, deLucas A, Rodríguez J (2008) Influence of operation conditions on the microencapsulation of PCMs by means of suspension-like polymerization. Colloid Polym Sci 286:1019–1027
44. Sánchez L, Lacasa E, Carmona M, Rodriǵuez JF, Sánchez P (2008) Applying an experimental design to improve the characteristics of microcapsules containing phase change materials for fabric uses. Ind Eng Chem Res 47:9783–90
45. Sánchez-Silva L, Carmona M, de Lucas A, Sánchez P, Rodríguez JF (2010) Scale-up of a suspension-like polymerization process for the microencapsulation of phase change materials. J Microencapsul 27:583–593
46. Li W, Song G, Tang G, Chu X, Ma S, Liu C (2011) Morphology, structure and thermal stability of microencapsulated phase change material with copolymer shell. Energy 36:785–791
47. Wang H, Wang JP, Wang X, Li W, Zhang X (2013) Preparation and properties of microencapsulated phase change materials containing two-phase core materials. Ind Eng Chem Res 52:14706–14712
48. Yin D, Ma L, Liu J, Zhang Q (2014) Pickering emulsion: an oval template for microencapsulated phase change materials with polymer–silica hybrid shell. Energy 64:575–581
49. Ma S, Song G, Li W, Fan P, Tang G (2010) UV irradiation-initiated MMA polymerization to prepare microcapsules containing phase change paraffin. Sol Energy Mater Sol Cells 94 (10):1643–1647
50. Alkan C, Sari A, Karaipekli A (2011) Preparation, thermal properties and thermal reliability of microencapsulated n-eicosane as novel phase change material for thermal energy storage. Energy Convers Manag 52:687–692
51. Baek KH, Lee JY, Kim JH (2007) Core/shell structured PCM nanocapsules obtained by resin fortified emulsion process. J Dispers Sci Technol 28:1059–1065
52. Alay S, Göde F, Alkan C (2010) Preparation and characterization of poly(methyl-methacrylate-co-glycidyl methacrylate)/n-hexadecane nanocapsules as a fiber additive for thermal energy storage. Fibers Polym 11:1089–1093
53. Sari A, Karaipekli A (2008) Preparation, thermal properties and thermal reliability of capric acid/expanded perlite composite for thermal energy storage. Mater Chem Phys 109:459–464
54. Alay S, Alkan C, Göde F (2011) Synthesis and characterization of poly(methyl methacrylate)/n-hexadecane microcapsules using different cross-linkers and their application to some fabrics. Thermochim Acta 518:1–8
55. SarI A, Alkan C, Karaipekli A (2010) Preparation, characterization and thermal properties of PMMA/n-heptadecane microcapsules as novel solid–liquid microPCM for thermal energy storage. Appl Energy 87:1529–1534
56. Wang Y, Zhang Y, Xia T, Zhao W, Yang W (2014) Effects of fabricated technology on particle size distribution and thermal properties of stearic–eicosanoic acid/polymethylmethacrylate nanocapsules. Sol Energy Mater Sol Cells Part B 120:481–490
57. Blackley DC (1975) Emulsion polymerization, theory and practice. Applied Science, London
58. Zhang H, Wang X, Wu D (2010) Silica encapsulation of n-octadecane via sol–gel process: a novel microencapsulated phase change material with enhanced thermal conductivity and performance. J Colloid Interface Sci 343:246–255
59. Yang R, Zhang Y, Wang X, Zhang Y, Zhang Q (2009) Preparation of n-tetradecane-containing microcapsules with different shell materials by phase separation method. Sol Energy Mater Sol Cells 93:1817–1822
60. Jin Y, Lee W, Musinab Z, Ding Y (2010) A one-step method for producing microencapsulated phase change materials. Particuology 8:588–590
61. Wang JP, Zhang XX, Wang XC (2011) Preparation, characterization and permeation kinetics description of calcium alginate macro-capsules containing shape-stabilize phase change materials. Renew Energy 36:2984–2991

62. Su J, Ren L, Wang L (2005) Preparation and mechanical properties of thermal energy storage microcapsules. Colloid Polym Sci 284:224–228
63. Zhang X, Tao XM, Yick K-L, Wang X-C (2004) Structure and thermal stability of microencapsulated phase-change materials. Colloid Polym Sci 282:330–336
64. Zhang X, Fan Y, Tao X, Yick K (2005) Crystallization and prevention of supercooling of microencapsulated n-alkanes. J Colloid Interface Sci 281:299–306
65. Trigui A, Karkri M, Boudaya C, Candau Y, Ibos L (2013) Development and characterization of composite phase change material: thermal conductivity and latent heat thermal energy storage. Compos Part B 49:22–35
66. Trigui A, Karkri M, Boudaya C, Candau Y, Ibos L, Fois M (2014) Experimental investigation of a composite phase change material: thermal-energy storage and release. J Compos Mater 48:49–62
67. Trigui A, Karkri M, Krupa I (2014) Thermal conductivity and latent heat thermal energy storage properties of LDPE/wax as a shape-stabilized composite phase change material. Energy Convers Manag 77:586–596
68. Aadmi M, Karkri M, El hammouti M (2014) Heat transfer characteristics of thermal energy storage of a composite phase change materials: numerical and experimental investigation. Energy 72:381–392
69. Krupa I, Nógellová Z, Špitalsky Z, Janigová I, Boh B, Sumiga B, Kleinová A, Karkri M, AlMaadeed MA (2014) Phase change materials based on high-density polyethylene filled with microencapsulated paraffin wax. Energy Convers Manag 87:400–409
70. Karkri M, Lachheb M, Nogellová Z, Boh B, Sumiga B, AlMaadeed MA, Albouchi F, Krupa I (2015) Thermal properties of phase-change materials based on high-density polyethylene filled with micro-encapsulated paraffin wax for thermal energy storage. Energy Build 88:144–152
71. Karkri M, Lachheb M, Albouchi F, Ben Nasrallah S, Krupa I (2015) Thermal properties of smart microencapsulated paraffin/plaster composites for the thermal regulation of buildings. Energy Build 88:183–192
72. Krupa I, Nogellova Z, Špitalský Z, Malíková M, Sobolciak P, Ouederni M, Karkri M, AlMaadeed M (2014) Phase change materials based on high density polyethylene filled with microencapsulated paraffin wax. Energy Convers Manag 87:400–409
73. AlMaadeed M, Labidi S, Krupa I, Karkri M (2014) Effect of expanded graphite on the phase change materials of high density polyethylene/wax blends. Thermochim Acta 600:35–44
74. Trigui I, Karkri M, Krupa I (2014) Thermal conductivity and latent heat thermal energy storage properties of LDPE/wax as a shape-stabilized composite phase change material. Energy Convers Manag 77:586–596
75. Hong Y, Xin-shi G (2000) Preparation of polyethylene/paraffin compound as a form–stable solid–liquid phase change material. Sol Energy Mater Sol Cells 64:37–44
76. Sari A (2004) Form–stable paraffin/high density polyethylene composites as solid–liquid phase change material for thermal energy storage: preparation and thermal properties. Energy Convers Manag 45:2033–2042
77. Kaygusuz K, Sari A (2007) High density polyethylene/paraffin composites as form–stable phase change material for thermal energy storage. Energy Sources Part A 29:261–270
78. Krupa I, Mikova G, Luyt A (2007) Phase change materials based on low-density polyethylene/paraffin wax blends. Eur Polym J 43:4695–4705
79. Cai Y, Hu Y, Song L, Lu H, Chen Z, Fan W (2006) Preparation and characterizations of HDPE–EVA alloy/OMT nanocomposites/paraffin compounds as a shape stabilized phase change thermal energy storage material. Thermochim Acta 451:44–51
80. Alkan C, Sari A, Uzun O (2006) Poly(ethylene glycol)/acrylic polymer blends for latent heat thermal energy storage. AICHE J 52:3310–3314
81. Sari A, Alkan C, Kolemen U, Uzun O (2006) Eudragit S (methyl methacrylate methacrylic acid copolymer)/fatty acid blends as form–stable phase change material for latent heat thermal energy storage. J Appl Polym Sci 101:1402–1406

82. Kaygusuz K, Alkan C, Sari A, Uzun O (2008) Encapsulated fatty acids in an acrylic resin as shape-stabilized phase change materials for latent heat thermal energy storage. Energy Sources Part A 30:1050–1059
83. Alkan C, Sari A (2008) Fatty acid/poly(methyl methacrylate) (PMMA) blends as form–stable phase change materials for latent heat thermal energy storage. Sol Energy 82:118–124
84. Zhang L, Zhu J, Zhou W, Wang J, Wang Y (2011) Characterization of polymethyl methacrylate/polyethylene glycol/aluminum nitride composite as form–stable phase change material prepared by in situ polymerization method. Thermochim Acta 254:128–134
85. Sari A, Karaipekli A, Akcay M, Onal A, Kavak F (2005) Polymer/palmitic acid blends as shape-stabilized phase change material for latent heat thermal energy storage. Asian J Chem 18:439–446
86. Sari A, Kaygusuz K (2006) Studies on poly(vinyl chloride)/fatty acid blends as shape-stabilized phase change material for latent heat thermal energy storage. Indian J Eng Mater Sci 13:253–258
87. Sarier N, Onder E (2007) Thermal characteristics of polyurethane foams incorporated with phase change materials. Thermochim Acta 454:90–98
88. Sarier N, Onder E (2008) Thermal insulation capability of PEG-containing polyurethane foams. Thermochim Acta 475:15–21
89. You M, Zhang XX, Li W, Wang XC (2008) Effects of microPCMs on the fabrication of microPCMs/polyurethane composite foams. Thermochim Acta 472:20–24
90. Ke GZ, Xie JHF, Ruan RP, Yu WD (2010) Preparation and performance of porous phase change polyethylene glycol/polyurethane membrane. Energy Convers Manag 51:2294–2298
91. Sari A, Kaygusuz K (2007) Poly(vinyl alcohol)/fatty acid blends for thermal energy storage. Energy Sources Part A 29:873–883
92. Sari A, Alkan C, Karaipekli A, Onal A (2008) Preparation, characterization and thermal properties of styrene maleic anhydride copolymer (SMA)/fatty acid composites as form stable phase change materials. Energy Convers Manag 49:373–380
93. Mengjin J, Xiaoqing S, Jianjun X, Guangdou Y (2008) Preparation of a new thermal regulating fiber based on PVA and paraffin. Sol Energy Mater Sol Cells 92:1657–1660
94. Chen C, Wang L, Huang Y (2009) Ultrafine electrospun fibers based on stearyl stearate/polyethylene terephthalate composite as form stable phase change materials. Chem Eng J 150:269–274
95. Chen C, Wang L, Huang Y (2008) Morphology and thermal properties of electrospun fatty acids/polyethylene terephthalate composite fibers as novel form–stable phase change materials. Sol Energy Mater Sol Cells 92:1382–1387
96. Cai Y, Ke H, Dong J, Wei Q, Lin J, Zhao Y et al (2011) Effects of nano-SiO2 on morphology, thermal energy storage, thermal stability, and combustion properties of electrospun lauric acid/PET ultrafine composite fibers as form–stable phase change materials. Appl Energy 88:2106–2112
97. Luyt AS, Krupa I, Assumption HJ, Ahmad EEM, Mofokeng JP (2010) Blends of polyamide 12 and maleic anhydride grafted paraffin wax as potential phase change materials. Polym Test 29:100–106
98. Fang Y, Kang H, Wang W, Liu H, Gao X (2010) Study on polyethylene glycol/epoxy resin composite as a form–stable phase change material. Energy Convers Manag 51:2757–2761
99. Zhang X, Deng P, Feng R, Song J (2011) Novel gelatinous shape-stabilized phase change materials with high heat storage density. Sol Energy Mater Sol Cells 95:1213–1218
100. Sari A, Karaipekli A (2007) Thermal conductivity and latent heat thermal energy storage characteristics of paraffin/expanded graphite composite as phase change material. Appl Therm Eng 27:1271–1277
101. Sari A, Karaipekli A, Kaygusuz K (2008) Fatty acid/expanded graphite composites as phase change material for latent heat thermal energy storage. Energy Sources Part A 30:464–474

102. Sari A, Karaipekli A (2009) Preparation, thermal properties and thermal reliability of palmitic acid/expanded graphite composite as form–stable PCM for thermal energy storage. Sol Energy Mater Sol Cells 93:571–576
103. Feng L, Zheng J, Yang H, Guo Y, Li W, Li X (2011) Preparation and characterization of polyethylene glycol/active carbon composites as shape-stabilized phase change materials. Sol Energy Mater Sol Cells 95:644–650
104. Zhang Z, Fang X (2006) Study on paraffin/expanded graphite composite phase change thermal energy storage material. Energy Convers Manag 47:303–310
105. Wang W, Yang X, Fang Y, Ding J, Yan J (2009) Preparation and thermal properties of polyethylene glycol/expanded graphite blends for energy storage. Appl Energy 86:1479–1483
106. Xia L, Zhang P, Wang RZ (2010) Preparation and thermal characterization of expanded graphite/paraffin composite phase change material. Carbon 48:2538–2548
107. Xing L, Hongyan L, Shujun W, Lu Z, Hua C (2006) Preparation and thermal properties of form stable paraffin phase change material encapsulation. Energy Convers Manage 47:2515–2522
108. Wang W, Yang X, Fang Y, Ding J (2009) Preparation and performance of form–stable polyethylene glycol/silicon dioxide composites as solid–liquid phase change materials. Appl Energy 86:170–174
109. Tang B, Qiu M, Zhang S (2012) Thermal conductivity enhancement of PEG/SiO2 composite PCM by in situ Cu doping. Sol Energy Mater Sol Cells 105:242–248
110. Zhang D, Zhou J, Wu K, Li Z (2005) Granular phase changing composites for thermal energy storage. Sol Energy 78:471–480
111. Karaipekli A, Sari A (2008) Capric–myristic acid/expanded perlite composite as form–stable phase change material for latent heat thermal energy storage. Renew Energy 33:2599–2605
112. Sari A, Karaipekli A, Alkan C (2009) Preparation, characterization and thermal properties of lauric acid/expanded perlite as novel form–stable composite phase change material. Chem Eng J 155:899–904
113. Karaipekli A, Sari A (2009) Capric–myristic acid/vermiculite composite as form–stable phase change material for thermal energy storage. Sol Energy 83:323–332
114. Li M, Wu M, Kao H (2011) Study on preparation, structure and thermal energy storage property of capric–palmitic acid/ attapulgite composite phase change materials. Appl Energy 88:3125–3132
115. Li M, Wu Z, Kao H (2011) Study on preparation and thermal properties of binary fatty acid/ diatomite shape-stabilized phase change materials. Sol Energy Mater Sol Cells 95:2412–2416
116. Karaman S, Karaipekli A, Sari A, Bicer A (2011) Polyethylene glycol (PEG)/diatomite composite as a novel form–stable phase change material for thermal energy storage. Sol Energy Mater Sol Cells 95:1647–1653
117. Mesalhy O, Lafdi K, Elgafy A (2006) Carbon foam matrices saturated with PCM for thermal protection purposes. Carbon 44:2080–2088
118. Wanga Y, Xia TD, Zheng H, Feng HX (2011) Stearic acid/silica fume composite as form–stable phase change material for thermal energy storage. Energy Build 43:2365–2370
119. Li M, Wu Z, Kao H, Tan J (2011) Experimental investigation of preparation and thermal performances of paraffin/bentonite composite phase change material. Energy Convers Manag 52:3275–3281
120. Mei D, Zhang B, Liu R, Zhang Y, Liu J (2011) Preparation of capric acid/halloysite nanotube composite as form–stable phase change material for thermal energy storage. Sol Energy Mater Sol Cells 95:2772–2777
121. Zhou M, Lin T, Huang F, Zhong Y, Wang Z, Tang Y et al (2013) Highly conductive porous graphene/ceramic composites for heat transfer and thermal energy storage. Adv Funct Mater 23:2263–2269

Part III
Biomass

Biorefineries: An Overview on Bioethanol Production

Juan Carlos Dominguez Toribio and Francisco Jesus Fernández Morales

Abstract The growing interest on bioethanol has increased the pressure over new feedstock production and processing schemes. Conventional edible crops are no longer interesting as raw materials for the production of bioethanol because of their prices and ethical concerns; thus, new substrates must be used. Attending to these new necessities, lignocellulosic substrates, mainly agricultural and forest wastes, seem to be a very interesting option for bioethanol production. However, it is necessary to previously solve several limitations in their processing. These limitations are mainly related to the pretreatment used in the production process, because this stage is essential in order to make more accessible the substrates and increase the concentration of fermentable sugars after the enzymatic hydrolysis. The selection of the most adequate pretreatment and the best operation conditions for its implementation will lead to higher bioethanol yields, making the process cost-effective and more competitive with other liquid fuels. In this work, an overview of the biorefinery concept and the bioethanol production is presented.

Keywords Bioethanol, Biorefinery, Lignocellulosic, Wastes

J.C.D. Toribio
Chemical Engineering Department Chemical Sciences Faculty, Universidad Complutense de Madrid, Avda. Complutense S/N, 28040 Madrid, Spain

F.J.F. Morales (✉)
Chemical Engineering Department, University of Castilla-La Mancha, Avda. Camilo Jose Cela S/N, 13071 Ciudad Real, Spain
e-mail: FcoJesus.FMorales@uclm.es

G. Lefebvre et al. (eds.), *Environment, Energy and Climate Change II: Energies from New Resources and the Climate Change*, Hdb Env Chem (2016) 34: 153–174,
DOI 10.1007/698_2015_333,
Published online: 1 April 2015

Contents

1 Introduction

The world population has experienced continuous growth during the last century. Current projections show that, with a continuous increase, the population will reach approximately nine billion inhabitants by the year 2050 [1]. This population will need to deal with two main problems: energy supply and environmental concerns. At the same time, the huge amount of wastes generated by the population will need to be adequately managed prior to disposal.

Nowadays, the energy model and therefore the economy are mainly based on fossil energy sources such as oil, coal, natural gas, etc. These are being used for the production of fuel, electricity, and chemicals [2]. However, the environmental problems related to the fossil fuel combustion – mainly global warming, due to the drastic increase in the greenhouse gas (GHG) emissions during combustion of fossil fuels [3] – and also the prognosis of a future scarcity of fossil fuel reserves [4] are forcing the evolution to a more sustainable scenario with less GHG emissions.

To restrain and even reduce the proportion of GHG in the atmosphere, it is necessary to decrease the consumption of fossil fuels and to increase the use of renewable resources. Therefore, the new energy and economic scenario is mainly based on renewable energy sources. In this scenario, green plants are an interesting candidate as renewable energy source, because they can fix atmospheric carbon dioxide, which is together with water vapor the most important GHG, during their photosynthesis by converting it into organic substrates such as sugars, polysaccharides, amino acids, proteins, lipids, aromatic compounds, etc. Later on, the substrates contained in the plants can be used as sustainable raw materials and energy sources for bio-based products and biofuels. The term biofuel is generally used to refer to liquid or gaseous fuels, made from plant matter and residues, mainly used in the transportation sector [5]. Because of the indicated advantages, biofuels seem to be an interesting alternative to fossil fuels. This interest had lead to a significant

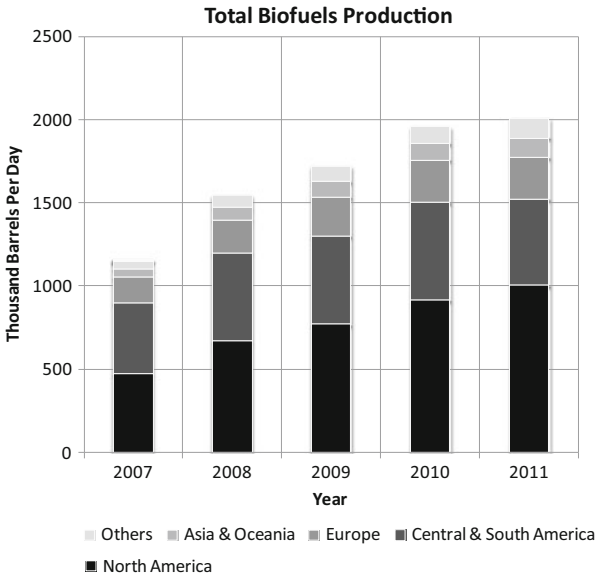

Fig. 1 Total biofuel production in thousand barrels per day. Data from US Energy Information Administration http://www.eia.gov

increase in the biofuel production during the last years. In Fig. 1, the world's total biofuel production in the period 2007–2011 is exhibited.

As can be seen in Fig. 1, almost 50% of the world's biofuel production is carried out in North America, mainly in the USA where it is produced about 95% of the North America production. Central and South America produce about 25% of the world's biofuel production; in this region Brazil is the main producer with about 85% of the production. Finally, the accumulated contribution of the rest of the globe accounts for a 25% of the world's production.

The shift from the fossil fuel economy to a bioenergy economy will allow advancing to a more sustainable growth. Mainly because these processes are based on renewable organic feedstock and also because a wide range of organic wastes and by-products could be used for chemical synthesis and bioenergy generation. Agricultural crops and residues, forest residues, farming wastes, agro-food wastes, organic fraction of municipal solid wastes (OFMSW), etc., are included among these wastes and by-products. Nowadays, the common ways for disposal of these wastes include landfilling, incineration, and feeding for animals. In the particular case of the OFMSW, it must be noted that currently most of these wastes are disposed in landfills, losing the opportunity of its valorization [6]. As an alternative, processing of these organic substrates could be used for adding value by means of transformation into interesting products with defined properties, with the economic and environmental advantages that this implies. This alternative processing of the organic substrates is in agreement with the biorefinery definitions in literature [7]. According to the American National Renewable Energy Laboratory (NREL): "A biorefinery is a facility that integrates biomass conversion processes and equipment to produce fuels, power, and chemicals from biomass.

The bio-refinery concept is analogous to today's petroleum refineries, which produce multiple fuels and products from petroleum. Industrial bio-refineries have been identified as the most promising route to the creation of a new domestic biobased industry."

The main advantages of biorefineries are the sustainable processing, mainly when they are based on microbial metabolisms, and the use of sustainable raw material, because they are organic substrates and sometimes even wastes. Therefore, biorefinery entails a double advantage: the raw material stabilization and the valorization of the chemicals or energy contained. Therefore, biorefinery deals with materials and energy. In this way, the reduction of the wastes or by-products could be linked to chemical and energy generation by means of one or more unit operations. In this sense it is important to remark that these unit operations could be carried out by microorganisms. This increases the sustainability of the process in both, the economical and the environmental, points of view [8]. Moreover, the biorefinery processes can be set to a zero waste concept. With this configuration, the wastes and/or by-products of a precedent unit operation could be used as the raw materials or source of energy for the following one, avoiding the generation of wastes.

In the particular case of the biofuels, they can be obtained by means of production processes based on raw biomaterials and/or bioprocesses according to the biorefinery concept. There are many different types of biofuels, which are produced from various crops and via different processes. Biofuels can be classified broadly as biodiesel and bioethanol and then subdivided into conventional or advanced fuels [9]. Because of its nature, the use of biofuels can contribute to the reduction of GHG emissions, providing a sustainable and clean energy source, at the same time that the economy in rural areas is increased. Nowadays, biofuels are mainly produced from biomass resources. Biomass is a very interesting feedstock for several main reasons: it is a renewable resource; it is balanced with the environment, resulting in no net releases of carbon dioxide; its very low sulfur content minimized the acidification of the environment; and in a future scenario with fossil fuel prices increasing, it will have a significant economic potential [10–12].

2 Biorefineries

Similar to the petroleum transformation in a conventional refinery, biorefinery uses different separation methods to obtain products with high added value [13] from biomass. Biomass presents a complex composition [14]. In the particular case of plant biomass, it is composed of basic carbohydrates, lignin, fats, proteins, dyes, etc. [15]. Because of that, a wide spectrum of products can be obtained from the processing of the plant biomass. With this aim, biorefineries combine unit operations in order to convert various types of feedstocks into industrial intermediates and final products. The flexibility of its used feedstock is the factor of first priority

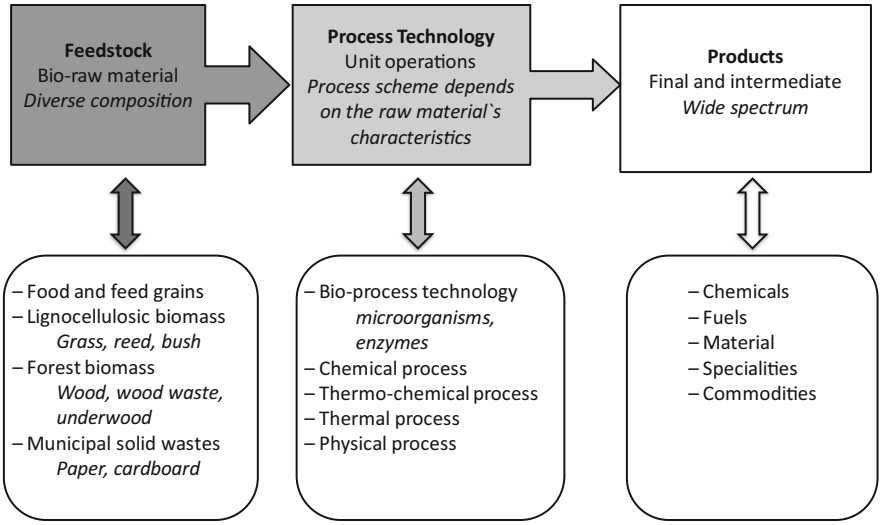

Fig. 2 Basic principles of the biorefinery concept

for adaptability toward changes in demand and supply. In Fig. 2 the basic principles of biorefinery are presented.

An adequate processing of the basic compounds contained in the biomass should be performed in order to achieve a feasible operation of biorefineries. Carbohydrates are one of the main substrates in biomass, accounting for about 75% of the total biomass. They are mainly present in the form of cellulose, hemicelluloses, starch, and saccharose. The lignin fraction in the biomass is also important, about 20%. The remaining 5% of biomass composition includes oils, proteins, and other compounds. Because of the prevalence of carbohydrates, most of the attention has been focused on its transformation into chemical bulk and final products. It is also important to remark that the glucose contained in the biomass, in the form of starch, cellulose, etc., presents an interesting value because of the wide range of chemical products that can be synthesized from glucose. Moreover, it must be highlighted that these transformations could be made by means of biotechnological processes, which is interesting from the energetic and the economical point of view [16].

Among the variety of products that can be obtained from glucose by means of microbial transformations stand up ethanol, lactic acid, acetic acid, levulinic acid, etc. Moreover, glucose could be used for synthesizing intermediates that could be employed in conventional processing lines. A scheme of possible intermediates and final products that could be obtained from biomass in a biorefinery is presented in Fig. 3.

The use of biotechnology in biorefineries is a significant step since it allows obtaining more sustainable intermediate and final products, because bioprocesses are based on microbial metabolisms and therefore does not produce any harmful substance to the environment. As an example, the following chemicals could be

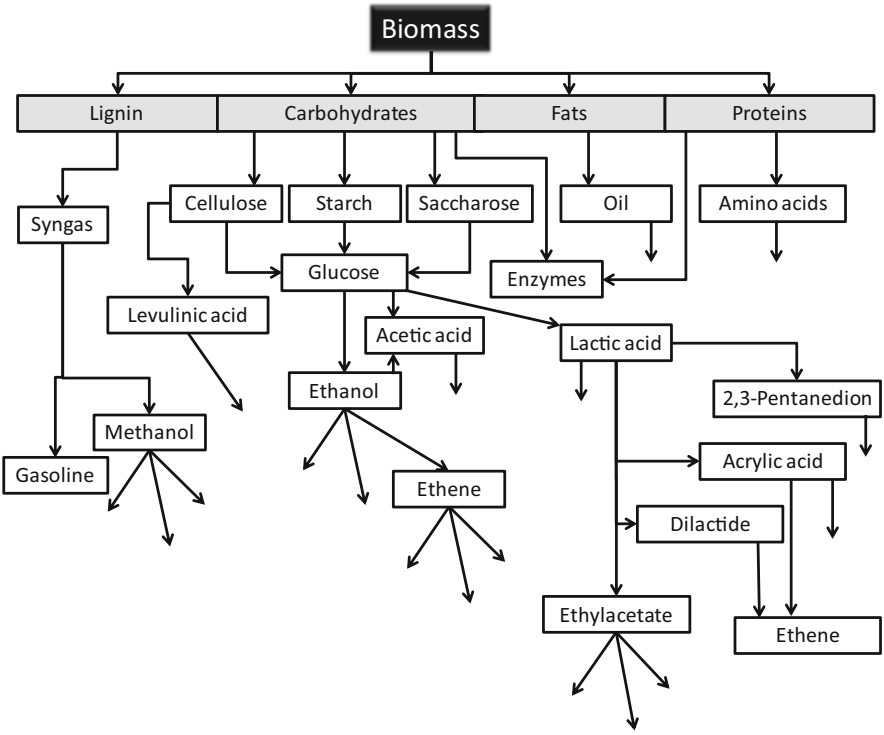

Fig. 3 Product line of biomass in a biorefinery, with special emphasis on carbohydrates

obtained from microbial transformation of glucose: acetaldehyde, propylene, malic acid, citric acid, methane, ethylene, lactic acid, acetic acid anhydride, 2,3-pentanedione, parasorbic acid, methanol, ethanol, propanediol, diethyl ether, itaconic acid, sorbic acid, acetic acid, propylene oxide, vinyl acetate, aconitic acid, acetone, *n*-butanol, isoascorbinic acid, etc.

After the biotransformation of the raw materials, the recovery of the product requires several steps such as filtration, extraction, distillation, etc.

2.1 Crop and Green Biorefinery

Crops like wheat, corn, etc., can be used as feedstock in biorefinery conforming the crop biorefinery. These crops are usually transformed in order to extract their main components: lignocellulosic material and starch. In the case of the green biorefinery, a wide spectrum of feedstocks such as grass, closure fields, lucerne, clover, etc., are used. When green crops are processed, cellulose, starch, and sugars are obtained. Moreover, the green juice obtained contains proteins, dyes, hormones, free amino acids, organic acids, etc. These compounds can be subsequently processed.

2.2 *Lignocellulosic Biorefinery*

As it was previously indicated, lignocelluloses are one of the main components of the biomass. Lignocelluloses are present in a number of raw materials such as straw, reed, grass, wood, etc. Their conversion products have a very good position on traditional and future chemical market.

Lignocelluloses mainly consist of three chemical fractions: lignin, cellulose, and hemicelluloses. An overview of the main products that could be obtained from a lignocellulosic biorefinery is presented in Fig. 4.

From microbial conversion of glucose, interesting fuels can be obtained such as hydrogen [17] and methane [18]. Another interesting product that could be obtained is the ethanol. Some yeasts can transform the glucose into ethanol with very high yields, around 90% w/w. Ethanol is a very important product because it can be used in conventional petrochemical refinery for ethylene production and its derived

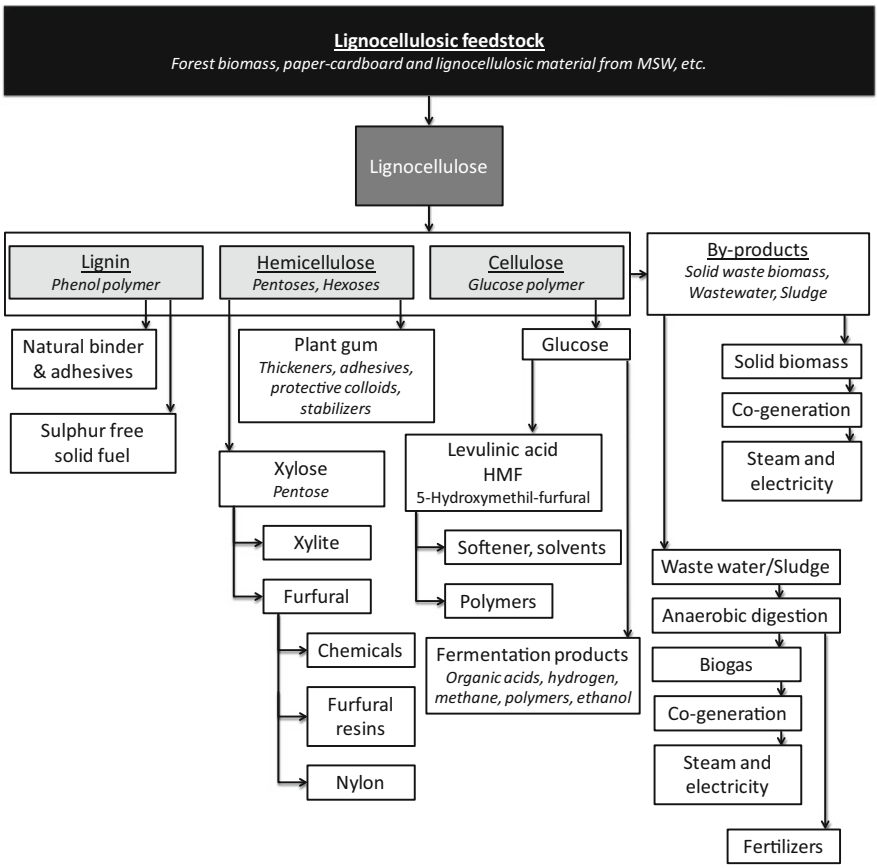

Fig. 4 Product line in a lignocellulosic biorefinery

commodities such as polyethylene and polyvinyl acetate. Moreover, ethanol can be used as fuel additive. The technology for biomass conversion into ethanol has great challenges mainly related to the feedstock processing. Because of that, special attention must be paid to a few aspects such as the price of the feedstock and its availability, uniformity, cleanliness, efficiency, and yield.

3 Bioethanol

Bioethanol and bioethanol–gasoline mixtures have been used as alternative transportation fuels since the beginning of the twentieth century [19]. This situation was stimulated during World War II due to the scarcity of petrol supply. However, the potential of bioethanol was ignored until the oil crisis of the beginning of the 1970s [20].

Since the beginning of the 1980s, there has been an increased interest in the use of bioethanol as an alternative fuel. This can be explained because during the last decades, governmental initiatives promoting the use of renewable fuels have been carried out. Many countries are shifting their focus toward renewable energy sources, mainly because of depleting crude oil reserves but also because biofuels can be produced anywhere, reducing the energetic dependence of the countries. Because of the global interest, the global market for biofuel has entered a phase of rapid growth.

Among the renewable fuel options, bioethanol seems to be one of the best because of its chemical properties. At the beginning, bioethanol was used as an octane enhancer to replace lead, but nowadays, its octane number, flammability limits, higher flame speeds, and higher heats of vaporization make bioethanol a very interesting fuel for transportation. These chemical properties allow bioethanol for a higher theoretical efficiency, compared to gasoline, when it is burned in an internal combustion engine [21].

Anyway, bioethanol presents several disadvantages, including the following: a lower energy density than gasoline, about a 30% lower, and a lower vapor pressure than gasoline which makes more difficult the cold starts of the engines [22]; also, it is a corrosive liquid and presents a very high chemical oxygen demand (COD), which leads to harmful effects on the environment when it is accidentally discharged.

One of the main advantages of bioethanol is that it is a liquid fuel that can be adapted to existing fuel supply systems, replacing at least partially fossil fuels in the transportation sector [23]. Bioethanol can be directly used in the engines or it can be blended with gasoline. Bioethanol can be used as a 5% blend with petrol under the EU quality standard EN 228. Moreover, the use of this blend is covered by vehicle warranties. Furthermore, bioethanol is most commonly blended with gasoline in a concentration ratio of 1:10 and in a less extension blended with gasoline in a mixture called gasohol composed of 24% bioethanol and 76% gasoline [24]. With engine modification, bioethanol can be used at higher levels, 85%

bioethanol, for example [12]. However, the higher production cost of bioethanol compared to that of fossil fuels is delaying the increase of bioethanol percentages in blends.

Bioethanol is seen as a good fuel alternative because the raw materials used are renewable and can be grown in most climates around the world. However, the use of starch or sugar feedstocks has directly increased food prices, generating ethical conflicts and also increasing the prices of the raw material used, which account for 40–75% of the total expenses of bioethanol production. Therefore, cheap and abundant nonfood materials are required as alternative biomass sources, e.g., agricultural by-products, forest residues, energy crops [25, 26], or even wastes.

The production of bioethanol according to the first-generation biofuels is based upon edible crops, mainly starch crops (corn and wheat) and from sugar crops (sugarcane and sugar beet). The main drawbacks of the bioethanol generated from edible feedstock are the concerns about competition with food supplies, which has important implications from the ethical point of view. Therefore, a second generation of biofuels was developed. In general, second-generation biofuels are produced from nonedible lignocellulosic feedstocks. These raw materials result in the production of more fuel per unit of agricultural land use and require less chemical and energy consumption, resulting in a higher yield in terms of net energy produced. Moreover, these lignocellulosic materials are considered not to directly compete with food. However, it must be noted that there is a clear competition for land use as well as for other potential use of the lignocellulosic materials, mainly for heat and power generation through combustion as solid biofuel.

Nonedible crops like *sweet sorghum* require less water or nutrients, having a shorter growing period and a higher fermentable substrate content than conventional sugar crops like sugarcane. Moreover, the whole *sweet sorghum* plant can be processed without leaving any waste. Additionally, the development of lignocellulosic treatment technology allowed extracting not only the energy content in starch and sugar crops but also in wood, in wastes from forestry, and even from the OFMSW.

These nonedible feedstocks are a more sustainable and ethical raw material source for the production of bioethanol, because of their abundance, widespread distribution, and noncompetitiveness with food supply. Second-generation bioethanol processes that use agro-industrial wastes have, besides their low cost and absence of ethical implications, the additional advantage of the valorization of the waste.

The use of these alternative nonedible substrates in the second-generation biofuels opens up new possibilities for the bioethanol production. In this way, they can compete with products derived from fossil resources in terms of economical and energetic sustainability, resource availability, supply reliability, and environmental friendliness.

Regarding the second-generation bioethanol, at the beginning of 2013, there were 48 projects under operation, 9 were under construction or under commissioning, and 14 projects were planned. The largest projects were the Neste Oil's facilities in Rotterdam (the Netherlands) and Singapore, Borregaard Industries in

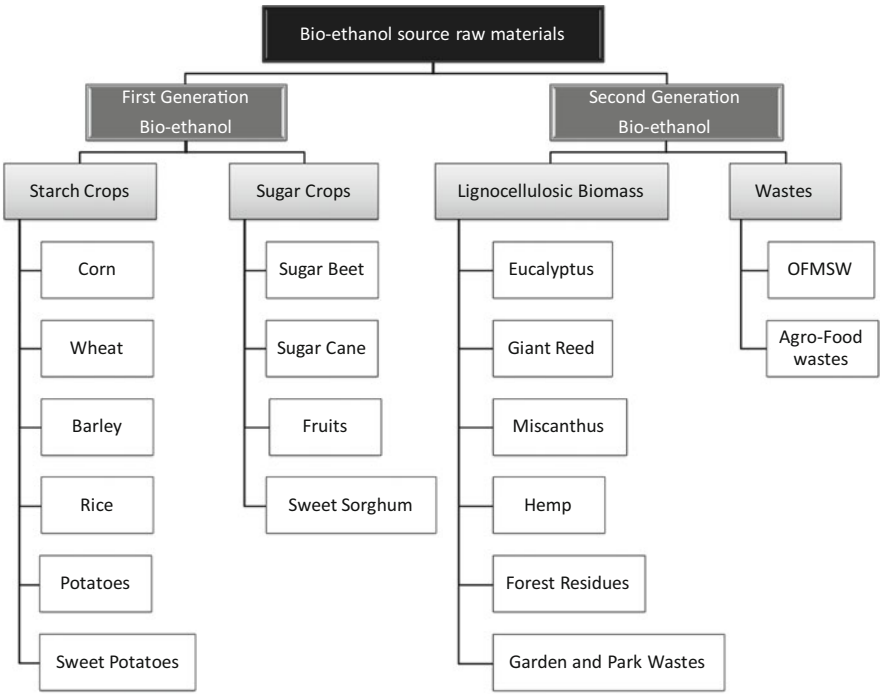

Fig. 5 Scheme of potential feedstocks for bioethanol production

Sarpsborg (Norway), and Tembec Chemical Group in Temiscaming (Canada), using chemical, biochemical, and thermochemical technology, respectively. The largest plants under construction for cellulosic bioethanol production were those of Abengoa in Hugoton, USA (75,000 t/year), and POET-DSM in Emmetsburg, USA (75,000 t/year).

In Fig. 5 a scheme of potential feedstock for bioethanol production is shown.

In this sense, research into new carbon sources among agro-food industry by-products and agricultural residues for use in second- and third-generation bioethanol production is essential for the successful development of renewable biofuels.

Additionally, the combustion of bioethanol can be considered as carbon dioxide neutral. This is because in the growing phase of the source substrate, generally biomass, carbon dioxide is fixed by means of photosynthesis and oxygen is released. Then, the bioethanol is combusted consuming oxygen as oxidant and releasing carbon dioxide in the same amount that was previously fixed. Therefore, the net carbon dioxide release, in a time horizon of about 1 year, is nil. Obviously, this is a clear advantage when comparing with fossil fuels in which the carbon dioxide emissions are uncoupled of the carbon dioxide fixation by millions of years. Moreover, fossil fuels release other pollutants.

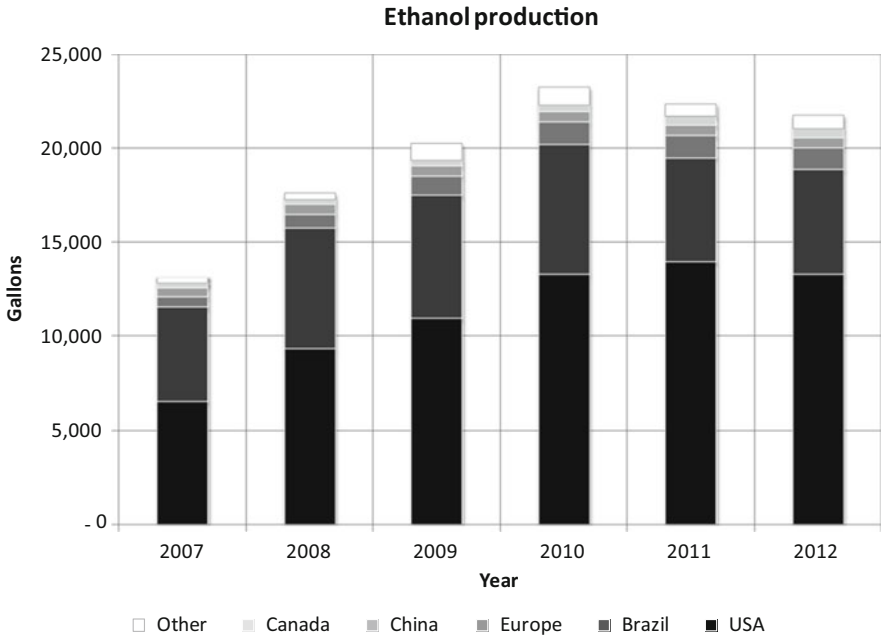

Fig. 6 Scheme of potential feedstocks for bioethanol production. Data from Renewable Fuels Association "2014 Ethanol Industry Outlook" http://www.ethanolrfa.org/pages/annual-industry-outlook

Regarding the global production of bioethanol, it peaked in 2010, being the USA the world's largest producer. Together, the USA and Brazil produce 87% of the world's bioethanol. The vast majority of US bioethanol is produced from corn, while Brazil primarily uses sugarcane. In Fig. 6 the global ethanol production by country or region, during the period 2007–2012, can be seen.

3.1 Substrates for Bioethanol Production

Although oil feedstock varies in a certain extension, their composition is much constant than that of the biomass. The main components of biomass are carbohydrates (cellulose, hemicelluloses, lignocelluloses, starch, and sugars), lipids (wax, fats, and oils), proteins, aromatic compounds (lignin), and ash (phosphorous, calcium, etc.). This biomass compositional variety is a disadvantage but also an advantage. The advantage of its heterogeneous composition is that a biorefinery can produce a wider spectrum of products, even more than a conventional oil refinery. The main disadvantage is the range of unit operations required for its processing, mainly for the conversion and separation of the raw materials and intermediate or final products.

As it was previously stated, one of the main products obtained from biorefineries is ethanol. Nowadays, large-scale production of ethanol is mainly based on sucrose from sugarcane and starch, mainly from corn and soybeans. As indicated above, ethanol production based on corn or sugarcane may not be desirable because they are edible crops. Not only ethics but also cost will be a key factor in the growth of the bioethanol market. This is because the economy of the ethanol production process from edible crops is dependent on the market of the product itself and its by-products. It must be also taken into account that, unfortunately, the market of the products and their by-products may not expand as that of ethanol in the future [27].

Because of the ethical and economical concerns, new substrates must be used for ethanol production [28]. In this sense, the use of lignocellulosic materials, a low-cost renewable raw material and easily available, avoids the existing competition of food versus fuel caused by edible crop-based bioethanol production [29]. At the same time, this represents a great opportunity for converting cheap substrates, sometimes considered as wastes, into a fuel. Because of that, lignocellulosic substrates are entitled to be one of the main feedstocks for bioethanol production in the medium and long term. Moreover, it must be highlighted that bioethanol production could be the route to the effective utilization of agricultural wastes produced every year. Although to use renewable plants, crop residues, and other biomass materials for bioethanol production is the best option, several concerns must be taken into account. Among them, attention should be focused on the implications of the composition of the biomass, destruction of vital soil resources, cultivation and land use practices, energy balance, pollutant gas emissions, pollution due to pesticides, soil erosion, effect over biodiversity and landscape value, transport and storage costs of the biomass, and water requirements and water availability [7].

Estimations indicate that about 442 million cubic meters of bioethanol could be produced from lignocellulosic biomass and that the bioethanol from crop residues and wasted crops could be about 491 million cubic meters per year. These numbers mean that they are about 16 times the actual world bioethanol production [30]. The lignocellulosic compounds can be obtained from a number of biomass sources, including rice straw, corn straw, wheat straw, sugarcane bagasse, grasses, wood chips, sawdust, etc. Because of the great expectations on lignocellulosic compounds, extensive research has been carried out on ethanol production from lignocelluloses in the past decades [14, 31, 32].

Waste biomass is very attractive as feedstock for bioethanol production because it is one of the most abundant and in certain extension homogeneous natural resources along the globe, contributing to sustainability [5, 33].

4 Pretreatments

The process to convert organic substrates into bioethanol encompasses upstream and downstream operations. When processing any complex raw material, such as lignocellulosic feedstocks, several stages are necessary. The aim of the first stage,

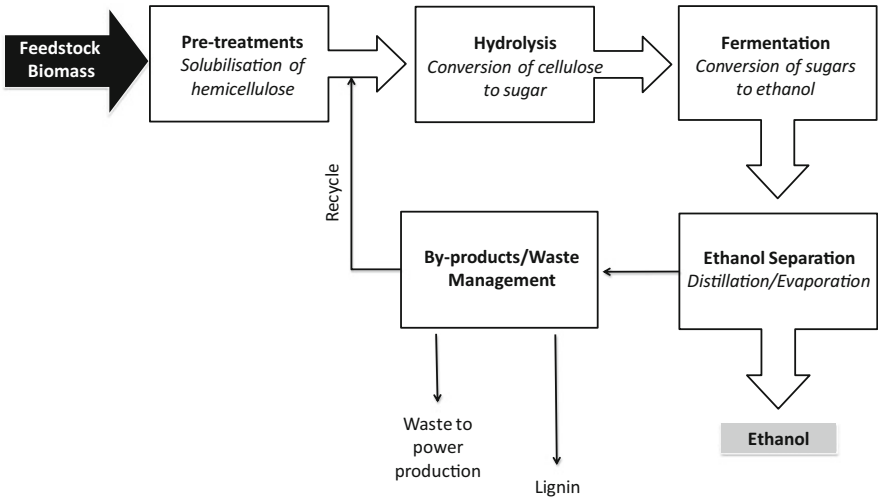

Fig. 7 Schematic diagram of the biomass conversion to bioethanol

called pretreatment, is to alter the structure of the biomass breaking the lining seal and hemicelluloses sheathing over cellulose and also disrupting the crystalline structure of cellulose. After that, the feedstock substrates will be more accessible for transformation during the following stages. The second stage is an enzymatic saccharification with enzymes, and then the third stage is the fermentation of the sugars obtained by means of yeast and bacteria. Finally, the final product recovery must be carried out [34]. A scheme of the main stages is presented in Fig. 7.

When treating biomass, the pretreatment is the crucial stage because it makes more accessible the carbohydrate polymers to the hydrolytic enzymes and therefore determines the final concentration of fermentable substrates available to produce bioethanol [35, 36]. In literature a number of pretreatments have been described. These pretreatments can be grouped into physical pretreatment, chemical pretreatment, thermal pretreatments, biological pretreatment, and their combinations.

Recently, also ionic liquids have been used in a pretreatment process [37]. Their main advantage is that they can act as solvents in a variety of chemical processes presenting the ability to dissolve wood species that are insoluble in conventional solvents.

The goals of an efficient pretreatment are the directly obtaining of glucose after the subsequent hydrolysis stage, avoiding any degradation of sugar content, and the formation of inhibitory compounds. These objectives must be obtained reducing the energy demands [38] in order to minimize the costs. It must be remarked that the pretreatment is one of the most expensive processing stages for the production of bioethanol. Therefore, the pretreatment must be balanced between the economical and production yield points of view [34, 39, 40]. In general, the selected pretreatment must be simple, energy efficient, and cost-effective, and the most

important issue is that it must avoid any fermentable substrate degradation, because this would reduce the bioethanol yield of the process.

4.1 Physical Pretreatments

The physical pretreatment processes normally are size reduction of raw materials by means of mechanical methods such as chipping, milling, and gridding [41–44] and microwave/ultrasound irradiation [45–49].

The *mechanical size reduction pretreatments* decrease the cellulose crystallinity, improving the efficiency of the subsequent hydrolysis [50, 41]. The main techniques used are dry and wet milling, vibratory ball, and compression milling [51, 52]. The main drawback of these processes is that they are very high-energy-consuming processes. Because of that, these pretreatments are not very often implemented in full-scale plants. Obviously, the energy consumption depends on the nature and moisture content of the feedstock and on the desired final size. Regarding the final size of the feedstock, it must be taken into account that, on one hand, a very big size does not enhance the subsequent hydrolysis, but, on the other hand, a very small size could generate clogging during the downstream processing and a significant increment in the operational costs. Moreover, size reduction pretreatments make easier the handling of the feedstock in the subsequent processing operations, avoiding mass and energy transfer limitations [36].

Microwave pretreatment is based on thermal and nonthermal effects caused by the short-wavelength radiation. Microwaves drastically increase the temperature of the water causing a hot spot which results in an explosion which disrupts the adjacent particles [53]. In the case of lignocellulosic feedstocks, the hydrolysis causes the release of acetic acid. This weak acid enhances the effects caused by the high temperature that reached in the process [38]. Regarding *ultrasounds*, its effects are similar to the thermal effects caused by microwaves. Ultrasounds create cavitation bubbles, and the implosion of these bubbles drastically increases the temperature of water, causing a hot spot [53] and causing the effects previously described for microwaves [45, 49, 54].

4.2 Physical–Chemical Pretreatments

These treatments are based on the solubilization of lignocellulosic biomass. Some of the most relevant physical–chemical pretreatments are described below in this section.

Liquid hot water treatment, also known as *autohydrolysis*, uses water at temperatures ranging from 160 to 230°C and pressures higher than 5 MPa with the aim to keep the water in the liquid state. Usually the pH is controlled in the range 4–7 in order to avoid the polysaccharide degradation [55]. In literature modifications of

this process by means of the addition of organic and mineral acids have also been described [34, 56].

Steam explosion has been one of the most often used pretreatments, showing successful results for a wide spectrum of lignocellulosic feedstocks. In this pretreatment the biomass is exposed to a high temperature and pressure steam, about 150–300°C and 20–50 bar, for several minutes. Then, the pressure and temperature are drastically decreased allowing the expansion of the condensed moisture within the lignocelluloses matrix and disaggregating them into individual fibers. The high yields obtained make this pretreatment interesting from the economical point of view [57].

Ammonia fiber explosion (AFEX) is an alkaline thermal pretreatment based on the combination of steam explosion and alkaline pretreatments. This pretreatment uses about 0.3–2 kg ammonia per kg of biomass, and it is performed at moderate temperatures, ranging from 40 to 140°C, and moderate pressures, ranging from 1.5 to 2.0 kPa, for several minutes [58]; then, the pressure and temperature are drastically reduced. In this pretreatment the presence of ammonia at moderate temperature and high pressure allows a combined physical and chemical effect that induces cleavage of lignin–carbohydrate complex, hemicellulose hydrolysis, and cellulose decrystallization. All these processes lead to an almost complete conversion of cellulosic and hemicellulosic compounds into fermentable sugars without the production of major inhibitors for enzymes or microbes. Unfortunately, this pretreatment presents high costs due to the use of ammonia. Because of that, the ammonia recovery and reuse is a key point in its full-scale implementation [59]. Hopefully, the volatility of ammonia allows its recovery and reuse, leaving the feedstock ready for the subsequent enzymatic hydrolysis [60–62]. Other ammonia-based pretreatments are *ammonia recycle percolation (ARP)*, *soaking in aqueous ammonia (SAA)*, *supercritical ammonia*, and *ammonia hydrogen peroxide* pretreatments. The main differences of these processes with *AFEX* are the thermodynamic state of the ammonia–water mixtures and the applied ammonia concentration.

Another pretreatment in this group is the *carbon dioxide explosion*. This pretreatment is similar to that of the ammonia and steam explosion. The main difference is that the carbon dioxide explosion is more cost-effective than the ammonia explosion and that it does not generate the inhibitors generated in the steam explosion [38].

4.3 Chemical Pretreatments

The chemical pretreatments used are based on either acid (hydrochloric acid and sulfuric acid) or alkaline (lime and sodium hydroxide) chemicals. Also, they can be implemented using organic solvents – known as organosolv treatments – carbon dioxide, and other chemicals. The yield of fermentable sugars released during the chemical pretreatment is influenced by a number of parameters such as

concentration, contact time, temperature, and feedstock-to-chemical ratio. These pretreatments, combined with high temperature or high pressure, have been extensively applied [35, 36, 63–65].

Acid hydrolysis can be divided into two groups of pretreatment: one based on concentrated acid at low temperature and the other one based on diluted acid at high temperature [59]. Regarding the acid concentration, it must be also taken into account that, on one hand, the use of concentrated acid allows the process to lower operational costs because the acid can be recovered after the pretreatment. However, on the other hand, the higher the acid concentration, the higher the corrosion problems. Diluted acid pretreatments are considered one of the most important pretreatments [66]. Usually, they are carried out using concentrations in the range 0.2–5% w/w and temperatures between 120°C and 220°C. The acid most commonly used is sulfuric acid although other acids such as hydrochloric, nitric, and trifluoroacetic acids have also been employed [59]. In these pretreatments, the acid attacks hemicelluloses and cellulose. Unfortunately, sometimes the acid pretreatments generate degradation products such as furfural, 5-hydroxymethylfurfural, phenolic acids, aldehydes, etc., which could act as inhibitory compounds in the microorganism's growth. Because of that, before the subsequent fermentation, the hydrolysate must be detoxified.

Alkaline pretreatments are mainly based on sodium and potassium hydroxide, lime, and ammonia. Alkaline pretreatments are commonly used for delignification of biomass under mild operating conditions with the aim to minimize sugar degradation avoiding the generation of inhibitory compounds [35, 36], being a process similar to the Kraft paper pulping technology. When used with lignocellulosic feedstock [46, 67], these chemicals enhance the cellulose and hemicellulose enzymatic degradation. After the pretreatment, the product can be divided into alkali-soluble lignin, hemicelluloses, and residue. This residue is rich in cellulose and can be used for paper and derivate production. Sodium hydroxide and lime are used in the range 0.05–0.15 g alkali/g biomass and temperatures in the range of 30–130°C with contact times ranging from 18 min until 18 h [59].

In literature the use of oxidant agents, such as air, oxygen, or hydrogen peroxide, in combination with alkaline pretreatment has been reported [68, 69]. This combination, known as *alkaline peroxide*, greatly improves the lignin removal. The reaction mechanisms are similar to that of the alkaline pretreatment, but it is complemented with the oxidation of the lignin by the oxygen peroxide. The main advantage of this combination is that it presents a faster kinetics at low temperature. This pretreatment has also been studied in combination with steam explosion and hydrothermal treatments.

Organosolv pretreatments are based on the differential solubilization and partitioning of feedstock components in organic solvents and water. After the treatment, the organic solvent can be easily removed allowing the recovery of the lignin [63]. Formic acid, acetic acid, methanol, ethanol, acetone, etc., can be used as organic solvents [63, 64]. This pretreatment helps in the delignification of lignocelluloses feedstocks. The solvent can be recovered by distillation and subsequently reused [36].

Recently, *ionic liquids* (ILs) have been used as pretreatment. ILs are able to establish hydrogen bonds with cellulose at high temperature. Usually, the ILs-to-feedstock ratio is about 10:1. Lignocellulosic feedstock pretreatment using ILs offers several attractive features when compared to conventional methods. These advantages include significantly lower temperatures, below 100°C, and less hazardous process chemicals and conditions [37]. As a drawback, the very high cost related to ILs must be also noted.

4.4 Biological Pretreatments

The biological pretreatments are based on the enzymatic modifications caused by microorganisms, mainly fungi such as rot, brown rot, and soft rot [38]. These enzymes degrade the biomass releasing the fermentable substrates. The biological pretreatments have been reported as powerful pretreatments of biomass [70]. The main disadvantages are that these pretreatments present low rates, which increases the length of the pretreatment, and that the used organisms consume some of the carbohydrates available, which reduces the final yield of the pretreatment [50, 58, 71]. However, the main advantages are that biological processes are non-energy-intensive processes and do not consume chemicals and the organisms used are self-sustained [36, 57, 58].

5 Concluding Remarks

The search for more sustainable fuels has drastically increased during the last years, mainly because they will allow reduction in the greenhouse gas emissions and also because they will provide energy independence. Bioethanol is one of the most promising options; however, the major problem with bioethanol production is the availability of raw materials for its production. In the future, the bioethanol from edible crops should be minimized only to production excess or out-of-specification products in order to avoid a severe competence with food provision. With regard to feedstock, the use of nonedible substrates, forest wastes, and even OFMSW seems a good option, allowing to obtain a sustainable fuel at the same time that wastes or at least nonedible crops are transformed. About the processing, the pretreatments stand up as one of the key stages, mainly because they make more accessible the substrates contained for the hydrolysis and fermentation stages, increasing the bioethanol yield.

References

1. Gonzalez del Campo A, Lobato J, Cañizares P, Rodrigo MA, Fernandez Morales FJ (2013) Short-term effects of temperature and COD in a microbial fuel cell. Appl Energy 101:213–217
2. Uihlein A, Schebek L (2009) Environmental impacts of a lignocellulose feedstock biorefinery system: an assessment. Biomass Bioenergy 33(5):793–802
3. Ballesteros I, Negro MJ, Oliva JM, Cabañas A, Manzanares P, Ballesteros M (2006) Ethanol production from steam-explosion pretreated wheat straw. Appl Biochem Biotechnol 130 (1–3):496–508
4. Laherrère J, Perrodon A (1997) Technologie et réserves. Petrole et Techniques 406:10–28
5. Balat M (2007) An overview of biofuels and policies in the European union. Energ Source Part B: Econ Plann Policy 2(2):167–181
6. Fernández FJ, Sánchez-Arias V, Rodríguez L, Villaseñor J (2010) Feasibility of composting combinations of sewage sludge, olive mill waste and winery waste in a rotary drum reactor. Waste Manag 30(10):1948–1956
7. Kamm B, Gruber PR, Kamm M (2008) Biorefineries – industrial processes and products: status quo and future directions, vol 1–2. Wiley, Weinheim
8. Harrison RG (2013) Bioseparations science and engineering. Topics in chemical engineering. Nota, Kbh
9. Hammond GP, Kallu S, McManus MC (2008) Development of biofuels for the UK automotive market. Appl Energy 85(6):506–515
10. Cadenas A, Cabezudo S (1998) Biofuels as sustainable technologies: perspectives for less developed countries. Technol Forecast Soc Chang 58(1–2):83–103
11. Demirbas A (2008) Biomethanol production from organic waste materials. Energ Source Part A: Recovery Utilization Environ Effects 30(6):565–572
12. Demirbas A (2008) The importance of bioethanol and biodiesel from biomass. Energ Sources Part B: Econ Plann Policy 3(2):177–185
13. Huang HJ, Ramaswamy S, Tschirner UW, Ramarao BV (2008) A review of separation technologies in current and future biorefineries. Sep Purif Technol 62(1):1–21
14. Orozco RS, Hernández PB, Morales GR, Núñez FU, Villafuerte JO, Lugo VL, Ramírez NF, Díaz CEB, Vázquez PC (2014) Characterization of lignocellulosic fruit waste as an alternative feedstock for bioethanol production. BioResources 9(2):1873–1885
15. Velázquez-Martí B, Sajdak M, López-Cortés I, Callejón-Ferre AJ (2014) Wood characterization for energy application proceeding from pruning Morus alba L., Platanus hispanica Münchh. and Sophora japonica L. in urban areas. Renew Energy 62:478–483
16. Wainwright M (1999) An introduction to environmental biotechnology. Kluwer, Boston
17. Infantes D, González Del Campo A, Villaseñor J, Fernández FJ (2011) Influence of pH, temperature and volatile fatty acids on hydrogen production by acidogenic fermentation. Int J Hydrog Energy 36(24):15595–15601
18. Rodríguez L, Villaseñor J, Fernández FJ, Buendía IM (2007) Anaerobic co-digestion of winery waste water. Water Sci Technol 56(2):49–54
19. Demirbas A, Karslioglu S (2007) Biodiesel production facilities from vegetable oils and animal fats. Energ Source Part A: Recovery Utilization Environ Effects 29(2):133–141
20. Balat M (2009) New biofuel production technologies. Energy Educ Sci Technol Part A Energy Sci Res 22(2):147–161
21. Balat M (2007) Global bio-fuel processing and production trends. Energ Explor Exploit 25 (3):195–218
22. MacLean HL, Lave LB (2003) Evaluating automobile fuel/propulsion system technologies. Prog Energy Combust Sci 29(1):1–69
23. Carroll A, Somerville C (2009) Cellulosic biofuels. Annu Rev Plant Biol 60:165–182
24. Dias De Oliveira ME, Vaughan BE, Rykiel EJ Jr (2005) Ethanol as fuel: energy, carbon dioxide balances, and ecological footprint. Bioscience 55(7):593–602

25. Demirbas A (2011) Competitive liquid biofuels from biomass. Appl Energy 88(1):17–28
26. Swain PK, Das LM, Naik SN (2011) Biomass to liquid: a prospective challenge to research and development in 21st century. Renew Sust Energ Rev 15(9):4917–4933
27. Taherzadeh MJ, Karimi K (2007) Acid-based hydrolysis processes for ethanol from lignocellulosic materials: a review. BioResources 2(3):472–499
28. Balat M, Balat H (2009) Recent trends in global production and utilization of bio-ethanol fuel. Appl Energy 86(11):2273–2282
29. Bjerre AB, Olesen AB, Fernqvist T, Plöger A, Schmidt AS (1996) Pretreatment of wheat straw using combined wet oxidation and alkaline hydrolysis resulting in convertible cellulose and hemicellulose. Biotechnol Bioeng 49(5):568–577
30. Kim S, Dale BE (2004) Global potential bioethanol production from wasted crops and crop residues. Biomass Bioenergy 26(4):361–375
31. Duff SJB, Murray WD (1996) Bioconversion of forest products industry waste cellulosics to fuel ethanol: a review. Bioresour Technol 55(1):1–33
32. Binod P, Sindhu R, Singhania RR, Vikram S, Devi L, Nagalakshmi S, Kurien N, Sukumaran RK, Pandey A (2010) Bioethanol production from rice straw: an overview. Bioresour Technol 101(13):4767–4774
33. Demirbas A (2008) Biofuels sources, biofuel policy, biofuel economy and global biofuel projections. Energy Convers Manag 49(8):2106–2116
34. Mosier N, Wyman C, Dale B, Elander R, Lee YY, Holtzapple M, Ladisch M (2005) Features of promising technologies for pretreatment of lignocellulosic biomass. Bioresour Technol 96 (6):673–686
35. Alvira P, Tomás-Pejó E, Ballesteros M, Negro MJ (2010) Pretreatment technologies for an efficient bioethanol production process based on enzymatic hydrolysis: a review. Bioresour Technol 101(13):4851–4861
36. da Costa Sousa L, Chundawat SP, Balan V, Dale BE (2009) 'Cradle-to-grave' assessment of existing lignocellulose pretreatment technologies. Curr Opin Biotechnol 20(3):339–347
37. Oliet M, Casas A, Domínguez JC (2012) Ionic liquids applications in biorefinery. In: The role of ionic liquids in the chemical industry. Nova Publishers Science, Madrid, pp 133–168
38. Sarkar N, Ghosh SK, Bannerjee S, Aikat K (2012) Bioethanol production from agricultural wastes: an overview. Renew Energy 37(1):19–27
39. Delgenes JP, Moletta R, Navarro JM (1996) Effects of lignocellulose degradation products on ethanol fermentations of glucose and xylose by *Saccharomyces cerevisiae*, *Zymomonas mobilis*, *Pichia stipitis*, and *Candida shehatae*. Enzym Microb Technol 19(3):220–225
40. Wyman CE (1999) Biomass ethanol: technical progress, opportunities, and commercial challenges. Annu Rev Energy Environ 24:189–226
41. Mais U, Esteghlalian AR, Saddler JN, Mansfield SD (2002) Enhancing the enzymatic hydrolysis of cellulosic materials using simultaneous ball milling. Appl Biochem Biotechnol 98–100:815–832
42. Cadoche L, López GD (1989) Assessment of size reduction as a preliminary step in the production of ethanol from lignocellulosic wastes. Biol Wastes 30(2):153–157
43. Vidal BC Jr, Dien BS, Ting KC, Singh V Jr (2011) Influence of feedstock particle size on lignocellulose conversion – a review. Appl Biochem Biotechnol 164(8):1405–1421
44. Yoo J, Alavi S, Vadlani P, Amanor-Boadu V (2011) Thermo-mechanical extrusion pretreatment for conversion of soybean hulls to fermentable sugars. Bioresour Technol 102 (16):7583–7590
45. Keshwani DR, Cheng JJ, Burns JC, Li L, Chiang V (2007) Microwave pretreatment of switchgrass to enhance enzymatic hydrolysis. ASABE Annual International Meeting, June 17–20, 2007. Minneapolis
46. Keshwani DR, Cheng JJ (2010) Microwave-based alkali pretreatment of switchgrass and coastal bermudagrass for bioethanol production. Biotechnol Prog 26(3):644–652

47. Subhedar PB, Gogate PR (2013) Intensification of enzymatic hydrolysis of lignocellulose using ultrasound for efficient bioethanol production: a review. Ind Eng Chem Res 52 (34):11816–11828
48. Rehman MSU, Kim I, Kim KH, Han JI (2014) Optimization of sono-assisted dilute sulfuric acid process for simultaneous pretreatment and saccharification of rice straw. Int J Environ Sci Technol 11(2):543–550
49. Ur Rehman MS, Kim I, Chisti Y, Han JI (2012) Use of ultrasound in the production of bioethanol from lignocellulosic biomass. Energy Educ Sci Technol Part A: Energy Sci Res 30(SPEC .ISS.1):359–378
50. Sun Y, Cheng J (2002) Hydrolysis of lignocellulosic materials for ethanol production: a review. Bioresour Technol 83(1):1–11
51. Da Silva AS, Inoue H, Endo T, Yano S, Bon EPS (2010) Milling pretreatment of sugarcane bagasse and straw for enzymatic hydrolysis and ethanol fermentation. Bioresour Technol 101 (19):7402–7409
52. Buaban B, Inoue H, Yano S, Tanapongpipat S, Ruanglek V, Champreda V, Pichyangkura R, Rengpipat S, Eurwilaichitr L (2010) Bioethanol production from ball milled bagasse using an on-site produced fungal enzyme cocktail and xylose-fermenting Pichia stipitis. J Biosci Bioeng 110(1):18–25
53. Sindhu R, Kuttiraja M, Elizabeth Preeti V, Vani S, Sukumaran RK, Binod P (2013) A novel surfactant-assisted ultrasound pretreatment of sugarcane tops for improved enzymatic release of sugars. Bioresour Technol 135:67–72
54. Rehman MSU, Umer MA, Rashid N, Kim I, Han JI (2013) Sono-assisted sulfuric acid process for economical recovery of fermentable sugars and mesoporous pure silica from rice straw. Ind Crop Prod 49:705–711
55. Mosier N, Hendrickson R, Ho N, Sedlak M, Ladisch MR (2005) Optimization of pH controlled liquid hot water pretreatment of corn stover. Bioresour Technol 96(18 SPEC. ISS):1986–1993
56. Van Walsum GP, Shi H (2004) Carbonic acid enhancement of hydrolysis in aqueous pretreatment of corn stover. Bioresour Technol 93(3):217–226
57. Hamelinck CN, Van Hooijdonk G, Faaij APC (2005) Ethanol from lignocellulosic biomass: techno-economic performance in short-, middle- and long-term. Biomass Bioenergy 28 (4):384–410
58. Balan V, Da Costa SL, Chundawat SPS, Vismeh R, Jones AD, Dale BE (2008) Mushroom spent straw: a potential substrate for an ethanol-based biorefinery. J Ind Microbiol Biotechnol 35(5):293–301
59. Carvalheiro F, Duarte LC, Gírio FM (2008) Hemicellulose biorefineries: a review on biomass pretreatments. J Sci Ind Res 67(11):849–864
60. Zhong C, Lau MW, Balan V, Dale BE, Yuan YJ (2009) Optimization of enzymatic hydrolysis and ethanol fermentation from AFEX-treated rice straw. Appl Microbiol Biotechnol 84 (4):667–676
61. Garlock RJ, Chundawat SPS, Balan V, Dale BE (2009) Optimizing harvest of corn stover fractions based on overall sugar yields following ammonia fiber expansion pretreatment and enzymatic hydrolysis. Biotechnol Biofuels 2(1):1–14
62. Sendich E, Laser M, Kim S, Alizadeh H, Laureano-Perez L, Dale B, Lynd L (2008) Recent process improvements for the ammonia fiber expansion (AFEX) process and resulting reductions in minimum ethanol selling price. Bioresour Technol 99(17):8429–8435
63. Wildschut J, Smit AT, Reith JH, Huijgen WJJ (2013) Ethanol-based organosolv fractionation of wheat straw for the production of lignin and enzymatically digestible cellulose. Bioresour Technol 135:58–66
64. Amiri H, Karimi K, Zilouei H (2014) Organosolv pretreatment of rice straw for efficient acetone, butanol, and ethanol production. Bioresour Technol 152:450–456
65. Duarte LC, Silva-Fernandes T, Carvalheiro F, Gírio FM (2009) Dilute acid hydrolysis of wheat straw oligosaccharides. Appl Biochem Biotechnol 153(1–3):116–126

66. Harun R, Danquah MK (2011) Influence of acid pre-treatment on microalgal biomass for bioethanol production. Process Biochem 46(1):304–309
67. Gabhane J, Prince William SPM, Gadhe A, Rath R, Vaidya AN, Wate S (2014) Pretreatment of banana agricultural waste for bio-ethanol production: individual and interactive effects of acid and alkali pretreatments with autoclaving, microwave heating and ultrasonication. Waste Manag 34(2):498–503
68. Martin C (2007) Wet oxidation biomass pretreatment for ethanol. Ind Bioprocess 29(3):9–10
69. Martín C, Thomsen AB (2007) Wet oxidation pretreatment of lignocellulosic residues of sugarcane, rice, cassava and peanuts for ethanol production. J Chem Technol Biotechnol 82 (2):174–181
70. Akin DE, Rigsby LL, Sethuraman A, Morrison Iii WH, Gamble GR, Eriksson KEL (1995) Alterations in structure, chemistry, and biodegradability of grass lignocellulose treated with the White rot fungi *Ceriporiopsis subvermispora* and *Cyathus stercoreus*. Appl Environ Microbiol 61(4):1591–1598
71. Talebnia F, Karakashev D, Angelidaki I (2010) Production of bioethanol from wheat straw: an overview on pretreatment, hydrolysis and fermentation. Bioresour Technol 101(13):4744–4753

Effects of External Resistance on Microbial Fuel Cell's Performance

A. González del Campo, P. Cañizares, J. Lobato, M. Rodrigo, and F.J. Fernandez Morales

Abstract Microbial fuel cells (MFCs) are bioelectrochemical devices able to convert chemical energy into electricity. This chapter describes the effect of the external resistance on the performance of a MFC. Firstly, the state of the art of this topic has been comprehensively revised, and the effect of external resistance on cell voltage, anode potential, current and power generated, microbial diversity, structure and morphology of the biofilm, microbial metabolism and organic matter removal, coulombic efficiency, and time of stability is reported. Also, different methods to the control of external resistance as a function of internal resistance changing are explained. After that, the effect of changes in the external resistance on power generated and COD removal in a microscale MFC, used to treat wastewater, was studied. The obtained results indicated that when external resistance was increased, the power decreased. However, hysteresis was observed due to change in microbial diversity in the anode. During the first phase of increment of external resistance, the maximum power exerted, 1.69×10^{-3} mW, was obtained with a 2,700 Ω load. However, when decreasing the external resistance, the maximum power, 1.27×10^{-3} mW, was obtained with a 2,200 Ω load. Regarding COD removal, the effluent COD decreased when external resistance was increased, that is, the wastewater treatment was enhanced when external resistance was higher.

Keywords Electricity, External resistance, Microbial fuel cell, Microscale

A. González del Campo and F.J. Fernandez Morales (✉)
Chemical Engineering Department, University of Castilla-La Mancha, ITQUIMA, Avenida Camilo José Cela S/N. 13071, Ciudad Real, Spain
e-mail: FcoJesus.FMorales@uclm.es

P. Cañizares, J. Lobato, and M. Rodrigo
Faculty of Chemical Sciences and Technologies, Chemical Engineering Department, University of Castilla-La Mancha, Building Enrique Costa Novella, Avenida Camilo José Cela S/N. 13071, Ciudad Real, Spain

G. Lefebvre et al. (eds.), *Environment, Energy and Climate Change II: Energies from New Resources and the Climate Change*, Hdb Env Chem (2016) 34: 175–198,
DOI 10.1007/698_2014_290,
Published online: 22 October 2014

Contents

1 Introduction

Microbial fuel cells (MFCs) are electrochemical devices that exploit the metabolic abilities of electrogenic microorganisms to facilitate the generation of electricity from chemical energy, mainly from organic matter. In a MFC, organic matter is oxidized at an anode by biological process where microorganisms deliver the electrons to the anodic electrode. These electrons flow through an external load and are released at the cathode where they are consumed to reduce an oxidant agent, usually oxygen. This biological system has the potential to oxidize a large variety of organic compounds producing at the same time electricity [1, 2]. In literature the electricity generation using MFCs has been studied using pure organic compounds, such as acetate, butyrate, and glucose, and also with waste streams [3–5]. Anyway, the main advantage of electrogenic microorganisms is their ability to oxidize wastes with simultaneous energy generation [6].

In this way, one of the most attractive energy sources for MFCs is wastewater, because electricity production is combined with the wastewater treatment [7]. The use of MFCs for wastewater treatment presents several advantages, such as economical savings in aeration and solid handling. Aeration alone can account for half of the operation costs at a typical treatment plant [8] and in MFC aeration is not necessary. The MFC process is inherently an anaerobic process; moreover, the sludge yields for an anaerobic process are approximately one-fifth of that for an aerobic process. Thus, the use of MFCs could drastically reduce solid production at a wastewater treatment plant, reducing also the operating costs for solid handling [1].

The major bottleneck of MFC application is its relatively low power density; nowadays, the actual power density exerted by MFC is not high enough for industrial applications. In order to solve this drawback, research on MFC has been focused on power density improvement by optimizing operating conditions such as COD loads [9], operational pH [10, 11], flow rate [12], and temperature [8]. Additionally, one of the main factors to enhance the power output is by means

of an integral component of the MFCs, the external resistance [13, 14]. The external resistance is used to dissipate the electrical energy when MFCs are operated independently of an electrical device and as an integrated part of an electrical grid that controls the output of fuel cells [15]. The external resistance controls the ratio between the current generation and the cell voltage [16]. A high external resistance results in a high cell voltage and low current, and a low external resistance results in a low cell voltage and high current. One way to minimize losses is to operate the MFC under optimal conditions for power production at an optimal external resistance [17]. Because of that, the effect of the external resistance on the activity of the biocatalyst and on the electricity production in MFCs is a key point that must be taken into account [18].

In this context, the aim of this chapter is to study the effect of change of external resistance on operation of MFCs and to indicate how to select the most appropriate external resistance.

1.1 Effect of External Resistance on Performance of MFC

The external resistance controls the ratio between the cell voltage, determined by the difference between the cathode potential and the anode potential, and the current (amount of electrons per unit of time which flow through the circuit). The Gibbs free energy which is available for the microorganisms during substrate oxidation is proportional to the number of electrons transferred to the electrode and the potential difference between the anode potential and the redox potential of the substrate [19]. In this way, the higher the anode potential and the higher the current, the more energy the microorganisms theoretically gain per unit of time [20, 21]. This would result in an increase of the current generation and a lowering of the cell voltage by the microorganisms, both influencing the power generation [13]. Taking into account these statements, it is clear that the external resistance has significant impact on MFC performance, including electricity production, COD removal and microorganism population evolution. In the literature the effect of external resistance on MFC performance has been addressed. In the following sections, the effect of external resistance on the main variables of the MFC operation will be revised and studied.

1.1.1 Influence of External Resistance on Anode and Cathode Potentials and Cell Voltage

The maximum cell voltage in a MFC is obtained at open circuit, that is, when external resistance is infinite. When the external resistance decreases, the voltage exerted by the MFC also decreases. According with Menicucci et al. [22], this is because of the limitations imposed on the electrode reaction kinetics, on mass transfer, and on charge-transfer processes at the current-limiting electrode (one of

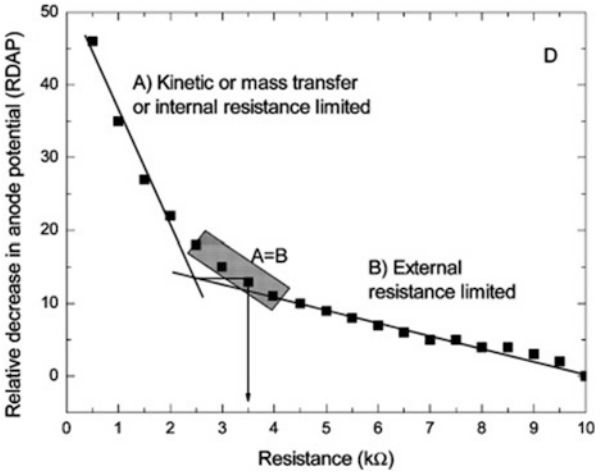

Fig. 1 Relative decrease in anode potential in a MFC as a function of external resistance (extracted from Menicucci et al. [22])

the two electrodes that exhibits the slower charge-transfer kinetics). In this research Menicucci et al. [22] evaluated the performance of MFC with different external resistances from 6 to 0.125 kΩ. The cell voltage decreased when external resistance decreased. The decrease was more significant when they applied an external resistance less than 3 kΩ. They used the relative decrease in anodic potential (RDAP) to select the external resistance to measure the maximum sustainable power of their MFC. In Fig. 1, the variation of percent deviation of anodic potential with respect to the applied external resistance in that work is shown.

When external resistance was high, the RDAP increased linearly with decreasing external resistance because external resistance limited the electron delivery to the cathode. When a low external resistance is applied, the electron delivery to the cathode is limited by kinetic and/or mass transfer (or internal resistance), and the RDAP increased linearly with decreasing external resistance. However, the RDAP also increased linearly with decreased external resistance, with different slopes, for external resistance-limited or internal resistance-limited conditions. When both lines intersected, they draw a horizontal line from the intersection to estimate the external resistance that allows them to measure sustainable power. Thus, in the study of Menicucci et al. [22] external resistance between 2.5 and 4 kΩ provided very close power values.

Ghangrekar and Shinde [23] also studied the effect of external resistance on MFC, and they observed that cell voltage increased with the increase in external resistance from 0 to 4,000 Ω; the maximum voltage of 358 mV was observed at an external resistance of 4,000 Ω.

Later on, Rismani-Yazdi et al. [15] obtained similar cathode potentials at different external resistances. However, anode potential varied under different external resistance employed. MFCs with lower external resistances resulted in higher anode potentials. This was also observed in the study of Song et al. [24] carried out using a sediment microbial fuel cell (SMFC). In that study, an increase

in external resistance was accompanied with a significant decrease in anode potential. The anode potential for SMFCs with an external resistance of 10 Ω was much higher than those with other external resistances, around 30 and 80 mV higher than those with external resistance of 100 and 1,000 Ω, respectively. However, the cathode potential for the SMFC with 10 Ω external resistance was only 2–8 mV lower than those for SMFCs with 100 Ω and higher external resistances, which were found to be quite similar.

Similar results were found in other studies. In the study of Chae et al. [25], the anode potential became more negative with the increased external resistance. Zhang et al. [26] used the same MFC configuration but with different external resistance, and they concluded that MFC with a lower external resistance showed a higher steady anode potential after start-up.

These results indicate that the external resistance in MFCs regulates anode potentials. In order to maximize electrical energy output of a MFC, the anode potential should be as low and the cathode potential as high as possible [16]. However, the anode potential controls the theoretical energy gain for microorganism [27]. At low anode potential, the redox potential at the anode was probably too low to make it a favorable electron acceptor for the microorganisms [28], that is, there is low energy per electron transferred available for growth and cell maintenance. In this way, the differences in MFC performance with different external resistances may be associated with variations in activation losses at the anode, which is a function of electrochemical activity of anode-reducing microorganisms [15]. Therefore, there existed an optimum anode potential enabling the microbial consortia to balance electrode reduction kinetics with potential energy gain, which could be easily achieved through selection of the desired external resistance [24]. The activation losses have little influence on the MFC operation under optimal or close to optimal external resistance, which occurs when external resistance is close to the internal one [7]. Schroder [21] suggested that the differences observed in the anode potential under various external resistances can select for different electrochemically active microorganisms.

1.1.2 Influence of External Resistance on Electric Current of MFC

When MFC is operated with a low external resistance, the MFC generated higher current [15, 24, 25, 29, 30] due to the highest electron transfer to the cathode supporting faster cathode reaction and high electrogenic activity.

In this way, various studies have observed that stepwise decreases in the external resistance of an MFC improved the current generation over time [13, 15, 31, 32]. In the study of Aelterman et al. [13], the descent of external resistance from 50 to 25 Ω and finally to 10.5 Ω resulted in a significant increase in the continuous current generation. Moreover, Aeltermant et al. [13] observed that when the MFCs were operated at lower resistances, the mass transfer or kinetic limitations observed during polarization lowered, resulting in a less steep descent of the current density.

In a SMFC, Song et al. [24] observed that while there was not much difference among the currents produced at five different external resistances during the initial 10 days of operation, currents produced by the SMFCs were different after that. The highest average current of 0.22 mA was produced from SMFCs with an external resistance of 100 Ω, followed by those at 10 Ω and then 400 Ω. This can be explained because when working at low external resistance, a slight increase in internal resistance can dramatically decrease a fuel cell's performance [33] which reduces the current production mainly because of the internal resistance but not due to the external one. The SMFCs with an external resistance of 1,000 Ω produced the lowest current [24]. Similar to previous studies, Zhang et al. [26] observed that a conventional MFC with a lower external resistance showed a higher current generation after start-up.

On the other hand, when operating at high external resistance that almost mimics an open circuit, microorganisms were unable to transfer their electrons to such an unfavorable electron acceptor. In this situation, the high external resistance restricts the current that is able to flow from anode to cathode, and this may affect which microorganisms are able to colonize the anode [28, 34]. In the study of Ghangrekar and Shinde [23], it was demonstrated that when external resistance is very high, the current was brought to minimum and nearly constant value. Moreover, in this case, the limiting factor is the external resistance, and the current production is almost independent of another factor, such as the distance between the electrodes and surface of the anode.

1.1.3 Influence of External Resistance on Electric Power of MFC

According to the information presented above, when external resistance is low, the cell voltage is low and current is high. Taking into account that the power is the product of current and cell voltage, a question arises: Which value of external resistance makes that power maximum?

In order to determine that, it is necessary to take into account the following argument: If external resistance is low, then the equilibrium potential of the cell initially generates a high instantaneous electric current, higher than the maximum sustainable rate of charge transfer to/from the current-limiting electrode. As a result, the potential across the cell decreases quickly and adjusts to the rate of charge transfer to the current-limiting electrode, effectively decreasing the current in the external circuit. However, if the external circuit has a relatively high electrical resistance, then the equilibrium potential of the cell generates an electric current lower than the maximum sustainable rate of charge transfer to/from the current-limiting electrode. The potential of the cell adjusts to the external resistance. In the latter case, the power generation is sustainable but lower than it could be if the resistance of the external circuit were lower [22].

In this way, the maximum power transfer theorem states that maximum power is drawn when the external resistance (R_{ext}) of electric power source equals the

internal resistance of power sources. Moritz von Jacobi published the maximum power (transfer) theorem around 1840, and it is also referred to as "Jacobi's law."

Then, the mathematical demonstration of maximum power transfer theorem for a DC circuit can be demonstrated as follows [35]:

Considering the MFC as a DC circuit, a voltage drop (V) drives an electric current (I) through internal (R_{int}) and external (R_{ext}) resistances. By Ohm's law,

$$I = \frac{V}{R_{ext} + R_{int}}$$

And the power (P) is

$$P = I^2 \cdot R_{ext} = \frac{V^2}{(R_{ext} + R_{int})^2} \cdot R_{ext} = \frac{V^2}{R_{int}^2/R_{ext} + 2R_{int} + R_{ext}} \cdot R_{ext}$$

P is maximum when the denominator is minimum. Differentiating the denominator with respect to R_{ext},

$$\frac{d\left(R_{int}^2/R_{ext} + 2R_{int} + R_{ext}\right)}{dR_{ext}} = -\frac{R_{int}^2}{R_{ext}^2} + 1$$

For maximum or minimum, the first derivative is zero, so

$$R_{int}^2/R_{ext}^2 = 1$$

Therefore, the power is maximum when $R_{ext} = R_{int}$.

If external resistance is higher or lower than internal resistance, generated power will decrease.

Because of its importance, multiple studies have been checking this theorem in MFC [13, 28, 34, 36–39].

Katuri et al. [36] observed that when external resistance was increased from 0.1 to 1 kΩ, the power density increased, reaching a maximum power density of 10.1 mW m^{-2}. A fall in power generation was observed at external resistance values from 10 to 50 kΩ. In the Fig. 2, the power generation in that work under different external resistances is shown. It is important to mention that internal resistance of the MFC used in that study was around 1 kΩ.

In the study of Lyon et al. [28], the internal resistance was 300 Ω, and the highest power production was obtained with an external resistance of 470 Ω, followed by 1,000 Ω, 100 Ω, 10 kΩ, and finally 10 Ω. The external resistance of 10 Ω produced the weakest power production as the resistance was too low compared to the internal resistance (300 Ω).

In the work of Ren et al. [34], the internal resistance of the MFCs was around 190 Ω, which explains why the peak power from MFCs was achieved at the 265 Ω external resistance. On the other hand, in that work the influence of increasing and

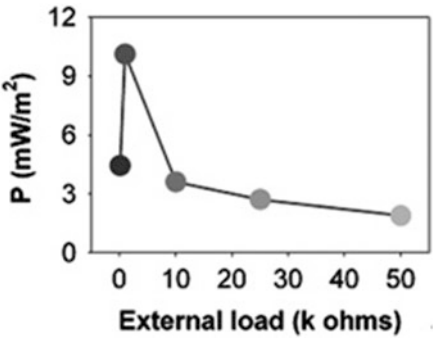

Fig. 2 Relationship between peak power generation and external resistance (extracted from Katuri et al. [36])

decreasing of external resistance at 25 min intervals on power density was studied. Higher power density values were observed when external resistances were changed from high to low (from 5,000 to 10 Ω) compared to low to high (from 10 to 5,000 Ω).

In other studies, although internal resistance was not measured, an increase in power was observed when external resistance was increased until a value, and then, when external resistance continued to increase, the power decreased [25, 26]. In the study of Zhang et al. [26], the power obtained after start-up increased from 1.96 to 6.05 mW when external resistance increased from 10 to 50 Ω. Then, when external resistance increased from 50 to 1,000 Ω, the power decreased to 0.64 mW. The best power of MFC with an external resistance of 50 Ω may come from the highest active biomass production on the surface of electrode. The lower performance with 10 Ω, despite the higher active biomass, might be due to the significant ohmic loss resulting from the existence of void spaces in the interior of the biofilm.

In the study of Chae et al. [25], the power density increased when external resistance increased from 10 to 100 Ω and showed a maximum value of 124 mW cm^{-2} at 100 Ω. When external resistance was increased from 100 to 2,500 Ω, the power density decreased.

It is important to remark that the theorem is not satisfied in several MFC studies [24, 40]. Song et al. [24] observed that power density increased with the increase in external resistance and the highest power density of 3.15 mW m^{-2} was obtained at an external resistance of 1,000 Ω. However, the internal resistance varied between 132 and 214 Ω. This fluctuation could be explained because internal resistance is not a system constant and depends on the external resistance applied to the MFC. In the study of Lee et al. [40], MFC with highest external resistance had better power densities.

1.1.4 Influence of External Resistance on Microbial Diversity

For practical purposes and in large-scale applications, mixed cultures are generally preferred over pure cultures because they are more readily obtainable in large quantities, more tolerant to environmental fluctuations, and more accommodating

to a variety of substrates [41]. But other microorganisms such as methanogens are ubiquitous in sludge used as inoculum in MFC. Because of that, it is important to control and inhibit the competing microorganisms in a MFC.

In literature the influence of external resistance on microorganism diversity has been studied. In all studies, a change in microorganism diversity was observed when external resistance was changed [15, 28, 34, 36, 39], and new knowledge has been generated.

In this way, the external resistance in an MFC directly influences the anode potential, which is equivalent to the anode availability as an electron acceptor; therefore, it influences on anode biofilm development and performance [42]. Low resistance leads to more positive potentials, which provide more free energy to the microorganisms and enable a higher flux of electrons through electrogenic metabolisms [26], imparting a selective advantage to electrogenic over competing microorganisms [15, 39]. Thus, several studies have demonstrated that low external resistance enhances the presence of electrogenic microorganisms in the MFC anode chamber [40, 43–46] and that high external resistance reduces the anode potential enhancing the presence of strictly anaerobic microorganisms [18, 40, 45, 46]. In this way, independent of the microbial composition of the inoculum, proliferation of the electrogenic microorganisms could only be achieved at external resistance values that are equal to or less than the MFC internal resistance [18].

In addition to influencing this competition with other groups, the external resistance (anode potential) also exerts a selective pressure on the electrogenic community composition due to their different attributes related to anode affinity and maximum substrate utilization rate [42, 47]. This presents an opportunity to tailor the anode biofilm structure and composition and potentially MFC performance with respect to power output and substrate utilization, through the adjustment of external resistance [34].

Lyon et al. [28] demonstrated that the microbial community structure in MFC's biofilm operated at external resistance appreciably above internal resistance (1 to 10 kΩ) was significantly different from that observed in the MFC operated at low external resistance (10, 100 and 470 Ω) [28]. As mentioned above, a low external resistance promotes growth and metabolic activity of the electrogenic microorganisms since electron transport to the cathode is facilitated [18].

Rismani-Yazdi et al. [15] proved that within the anode-attached microorganisms, samples from MFCs with lower external resistance (higher anode potential), 20 and 249 Ω, had more similarity (75%) than those with higher external resistances (65% similarity between 480 and 1,000 Ω). It is because, as has been explained, operating the MFCs at low external resistance selects for microorganisms that have higher activity of electron transfer to the anode [48–50]. This interpretation is supported by Liu et al. [51] and Torres et al. [42], who suggest that a more positive anode potential is associated with greater colonization of anode-reducing microorganisms on the electrode.

Katuri et al. [36] also observed that different communities were selected at different external resistance which may represent selection of electrogenic organisms at lower external resistance. In the study of Jung and Regan [39], increasing

external resistance to 9,800 Ω, the anode microorganism communities changed significantly, while continued operation at 970 Ω and a reduction to 150 Ω had little effect on them, although, in general, the modification of the external resistance load did not consistently affect the abundance of these functional groups.

In the study of Lyon et al. [28], with high external resistance, different electrode-reducing microorganisms colonized the anode that when external resistance was low. Regardless of the high external resistance, some microorganism species were still able to use the anode as an electron transfer intermediate. When external resistance is increased from 470 to 10 kΩ, the maximum power was slightly increased. However, during the initial period of higher maximum power output, there were two peaks that appear on the polarization curve. This could indicate two separate populations of microorganisms that were capable of producing electricity. Therefore, community structure changed with external resistance; however, different communities were capable of producing the same level of power production.

In the work of Ren et al. [34], bacteria with a filamentous structure dominated and formed relatively thin and patchy biofilm (0–30 μm) on the anodes under high external resistances (1,000 and 5,000 Ω), while rod-shaped cells accumulated and formed dense biofilms (more than 50 μm) that covered the anodes under lower resistances (10, 50 and 265 Ω). As the external resistance decreased, the biofilm cells tended to aggregate and finally covered the whole anode with thick biofilm.

1.1.5 Influence of External Resistance on Structure and Morphology Biofilm

Previously, the relationships between the microorganism diversity and the external resistance in a MFC have been studied. Moreover, the external resistance may also affect the structure and morphology of the biofilm in the anode. Therefore, in some research, the influence of external resistance on structure and morphology of the biofilm has been studied.

At low external resistance (higher anode potential and current), more electrogenic microorganisms should be able to transfer electrons to the anode and gain more energy; it leads to a more diverse and denser anode biofilm [26, 34]. Following this argument, Ren et al. [34] obtained different biofilm morphologies and densities in the MFCs under different external resistances (10–1,000 Ω).

Mclean et al. [32] described how the differences in external resistances affect cellular electron transfer rates on a per cell basis and overall biofilm development in *Shewanella oneidensis* strain MR-1 by monitoring the real-time microscopic imaging of anode population. They found that the anode of a MFC started up at a low external resistance (100 Ω) had a thinner biofilm and higher current per cell, compared with that at a high external resistance (1 MΩ).

Another effect of external resistance on morphology and structure of the biofilm was discovered by Zhang et al. [26]. They observed that although the biofilm formed at 10 Ω contained less active biomass than that at 50 Ω, both biofilms were of similar thickness. This is because the microorganisms were more loosely

packed in the biofilm developed and the extensive voids were found to be distributed within biofilm at 10 Ω (the less external resistance). These voids were beneficial for mass transport within the biofilm by forming water channels that facilitate the substrate and buffer supply, as well as product removal. However, void spaces also lead to imperfect contact between the electrogenic microorganisms and the anodes, causing a decrease in the electrical conductivity of the biofilm matrix and consequently reduced the performance of the MFCs. By contrast, the biofilm formed at 50, 250, and 1,000 Ω appeared quite homogeneous and showed a compact structure, in which cells were tightly linked together by visible polymeric viscous materials.

1.1.6 Influence of External Resistance on Microbial Metabolism and Organic Matter Removal

The external resistance also influences on the microbial metabolism. The differences in MFC performance with different external resistances result mainly from the differences in the catalytic activity at the anodes [24] affecting therefore the microbial metabolisms and organic matter removal.

In this way, Aelterman et al. [13] observed that at the highest external resistance (50 Ω), feeding the biomass with an increased loading rate did not result in a rise of the continuous current generation. The amount of energy which was available for growth and maintenance, as determined by the external resistance, was probably too low to sustain a higher metabolic activity of the microorganisms. Therefore, no increase of the current generation at higher loading rates could be noted. Only during polarization or at lower external resistances, when higher electron fluxes and lower anode potentials were allowed, enabling a higher energy gain for the microorganisms, significant increases of the current generation and power outputs were observed.

At lower external resistance, the COD removal was higher, and with the increase in external resistance, a decrease in COD removal occurs [5, 29, 30, 36, 39, 40]. This is because, at higher external resistances, there is a lower anode potential, which may alter the metabolic activities of the anodic microbial community, and the presence of different microbial species could provide different mechanisms for efficient utilization of organic matter [36]. MFCs operated at higher anode potential (low external resistance) may lead to enhanced wastewater treatment since drawing a greater current from the MFC accelerates the COD removal [36]. In the work of Sajana et al. [52] carried out in a SMFCs, better COD and TN removal were observed when the system operated with lower external resistance than when operated with higher ones.

According to this argument, the total SCFA concentration of the anolyte increases with external resistance [36], and it can affect pH in the anode biofilm [53, 54]. The increased production of SCFAs with high external resistance may result from a high competition for organic matter in the anode and/or reduced consumption of metabolites with higher external resistance because of lower rates

of respiration and anodic electron transfer activity. Also, Pinto et al. [7] observed that methane production was higher when MFC was operated at higher external resistance.

On the other hand, in various studies [26, 36, 45], a lower biomass yield at low external resistances has been obtained. Microorganisms may also produce extracellular polymeric substance (EPS) during growth on the anode surface, consuming energy which is available for microorganism growth [55]. Therefore, a higher portion of energy is consumed for the synthesis of EPS rather than for microorganism growth in the case of MFC with lower external resistance. In the study of Zhang et al. [26], EPS content of biofilm decreased from 296.8 to 51.9 mg g^{-1} as the external resistance increased from 10 to 1,000 Ω. Considering that the active biomass of the biofilm developed at 10 Ω was lower than that of 50 Ω, whereas the energy gain was higher, this result suggested that a greater portion of energy was consumed for EPS synthesis in the case of the biofilm developed at 10 Ω. Low sludge yield was reported to be advantageous in the water industry as it accounts for around 25–65% of total plant operating costs [56].

1.1.7 Influence of External Resistance on Coulombic Efficiency

Coulombic efficiency is the ratio of total recovered coulombs by integrating the current over time to the theoretical amount of coulombs that can be produced from organic matter removal. Therefore, taking into account that current and organic matter removal is influenced by external resistance, coulombic efficiency is also influenced by external resistance.

Generally, coulombic efficiency increases when external resistance is decreased. It is because current is increased [15, 40], anode potential is increased [39], and the share of fermentative and anaerobically respiring microorganisms is reduced [25, 34, 36, 57].

In this way, in the study of Rismani-Yazdi et al. [15], a maximum coulombic efficiency of 19% was obtained in MFCs with 20 Ω external resistance, and with 1,000 Ω the coulombic efficiency was 12%. It was due to changes in microbial diversity and the differences in current flow induced at various external resistances and other factors: accumulation of metabolites, biomass growth, substrate crossover, and competing reactions for electrons or reduction of O_2 diffusion through the membrane.

Lee et al. [40] observed that the coulombic efficiency values appeared to be decreased with increasing external resistance. High external resistance would bring high ohmic losses for electron transfer, thus probably resulting in a lower coulomb efficiency.

In the study of Jung and Regan [39], the high availability of the anode with low external resistance resulted in high coulombic efficiency.

Katuri et al. [36] obtained a maximum coulombic efficiency of 6.15% for MFC operated under the lowest external resistance (0.1 kΩ), and it decreased until 0.44% when external resistance increased until 50 kΩ. This behavior was perhaps due to

competition for electron donor between electrogenic microorganisms and fermentative and anaerobically respiring microorganisms when external resistance was increased.

In the study of Juang et al. [57], it was observed that when external resistance ranged from 10 to 1,000 Ω, a lower resistance corresponded to a higher coulombic efficiency. It means that some electrons were consumed by some mechanisms other than the cathode reaction [58].

Chae et al. [25] determined that lowering the resistance from 600 to 50 Ω reduced the methanogenic electron loss by 24%. When the external resistance was lowered to 50 Ω after a run at 600 Ω for a period of 5 months, the level of methanogenic electron loss reduced from 53.2 to 40.6%, indicating its potential for controlling the methanogens. This resulted in a corresponding increase in coulombic efficiency from 32 to 42.8%, similar to the amount of saved electrons calculated by reducing methanogenesis. The undefined electron losses, including electron sink for microorganism growth, were about 4–10%.

In the work of Ren et al. [34], the average coulombic efficiency for the 10 Ω external resistance MFCs was 45%, while the average value for 5,000 Ω external resistance MFCs was only 6%. The low electron recovery at high external resistances was mainly due to the long batch duration, which resulted in more electron loss to non-electricity-related reactions such as aerobic respiration and perhaps methanogenesis, though the latter was not measured.

1.1.8 Influence of External Resistance on Time of Stability

When the external resistance is changed, the electrochemical response of the biofilm established at the antecedent quickly stabilizes. However, the biofilm takes much longer to stabilize, with changes in biofilm structure and community composition potentially leading to a long-term stable performance that differs from the short-term electrochemical response [34].

In the study of Jadhav and Ghangrekar [29], when the resistance was increased from 50 to 100 Ω, with initial sudden drop, the produced current increased with time and got stabilized within 20 min. However, when resistance was increased from 500 to 1,000 Ω, after initial sudden drop, the current slowly increased and got stabilized after 2 h. At lower resistance change, from 50 to 100 Ω, the current reached the stable value with less time after changing the resistance, but at higher resistance changes, it took long time for the current to reach the stable value.

Katuri et al. [36] also observed that the time taken to attain the peak current density decreased with decreasing external resistance. These observations may be due to different electron transfer rates under different external resistances and/or variations in microbial metabolic activities and kinetic differences in substrate utilization [46].

However, in the work of Menicucci et al. [22] only when the external resistance was large enough did the power generation reached a sustainable level quickly. The lower the external resistance, the longer the time needed for the cell to equilibrate

and produce the sustainable power. In another study, He et al. [33] measured the power of their MFC and reported the maximum power that occurred when a 66 Ω resistor was applied. However, when they applied a larger external resistance, 100 Ω, the current decreased in time. When they applied a 470 Ω external resistance, the current did not change, showing the sustainable conditions.

In the work of Ren et al. [34], where the long-term operation of MFCs at different fixed resistances and the performances, architectures, and compositions of these different steady-state biofilms were studied, it was also observed that MFC under higher resistance showed reduced periods before reaching steady-state voltage. The lag time for 5,000, 1,000, 265, 50, and 10 Ω MFC to reach 80% of their maximum voltage was 91, 104, 106, 108, and 120 h, respectively. Higher external resistance could accelerate the biofilm acclimation process by providing a lower anode potential for a faster MFC start-up.

1.2 Control of External Resistance as a Function of Internal Resistance Changing

As it has been previously stated, the MFC power output is maximized when the external resistance connected to the cell is equal to the total internal resistance. An incorrect selection of external resistance, either larger or smaller than the internal resistance, may lead to large losses in power output. Meanwhile, variations in operating conditions (temperature, pH, influent strength, influent composition, and other factors) and the processes of biofilm growth and decay lead to significant changes of the internal resistance over time [22]. This inevitably results in a mismatch between the internal and the external resistances and, therefore, may lead to large losses in power output. For it, the external resistance control is an important requirement for industrial application of MFCs.

Premier et al. [59] demonstrated that the power production and coulombic efficiency of MFCs can be substantially improved using an automatic control strategy of external resistance.

The problem of optimizing the external load for power sources has been addressed before by online control, and it is often referred to as maximum power point tracking (MPPT). Thus, when internal resistance is increased or decreased due to the change in operation conditions, the MPPT algorithm decreases the external resistance value [18].

Woodward et al. [60] studied a method for external resistance control, which uses an online perturbation/observation (P/O) algorithm for maximizing the power output.

The P/O algorithm demonstrated excellent stability and fast convergence so that external resistance always remained close to internal resistance. This strategy might prevent MFC operation at external resistance values below its internal resistance,

thus helping to avoid voltage reversal [61] after a feed disruption or another operating problem.

In this way, in the study of Pinto et al. [18], MFC-1, which was operated at a high external resistance, always had a low current density and a low coulombic efficiency, while MFC-2, which was operated at the lowest external resistance, and MFC-3, which was operated at an optimal external resistance by the P/O algorithm, showed larger values.

Also, a logic-based control approach for adjusting the external resistance has recently been proposed in literature [59].

Both methods provide real-time optimization of the external resistance; however the practical implementation of these methods would require a device with a variable electrical load that can be fitted on demand. Meanwhile, the electrical loads are not always adjustable.

Another mode of operation is described by a duty cycle, which suggested that by operating an MFC with intermittent connection/disconnection of the external resistance, the MFC power output could be improved without significant losses in power output even at external resistance values below internal resistance [62].

Coronado et al. [63] elaborated on the approach of intermittent (periodic) connection of the electrical load by analyzing the MFC frequency response in a range of 0.1–1,000 Hz and operating the MFC at a sufficiently high switching frequency, equivalent to a pulse-width modulated connection for the external resistance (R-PWM mode of operation). In the study of Coronado et al. [63], external resistance was disconnected during a time in each duty cycle in the R-PWM mode of operation. In this way, by comparing power outputs of MFCs operated in the R-PWM mode and with a constant resistance equal to the estimated total internal resistance value, the R-PWM mode operation was demonstrated to improve MFC performance by up to 22–43%.

In a stack of MFCs, the initially small difference in potential between cells can eventually dominate and suppress the performance of neighboring cells [64]. This voltage reversal can detract from the expected total power output in serial connection and can also deleteriously affect the electrogenic biofilm on the electrode [61]. Grondin et al. [65] used intermittent and periodic connection of the load as an alternative to MPPT operation to match internal and external impedance in order to obtain maximum power transference. Several duty cycles of open and closed circuit operation in benthic MFCs increased power output; however little or no effect on the anode community development was seen [66].

2 Experimental Procedure

2.1 Experimental Setup

The setup used in this study (see Fig. 3) consisted of a two-chambered microscale MFC separated by a proton exchange membrane, PEM (Sterion®) [9, 67]. Both the anodic and cathodic chambers were built on a graphite plate; the anode chamber volume was 0.95 cm^3 and the cathode chamber volume with serpentine channels was 0.5 cm^3. Toray carbon papers TGPH-120 (E-TEK, USA) (3 × 3 cm) were used as electrodes in the anodic and the cathodic chambers. The anodic electrode contained 20% of Teflon, and the cathodic electrode contained 10% in order to improve the mechanical properties of the carbon support [68]. At the cathode, a catalytic layer with 0.5 mg Pt/cm^2 loading was deposited onto a microporous layer [69]. The membrane-electrode assembly was performed according to literature [8]. The active areas of the anodic and cathodic electrode were 4.65 and 2.85 cm^2, respectively. Both electrodes were connected by an external resistance of 120 Ω (initial conditions) [70]. A scheme of the setup used is shown in Fig. 3.

The anodic compartment was inoculated with activated sludge from Ciudad Real Wastewater Treatment Plant and operated in the fed-batch mode until steady state was reached [9]. After acclimatization, the MFC was operated in continuous mode. To do that, the anodic chamber was fed with a synthetic wastewater, which contained 9 g L^{-1} glucose and fructose as organic substrates and COD 343 mg L^{-1} and trace minerals, at a flow rate of 0.5 mL min^{-1}. In order to avoid the degradation of the wastewater during its storage, it was sterilized for 30 min at 105°C. The composition of the synthetic wastewater used in the experiments can be found elsewhere [71].

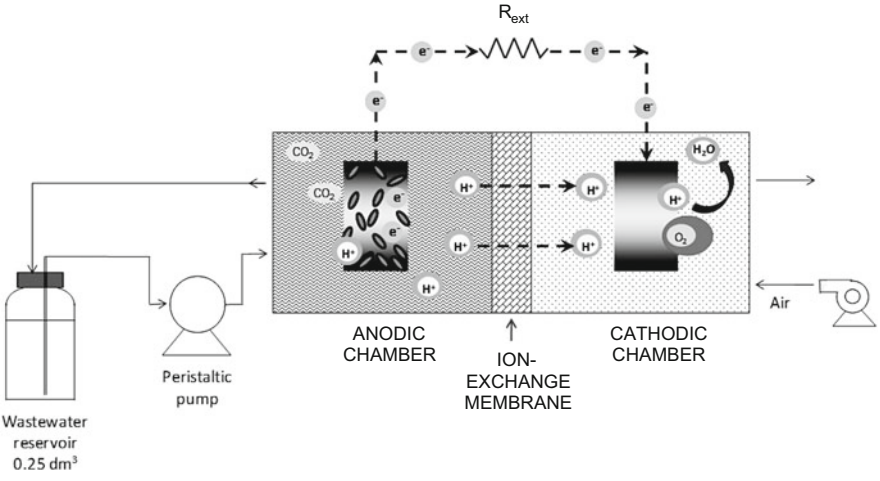

Fig. 3 Schematic view of the setup

An air-breathing cathode was used. Air-breathing systems use free convection airflow to supply oxygen to the cathode.

2.2 Characterization Techniques

A digital multimeter was connected to the system to monitor continuously the cell voltage at the value of the external load (R_{ext}). These cell voltages (V) are directly related to the current flowing between the electrodes (I) by the Ohms law. Power was calculated from current and voltage.

The effluent's COD from anodic compartment was determined by photometric methods with a MERCK COD cell test and Pharo 100 MERCK spectrophotometer.

3 Results and Discussion

In this study, the influence of the external resistance over the power and wastewater treatment capacity of a microscale MFC was evaluated. In this way, the first external resistance studied was 120 Ω, external load used for the normal operation of the cell. Gradually, the external resistance was stepwise increased from 120 to 3,300 Ω. The maximum resistance was selected in order to overcome the internal resistance of MFC, which was around 2,200 Ω. Afterward, the external resistance was decreased from 3,300 to 120 Ω, in order to evaluate the effect of the lowering of the external resistance on the MFC.

In this way, each external resistance was kept in the system of MFC until the steady state was reached.

3.1 External Resistance Effect on Power Production

The effect of the external resistance on power generation was studied. In Fig. 4 the generated power in the steady state for each evaluated resistance is shown.

The generated power by MFC increased with the increment of external resistance. When the external resistance increases from 120 to 560 Ω, a great increment in power from 3.76×10^{-4} to 1.57×10^{-3} mW was observed. From 1,000 Ω power stayed constant around 1.6×10^{-3} mW; this is because the increment of external resistance adversely affects the electricity production. In the phase of decrement of external resistance, a decrement of power from 1.6×10^{-3} to 4.8×10^{-5} mW was observed. It is important to highlight that this loop has hysteresis. In this way, the obtained power for each external resistance was always higher in the phase of increment of the external resistance than in the phase of decrement of the external resistance. Lyon et al. [28] noted changes in microbial community structure both at

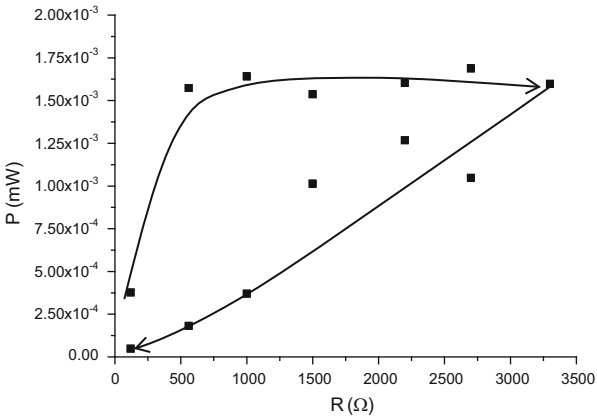

Fig. 4 Power in steady state at every external resistance

the highest external resistance and when the resistances were changed. It could be the reason for the reduction observed in the power exerted when the systems worked with high external resistance and also to the existence of a hysteresis loop. The difference in MFC performance with different external resistances may be associated with variations in activation losses at the anode, which is a function of electrochemical activity of anode-reducing microorganisms [15]. It has been suggested that differences observed in the anode potential under various external resistances can select for different electrochemically active microorganisms [21].

On the other hand, during the first phase of increment of external resistance, the maximum power, 1.69×10^{-3} mW, was obtained with 2,700 Ω. The reason for this is that the behavior of MFC changed during the phase of increment of external resistance, and it is possible that the internal resistance also changed. However, in the phase of lowering of the external resistance, the maximum power, 1.27×10^{-3} mW, was obtained with 2,200 Ω.

3.2 External Resistance Effect on Wastewater Treatment

In the MFC, the microorganisms of the anodic compartment oxidize the organic substrate to carry out its vital functions, thereby removing organic pollutants from wastewater. In this section, the effect of external resistance on the purifying capacity of MFC is studied.

In Fig. 5, the effluent COD as a function of external resistance is observed. As it can be seen, the COD of the effluent decreased when the external resistance was increased; therefore, the consumed substrate by microorganisms increased. In this way, the purifying capacity of the MFC enhanced when the external resistance was increased. However, taking into account that the electricity production decreased, it is clear that greater consumption of organic matter was not caused by the improvement in the behavior of electrogenic microorganisms. Thus, at the anodic compartment, there were other microorganisms (not electrogenics) that degraded organic matter of wastewater.

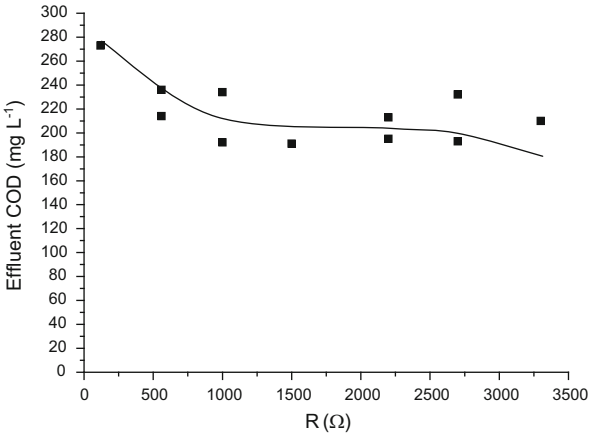

Fig. 5 Effluent COD in steady state at every external resistance

Concluding Remarks

The external resistance directly influences on anode potential and current, and they influence on other variables in a MFC, such as microbial diversity, biofilm morphology, power generated, coulombic efficiency, and MFC stability among other variables. In this way, the selection of the optimal external resistance in order to get the best performance in the MFC is very important. Moreover, it is necessary to take into account that modifications in the operational conditions could change the internal resistance and, therefore, the optimal performance of MFC. Therefore, it is necessary to control the external resistance as a function of internal resistance. Based on the observation made, it can be also concluded that the external resistance select the microbial population growing in the anodic chamber of the MFC. As a consequence of higher external resistance, microbial diversity changed and the lower power was obtained for the same external resistance. It was also observed that when working with high external resistance, the COD removal from the wastewater was higher.

Acknowledgments The authors thank the JCCM for the financial support through the Project POII10-0329-5194.

References

1. Logan BE (2008) Microbial fuel cells. Wiley, New Jersey
2. Debabov V (2008) Electricity from microorganisms. Microbiology 77(2):123–131
3. Chaudhuri SK, Lovley DR (2003) Electricity generation by direct oxidation of glucose in mediatorless microbial fuel cells. Nat Biotechnol 21:1229–1232

4. Min B, Logan BE (2004) Continuous electricity generation from domestic wastewater and organic substrates in a flat plate microbial fuel cell. Environ Sci Technol 38:5809–5814
5. Liu H, Cheng SA, Logan BE (2006) Production of electricity from acetate or butyrate using a single-chamber microbial fuel cell. Environ Sci Technol 39:658–662
6. Lovley DR (2006) Bug juice: harvesting electricity with microorganisms. Nat Rev Microbiol 4:497–508 (Nature Publishing Group)
7. Pinto RP, Srinivasan B, Manuel MF, Tartakovsky B (2010) A two-population bio-electrochemical model of a microbial fuel cell. Bioresour Technol 101:5256–5265
8. Fernández FJ, Castro MC, Rodrigo MA, Cañizares P (2011) Reduction of aeration costs by tuning a multi-set point on/off controller: a case study. Control Eng Pract 19(10):1231–1237
9. González del Campo A, Lobato J, Cañizares P, Rodrigo M, Fernández FJ (2013) Short-terms effects of temperature and COD in a microbial fuel cell. Appl Energy 101:213–217
10. Rozendal RA, Hamelers HVM, Buisman CJN (2006) Effects of membrane cation transport on pH and microbial fuel cell performance. Environ Sci Technol 40(17):5206–5211
11. Oliveira VB, Simoes M, Melo LF, Pinto AMFR (2013) Overview on the developments of microbial fuel cells. Biochem Eng J 73:53–64
12. Ieropoulos I, Greenman J, Melhuish C (2010) Improved energy output levels from small-scale microbial fuel cells. Bioelectrochemistry 78:44–50
13. Aelterman P, Versichele M, Marzorati M, Boon N, Verstraete W (2008) Loading rate and external resistance control the electricity generation of microbial fuel cells with different three-dimensional anodes. Bioresour Technol 99(18):8895–8902
14. Woodward L, Perrier M, Srinivasan B, Tartakovsky B (2009) Maximizing power production in a stack of microbial fuel cells using multiunit optimization method. Biotechnol Prog 25 (3):676–682
15. Rismani-Yazdi H, Christy A, Carver SM, Yu Z, Dehority BA, Tuoviven OH (2011) Effect of external resistance on bacterial diversity and metabolism in cellulose-fed microbial fuel cells. Bioresour Technol 102:278–283
16. Logan BE, Hamelers B, Rozendal R, Schöder U, Keller J, Freguia S, Aelterman P, Verstraete W, Rabaey K (2006) Microbial fuel cells, methodology and technology. Environ Sci Technol 40:5181–5192
17. Clauwaert P, Aelterman P, Pham TH, De Schamphelaire L, Carballa M, Rabaey K, Verstraete W (2008) Minimizing losses in bio-electrochemical systems: the road to applications. Appl Microbiol Biotechnol 79:901–913
18. Pinto RP, Srinivasan B, Guiot SR, Tartakovsky B (2011) The effect of real-time external resistance optimization on microbial fuel cell performance. Water Res 45:1571–1578
19. Thauer RK, Jungermann K, Decker K (1977) Energy-conservation in chemotropic anaerobic bacteria. Bacteriol Rev 41:100–180
20. Aelterman P, Freguia S, Keller J, Verstraete W, Rabaey K (2008) The anode potential regulates bacterial activity in microbial fuel cells. Appl Microbiol Biotechnol 78:409–418
21. Schroder U (2007) Anodic electron transfer mechanisms in microbial fuel cells and their energy efficiency. Phys Chem Chem Phys 9:2619–2629
22. Menicucci J, Beyenal H, Marsili E, Veluchamy RA, Demir G, Lewandowski Z (2006) Procedure for determining maximum sustainable power generated by microbial fuel cell. Environ Sci Technol 40:1062–1068
23. Ghangrekar MM, Shinde VB (2007) Performance of membrane-less microbial fuel cell treating wastewater and effect of electrode distance and area on electricity production. Bioresour Technol 98(15):2879–2885
24. Song T-S, Yan Z-S, Zhao Z-W, Jiang H-L (2010) Removal of organic matter in freshwater sediment by microbial fuel cells at various external resistances. J Chem Technol Biotechnol 85:1489–1493
25. Chae K-J, Choi M-J, Kim K-Y, Ajayi FF, Park W, Kim C-W, Kim IS (2010) Methanogenesis control by employing various environmental stress conditions in two-chambered microbial fuel cells. Bioresour Technol 101:5350–5357

26. Zhang L, Zhu X, Li J, Qiang L, Ye D (2011) Biofilm formation and electricity generation of a microbial fuel cell started up under different external resistances. J Power Sources 196:6029–6035
27. Wagner RC, Call DF, Logan BE (2010) Optimal set anode potentials vary in bioelectrochemical systems. Environ Sci Technol 44:6036–6041
28. Lyon DY, Buret F, Vogel TM, Monier J-M (2010) Is resistance futile? Changing external resistance does not improve microbial fuel cell performance. Bioelectrochemistry 78:2–7
29. Jadhav GS, Ghangrekar MM (2009) Performance of microbial fuel cell subjected to variation in pH, temperature, external load and substrate concentration. Bioresour Technol 100:717–723
30. Jang JK, Pham TH, Chang IS, Kang KH, Moon H, Cho KS, Kim BH (2004) Construction and operation of a novel mediator and membrane-less microbial fuel cell. Process Biochem 39 (8):1007–1012
31. Borole AP, Hamilton CY, Vishniverskaya TA, Leak D, Andras C, Morrell-Falvey J, Keller M, Davison B (2009) Integrating engineering design improvements with exoelectrogen enrichment process to increase power output from microbial fuel cells. J Power Sources 191:520–527
32. McLean JS, Wanger G, Gorby YA, Wainstein M, McQuaid J, Ishill SI, Bretschger O, Beyenal H, Nealson KH (2010) Quantification of electron transfer rates to a solid phase electron acceptor through the stages of biofilm formation from single cells to multicellular communities. Environ Sci Technol 44:2721–2727
33. He Z, Minteer SD, Angenent LT (2005) Electricity generation from artificial wastewater using an upflow microbial fuel cell. Environ Sci Technol 39:5262–5267
34. Ren Z, Yan H, Wang W, Mench MM, Regan JM (2011) Characterization of microbial fuel cells at microbially and electrochemically meaningful time scales. Environ Sci Technol 45:2435–2441
35. Stephen NG (2006) On the maximum power transfer theorem within electromechanical systems. Proc IME C J Mech Eng Sci 220:1261–1267
36. Katuri KP, Scott K, Head IM, Picioreanu C, Curtis TP (2011) Microbial fuel cells meet with external resistance. Bioresour Technol 102:2758–2766
37. Logan BE, Regan JM (2006) Electricity-producing bacterial communities in microbial fuel cells. Trends Microbiol 14:512–518
38. Manohar AK, Bretschger O, Nealson KH, Mansfeld F (2008) The use of electrochemical impedance spectroscopy (EIS) in the evaluation of the electrochemical properties of a microbial fuel cell. Bioelectrochemistry 71:149–154
39. Jung S, Regan JM (2011) Influence of external resistance on electrogenesis, methanogenesis, and anode prokaryotic communities in microbial fuel cells. Appl Environ Microbiol 77:564–571
40. Lee C-Y, Chen J-H, Cai Y-Y (2010) Bioelectricity generation and organic removal in microbial fuel cells used for treatment of wastewater from fish-market. J Environ Eng Manage 20:173–180
41. Infantes D, González Del Campo A, Villaseñor J, Fernández FJ (2011) Influence of pH, temperature and volatile fatty acids on hydrogen production by acidogenic fermentation. Int J Hydrogen Energy 36(24):15595–15601
42. Torres CI, Krajmalnik-Brown R, Parameswaran P, Marcus AK, Wanger G, Gorby YA, Rittmann BE (2009) Selecting anode-respiring bacteria based on anode potential: phylogenetic, electro-chemical, and microscopic characterization. Environ Sci Technol 43:9519–9524
43. Jung S, Regan JM (2007) Comparison of anode bacterial communities and performance in microbial fuel cells with different electron donors. Appl Microbiol Biotechnol 77:393–402
44. Lee HS, Parameswaran P, Kato-Marcus A, Torres CI, Rittmann BE (2008) Evaluation of energy-conversion efficiencies in microbial fuel cells (MFCs) utilizing fermentable and non-fermentable substrates. Water Res 42:1501–1510
45. Picioreanu C, Head IM, Katuri K, Van Loosdrecht MCM, Scott K (2007) A computational model for biofilm-based microbial fuel cells. Water Res 41:2921–2940

46. Picioreanu C, Katuri KP, Head IM, van Loosdrecht MCM, Scott K (2008) Mathematical model for microbial fuel cells with anodic biofilms and anaerobic digestion. Water Sci Technol 57:965–971
47. Torres CI, Marcus AK, Lee HS, Parameswaran P, Krajmalnik-Brown R, Rittmann BE (2010) A kinetic perspective on extra-cellular electron transfer by anode-respiring bacteria. FEMS Microbiol Rev 34:3–17
48. Rabaey K, Boon N, Siciliano SD, Verhaege M, Verstraete W (2004) Biofuel cells select for microbial consortia that self-mediate electron transfer. Appl Environ Microbiol 70:5373–5382
49. Finkelstein DA, Tender LM, Zeikus JG (2006) Effect of electrode potential on electrode-reducing microbiota. Environ Sci Technol 40:6990–6995
50. Srikanth S, Mohan SV, Sarma PM (2010) Positive anodic poised potential regulates microbial fuel cell performance with the function of open and closed circuitry. Bioresour Technol 101:5337–5344
51. Liu Y, Harnisch F, Fricke K, Sietmann R, Schröder U (2008) Improvement of the anodic bioelectrocatalytic activity of mixed culture biofilms by a simple consecutive electrochemical selection procedure. Biosens Bioelectron 24:1006–1011
52. Sajana TK, Ghangrekar MM, Mitra A (2014) Effect of operating parameters on the performance of sediment microbial fuel cell treating aquaculture water. Aquacult Eng 61:17–26
53. Franks AE, Nevin KP, Jia H, Izallalen M, Woodard TL, Lovley DR (2009) Novel strategy for three-dimensional real-time imaging of microbial fuel cell communities: monitoring the inhibitory effects of proton accumulation within the anode biofilm. Energy Environ Sci 2:113–119
54. Torres CI, Kato Marcus A, Rittmann BE (2008) Proton transport inside the biofilm limits electrical current generation by anode-respiring bacteria. Biotechnol Bioeng 100:872–881
55. Qureshi N, Annous BA, Ezeji TC, Karcher P, Maddox IS (2005) Biofilm reactors for industrial bioconversion processes: employing potential of enhanced reaction rates. Microb Cell Fact 4:24
56. Liu Y, Tay JH (2011) Strategy for minimization of excess sludge production from the activated sludge process. Biotechnol Adv 19:97–107
57. Juang DF, Yang PC, Chou HY, Chiu LJ (2011) Effects of microbial species, organic loading and substrate degradation rate on the power generation capability of microbial fuel cells. Biotechnol Lett 33:2147–2160
58. Gil GC, Chang LS, Kim BH, Kim M, Jang JK, Park HS, Kim HJ (2003) Operational parameters affecting the performance of a mediator-less microbial fuel cell. Biosens Bioelectron 18:327–334
59. Premier GC, Kim JR, Michie I, Dinsdale RM, Guwy AJ (2011) Automatic control of load increases power and efficiency in a microbial fuel cell. J Power Sources 196:2013–2019
60. Woodward L, Perrier M, Srinivasan B, Pinto RP, Tartakovsky B (2010) Comparison of real-time methods for maximizing power output in microbial fuel cells. AIChE J 56:2742–2750
61. Oh SE, Logan BE (2007) Voltage reversal during microbial fuel cell stack operation. J Power Sources 167(1):11–17
62. Grondin F, Perrier M, Tartakovsky B (2012) Microbial fuel cell operation with periodic connection of the external resistance. In: 8th IFAC symposium on advanced control of chemical processes, Furama Riverfront, Singapore, pp 120–124
63. Coronado J, Perrier M, Tartakovsky B (2013) Pulse-width modulated external resistance increases the microbial fuel cell power output. Bioresour Technol 147:65–70
64. Fradler KR, Kim JR, Boghani HC, Dinsdale RM, Guwy AJ, Premier GC (2014) The effect of internal capacitance on power quality and energy efficiency in a tubular microbial fuel cell. Process Biochem 49:973–980
65. Grondin F, Perrier M, Tartakovsky B (2012) Microbial fuel cell operation with intermittent connection of the electrical load. J Power Sources 208:18–23

66. Gardel EJ, Nielsen ME, Grisdela PT, Girguis PR (2012) Duty cycling influences current generation in multi-anode environmental microbial fuel cells. Environ Sci Technol 46:5222–5229
67. Lobato J, González del Campo A, Fernández FJ, Cañizares P, Rodrigo MA (2013) Lagooning microbial fuel cells: a first approach by coupling electricity-producing microorganisms and algae. Appl Energy 110:220–226
68. Lobato J, Cañizares P, Rodrigo MA, Linares JJ, Fragua AF (2006) Application of Sterion membrane as polymer electrolyte for DMFCs. Chem Eng Sci 61:4773–4782
69. Fernandez FJ, Seco A, Ferrer J, Rodrigo M (2009) Use of neurofuzzy networks to improve wastewater flow-rate forecasting. Environ Model Software 24(6):686–693
70. Lobato J, Cañizares P, Fernandez FJ, Rodrigo MA (2012) An evaluation of aerobic and anaerobic sludges as start-up material for microbial fuel cell systems. N Biotechnol 29 (3):415–420
71. González del Campo A, Cañizares P, Rodrigo MA, Fernández FJ, Lobato J (2013) Microbial fuel cell with an algae-assisted cathode: a preliminary assessment. J Power Sources 242:638–645

The Avocado and Its Waste: An Approach of Fuel Potential/Application

María Paz Domínguez, Karina Araus, Pamela Bonert, Francisco Sánchez, Guillermo San Miguel, and Mario Toledo

Abstract With a global production exceeding 4 million tons per year in 2011, avocado has become a major agroindustrial commodity. Most of the production and the transformation industry is located in North and Central America, although consumption is growing fast primarily in developed countries like the USA and the European Union. The principal use of the avocado fruit is human consumption, although other applications related to the production of cosmetics, nutritional supplements and livestock feed have been reported.

Only the avocado pulp is employed for commercial applications, while other fruit elements like the seed and peel have no practical use and are disposed of by landfilling. Avocado seeds, which represent up to 26 wt % of the fruit mass, are produced in large amounts in centralized avocado transformation plants. Despite their high starch content, the seeds cannot be used for livestock feeding due to the high concentration of polyphenols, which impart a bitter taste and may be toxic at high levels. This chapter presents an introduction into the characteristics of avocado seeds and its potential use as a fuel using different technologies. Information is provided about the chemical, physical and thermal properties of the material. Preliminary results are also included describing its thermochemical transformation using a rotary kiln and a porous media reactor. Product yields and compositions are

M.P. Domínguez (✉), F. Sánchez, and G. San Miguel
Departamento de Ingeniería Energética y Fluido Mecánica, Escuela Técnica Superior de Ingenieros Industriales (ETSII), Universidad Politécnica de Madrid, C/ José Gutiérrez Abascal 2, 28006 Madrid, Spain
e-mail: maria.dominguezd@alumnos.upm.es

K. Araus and M. Toledo
Departamento de Ingeniería Mecánica, Universidad Técnica Federico Santa María, Av. España 1680, Valparaíso, Chile

P. Bonert
Universidad Técnica Federico Santa María, Centro de Economía y Administración de Residuos Sólidos, C/ General Bari No 699, Co Placeres, Valparaíso, Chile

G. Lefebvre et al. (eds.), *Environment, Energy and Climate Change II: Energies from New Resources and the Climate Change*, Hdb Env Chem (2016) 34: 199–224,
DOI 10.1007/698_2014_291,
Published online: 16 October 2014

described for the gasification and pyrolysis of this material using different operating conditions. The chapter also shows preliminary analysis regarding mechanical densification for the production of pellets.

Keywords Avocado seeds, Energy, Gasification, Pellets, Pyrolysis, Valorization

Contents

1 Introduction

The avocado (*Persea americana* Mill.) is a highly nutritious subtropical fruit, with a high content of unsaturated fats and vitamins [1]. With a production exceeding four million tons in 2011, the industrial transformation of this fruit for the production of guacamole and avocado oil generates large amounts of by-products, primarily husks and seeds [2]. These residues may be used as forage for domestic animals, although its nutrient value is limited [3]. This chapter presents an overview of the avocado fruit including composition, botanical aspects and production and also an analysis of the potential of using the by-products from its industrial transformation (mainly the seed) as an energy source.

2 The Avocado: Botanical Aspect, Market and Research for Energy Uses

2.1 Botanical Aspect

2.1.1 Botanical Description and Varieties

The avocado tree (*P. americana* Mill.) belongs to the family *Lauraceae* and to the genus *Persea*. This species originates from Central America and has been widely planted in many tropical and subtropical areas all over the world. Nowadays it is also cultivated under irrigation in several warm dry areas like Mediterranean countries and California. The avocado tree is characterized by a rapid growth rate. It may reach 30 m in height, though specimens in orchards are usually grown to a smaller size (usually below 8 m) so pruning and harvesting can be done more readily [4]. The root system is usually shallow ($\leq$1 m). Leaves are alternate, stalked and perennial [5]. Flowers are inconspicuous and occur in panicles. Avocado exhibits a type of flowering behaviour known as "synchronous dichogamy": The flower can expose the female organ in the morning, so the stigma is receptive to pollen for a couple of hours, closes itself and reopens as male in the afternoon of the day after (type A) or opens as female in the afternoon and as male in the morning of the following day (type B). This condition is not conducive to self-pollination [4, 6]. The fruit (which is the harvestable product – the avocado itself) is an ellipsoidal or ovate berry with one single seed.

There are three main botanical varieties of avocado: *drymifolia* (Mexican), *guatemalensis* (Guatemalan) and americana (West Indian). *P. americana* var. *drymifolia* is native to central Mexico, resists cold temperatures (down to −9°C) and has small leaves with essential oils that provide them with a distinctive anise flavour. The fruits are small (80–250 g) and contain a high percentage of lipids (up to 30%, fresh matter basis – f.m.b.). Fruit skin is thin, smooth and, ordinarily, pale green, and the pulp has very low fibre content. According to [5], more than ten commercial varieties belong to this botanical variety. Among them are the following: Puebla, Duke, Gottfried and Topa Topa (type A) and Zutano and Bacon (type B).

Figure 1 shows a taxonomical adscription of various commercial varieties of avocado. *P. americana* var. *guatemalensis* is native to Mexico and Guatemala, resists mild winters (with minimum temperatures down to −5°C) and has big dark green leaves. The fruit weight varies between 200 and 1,000 g. Lipid content in pulp is around 20% (f.m.b.). Fruit skin is thick and hard, dark green or even dark purple. According to [5] almost 40 commercial varieties belong to this botanical variety, for example, Reed, Pinkerton and Mayapan (type A) and Edranol, Itzamna, Linda and Nabal (type B).

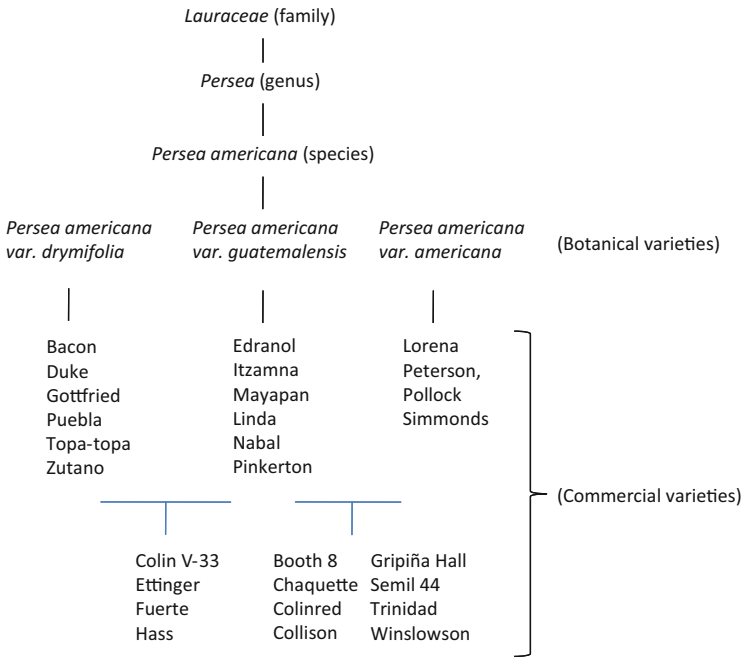

Fig. 1 Taxonomical adscription of some commercial varieties of avocado

P. americana var. *americana* is native to Central-South American lowlands and does not resist temperatures below −2°C. The fruit weight oscillates between 250 and 2,500 g, and the lipid content in the pulp is low (between 5 and 15%, f. m.b). Fruit skin is thin and flexible, smooth or rough, and green, yellow, or yellow-reddish coloured. According to [5] almost 14 commercial varieties belong to this botanical variety. Among them are the following: Peterson and Simmonds (type A) and Lorena, Trapp and Pollock (type B).

Avocado tree has a high level of allogamy (cross-pollination) so many commercial varieties were originated from hybridization between the previously described varieties. Among them, the following stand out:

– Mexican x Guatemalan: Hass (type A) and Fuerte, Ettinger and Colin V-33 (type B)
– Guatemalan x West Indian: Choquette, Colinred, Collison, Semil 44 and Trinidad (type A) and Booth 8, Gripiña, Hall and Winslowson (type B)

Their main characteristics are intermediate between those corresponding to the parental varieties. Hass, the most important avocado variety in the world, is closely related to the old Guatemalan variety Lion, and it is considered to be 85–90% Guatemalan and 10–15% Mexican. Hass fruits are medium sized (150–400 g) with

a rough green skin that turns black when ripens. Pulp has lipid content between 15% and 21% (f.m.b.) and very good organoleptic properties [5, 7]. Hass is the variety used in all of the experimental sections of this chapter.

2.1.2 Agroecology

The main topics concerning avocado's agroecology are summarized in an extensive publication by [5]. Thermal requirements depend on varieties, as it has been previously stated. Besides the extreme values mentioned above, optimal mean temperatures for avocado growth are as follows: 5–17°C (*P. americana* var. *drymifolia*), 4–19°C (*P. americana* var. *guatemalensis*) and 18–26°C (*P. americana* var. *americana*). Concerning humidity, avocado tree has a very good adaptability to low humidity climates, but adaptation depends on varieties, according to the following order: *drymifolia* > *guatemalensis* > *americana*. There are avocado plantations in rainfed areas where precipitation ranges between 665 and 2,000 mm/year, and water needs also depend on varieties according to the same previous order. Wind barriers are commonly used in orchards because of the sensibility of avocado trees to strong winds. When speed reaches values over 20 km/h, branches can be broken and flowers or fruits may drop. Some varieties are more resistant to strong winds (Duke, Bacon), while others, like Zutano, are highly sensitive. Regarding edaphic conditions, well-drained soils are required; otherwise, diseases (rottenness) will attack the plantation. Loamy and sandy soil textures are, therefore, preferred.

2.1.3 Propagation and Crop Management

Propagation of avocado plants is done using cuttings from selected varieties and grafting on rootstocks that have higher tolerance to drought, salinity or diseases. Plant density ranges between 100 and 462 plants/ha. Pruning is less intensive than in other species, but shaping, maintenance and rejuvenation pruning are frequently done in avocado orchards. Bark ringing of 2 or 3 branches per tree is sometimes used to avoid alternation in fruit production (masting) and to enhance flower occurring or fruit weight gain [5]. Fertilization requirements deeply depend on the chosen variety and the soil composition, but in general terms, avocado is a crop with a high demand of potassium [8]. Weeding is uncommonly needed once trees have grown. In the meantime, mechanical and chemical procedures, as well as mulching, can be used to fight weeds [9]. Phytochemicals are usually applied to fight pests (insects) and diseases (among them, the most important is the rottenness caused by the fungus *Phytophthora cinnamomi* var. *cinnamomi* Rands) [10, 11]. Harvest is done manually by cutting the stalk. Yields commonly range between 8 and 13 ton/(ha year).

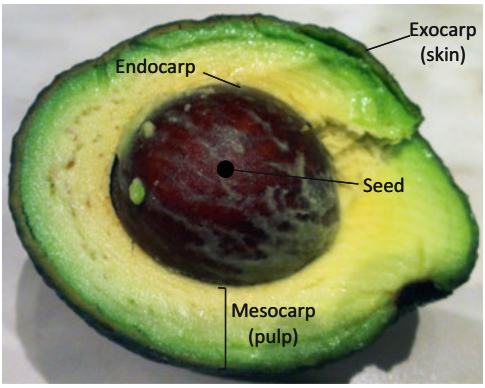

Fig. 2 Anatomy of the avocado berry

2.1.4 Fruit Morphology and Chemical Composition

Avocado is a berry consisting of a single carpel and a single seed [6]. It may show different shapes (elliptical, ovate, spherical, oblate, rhomboidal, globular, etc.) and many different colours (pale green, dark green, yellowish green, yellow, reddish yellow, light purple, dark purple and black). From a botanical point of view, the skin represents the berry's exocarp, the edible pulp is the mesocarp and the thin layer coating the seed is the endocarp, as shown in Fig. 2. The seed itself consists of two fleshy cotyledons, plumule, hypocotyl, radicle and two thin seed coats adhering to each other [6].

The relative proportion of the different parts varies greatly. Among the commercial varieties above-mentioned (and considering fresh weight), skin percentage ranges between 3% (Choquette) and 13.5% (Booth 8), pulp between 64% (Puebla) and 80% (Choquette), and seed between 10% (Nabla, Pinkerton, Lorena) and 26% (Zutano). Regarding Hass, the relative proportion is about 8.5:72:11% (skin/pulp/seed) [5].

To the best of our knowledge, avocado skin composition has been poorly researched. Sadir [12] reported the following values for Wagner variety skin: 4.2% sugars, 3.9% proteins, 12.7% lipids, 24.1% fibre and 3.9% ashes (dry matter basis – d.m.b.). Bressani et al. [13] studied the composition of lyophilized skin from several varieties (both native and commercial) and reported the following mean values for major components: 9.8% moisture, 73.7% carbohydrates, 4.0% proteins, 4.4% lipids, 51.9% crude fibre and 4.0% ashes. Moisture average value in fresh matter was 66.6%. It seems probable that, due to chosen methods, fibre and carbohydrate contents overlap. Concerning Hass variety, values in the same report were 14.5% moisture, 62.0% carbohydrates, 8.3% proteins, 9.1% lipids, 50.7% crude fibre and 6.1% ashes.

Pulp is mainly composed of water (65–77%) and lipids (3–32%), mainly triglycerides. In Hass avocado, the most important fatty acids are oleic (47–59% of total fatty acids), palmitic (17–23%), linoleic (13–26%) and palmitoleic (9–10%) [7, 14, 15]. Carbohydrates represent about 8.6% of total fresh weight (6.8% fibre,

Table 1 Chemical composition of lyophilized avocado seeds according to Bressani et al. [13], 2009 (%, d.m.b.)

	Pool of varieties		Hass	
	Peeled seed	Tegument[a]	Peeled seed	Tegument[a]
Moisture before lyophilization	60.5	61.5	60.1	60.1
Moisture	8.7	10.2	7.7	11.5
Carbohydrates	71.9	74	79.5	74.4
Proteins	4.8	5.7	3.4	5.8
Lipids	4.6	3	5.5	3.9
Crude fibre	3.9	29.9	4.0	26.5
Ashes	3.4	3.9	4.2	4.4

[a]Tegument relative weight was always below 5% of whole seed weight (f.m.b.)

0.3% sugars and 0.11% starch, according to [7]). The protein content is about 2% [6, 7]. Ashes represent about 1.77% (f.m.b), and potassium is, by far, the most important element [507 mg/100 g, a content almost ten times higher than phosphorous (54 mg/100 g), which is the second most important element] [7].

Regarding seeds, Bressani et al. [13] studied the composition of lyophilized peeled seeds and peel (tegument) from several varieties (both native and commercial) and reported values showed in Table 1 for major components. Weatherby and Sorber [16] were more specific about carbohydrate composition when they studied drymifolia and Fuerte peeled seeds and determined values for sucrose (1.2–1.9%, d.m.b.), arabinose (4.1–4.5%, d.m.b.), total sugars (4.5–7.3%, d.m.b.) and starch (57.2–59.9%, d.m.b.). The crude fibre content found by these latest authors was significantly higher (7.3–9.1%), closer to those values reported by Bora et al. [17] for Fuerte unpeeled seeds (11.6%, d.m.b.). The lipid content, however, was plainly lower (1.7–2.2% d.m.b).

Concerning minor compounds, total polyphenols and tannins in avocado seeds have received increasing attention due to their antioxidant properties [18]. Bressani et al. [13] reported average values of 448 mg catechol/100 g (d.m.b.) and 259 mg tannic acid/100 g (d.m.b.) for both groups of components, respectively, in a pool of avocado varieties. For Hass avocado, values of 602.5 ± 278.51 mg catechol/100 g (d.m.b.) and 332.82 ± 61.49 mg tannic acid/100 g (d.m.b.) were found.

2.2 The Avocado Market

The international market for avocado fruit and its derivates (primarily guacamole and avocado oil) has been growing rapidly in the last decade. Data about production, exports and imports of this fruit are available from the Food and Agriculture Organization of the United Nations (FAO) (http://faostat3.fao.org/faostat-gateway/go/to/home/E).

2.2.1 Production

Commercial production of avocado in 2011 exceeded 4 millions of tons (4,276,592 ton), with the Hass variety being the most popular. American countries remain the largest producers of this fruit, but contribution from African, European and Asian countries is growing rapidly. As shown in Fig. 3, Mexico was by far the main producer, representing 29.6% of the world's market.

2.2.2 Exports and Imports

Mexico is also the largest exporter of avocados, with nearly 350,000 ton/year. This represented around 40% of the world market in 2011. As shown in Fig. 4, four other countries (Chile, the Netherlands, Peru and Spain) have export volumes between 120,000 and 70,000 tons, representing in combination an additional 40%. The top ten exporters accumulated around of 90% of the 800,000 ton exported in 2011.

The USA imported over 415,000 ton of avocados in 2011, representing 36% of the world's imports. This was followed at a distance by the Netherlands, France, Japan, Canada, the UK, Spain and Germany. The Netherlands and France represented the second most important group of importers, with a 20% of the worldwide market (Fig. 5).

2.2.3 Avocado Uses

Most of the avocado in the world is commercialized by the retailer and food industry for human consumption, either directly as fresh fruit or after processing in the form of different avocado derivates (guacamole, sauces, avocado oil, flavouring agents, etc.). Avocado oil is also employed for cosmetic applications. These products derive from the pulp of the avocado, while the rest of the fruit (peel, seed) has no commercial use and is managed as a waste.

2.3 Avocado and Energy: An Overview

Waste derived from the transformation of avocado fruits may be used for its energy content, which may become an additional source of revenues for this industry and may also reduce the environmental burden associated with this commercial activity. These wastes are produced in large amounts in centralized avocado transformation plants. This section provides a review about the potential of using avocado by-products derived from its industrial transformation as an energy resource.

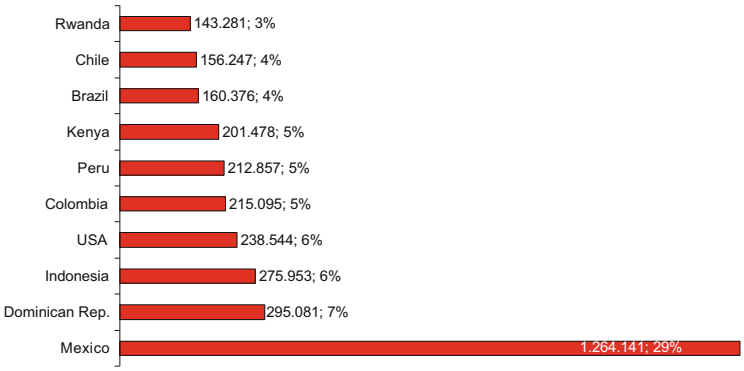

Fig. 3 Main producers of avocado worldwide (values in ton/year) (Faostat 2014)

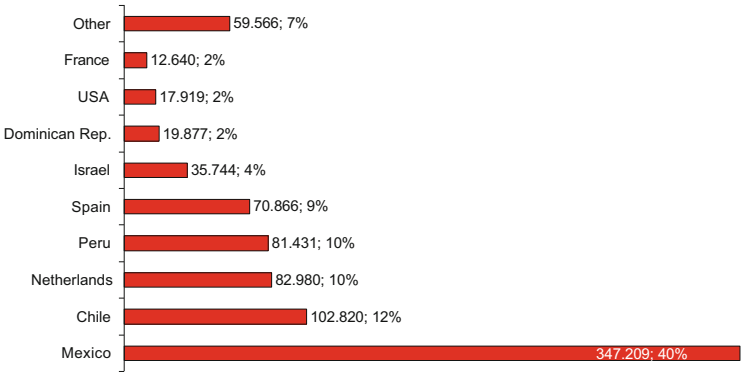

Fig. 4 Main exporters of avocado (values in ton/year) (Faostat 2014)

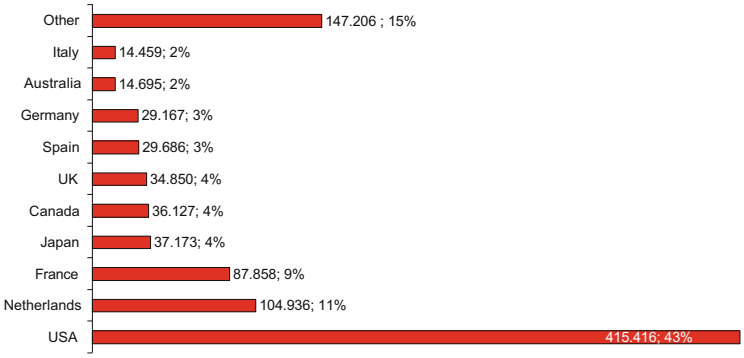

Fig. 5 Main importers of avocado (values in ton/year) (Faostat 2014)

2.3.1 Avocado Pulp Oil

The pulp in avocado fruits contains high concentrations of triglyceride oils. However, this oil is not suitable for widespread utilization as cooking oil due to its strong bitter taste [19]. In the 1980s a few publications were produced aimed at optimizing the production and application of avocado oil. Werman and Neeman [20] analysed the effect of different parameters on the extraction of avocado pulp oil by centrifugal processing including temperature, pH and NaCl concentration. Potential applications of avocado oils in the cosmetic industry are discussed in [21].

The use of avocado pulp oils for the production of biodiesel has been reported in various publications. Cabrera et al. [22] present a preliminary analysis of yields, composition and energy properties of biodiesel produced from different tropical fruits, including avocado. The experimental results evidence the production of high-quality methyl esters from crude avocado oils. This paper describes lower heating values and higher viscosity values in the avocado fuel, compared to conventional diesel. Giraldo and Moreno-Piraján [23] describe the benefits of using lipases to improve the yields in the synthesis of biodiesel from avocado pulp oil. Knothe [24] provides a chemical characterization of methyl esters from an avocado oil biodiesel.

2.3.2 Avocado Seed Oil

Some articles report the production of triglyceride oils and biodiesel from avocado seeds. Weatherby and Sorber [16] present a complete analysis of the chemical composition of avocado seed. The authors suggest that human consumption of these oils requires a pretreatment to minimize its bitter astringent taste. Rachimoellah et al. [25] provide results for biodiesel production from avocado seed oil using homogeneous catalysts. Characterization of the resulting biodiesel shows that it satisfies the quality standards required for diesel.

2.3.3 Other Uses of Avocado Seed

Another use for avocado seed relates to the production of carbonized materials and adsorbents. Elizalde-González et al. [26] describe the pore characteristics and adsorption capacity of chars and activated carbons produced from this material. Activated carbons from avocado seeds showed improved adsorption characteristics than the ones produced from corncob and plum kernels. Alvares et al. [27] describe that activated carbons from avocado seeds exhibited high phenol adsorption capacity.

3 Avocado Seed Characterization

Avocado seeds from ripe fruits of the Hass variety were produced in Malaga (Spain). The samples were cut and milled, homogenized and characterized for its chemical, fuel and thermal properties. These same samples were also employed to investigate energy transformation and valorization using different technologies: combustion/gasification in a porous media reactor, pyrolysis in a rotary kiln and mechanical densification using a pelletizer. The following sections show preliminary results from these analyses and trials.

3.1 Elemental Analysis

The results were obtained using a Thermo Finnigan Flash EA (model 1112) elemental analyser. Values represent the average of duplicate analyses, expressed as percentage of the original sample mass (dry matter basis) (Table 2).

The results show that the avocado seeds present a high quantity of carbon and oxygen and low percentage of hydrogen and nitrogen. This composition is in agreement with the high starch concentration in the avocado seeds described in Sect. 2.1.4.

3.2 Proximate Analyses

Values are expressed as mass percentage in wet matter basis for humidity and dry matter determinations and in dry matter basis for the other parameters. The results represent the mean values of duplicate determinations. Table 3 also shows the standardized methods employed.

3.3 Heating Values

Heating values were determined according to standard method ASTM D-240. Table 4 shows the average results of duplicate determinations on wet and dry matter basis.

Table 2 Elemental analysis (dry matter ash free basis) of avocado seeds

	Value (wt %)
Carbon	48.3 ± 0.2
Hydrogen	7.5 ± 0.1
Nitrogen	<0.5
Oxygen	43.4 ± 0.2

Table 3 Proximate analysis of avocado seeds

	Value (wt %)	Standard method
Humidity[a]	45.3	EN 14774-1:2010 [28]
Dry matter[a]	54.7	EN 14774-1:2010 [28]
Volatile solids[b]	78.7	EN 15148:2009 [29]
Ash[b]	2.6	EN 14775:2009 [30]
Fixed carbon[b]	18.7	By difference

[a]Wet basis
[b]Dry basis

Table 4 Heating values of avocado seeds

	Wet basis	Dry basis
High heating value (MJ/kg)	7.7	16.6
Low heating value (MJ/kg)	5.7	14.6

3.4 Thermogravimetric Analysis (TGA)

The TGA analysis was conducted under flowing (55 mL/min) nitrogen, with a heating rate of 10°C/min to a maximum temperature of 900°C using a TA Instrument TGA/DTA, model TGA 2050. The seeds were dried prior to TGA analysis at 70°C for 24 h.

The results shown in Fig. 6 describe two areas of mass loss. The first one (A), at temperatures around 100°C, relates to moisture content. The second (B), at temperatures between 250 and 350°C, relates primarily to thermal degradation of starch, the main polymeric component of the avocado seeds [16, 17]. The thermal degradation of other structural polymers (cellulose, hemicellulose and lignin) is masked by the prevalence of the peak corresponding to starch.

4 Combustion/Reforming of Avocado Seeds in a Porous Media Reactor

4.1 Description of Technology

Inert porous media reactors represent a more efficient alternative to free flame combustion systems for the energy utilization of gas fuels. The reactor is filled with an inert media through which the flame is transmitted. The result is the formation of a flame front (combustion wave) formed by small flames, which is transferred from one end of the other of the reactor. This flame front improves heat transfer capacity of the system, resulting in reduced pollutant emissions and increased efficiency compared to free flame systems [31].

Various papers describe the adaptation of inert porous media technology to different fuels and operating conditions [32]. A special case involves hybrid filtration combustion, where solid fuels are incorporated into the inert porous

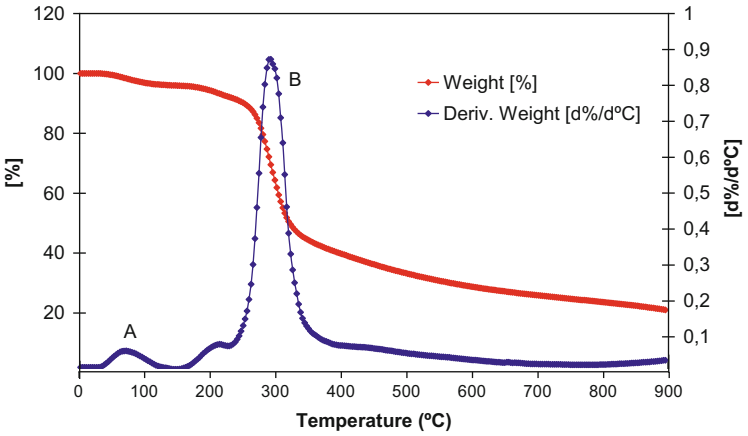

Fig. 6 TGA-DTA analysis of avocado seed

media for improved combustion conditions and energy valorization of the solid fuel [33–35]. Flame propagation in the heterogeneous media is more complex, resulting in higher process temperature and propagation velocities. This section shows preliminary results from a combustion/reforming process conducted in a hybrid filtration system. Avocado seeds are added to the inert porous media and the combustion process is enriched with addition of methane.

4.2 Methodology

The hybrid filtration combustion system consists of a 340 mm long quartz tube with an internal diameter of 40 mm which is covered with insulation. In hybrid configuration (Fig. 7), the tube is filled with a uniformly mixed aleatory alumina spheres (5.6 mm diameter) and avocado seeds (cut to at a similar alumina sphere size) with volume fraction of 50%. The packed bed formed in this way occupied 130 mm of the tube length with a porosity of 40%. In conventional configuration the tube is filled only with alumina spheres.

Air and natural gas (96% methane), metered using Aalborg mass flow controllers, are premixed and introduced into the reactor through the distribution grid at the reactor bottom. The upstream propagating combustion wave was initiated with a lighter at the reactor exit which opens to the atmosphere, and the wave was turned off when it reached the reactor bottom. In all cases the alumina spheres were slowly shifted downwards occupying the space of the avocado seeds pellets consumed by the moving combustion wave. It was found that in all cases the avocado seeds pellets were completely consumed.

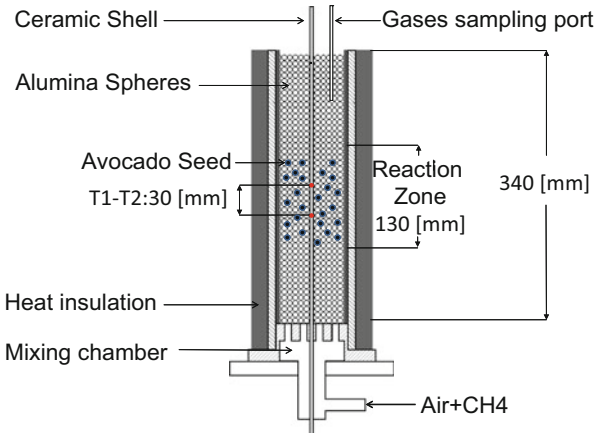

Fig. 7 Schematic representation of the porous media reactor

The axial temperature distribution of the reactor is measured by two S-type thermocouples. These thermocouples are housed in a multibore ceramic shell 8 mm in diameter. A data acquisition system was used to read and record the temperatures. The error in the wave velocity measurements performed based on displacement of thermal profile along the reactor length was 10%. Chemical composition of the output gases was measured using a PerkinElmer (Clarus 500) Gas Chromatograph, equipped with a thermal conductivity detector (TCD). The accuracy of chemical sampling was close to 10%.

4.3 Results

Figure 8 shows the flame propagation velocities and the process temperatures observed when the porous media reactor was operated in conventional and hybrid configurations, as a function of the gas fuel equivalence ratio (φ). The results illustrate the lowest flame propagation velocity in conventional operation of the reactor at $\varphi = 0.6$ (-0.00143 cm/s). The flame propagation profile changed with the incorporation of biomass to exhibit a minimum at $\varphi = 1.0$ (-0.0023 cm/s). Regarding process temperature, the experimental results show minimum values at $\varphi = 1.0$ in both configurations. This may be associated with the progressive contribution of endothermic processes and reactions (volatilization and steam reforming) reached at that equivalence ratio. Comparatively lower minimum temperatures were observed when the reaction zone contained biomass (817°C compared to 920°C in conventional configuration), which may be associated with the evolution of water and volatile products. Maximum process temperatures in both configurations were found at $\varphi = 1.2$ (above 1,053°C), which has been attributed to predominance of exothermic reactions.

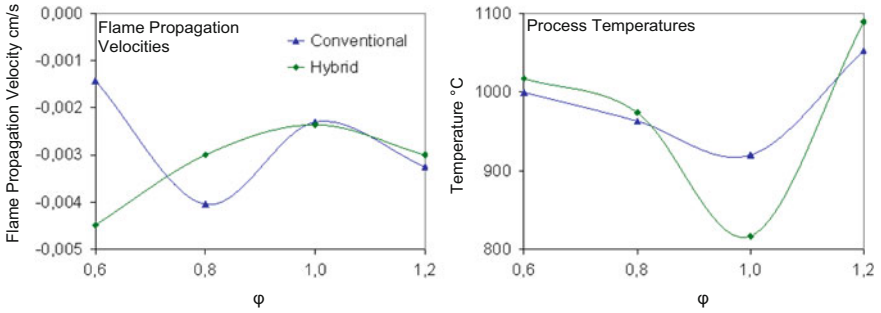

Fig. 8 Flame propagation velocities and process temperatures as a function of gas fuel equivalence ratios (φ)

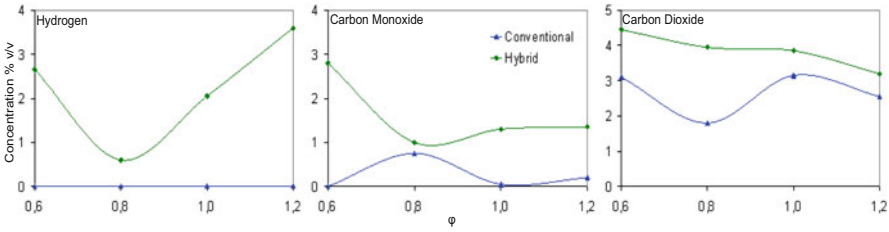

Fig. 9 Gas concentrations as a function of gas fuel equivalence ratios (φ)

The concentration of methane in the evolved gases was negligible at $\varphi \leq 1.0$. However, methane levels of 1.3 and 5.7 % v/v were observed at $\varphi = 1.2$ when operating in conventional and hybrid configuration, respectively.

Figure 9 shows the formation of H_2, CO and CO_2 as a function of the equivalence ratio. The results show that the concentration of hydrogen is below detection limits when operating the reactor in conventional configuration. In contrast, hydrogen concentrations in the range between 0.6 and 3.6 % v/v were observed when operating in hybrid mode, with a minimum at $\varphi = 0.8$. Regarding carbon monoxide, the experiments show very low concentrations in the case of conventional operation, with a maximum of 0.75 % v/v at $\varphi = 0.8$. In contrast, operation in hybrid configuration generated higher carbon monoxide concentrations, with a maximum at $\varphi = 0.6$ (2.8 % v/v) and minimum at $\varphi = 0.8$ (1.0 % v/v). Carbon dioxide concentrations remained within 1.8 and 3.2 % v/v when operating the reactor in conventional configuration. These values were higher (between 3.2 and 4.5% v/v) as a result of incorporating biomass into the reactor, with a maximum at $\varphi = 0.6$.

The results show similar trends that the results of other researches with this technology [33, 34], but is not possible to comparison with other studies in avocado seed, because for this material no results reported.

4.4 Conclusions

The experimental results show that incorporation of biomass (avocado seeds) into a porous media reactor operating with methane/air mixtures results in a notable alteration of its operating conditions in terms of process temperature, flame propagation velocity and gas composition. The presence of biomass resulted in an increase in the concentration of syngas-related gases (H_2, CO) and also CO_2, primarily when operating at high gas fuel equivalence ratios.

5 Torrefaction and Pyrolysis

5.1 Description of Technology

Biomass is a renewable energy source, which can mitigate the greenhouse effect because carbon dioxide (CO_2) levels emitted into the atmosphere during combustion are compensated when absorbed during photosynthesis; furthermore, their use could reduce dependence on fossil fuels [36, 37]. The biomass is mainly composed of natural polymers like cellulose, hemicellulose and lignin [38]. It is available in a diverse array of forms and types: animal refuse, forestry, industrial and urban residues and agriculture waste [39]. Currently, there is a worldwide interest in biomass, which is focusing on the conversion of its fuel in the production of heat and electricity [40].

Potential of biomass to be used as an alternative to fossil fuels is mainly reduced by its low energy density, high costs associated with transportation and storage [41, 42], and disadvantages relating to characteristics of the raw biomass, such as high moisture content, hygroscopic behaviour and large particle size [43]. However, these disadvantages can be resolved by subjecting the raw biomass to thermal pretreatments, e.g. torrefaction and pyrolysis [39, 43]. During the torrefaction process, the biomass is heated at temperatures between 200°C and 300°C, at atmospheric conditions and in the absence of oxygen (O_2). Several pieces of research have reported that torrefied biomass has various advantages over the raw biomass, such as increased calorific, reduction in moisture content, hydrophobic behaviour, easy particle size reduction (milling), densification biomass and easy storage and transport [44–50]. Pyrolysis is defined as a thermal decomposition of biomass, when exposed to temperatures between 400°C and 800°C and in the absence of O_2. Depending on the operating conditions, it may favour the production of biochar (solid products), bio-oil (liquid products) and syngas (gaseous products). Bio-oil may be transported and stored more readily and may be used in different energy applications (boilers, furnaces, internal combustion engines, turbines) [51–54].

The literature has reported recent research on energy recovery from several waste (biomass) sources, derived from human consumption or food industries,

e.g. olive seeds [55–59]. Specifically, research on energy recovery of avocado seeds using torrefaction or pyrolysis has not been reported, considering that their seed is 10–13 % wt. of fresh fruit and is discarded after consumption [26]. The aim of this study is to investigate the potential of avocado seeds as a fuel, through thermochemical conversion of biomass using a rotary furnace under an inert atmosphere and at temperatures in the range of 150–900°C. Yields of solid, liquid and gas fractions for each experimental condition were determined gravimetrically, and furthermore the experimental results were discussed.

5.2 Methodology

Avocado (*P. americana* Mill.) seeds were supplied by a Spanish restaurant (Punto MX, Madrid). The biomass sample was ground by a knife mill (Retsch GM 200). The initial moisture content of sample was 51 % wt., and it was measured in a thermobalance (PCE-MB Series). The samples were oven dried for 24 h at 40°C to decrease their moisture content at values between 8 and 15 % wt. (ASTM E1756-08) for analysis by torrefaction or pyrolysis.

Torrefaction and pyrolysis experiments were performed in a rotary furnace (Fig. 10) by batch operation. The sample of biomass (150 g) was charged in the reactor vessel (a quartz cylinder with 470 mm L 150 mm ID) in each experiment. The rotation speed used was 3 rpm and the biomass was heated at a rate of 10°C/min from room temperature to a desired temperature (range from 150°C to 900°C) under a nitrogen flow rate of 0.2 L/min. The temperature in the reactor vessel was set using an electric furnace controlled by a PID controller. The residence time at the torrefaction or pyrolysis temperature was 15 min. Previously the system was purged with 0.2 L/min of preheated nitrogen for 15 min. Depending on the temperature at which the experiment was performed (torrefaction or pyrolysis),

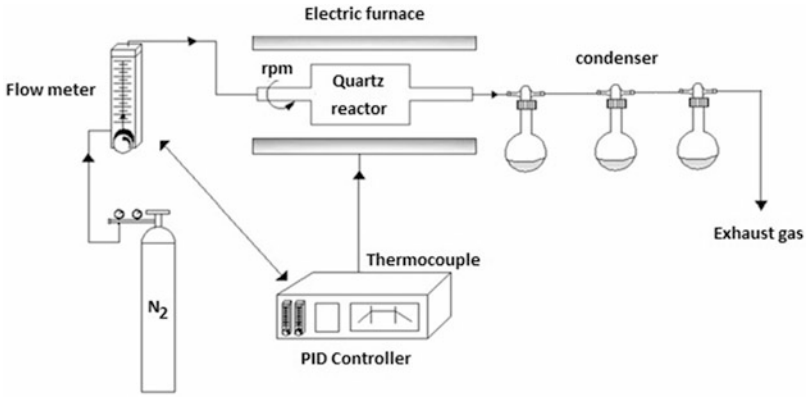

Fig. 10 Rotary furnace and experimental setup for the thermal treatment of avocado seeds

the resulting products were a gas, a liquid, and a solid. The liquid phase was collected into a glass flask placed in an ice-cooled condenser (cold trap). The exhausted solid phase was collected into the reactor. Yields of liquid and solid products were obtained gravimetrically, and yields of gaseous products were calculated by difference.

5.3 *Product Yields*

Figure 11 shows the product yields obtained during the torrefaction and pyrolysis of avocado seeds at different temperatures. The experimental results showed a gradual transformation of the original biomass into the different fractions: liquid, solid and gas.

The results show a reduction in the solid fraction yield with temperature as a result of progressive thermal degradation of the biomass. At temperatures between 150°C and 250°C, most of the condensable fraction is formed by water. In that temperature range, the biomass is subjected to drying and dehydration reactions. Thermal degradation of the polymeric constituents of the avocado seeds (mainly starch but also cellulose, lignin and hemicellulose) takes place primarily at temperatures between 250°C and 500°C, resulting in the formation of a condensable and a gas fraction. In that temperature range, the solid fraction yield is reduced from 90% to 25% wt. At temperatures above 500°C, product yields (solid, liquid and gas) remained relatively constant (21–24 % wt. approximately), which suggests completion of the thermal degradation process. Characterization of the chemical, physical and fuel properties of the resulting products is ongoing at present.

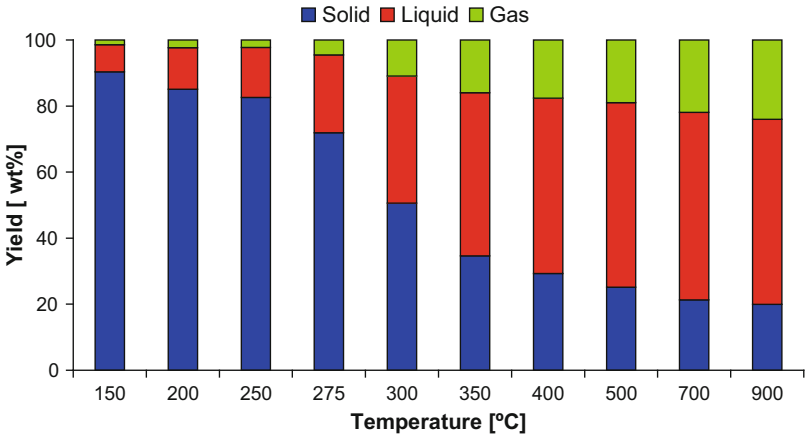

Fig. 11 Thermal treatment of avocado seed: effect of temperature on product yields

5.4 Conclusions

Preliminary results describe the thermal behaviour of avocado seeds during torrefaction and pyrolysis in a rotary kiln. Preliminary results suggest that there may be a commercial potential for large-scale production of charcoal and liquid fuels from avocado seeds by torrefaction and pyrolysis.

6 Densification Analysis of Avocado Seed

6.1 Description of Technology

One of the major drawbacks of biomass, when compared to fossil fuel, is its low energy density. Mechanical densification is a technology based on the use of pressure and mild temperatures to compact the biomass and, therefore, increase its density. There are two commercial products based on biomass densification: briquettes and pellets. According to Spanish standard UNE-EN_14961-1 = 2011 [60], briquettes have cylindrical or prismatic shape and a length between 50 and 400 mm (with diameters that usually range between 25 and 125 mm). Pellets have cylindrical shape, their length ranges between 3.15 and 50 mm and their diameters range between 6 and 25 mm.

The densification process that leads to the production of pellets is known as pelletization. Pressure, temperature, moisture content and the presence or absence of binders are the critical operation conditions [61]. This section studies the mechanical behaviour of pellets produced from different proportions of avocado seed and California pine (*Pinus radiata* D. Don) sawdust.

6.2 Methodology

The raw materials were ground and sieved to a particle size below 3.15 mm and dried to a moisture content of $10 \pm 0.3\%$. The pellets were produced in an experimental laboratory scale pelletizer. This device generates pellets by compacting biomass between two blunt needles made of steel in a cylindrical die provided with a heating jacket. Pressure, temperature and residence time can be controlled (Fig. 12).

The experimental conditions were as follows: die diameter, 8 mm; pressure, 919 bar; temperature, 80°C; and residence time, 3 min. Table 5 shows the pellets analysed in this trial with their respective mixing ratios [wt%] for avocado seed and pine sawdust. Total weight of each pellet was about 1 g. The results represent average values of triplicate values. The length and the diameter of the pellets were measured using a digital calliper. Weight was determined using a calibrated scale.

Fig. 12 Laboratory scale pelletizer

Table 5 Mixing ratios of pellets and identification name

Biomass		
Avocado seed (%)	Pine sawdust (%)	Identification code
0	100	0.A/100.P
10	90	10.A/90.P
30	70	30.A/70.P
50	50	50.A/50.P
70	30	70.A/30.P
90	10	90.A/10.P
100	0	100.A/0.P

Density was calculated considering the cylindrical shape of the pellets. Durability analyses were performed according to standard UNE-EN 15210-1 [62], by the determination of the remaining mass of pellets after mechanical stress.

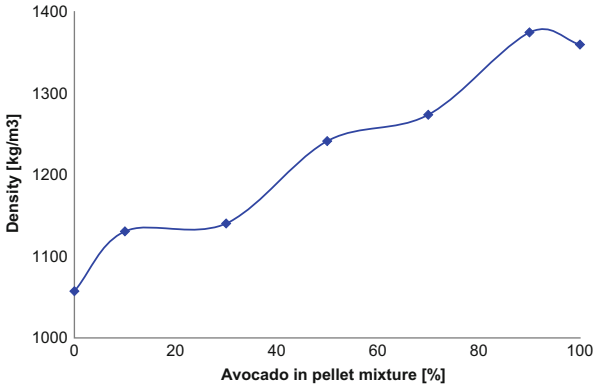

Fig. 13 Average densities of pellets produced from pinewood and avocado seeds

6.3 Results

6.3.1 Compaction Analysis

Average density of produced pellets is shown in Fig. 13. The results show that pellets produced from avocado seeds exhibited a higher mass density (1,378 kg/m^3) than those produced from pinewood (1,058 kg/m^3). A correlation between the avocado seed content in the pellet and its mass density was also observed. Lignocellulosic tissues are known to exhibit lower mass densities than starch.

6.3.2 Durability Analysis

Durability results in Fig. 14 show some degree of variability. The values suggest that pellets made of 100% avocado seed had less durability than all the other ones. On the other hand, a high percentage of avocado seed in the mixture (50–90%) seems to enhance durability. This effect could be a consequence of the binding properties of starch, which may only become clear when the biomass mixture contains a certain amount of lignocellulosic constituents. When seed percentage reaches 100%, those properties may not be enough to compensate the lack of rigid structures that woody tissues provide, and so, durability decreases. These structures (dead cell walls) may play the same role that corrugated steel rods inside reinforced concrete beams: providing them with better mechanical resistance. Further research is ongoing on this matter.

6.4 Conclusions

Results on densification and durability show that avocado pellets exhibit good densification but high fragility. Mixing avocado seed with a lignocellulosic biomass

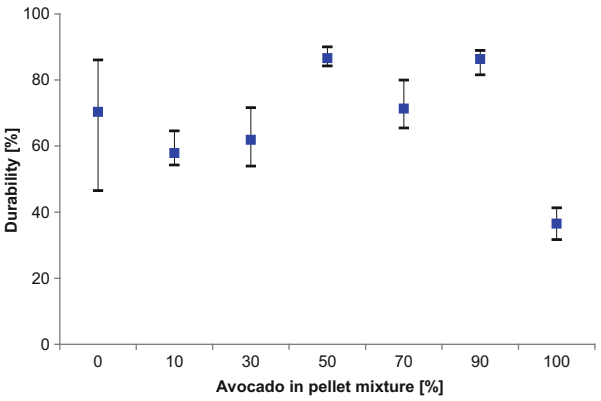

Fig. 14 Average durability of pellets produced from pinewood and avocado seeds

(pine sawdust) decreases pellet density but increases durability. If avocado seed pellets are intended to be used in industrial processes, further research is needed to optimize the mixing ratio and production conditions.

General Conclusions

- The concentration of starch in avocado seeds is significantly higher than in other plant seeds (like olive stone) which affects its use in energy applications.
- Avocado production is growing rapidly around the world with Mexico being the main producer and exporter and the USA the main importer. Hass is the variety most commercialized around the world.
- The pulp is the only part of the fruit that has commercial value while the rest of the fruit (peel, seed) is managed as a waste. Very little research has been conducted to evaluate the energy potential of avocado by-products (peel and seed).
- The experimental results show that incorporation of biomass (avocado seeds) into a porous media reactor operating with methane/air resulted in an increase in the concentration of syngas-related gases (H_2, CO) and also CO_2, primarily when operating at high gas fuel equivalence ratios.
- Regarding torrefaction and pyrolysis, preliminary results suggest that there may be a commercial potential for large-scale production of charcoal and liquid fuels from avocado seeds.
- Mixing avocado seed with a lignocellulosic biomass (pine sawdust) results in a reduction in the density of the resulting pellets but an increase in its durability, compared with avocado seeds.

In general, the size of the avocado market, the yield and quality of the by-products generated from the industrial transformation of avocados (mainly peel and seed) and the preliminary results obtained for energy valorization and densification of avocado seeds show a notable energy potential of this waste. Further research is necessary to produce conclusive results.

Acknowledgements The authors are grateful to the European Commission for financial support under Marie Curie Actions (Grant Agreement no 318927) and to Universidad Politécnica de Madrid for financial support under Project AL13-PID-16 for Research Activities with Latin America. We are also grateful to restaurant Punto MX (Madrid, Spain) and to Frumaco SL (Málaga, Spain) for provision of avocado seeds.

References

1. Seymour GB, Tucker GA (1993) Avocado. In: Seymour C, Taylor J, Tucker C (eds) Biochemistry of fruit ripening. Chapman & Hall, London. ISBN 0412 40830 9
2. Cowan AK, Wolstenholme BN (2003) Avocados. In: Caballero B, Finglas P, Trugo L (eds) Encyclopedia of food sciences and nutrition, 2nd edn. Elsevier Science Ltd
3. Arriola MC, Menchú JF (1979) The avocado. In: Inglett GE, Charalambous G (eds) Tropical foods: chemistry and nutrition, vol 2. Academic, New York
4. Donetti M (2011) Postharvest biochemical and physiological characterization of imported avocado fruit. Doctoral thesis, Cranfield University
5. Bernal JA, Díaz CA (2008) Generalidades del cultivo. In: Bernal JA, Díaz CA (eds) Tecnología para el cultivo del aguacate. Corporación Colombiana de Investigación Agropecuaria (Colombia). ISBN: 978-958-8311-74-6
6. Biale JB, Young RE (1971) The avocado pear. In: Hulme AC (ed) The biochemistry of fruits and their products. Academic, New York. ISBN 12-361202-0
7. USDA (United States Department of Agriculture) (2011) Avocado, almond, pistachio and walnut composition. Nutrient Data Laboratory. USDA national nutrient database for standard reference, Release 24. USDA, Washington
8. Tamayo A (2008) Nutrición y Fertilización. In: Bernal JA, Díaz CA (eds) Tecnología para el cultivo del aguacate. Corporación Colombiana de Investigación Agropecuaria (Colombia). ISBN: 978-958-8311-74-6
9. Córdoba OJ (2008) Arvenses. In: Bernal JA, Díaz CA (eds) Tecnología para el cultivo del aguacate. Corporación Colombiana de Investigación Agropecuaria (Colombia). ISBN: 978-958-8311-74-6
10. Londoño ME (2008) Insectos. In: Bernal JA, Díaz CA (eds) Tecnología para el cultivo del aguacate. Corporación Colombiana de Investigación Agropecuaria (Colombia). ISBN: 978-958-8311-74-6
11. Tamayo PJ (2008) Enfermedades y desórdenes abióticos. In: Bernal JA, Díaz CA (eds) Tecnología para el cultivo del aguacate. Corporación Colombiana de Investigación Agropecuaria (Colombia). ISBN: 978-958-8311-74-6
12. Sadir R (1972) Olio di avocado: tecnología dell' estrazione e industrializacione di revani. Rivista Italiana Delle Sostanze Grasse 49:90–93 [Cited by Bressani R, Rodas B, Ruiz AS (2006) La composición química, capacidad antioxidativa, y valor nutritivo de la semilla de variedades de aguacate. Final Report of the Project FODECYT 02-2006, Universidad del Valle (Guatemala)]
13. Bressani R, Rodas B, Ruiz AS (2006) La composición química, capacidad antioxidativa, y valor nutritivo de la semilla de variedades de aguacate. Final Report of the Project FODECYT 02-2006 (National Science and Technology Fund), Universidad del Valle (Guatemala)
14. Ozdemir F, Topuz A (2003) Changes in dry matter, oil content and fatty acids composition of avocado during harvesting time and post-harvesting ripening period. Food Chem 86:79–83
15. Meyer MD, Terry LA (2010) Fatty acid and sugar composition of avocado, cv. Hass, in response to treatment with an ethylene scavenger or 1-methylcyclopropene to extend storage life. Food Chem 121:1203–1210

16. Weatherby LS, Sorber DG (1931) Chemical composition of avocado seed. Ind Eng Chem 23 (12):1421–1423
17. Bora PS, Narain N, Rocha RVM, Paulo MQ (2001) Characterization of the oils from the pulp and seeds of avocado (cultivar: Fuerte) fruits. Grasas y Aceites 52(3–4):171–174
18. Soong Y-Y, Barlow PJ (2004) Antioxidant activity and phenolic content of selected fruit seeds. Food Chem 88:411–417
19. Jamieson G, Raymond W, Hann M (1928) Avocado oil: the composition and constants of a little-known pericarp oil. Oil Fat Ind 5:202–207
20. Werman MJ, Neeman I (1987) Avocado oil production and chemical characteristics. J Am Oil Chem Soc 64(2):229–232
21. Swisher HE (1988) Avocado oil from food use to skin care. J Am Oil Chem Soc 65(11):1702–1712
22. Cabrera G, Burbano JC, García JI (2011) Preliminary analysis of biomass potentially useful for producing biodiesel. Dyna 170:144–151. ISSN 0012-7353
23. Giraldo L, Moreno-Pirajᾶn JC (2012) Lipase supported on mesoporous materials as a catalyst in the synthesis of biodiesel from *Persea americana* Mill. oil. J Mol Catal B Enzym 77:32–38
24. Knothe G (2013) Avocado and olive oil methyl esters. Biomass Bioenergy 58:143–148
25. Rachimoellah HM, Resti DA, Zibbeni A, Susila DIW (2009) Production of biodiesel through transesterification of avocado (*Persea gratissima*) seed oil using base catalyst. Jurnal Teknik Mesin 11(2):85–90
26. Elizalde-González MP, Mattusch J et al (2007) Characterization of adsorbent materials prepared from avocado kernel seeds: natural, activated and carbonized forms. J Anal Appl Pyrolysis 78:185–193
27. Alvares L, Caetano M et al (2011) Phenol removal from aqueous solution by activated carbon produced from avocado kernel seeds. Chem Eng J 174:49–57
28. AEN/CTN 164 (2010) EN 14774-1:2010 Solid biofuels – determination of moisture content – oven dry method – part 1: total moisture – reference method
29. AEN/CTN 164 (2010) EN 15148:2009 Solid biofuels. Determination of the content of volatile matter
30. AEN/CTN 164 (2010) EN 14775:2009 Solid biofuels. Determination of ash content
31. Howell JR, Hall MJ, Ellzey JL (1996) Combustion of Hydrocarbon Fuels within Porous Inert Media. Prog Energy Combust Sci 22:121–145
32. Mujeebu MA, Abdullah MZ et al (2009) Applications of porous media combustion technology – a review. Appl Energy 86:1365–1375
33. Toledo M, Vergara E, Saveliev A (2011) Syngas production in hybrid filtration combustion. Int J Hydrogen Energy 36:3907–3912. doi:10.1016/j.ijhydene.2010.11.060
34. Toledo M, Utria K, Gonzalez F et al (2012) Hybrid filtration combustion of natural gas and coal. Int J Hydrogen Energy 37:6942–6948. doi:10.1016/j.ijhydene.2012.01.061
35. Gentillon P, Toledo M (2013) Hydrogen and syngas production from propane and polyethylene. Int J Hydrogen Energy 38:9223–9228. http://dx.doi.org/10.1016/j.ijhydene.2013.05.058
36. United Nations (1998) Kyoto protocol to the United Nations framework convention on climate change
37. Demirbas A (2005) Potential applications of renewable energy sources, biomass combustion problems in boiler power systems and combustion related environmental issues. Prog Energy Combust Sci 31(2):171–192
38. Wu Y, Zhao Z, Li H, He F (2009) Low temperature pyrolysis characteristics of major components of biomass. J Fuel Chem Technol 37(4):427–432
39. Părpăriţa E, Brebu M, Azhar Uddin M, Yanik J, Vasile C (2014) Pyrolysis behaviors of various biomasses. Polym Degrad Stab 100:1–9
40. Megaritis A, Yap D, Wyszynski ML (2007) Effect of water blending on bioethanol HCCI combustion with forced induction and residual gas trapping. Energy 32(12):2396–2400
41. Hamelinck CN, Suurs RAA, Faaij APC (2005) International bioenergy transport costs and energy balance. Biomass Bioenergy 29(2):114–134

42. Hamelinck CN, Faaij APC (2006) Production of advanced biofuels. Int Sugar J 108 (1287):168–175
43. Chen WH, Kuo PC (2011) Torrefaction and co-torrefaction characterization of hemicellulose, cellulose and lignin as well as torrefaction of some basic constituents in biomass. Energy 36 (2):803–811
44. Chen WH, Kuo PC (2010) A study on torrefaction of various biomass materials and its impact on lignocellulosic structure simulated by a thermogravimetry. Energy 35(6):2580–2586
45. Prins MJ, Ptasinski KJ, Janssen FJJG (2006) More efficient biomass gasification via torrefaction. Energy 31(15):3458–3470
46. Couhert C, Salvador S, Commandre JM (2009) Impact of torrefaction on syngas production from wood. Fuel 88(11):2286–2290
47. Prins MJ, Ptasinski KJ, Janssen FJJG (2006) Torrefaction of wood – part 1. Weight loss kinetics. J Anal Appl Pyrolysis 77(1):28–34
48. Prins MJ, Ptasinski KJ, Janssen FJJG (2006) Torrefaction of wood – part 2. Analysis of products. J Anal Appl Pyrolysis 77(1):35–40
49. Bridgeman TG, Jones JM, Shield I, Williams PT (2008) Torrefaction of reed canary grass, wheat straw and willow to enhance solid fuel qualities and combustion properties. Fuel 87 (6):844–856
50. Repellin V, Govin A, Rolland M, Guyonnet R (2010) Modelling anhydrous weight loss of wood chips during torrefaction in a pilot kiln. Biomass Bioenergy 34(5):602–609
51. Kaminsky W (1985) Thermal recycling of polymers. J Anal Appl Pyrolysis 8:439–448
52. Scott DS, Majerski P, Piskorz J, Radlein D (1999) A second look at fast pyrolysis of biomass – the RTI process. J Anal Appl Pyrolysis 51(1–2):23–37
53. Senneca O (2007) Kinetics of pyrolysis, combustion and gasification of three biomass fuels. Fuel Process Technol 88(1):87–97
54. Uslu A, Faaij APC, Bergman PCA (2008) Pre-treatment technologies, and their effect on international bioenergy supply chain logistics. Techno-economic evaluation of torrefaction, fast pyrolysis and pelletisation. Energy 33(8):1206–1223
55. Blanco MC, Blanco CG, Martínez A, Tascón JMD (2002) Composition of gases released during olive stones pyrolysis. J Anal Appl Pyrolysis 65(2):313–322
56. Jauhiainen J, Conesa JA, Font R, Martín-Gullón I (2004) Kinetics of the pyrolysis and combustion of olive oil solid waste. J Anal Appl Pyrolysis 72(1):9–15
57. Pattara C, Cappelletti GM, Cichelli A (2010) Recovery and use of olive stones: commodity, environmental and economic assessment. Renew Sustain Energy Rev 14(5):1484–1489
58. Rodríguez G, Lama A, Rodríguez R, Jiménez A, Guillén R, Fernández-Bolaños J (2008) Olive stone an attractive source of bioactive and valuable compounds. Bioresour Technol 99 (13):5261–5269
59. Zabaniotou AA, Kalogiannis G, Kappas E, Karabelas AJ (2000) Olive residues (cuttings and kernels) rapid pyrolysis product yields and kinetics. Biomass Bioenergy 18(5):411–420
60. Asociación Española de Normalización y Acreditación (AENOR) (2011) Biocombustibles Sólidos. Especificaciones y clases de combustibles. Parte 1: Requisitos generales (UNE-EN_14961-1 = 2011). In: AENOR (ed)
61. Kaliyan N, Morey RV (2009) Factors affecting strength and durability of densified biomass products. Biomass Bioenergy 33:337–59
62. Asociación Española de Normalización y Acreditación (AENOR) (2010) Determinación de la durabilidad mecánica de pélets y briquetas. Parte 1: Pélets (UNE-EN 15210-1). In: AENOR (ed)

Part IV
Socio-economy of Energy

Agency and Learning Relationships Against Energy-Efficiency Barriers

I. Martín-Rubio, A. Florence-Sandoval, and E. González-Sánchez

Abstract Despite the need for increased industrial energy efficiency, studies indicate that cost-efficient energy conservation measures are not always implemented, explained by the existence of energy efficiency barriers. The main objective of this chapter is to understand how to overcome energy efficiency barriers from a learning system perspective view after having a comprehensive insight of the agency relationship developed between stakeholders in this energy efficiency industry.

Nowadays, ESCOs (energy service companies) play an important role in promoting energy efficiency. ESCOs are constantly adding new measures to their projects that can be introduced in the energy performance contracting (EPC) to guarantee the savings of the project. Energy service companies are facing the energy efficiency barriers, specially the traditional market failures, through better communications of the elements included in energy performance contracting. In this process, ESCOs interact with financial institutions, customers, government, and other stakeholders.

Our framework clarifies the role of the different stakeholders in order to improve the funding, knowledge, competences, and values that are behind the barriers identified in the previous literature. It should be noted that our aim is not to criticize previous theoretical approaches but to present the community of practice as an instrument to characterize the interactions and learning of whole energy efficiency system.

I. Martín-Rubio (✉) and A. Florence-Sandoval
Departamento de Ingeniería de la Organización, AE y E, Escuela Técnica Superior de Ingeniería y Diseño Industrial ETSIDI, Universidad Politécnica de Madrid, Ronda de Valencia, 3, Madrid, Spain
e-mail: Irene.mrubio@upm.es; Antonio.florence.sandoval@upm.es

E. González-Sánchez
ANESE, Asociación de Empresas de Servicios Energéticos, Madrid, Spain
e-mail: egonzalez@anese.es

G. Lefebvre et al. (eds.), *Environment, Energy and Climate Change II: Energies from New Resources and the Climate Change*, Hdb Env Chem (2016) 34: 227–260,
DOI 10.1007/698_2014_305, © Springer International Publishing Switzerland 2014,
Published online: 25 December 2014

Keywords Agency relationship, Community of practice, Energy-efficiency barriers, Performance contracting

Contents

1 Introduction

Persistent barriers inhibit many cost-effective energy-efficiency projects and prevent the full development of this industry. It is widely discussed and recognized that the presence of certain barriers is the reason for the "energy-efficiency gap," a term coined by Jaffe and Stavins [1] to explain the "paradox of gradual diffusion of apparently cost-effective energy efficient technologies." The energy-efficiency gap is explained by the existence of barriers to energy efficiency, which inhibits the adoption of cleaner equipments and manufacturing experiences, as well as learning from the experience of other countries [2, 3].

In 1993 DeCanio presented the barriers within firms to energy-efficient investments. In thinking about why firms may not always behave optimally, he remembered that a firm is a collection of individuals, brought together under a complex set of contracts both written and unwritten, but that the firm itself is not an entity acting with a single mind. The behavior of the firm is the outcome of the interplay of the motivations of the individuals comprising it, the rules and conventions governing their interaction, and the environment within the firms operates. He found barriers in these interactions due to principal-agent problems.

Jaffe and Stavins [1] demonstrated that the necessary preconditions for identifying the right measure of the "energy-efficiency gap" include understanding and disentangling market failure and nonmarket failure for the gradual diffusion of energy-efficient technologies. They consider that the sources of potential market failure, that is, the availability of information to adopt new technology, arises the problem of principal-agent. Also, they found nonmarket failure explanations of the energy-efficiency gap based on the uncertainty about future energy prices and the actual savings from the use of energy optimizing technologies, combined with the irreversible nature of the efficiency investment. Finally, another way of

characterizing the energy-efficiency gap itself is to say that inertia exists in consumer's adoption behavior; this is not an explanation, but an additional characterization of the problem. They also showed market failure that does not bear on the paradox but which are relevant to policy debates about the energy-efficiency gap; these are the actual energy prices, discount rates, and environmental consequences.

Weber [3] proposed a methodological background to introduce the concept of barrier models (for energy efficiency) in which three specific features were addressed. The three features were the objective obstacle, the subject hindered, and the action hindered.

DeCanio [4] explored this paradox with data from one of the US Environmental Protection Agency's voluntary pollution prevention programs. He has indicated that a strong empirical anomaly stands at the center of the study of the economics of energy efficiency. For both firms and consumers, there is abundant evidence that highly profitable energy-saving opportunities exist, yet the technologies embodying these opportunities have not spread universally throughout the economy. He found that both economic and organizational factors account for some of the variation in observed returns to these investments, but the results suggest a need for improved and more comprehensive theories of the investment behavior of firms and other organizations.

Later, data from different countries enables this paradox to be explored statistically (e.g., [5–10]). Both economic and organizational factors account for some of the variation in observed returns to these investments, but the results suggest a need for improved and more comprehensive theories of the investment behavior of firms and other organizations.

Chai and Yeo [11] indicated that empirical evidence of barriers to the adoption of energy-efficient technologies has been widely reported in the literature and they proposed a system thinking perspective to barrier analysis by considering interactions between the barriers taking into account stakeholders and government policies.

In this work, we try to go further by considering the relationships among different stakeholders and the energy-efficiency barriers through the lens of agency theory. Agency theory is concerned with resolving the problems that occur in agency relationships. When information and knowledge is moved, the agency relationship evolves.

The principal-agent model, as applied in such disciplines as sociology, political science, and political administration, is in essence a theory about contractual relationships between buyers and sellers [12]. In its simplest form, agency theory assumes that social life is a series of contracts. Conventionally, one member the "buyer" of goods or services is designated the "principal," and the other, who provides the goods or service is the "agent"—hence termed "agency theory." The principal-agent relationship is governed by a contract specifying what the agent should do and what the principal must do in return [13]. A common application in economics is the market for professional services. Assuming that both principal and agent are rational utility maximizers, they are likely to have different goals. In short, an information asymmetry exists, with an advantage to the agent. Principals

seek to manipulate and mold the behavior of agents so that they will act in a manner consistent with the principals' preferences. The contractual arrangement is one tool for accomplishing this goal.

The companies engaged in developing, installing, and financing performance-based projects are the energy service companies (ESCOs). ESCOs are seen as important vehicle for promoting energy efficiency around the world. Persistent barriers inhibit many cost-effective energy-efficiency projects and prevent the full development of the ESCO industry internationally. Vine [14] examined the ESCO activity internationally in 38 countries outside the USA in 2002 with a survey collecting information about the number of ESCOs, the key sectors targeted by ESCOs, and the four most important barriers facing the ESCO industry.

In the marketplace, an ESCO is an agent that perform a service to another company or user called principal. They have different goals and/or preferences. Obviously, agents want to make as much money as possible, while principals want to pay as little as possible for services. The contractual arrangement between ESCO company and its client is the EPC "energy performance contracting" that can guarantee the results and energy savings.

It is important to create more information for the actors implicated in the ESCO projects. A critical factor in the success of ESCOs is the ability to demonstrate successful applications of the ESCO concept [14]. Gluch et al. [15] found that within the field of sustainable development, collaborative and interdisciplinary actions are imperative for the development and implementation of proactive, holistic renovation solutions. They try to understand how knowledge sharing between different professional groups and practice may be facilitated, in this case, between various research organizations, municipal housing companies, energy suppliers, and various research organizations. Specific focus has been on identifying mechanism for interaction and knowledge sharing between actors (stakeholders) that normally do not meet in their everyday practice. Gluch et al. [15] introduce elements of community of practice (CoP) perspective in the development and innovation for low-energy housing. CoPs are individuals actively engaged in an arena of concern (domain) that form a community focused on growing the knowledge of the domain through group meaning-making in a situated practice [16]. Relevant collective practice [16, 17] suggests it is fruitful to look where are distinct fields of knowledge. In order to improve agency relationships it is relevant to understand how information flows and is interpreted in the principal-agent relationship.

The interaction among different stakeholders when facing energy-efficiency barriers is needed to be studied deeply. Agency theory is the start point to understand the problems of information asymmetry and goal conflict. We try to go a step further and present a CoP to develop the EPC needed in the society for developing energy-efficiency programs.

In this chapter, we complement agency theory with CoP theory to capture the greater complexity of agency relationships evolution. We explore agency relationships and organizational behavior topics that relate to information asymmetry in cooperative situations.

In this work, we contribute to understand the contract relationships ESCOs develop in a complex environment full of energy-efficiency barriers. First, we summarize the most relevant perspectives in energy-efficiency barriers and suggest that information asymmetry is the key barrier in the relationships in this industry. Second, we review the different stakeholders that interact in energy-efficiency industry. Third, we propose agency theory to understand the relationships, and, finally, we suggest communities of practice as learning perspective to move knowledge and foster collaboration in this industry. Finally, we conclude with a focus on lessons learned to improve EPC projects.

2 Theoretical Background: Energy-Efficiency Barriers, Agency Relationships Between Stakeholders, and Learning Perspective

Discussion of the energy-efficiency gap builds on the assumption that there are technologies, methods, or processes that may reduce energy use in an industry, but that barriers hinder the implementation. If industrial actors would only act rationally, this gap would not exist. It is needed not only an economic perspective to understand these barriers but also a sociotechnical perspective to have a better comprehensive approach of these barriers in order to understand the implementation process of new energy-efficiency measures.

There are different approaches to barrier analysis among the aforementioned studies in the introduction. In the early years, barriers to energy efficiency were often explained using theories from the mainstream economics. The energy-efficiency gap was largely attributed to market failures. Commonly reported market failures include information problems and unpriced energy costs (split incentives). However, market failures can only account for part of the energy-efficiency gap. Increasingly, energy efficiency is a multifaceted topic entailing technical, economic, and organizational challenges.

Later, researchers in other disciplines have also taken an interest in energy efficiency. Owens and Driffill [18] and Stephenson et al. [19] argued that behavioral and attitude changes to energy consumption contribute to energy efficiency. These perspectives largely discuss social barriers to technology adoption and innovation diffusion [20, 21]. Palm and Thollander [8] highlighted the interdisciplinary nature of energy efficiency and investigated the effects of social networks and regimes on energy-efficient technology diffusions.

Collectively, previous studies have identified a somewhat comprehensive list of barriers to adoption of energy efficient. However, there is no consensus on which barriers are the most important [11]. Perhaps more importantly, it is unclear whether overcoming the most significant barriers will automatically lead to better energy-efficiency adoption, especially if the barriers are interconnected. It is needed to understand the relationships and interactions among stakeholders when they

implement energy-efficiency projects. Agency theory is concerned with resolving the problems that occur in agency relationships.

The agency theory paradigm, first formulated in the academic economics literature in the early 1970s [12, 22], has diffused into the business and management literature by the 1990s, representing a new zeitgeist and becoming the dominant institutional logic of corporate governance [23]. However, Mitnick [24] said that agency is simply a general social theory of relationships of "acting for" or control in complex systems. Classical agency theory misunderstands not only the source of goal conflict but also the social conditions that inflame it. The sociology of professions provides a window on agency as expertise, problems of asymmetric information, and one kind for delivering agency services [25].

Given the multidisciplinary nature of energy efficiency, it is not surprising that researchers with different backgrounds, ranging from ecology to economics, have engaged in this line of research. Due to this, advice on how to promote energy efficiency differs depending on the adopted perspective. Despite the myriad of studies, there remains no consensus on which barriers are the most important. The attempt to classify barriers into different categories, while interesting, reveals nothing new on the nature of these barriers.

However, market failures can only account for part of the energy-efficiency gap. Increasingly, analysts as well as policy-makers are seeing industrial energy efficiency as a multifaceted topic entailing technical, economic, and organizational challenges that arise from information asymmetry and incentives.

Agency theory is concerned with resolving two problems that can occur in agency relationships. The first is the agency problem that arises when (a) the desires or goals of the principal and agent conflict and second (b) it is difficult or expensive for the principal to verify what the agent is actually doing. The problem here is that the principal cannot verify that the agent has behaved appropriately. The second is the problem of risk sharing that arises when the principal and agent have different attitudes toward risk. The problem here is that the principal and the agent may prefer different actions because of the different risk preferences [26].

The agency structure is applicable in a variety of settings, ranging from macrolevel issues such as regulatory policy to microlevel dyad phenomena such as impression management, lying, and other expressions of self-interest. Most frequently, agency theory has been applied to organizational phenomena. Overall, the domain of agency theory is relationships that mirror the agency structure of a principal and an agent in cooperative behavior, but have different goals and different attitudes toward risk.

2.1 Energy-Efficiency Barriers

There is a large body of literature on the nature of barriers to energy efficiency, which draws on overlapping concepts from neoclassical economics, institutional economics (principal-agency theory), behavioral economics, sociology, and

Table 1 A review of relevant references on energy-efficiency barriers

Relevant references	Perspective	Barriers	Theories
DeCanio [2, 4] "efficiency paradox"	Economic: financial aspects	Financial aspects Discount rate Energy price	Economic Theory Optimization Agency Theory
	Organizational	Shortsightedness of management Human capital Corporate culture Incentives Agency, incentives, and information	
Jaffe and Stavins [1] "energy-efficiency gap"	Economic: technology, financial, and end-user markets	Market failure: information and principal-agent problems Market failure that does not affect the gap: Energy prices, environmental consequences, discount rate	Technology Difussion model Economic Theory Optimization Agency Theory
Paradox of gradual diffusion of energy-efficiency technologies		Nonmarket failure: uncertainty and cost of adoption new technologies	
Weber [3]	Methodology of barrier models: organizational, behavioral and institutional	Objective obstacle Subject hindered Action hindered	Organizational & Institutional Theory
Vine [14]	Key barriers to end users (ESCO industry)	Financing Perception of risk Information/awareness (knowledge) EPC expertise Access to energy-efficiency equipment and technology Reliability Trust and credibility	Stakeholders: ESCOs Economic and Organizational Theory
	Key policy barriers for promoting ESCO industry	Lack of governmental policy on ESCO industry Low cost of energy Lack of budgeting and standardized public procedures for ESCO services Large economic and potential uncertainty Conflicts with other government policies No existing legal framework for protecting the interests of EPC participants	

(continued)

Table 1 (continued)

Relevant references	Perspective	Barriers	Theories
Rohdin et al. [6]	Economic	Hidden cost, access to capital, risk, heterogeneity, imperfect information, principal-agent relationships, adverse selection, split incentives	Economic Theory
	Behavioral	Bounded rationality, inertia, credibility and trust, form of information, values	Agency theory
	Organizational	Culture and power	Psychology and Organizational Theory
Sardianou [9]	Economic	Financial and market barriers Limited access to capital Cost of energy conservation measures Return of investments Investment on training of employees High transaction costs Uncertainty about energy prices Lack of information with regard to the profitability of energy saving measures Limited investment action	Economic Theory
	Organizational	Organizational and human factors Lack of know-how Lack of skilled technical personnel Focus on operative problems Difficulties with training of employees on energy measures Bureaucratic procedures to get financial support	Organizational Theory

(continued)

Table 1 (continued)

Relevant references	Perspective	Barriers	Theories
Sorrel et al. [27], Schleich [28]	Economic	Imperfect Information Hidden costs Access to capital Split incentives and appropriability Bounded rationality	Economic Theory
Palm and Thollander [8]	Economic	Imperfect and asymmetric information, hidden cost, risk Possible for performance of equipment (technical risk) Lack of budget funding	Interdisciplinary Perspective: Economic and Organizational Social Networks and Collaboration/Knowledge Management
	Behavioral	Inability to process information, form of information, trust, inertia, lack of awareness	
	Organizational	Energy managers lack power and influence Organizational culture leads to neglect of energy environmental issues Goals, routines, culture, power Lack of technical skills	
Fleiter et al. [29]	Economic: energy demand	Activity parameters: value-added, physical production. Technology stock Demand for end users/ energy services (useful energy) Energy-efficiency technologies Demand for final energy	Bottom-up model Accounting models Optimization to model energy supply and energy demand

(continued)

Table 1 (continued)

Relevant references	Perspective	Barriers	Theories
Chai and Yeo [11]	Economic nonmarket failure or market barriers	Low priority of energy issues Cost of production disruption Other priorities for capital investments Lack of investment capability Lack of funding/financing capability Lack of management support Capital market barriers Cost of energy Cost of identifying opportunities	Economic & Organizational Theory Technology Difusion Model
	Economic market failure	Split incentives Unpriced costs and benefits Insufficient and inaccurate information Lack of expertise in technology and management Difficulties in obtaining information Lack of technical skills Lack of trained manpower	
	Behavioral and organizational	Lack of information on profitability Lack of information about opportunities Resistance to change Lack of sense of corporate social responsibility Lack of incentives Lack of environmental policies in companies Energy managers lack influences	
	Physical constraints	Inappropriate technology at site Inappropriate industrial framework	

psychology [1, 9, 27]. It should be considered also a sociotechnical approach to understand the implementation of energy-efficiency measures in their context [8].

Barrier models describe the non-implementation of cost-effective energy-efficiency investment and specify three pertinent features of the non-implementation [3], that is, the objective obstacle, the subject hindered, and action hindered. Weber established the methodological question to ask when formulating a barrier model:

What is the obstacle, whom does it affect, and what aspect of energy conservation does it affect? Barriers to energy efficiency may be divided into three broad perspectives, namely, economic, organizational, and behavioral barriers as we see in Table 1.

Chai and Yeo [11] see an increasing number of other social sciences perspectives on barriers to industrial energy that largely discusses social barriers to technology adoption and innovation diffusion [11]. For instance, Owens and Driffill [18] and Stephenson et al. [19] argued that behavioral and attitude changes to energy consumption contribute to energy efficiency. Similar and newer perspectives on identifying and creating sociotechnical perspectives have also been introduced [6, 9, 20, 21]. Palm and Thollander [8] highlighted the effects of social networks and regimes on energy-efficient technology diffusions. They emphasized the need for analysts to steer away from traditional approaches to barrier analysis.

2.1.1 Economic Barriers: Market Failures and Financial Barriers

There may be a host of financial, economic, and market factors that could prevent an industrial firm from immediately investing in energy-saving technologies, thus resulting in "energy-efficient gap." Limited access to capital may prevent energy-efficiency measures from being implemented [1, 2].

The energy-efficiency gap was largely attributed to market failures, which occur due to flaws in the way markets operate. Mainstream economist argued that an imperfect market is a major source for slow adoption of energy-efficiency technologies and suboptimal energy-efficiency investment. Commonly reported market failures include information problems and unpriced energy costs.

Information problems include lack of information, asymmetric information, and the principal-agent problem for the control of the energy-efficiency program. DeCanio [4] and Jaffe and Stavins [1] introduced the relevance of agency problems in the study of energy-efficiency barriers.

Asymmetric information problems occur when one party involved in a transaction has more information than the other, which may lead to suboptimal energy-efficiency decisions. The fact that energy efficiency cannot be observed further intensifies this asymmetric information barrier.

Financial economists also believe that a correctly priced energy cost would spur energy efficiency almost automatically. Mechanisms that try to incorporate negative externalities into energy prices include practices such as domestic carbon trading. Such schemes increase the business operating costs of the companies. Furthermore, managers are more concerned about initial costs rather than annual savings when deciding to invest in an energy program.

However, market failures can only account for part of the energy-efficiency gap. Increasingly, analysts as well as policy-makers are seeing industrial energy efficiency as multifaceted topic entailing technical, economic, and organizational challenges. Typically, barriers are identified, classified, and discussed according to their nature [6]. In addition UNEP [30] classify barriers into areas of

management, information, knowledge, and financing and governing policy. Based on these classifications, suggestions may be offered on possible remedies to overcome these barriers.

While analysts such as Nagesha and Balachandra [31] and Rohdin et al. [6] concluded that financial barriers are the most significant barriers, others have identified production risk and information barriers as the most significant barriers [29]. Perhaps more importantly, it is unclear whether overcoming the most significant barriers will automatically lead to better energy-efficiency adoption, especially if the barriers are interconnected.

Another point in the literature is the perceived risk of energy-saving investments. The uncertainty about future energy prices, especially in the short term, and the slow rate of return of investments often seem to lead to higher perceived risks and therefore to more stringent investment criteria and a higher rate (Sardianou [9]). Jaffe and Stavins [1] reviewed market failures and market barriers for suggesting notions of economic potential and social optimum of energy efficiency.

2.1.2 Implementation Barriers: Organization and Behavioral Perspective

In recent years, researchers in other disciplines have also taken an interest in energy efficiency. In particular, we see an increasing number of other social science perspectives on barriers to industrial energy that largely discusses social barriers to technology adoption and innovation diffusion.

Owens and Driffill [18] and Stephenson et al. [19] argued that behavioral and attitude changes to energy consumption contribute to energy efficiency.

Palm and Thollander [8] highlighted the interdisciplinary nature of energy efficiency and investigated the effects of social networks and regimes on energy-efficient technology diffusions. They emphasized the need for analysts to steer away from traditional approach to barrier analysis and found that researcher are adopting a more inclusive and open approach by conducting interviews and surveys (questionnaires) and performing case studies to identify barriers.

Some researchers have also attempted to identify the most significant barrier in their respective areas of study. These studies are contingent, that is, the degree of importance of the barriers is applicable only at the place and time at which the survey was conducted, and therefore the findings may not be applicable to other countries and/or industrial sectors. Nevertheless, the list of identified barriers remains fairly similar despite the different rankings and classifications by different analysis.

The behavioral barriers include bounded rationality, inertia, credibility and trust, forms of information, and values [6]. Palm and Thollander [8] combine engineering and social science approach to enhance our understanding of industrial energy efficiency. They show that actors in different industrial sectors highlight different barriers to energy efficiency and that the identified classical economic barriers can be problematized in relation to the social context to understand their existence and how to resolve them. Their analysis indicates that different sectors of rather closed

communities have established their own tacit knowledge, perceived truths, and routines concerning energy-efficiency measures. According to this perspective, energy efficiency depends on social relationships and discussions, negotiations, and agreements developed in actor networks. One outcome of this perspective is that energy-saving measures in one sociocultural domain may be useless in another. Experiences, routines, and habit established and negotiated in a particular network will then determine what energy-efficiency measures will be implemented. The perception barriers according to some values, as outlined by social science researchers, should not be neglected and should be emphasized in energy-efficiency research. Credibility and trust in the information provider is of utmost importance if information regarding energy-efficiency investments is to be accepted. In order for information to be accepted, it should also be vivid, personal, simple, and specific.

Schleich [28] identify the culture barrier and the presence of empowered manager to face energy-efficiency strategy. These findings suggested that organizational failures are not easily solved through governmental energy policy activities like energy information campaigns. Organizations need to start looking their embedded values and managerial competences to be able to challenge these barriers. A start for doing this is mapping energy performance figures in the company's annual report. By stating the extent of cost-effective potential measures available at a company in the annual report, as well as other energy figures, it could empower energy management. He found also that in many industrial firms, there is often a shortage of trained and capable technical personnel. The lack of skilled personnel leads to difficulties with respect to installation of new, energy-efficient equipment.

Focusing barriers on the organizational level could throw new light on why energy-efficient technology is not implemented, even if it can be both economically and technologically rational for the organization to do so. Decisions how firms use energy and energy efficiency are made in organizational contexts.

The fact that managers do not consider energy efficiency as a "core" business activity can be found in some sectors as food and drink industries as Sardianou [9] found in his study in Greece—he found an opposite pattern in metal sector. A review of studies on barriers to energy efficiency shows that country-specific, region-specific, and theoretical economic studies have been conducted.

Vine [14] studied the barriers to the development of an ESCO industry in countries outside the USA. He found several barriers are common:

- Projects compete with more traditional investments such as small power plants and industrial expansion.
- Energy-efficiency projects and EPC are perceived to be more risky than supply side projects because they are often non-asset-based investments.
- Many energy-efficiency projects and ventures are too small to attract the attention of large multilateral financial institutions.
- The legal and regulatory frameworks are not compatible with energy-efficiency investments, particularly EPC. In particular, measurement and verification protocols for assuring performance guarantees are not understood.
- Few in-country financial institutions have experience financing energy-efficiency projects or ventures, especially through ESCOs.

– Utility companies' negative response to ESCOs for fear of decreased revenues.
– Lack of government support for EPC, especially in residential sector where local banks and private investors are reluctant to participate.

Researchers as Rohdin et al. [6] have adopted a more inclusive and open system approach by conducting interviews and surveys and performing case studies to identify barriers presented in the industrial sector. In recent years, we find two aspects:

1. Lack of confidence in government-sponsored energy audit but high trust in information and energy strategies sponsored by associations and colleagues. When colleagues are used as a source of information, energy efficiency tends to prevail; another way is through seminars and conferences. Actors from different companies and sectors meet and discuss energy efficiency from different perspectives [8].
2. Typically, barriers are identified, classified, and discussed according to their nature. Nonetheless, the list of identified barriers remains fairly similar despite the different rankings and classifications by different analysts.

Credibility and trust in the information provider is of utmost importance if information regarding energy-efficiency investments is to be accepted. In order for information to be accepted, it should be vivid, personal, and specific. Rohdin et al. [6] specify the top four sources of information are related to more personal conditions as colleagues: colleagues within sector, staff of associations related to associations, consultants performing energy audits and seminars.

Transparense report [55] concludes that the main barriers for the EPC business in Europe are the following: regulatory (lack of support from the government, subsidy, and policy uncertainty), structural (lack of trust in ESCO industry and lack of information), and financial (financial crisis and raising affordable finance). The main drivers are increasing energy prices and pressure to reduce costs. The 20 countries involved in Transparense project are at different stages of development of their EPC market. For the benefit of this project, it was recognized at the start that each country may have different needs, expectations, and characteristics depending on the level of advancement of its EPC industry. The results from the Transparense survey at EU-wide level make it clear that the energy policies from individual European governments are mostly seen as ineffective.

Researchers as Fleiter et al. [29] provide an overview of the current status of bottom-up models for industrial energy demand, with special focus on their capability to model barriers to the adoption of energy-efficient technologies. The state-of-the-art bottom-up model is based on an explicit representation of the technology stock and considers the costs of energy-efficiency options in detail. But with regard to barriers, most models only make use of an adjusted discount rate. They consider technology costs and energy prices in bottom-up models. Bottom-up models are traditionally based on a detailed representation of energy end uses. The evolution of the end uses and of their energy efficiency over time determines the future energy demand. Some bottom-up models determines the future energy demand. They explicitly model firm's investment decisions by applying a three-phase decision

model that breaks down the technology adoption into a knowledge phase, an economic evaluation phase, and an implementation phase. All phases are influenced by barriers.

A key determinant of the market diffusion of new energy-efficient projects is the technology adoption behavior of firms. As we have seen, barriers can be very different in nature, varying from the availability of information or capacity within firms, to dealing with risk and how it is perceived, to firm internal processes or the availability of financial resources.

2.2 Stakeholders

Discussion of the energy-efficiency gap builds on the assumption that there are technologies, methods, or processes that may reduce energy use in industry, but energy-efficiency barriers hinder their implementation. If actors would only act rationally, this gap would not exist. If we want to understand barriers and information asymmetry, we need to understand the role of every stakeholder in its social and institutional context. Palm and Thollander [8] suggest that energy efficiency depends on social relationships and discussions, negotiations, and agreements developed in actor networks.

After reviewing the major energy-efficiency barriers, now we present the role of stakeholders that improve the energy-efficiency system.

2.2.1 Government

Governments can help to overcome behavioral and implementation barriers through regulation of standard protocol for energy-efficiency management. One criticism of energy policies and programs is that technological advances and rising energy prices will cause energy-efficiency measures to be implemented in any case, even without government intervention [32].

Depending on the country's culture and legal tradition, the extent of regulation and legislation measures varies. Chai and Yeo [11] review now policies which aim to promote energy efficiency:

- Energy Acts. Japan has a history of strong legal tradition since Japan's Energy Conservation Act of 1979 under which an energy-efficiency program took place. European Union's Treaty of Lisbon places energy at the heart of European activity (An Energy Policy for Europe). It effectively gives it a new legal basis which it lacked in the previous treaties. Based on this, specific Directives such as 2010/31 [33] and 2012/27 [34] have been delivered on the subject energy efficiency. Beside this framework, some European Union countries like the UK also experienced some success with industrial energy regulatory policies. Industrial regulations and legislation programs include minimum efficiency standards for common equipment such as air compressors and combined heat

and power plants, mandatory energy audits, and factory energy conservation plans.

- Voluntary Agreements. More countries (e.g., Netherlands and Germany) took to voluntary agreements and fiscal measures to stimulate industrial energy-efficiency improvements. Voluntary measures have been more popular with governments because, compared with regulations, voluntary measures have fewer negative impacts on industrial competitiveness. The details and rigors of voluntary agreements differ in different countries, but generally, they are complemented by fiscal measures such as tax incentives, subsidies or exemptions, and investment grants [35].
- Fiscal Measures. Although fiscal measures alone already provide some form of motivation for organizations to adopt energy-efficiency technology, voluntary agreements create and increased awareness about the available government financial incentives.
- Educational and Informative Programs Are also Commonly Implemented. For example, energy labeling program serves to inform consumers about the energy consumption of equipment and buildings.
- Energy-Efficiency Financing Evolution. A relatively new development in the arena of energy-efficiency measures is energy-efficiency financing where organizations (borrowers) can obtain financial support from ESCOs themselves or from a third-party financer such as large commercial banks and international financial institutions like the World Bank. The financial support occurs in a manner that allows the borrower to repay the lender from the energy savings.

  International Standards. The first relevant effort in supranational standardization in energy efficiency could be the EN 16001:2009 *Energy management systems. Requirements with guidance for use* developed by the European Committee for Standardization (CEN). In April 2007, a United Nations Industrial Development Organization (UNIDO) stakeholders meeting decided to ask ISO to develop an international energy management standard. Therefore, ISO 50001:2011 *Energy management systems—Requirements with guidance for use* was published on June 17, 2011, being internationally accepted as reference standard.

Clearly, various policies have been deployed in order to promote energy efficiency over the years in many countries. However, there is no established advice or theory on when and what policies should be applied. The disparity between promise and actual progress suggests that there is an urgent need to develop a framework which links these policies together.

2.2.2 Industrial Organizations: The Role Energy Managers of Companies

Industrial organizations often pursue energy efficiency to reduce costs and display corporate social responsibility. Seeking help from technical consultants and

appointing energy managers are ways to reduce behavioral and implementation barriers in organizations.

Energy managers of companies are important stakeholders for the promotion of ESCOs. These professional and qualified individuals should be familiar with the service and capabilities offered by ESCOs and should be able to rely on them for implementing projects in their company [14].

2.2.3 Customers

Customers are the reason for a company's existence. Their demands will direct the company's market and developmental policies. As far as green clients increase, it will increase the motivation for energy efficiency.

It is crucial the interaction between energy end users and energy experts. Energy end users rarely see the world in the same way as energy experts. Thus, getting to know the end users and their context and finding the best ways to interact with them are key issues for energy-efficiency practitioners [36].

2.2.4 Research and Academic Institutions also Play a Part in the Energy-Efficiency System

They develop new energy-efficiency products and review the whole system from different points of views, as this paper show.

2.2.5 Financial Institutions

Banks and financial institutes provide credit if they rely on the way the whole system operate. It is important how they consider their involvement in the EPC together with ESCOs in supporting the financing for long-term projects. This is especially relevant when there is a shortage of credit in the country, as it is the case of Spain.

2.2.6 ESCOs and EPC: The Role of General Manager, Energy Auditor, and Employees

An ESCO is a company that provides energy efficiency-related and other value-added service and for which performance contracting is a core part of its energy-efficiency service business [37,38]. This definition is in line with the European Commission Directive (2006/32/EC) on energy end-use efficiency and energy services (ESD) standard definition of an ESCO [39].

The ESCO industry has consolidated in the developed world since 2000. Utility companies abandoned the business as deregulation stalled, and about 80% of the

total EPC business is conducted by ESCO subsidiaries of large companies, primarily equipment manufacturers, and the rest are small companies [40]. The European market for EPC is very heterogeneous. Some countries have well-developed markets with several large ESCOs acting in it. Other countries are at a very early stage of development, and some can be characterized as emerging markets [41].

Among the three major energy-consuming sectors in the economy (i.e., transportation, industry, and buildings), ESCOs have been the most active in the buildings sector. Among nonresidential customers, ESCOs have had most success in developing projects in public and institutional markets—federal, state, and local government facilities, schools, universities, and hospitals. Customers in the institutional sector tend to manage their own facilities and are often subject to legislative or executive energy mandates. ESCOs are also active in the commercial and industrial sectors but have more limited access in penetrating these markets. Relatively few ESCOs operate in the residential market; these ESCOs that are active in this market typically target larger multifamily and public housing facilities. Other types of energy service providers including equipment and controls manufacturers, engineering and construction firms, various types of contractors (heating and air conditioning, controls, windows, lighting, and insulation specialists), and energy consulting firms also provide efficiency services to residential, commercial, and industrial customers. The "MUSH" markets—municipal and state governments, universities and colleagues, and schools and hospitals—have historically hosted the large share of US ESCO projects [41].

The number of ESCOs varies in each country. One of the most important steps a country can take to promote the ESCO industry in their country is to establish an association of ESCOs. In 2005, over a dozen countries have created ESCO association [14]. The associations often are created with a few members initially, but they grow in size as the association develops. The ESCO industry has evolved significantly over the last decade. The next decade will engender more change.

ESCOs can guarantee the results and take on the performance risk, funding the improvements from the savings they deliver. This solution is termed "EPC," and while it has been implemented with great success in a number of EU member states, based on this success, it is currently gaining great interest and traction across the world. Public authorities are using EPC since more than 20 years. The EPC financed retrofitting of public buildings started in North America. Meanwhile EPC projects have become common also in the European Union. Thousands of public buildings, universities, and schools have been modernized thanks to EPC. And the number of success stories in private sector is continuing to increase.

In an EPC, an ESCO can provide the full range of services required to complete the project, including energy audit, design engineering, construction management, arrangement of long-term project financing, commissioning, operations and maintenance, savings, and monitoring and verification (M&V).

EPC management process consists of a four-stage process: preliminary study, detailed analysis, implementation, and guarantee phase. EPC is a turnkey service, sometime compared to design/build construction contracting which provides customers with a comprehensive set of energy efficiency, renewable energy, and

distributed generation measures and often is accompanied with guarantees that the saving produced by a project will be sufficient to finance the full cost of the project [40]. A typical EPC project is delivered by an ESCO and consists of the following elements:

1. Turnkey Service: The ESCO provides all of the services required to design and implement a comprehensive project at the customer facility, from the initial energy audit through long-term monitoring and verification (M&V) of project savings. In an EPC, an ESCO can provide the full range of services required to complete the project, including energy audit, design engineering, construction management, arrangement of long-term project financing, commissioning, operations and maintenance, and savings M&V.
2. Comprehensive Measures: The ESCO tailors a comprehensive set of measures to fit the needs of a particular facility and can include energy efficiency, renewable, distributed generation, water conservation, lighting, building envelopment improvements (insulation, roofs, windows, etc.), and sustainable materials and operations.
3. Project Financing: The ESCO arranges for long-term project financing that is provided by a third-party financing company. In the early days of EPC, ESCOs typically provided both project technical services and project financing, because financial institutions did not understand EPC and were unwilling to finance EPC projects. The main feature is the financing of the investments via the guaranteed cost savings achieved through improved energy efficiency within the terms of contract.
4. Project Savings Guarantee: The ESCO provides a guarantee that the savings produced by the project will be sufficient to cover the cost of project financing for the life of the project. The form of the guarantees varies between projects, because the guarantees are designed to fit the requirements of particular customers, as well as federal and state legislation and regulation.

EPC means operating (and financing) procedures for the provision of specific energy services. These procedures aim at saving energy and cutting costs by modernizing and optimizing necessary functions of installations. The aim is to achieve the guaranteed improvement of results in particular with regard to economic efficiency, energy saving, and net asset value of installations [41].

The main actors involved in the EPC inside an ESCO could be characterized as follows:

1. *Employees*: Performing an energy service involves assembling and delivering the output of a mix of physical facilities and mental labor. Often customers are involved in helping to create the service product, increasingly as the energy-efficiency values and culture of the client evolve. The lack of technical knowledge of the employee fails to realize the estimated savings on the energy-efficiency improvements. Engineers and employees need to update continuously their competence about M&V (monitoring and verification). New systems are

required to make the calculation of project savings more understandable to nontechnical client.

Recognizing that service personnel are also "internal customers" of the organization, marketers and human resource managers should work together to identify employee needs and concerns. Improving the working environment and increasing employee job satisfaction are often key steps in improving service for "external customers."

ESCOs are struggling to find the skilled engineering and technical personnel required to implement large-scale energy-efficiency programs and to maintain and operate energy-efficiency technologies.

2. *Managers*: The key responsibilities of this individuals is to manage sales team and maintain contact with established customers and source new business through prospecting new customers and generating business through sales leads. Also, it is their crucial responsibility to lead, train, motivate, and engage engineers and other employees who can work well together for a realistic compensation package to balance the twin goals of customer satisfaction and operational effectiveness.

   Managers coordinate the involvement of company personnel, including support, service, and management resources, in order to meet account performance objectives and customer's expectations. Developing energy projects means developing business plans that support the customer.

   Creating relationships with specific types of customers by delivering a carefully defined service package of consistent quality that meets their needs is perceived as offering superior value to competitive alternatives. The marketing competencies include not only the delivery system but also additional components such exposure to advertising and receiving feedback about their commercial practices. Communication and cooperation in the relationship is crucial as well as education of the customer not only in organization in energy thinking and how to optimize building performance but also in managing and relying on EPC. Each of the major ECP market segments suffers from its own constraints.

   The position requires formulation of and participation in the total go-to-market process: from product/marketing material development to the creation, and execution of business plans, establishment/achievement of sales targets for assigned ESCO accounts. Manager is responsible for driving revenue through business planning and customer/end-user development.

3. *Energy Analyst or Utility Bill Auditor*: Analysts are responsible for one day-to-day collection and tracking of client, supplier, and utility information. They assist in the construction of energy-related billing models and using them to analyze the client's energy bills. They are analytical thinker and strong communicators. They work directly with managers in forming and executing risk management strategies for their clients for electricity and natural gas. They serve as point of contact for the utility bill auditing process.

2.3 Agency Theory

The information asymmetry between the principal and agent is at the heart of energy-efficiency barriers. As Perrow [13] observed, the principal-agent model is fraught with the problems of cheating, limited information, and bounded rationality in general. Hence, the probability of shirking increases if the preferences of principals and agents diverge, if there are high levels of uncertainty, or if the agent has a distinct information advantage. Under these circumstances, the principal must reduce uncertainty by acquiring offsetting information, which as Mitnick [24] noted is not a costless undertaking. Asymmetric information problems occur when one party involved in a transaction has more information that the other, which may lead to suboptimal energy decisions. The fact that energy efficiency cannot be observed (i.e., it is "invisible") further intensifies this asymmetric information barrier.

Because the unit of analysis is the contract governing the relationship between the principal and the agent, Eisenhardt [26] indicated that the focus of the theory is on determining the most efficient contract governing the principal-agent relationship given assumptions about people (e.g., self-interest, bounded rationality, risk aversion), organizations (e.g., goal conflict among members), and information (e.g., information is a commodity which can be purchased). Specifically, the question becomes this: if it is a behavior-oriented contract (e.g., salaries, hierarchical governance) more efficient than an outcome-oriented contract (e.g., commissions, stock options, transfer of property rights, market governance).

The principal-agent stream is more directly focused on the contract between the principal and the agent. Whereas the positivist stream lays the foundation (i.e., that agency problems exist and that various contract alternatives are available), the principal-agent stream indicates the most efficient contract alternative in a given situation. The common approach in these studies is to use a subset of agency variables such as task programmability, information systems, and outcome uncertainty to predict whether the contract is behavior or outcome based. The principal-agent stream is more directly focused on the contract between the principal and the agent.

The introduction of multiple principals with externalities is certainly problematic for the principal-agent model [43]. Moe [44] wrote "The simple principal-agent model focuses for convenience on one principal and one agent, highlighting the determinants of controls in dyadic relationships." But such a dyadic relationship is unrealistic. A simple dyadic principal-agent model is incapable of capturing this dynamic interaction between multiple principals and agents.

According to Eisenhardt [26], it is possible to identify some characteristics or elements of agency relationships. Elements of agency relationships involve careful specification of assumptions about information asymmetry, risk aversion goal conflict, and other aspects as task programmability and outcome measurability (see Fig. 1):

1. Information asymmetry:

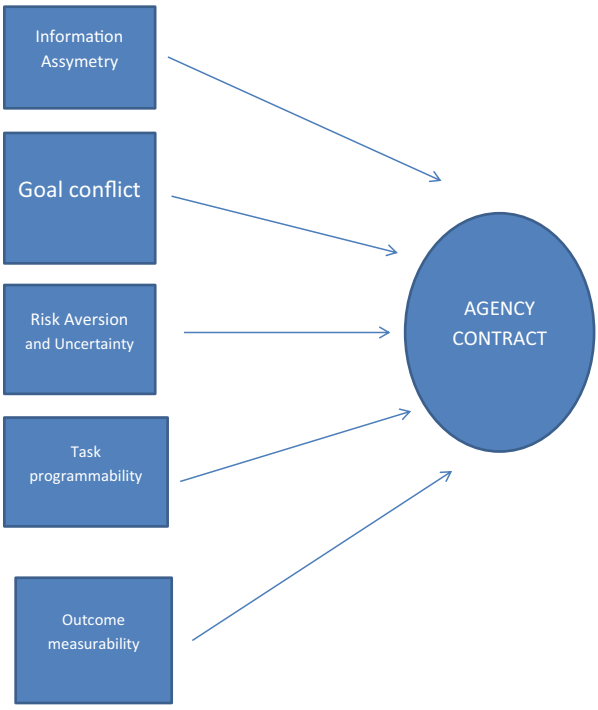

Fig. 1 Elements of agency contract

As we have noted, the information asymmetry is a critical assumption of the principal-agent model. Following Waterman and Meier [43], we don't need the information asymmetry as a constant in a model; the level of information between principals and agents can vary. In some highly technical fields, agents may have more information than their principals have. In others where technical expertise plays a lesser role, the information asymmetry and the "agency problem" should not be apparent. We need to keep this point in mind when we are devising a more generalizable theory.

As noted before, the information asymmetry is a critical assumption of the principal-agent model. The information asymmetry is simply the claim that agents have more information than their principal possesses. Waterman and Meier [43] acknowledge that agents have an information advantage, but also identify the limits of this information asymmetry, because the level of information between principals and agents can vary.

Treating information as a variable rather than as a constant really consists of two variables—the information possessed by the agent and the information possessed by the principal. When these variables are arrayed in two dimensions, in a dyadic relationship with one principal and one agent only, the standard form of information asymmetry is obviously only one of four possible situations.

Case A: both principal and agent possess a great deal of information.
Case B: neither possesses a great deal of information.

Case C: the principal possesses a great deal of information, but the agent does not.
Case D: the agent possesses a great deal of information, and the principal does not.

This is the traditional model principal-agent model.

Principal-agent models are supposed to be dynamic, not static. They characterize relationships that develop and evolve. All the stakeholders involved in energy-efficiency projects can learn over time about energy and efficiency. This change in the pattern of information has the potential to move a relationship in a way that energy-efficiency barriers are removed.

Therefore, it is relevant to combine information (e.g., technical expertise) and goal conflict as variables, into a more dynamic model of the interaction between principals and their bureaucratic agents.

2. Risk aversion and uncertainty:

A key aspect that defines the agency relationship is the trade-off between the cost of measuring behavior and the cost of measuring outcomes and transferring risk to the agent. Individuals vary widely in their risk attitudes. Uncertainty is viewed in terms of risk/reward trade-offs, not just in terms of inability to plan. This implication is that outcome uncertainty coupled with difference in willingness to accept risk about influence contracts between principal and agent.

A number of extensions to the simple model of contract are possible if we consider risk aversion. One is to relax the assumption of a risk-averse agent. As the agent becomes increasingly less risk averse (e.g., a wealthy agent), it becomes more attractive to pass risk to the agent using an outcome-based contract. Similarly, as the principal becomes more risk averse, it is increasingly attractive to pass risk to the agent.

3. Goal conflict:

In the market place, principal and agents clearly have different goals and/or preferences. Obviously, agents want to make as much money as possible, while principals want to pay as little as possible for services. Consequently, if we treat preferences between principals and agents, or what we call goal conflict, as a variable with different values rather than as a constant, different types of relationships between principals and agents should become apparent.

Another extension of the contract is to relax the assumption of goal conflict between the principal and agent. This might occur either in situations in which self-interest gives way to selfless behavior. As goal conflict decreases, there is a decreasing motivational imperative for outcome-based contracting, and the issue reduces to risk-sharing considerations.

The solution to this agency issue is to come up with incentives that will align the interests of the agents with those of the principal.

Conflicts between the agent and those of the principal are the least of the agent's problems. The real problem is that the agent is most likely serving many stakeholders, many of them with conflicting interest. Even if the agent is able to silence his or her own interests, there is the matter of how to maneuver through the tangled

loyalties he or she owes to many different principals and/or stakeholders and how to negotiate through their competing interests and sometimes irreconcilable differences. Shapiro [25] indicates that classical agency theory misunderstands not only the source of goal conflict but also the social conditions to inflame it. This is a matter for sociological inquiry.

4. Another set of extensions relates to the task performed by the agent:

(a) *Task programmability* is defined as the degree to which appropriate behavior by the agent can be specified in advance. The behavior of agents engaged in more programmed jobs is easier to observe and evaluate. Therefore, the more programmed the task, the more attractive are behavior-based contracts because information about the agent's behavior is more readily determined.

(b) *Measurability of the outcomes*. This variable assumes that outcomes are easily measured. When outcomes are measured with difficulty, outcome-based contracts are less attractive. In contrast, when outcomes are readily measured, outcomes-based contracts are more attractive.

Agency thinking reestablished the importance of incentives and self-interest in organizational thinking [13].

Despite Perrow's [13] assertion that agency theory is very different from organization theory, Eisenhardt [26] indicates that agency theory has several links to organizational perspectives. At its roots, agency theory is consistent with the classic works of Barnard [45] on the nature of cooperative behavior and March and Simon on the nature of organizations [46]. As in the earlier work, the heart of agency theory is the goal conflict inherent and information asymmetry when individuals with difference preference engage in cooperative effort, and the essential unit is the contract. Agency theory also is similar to information processing approaches to contingency theory [47,48].

Finally, when principals and agents engage in a long-term relationship, it is likely that the principal will learn about the agent and so will be able to assess behavior more readily. Conversely, in short-term agency relationships, the information asymmetry between principal and agent is likely to be greater, thus making outcome-based contracts more attractive.

2.4 Learning Perspective: Communities of Practice

Barriers to energy efficiency cannot be properly studied by looking at them in isolation, which is what was observed in many prior studies [11]. Often, recommendations were proposed for one barrier or a group of barriers with similar nature, disregarding the possible interactions between barriers which may well render the recommendation ineffective.

We follow Chai and Yeo proposition to start to define our framework from a learning perspective. Their framework offers a way to understand the roles and responsibilities of major stakeholders such as governments and ESCOs in driving

energy efficiency which allows the assessment and identification of weak links in energy-efficiency policies.

From this start point, we want to highlight the interaction among stakeholders to *learn* to improve their competence and results, dynamic aspect not studied by Chai and Yeo. We consider this system as CoP.

The exchange of energy-efficiency knowledge among experts and lay people reflects a fundamental problem in innovation. Information about user's needs, manufacturers' capabilities, and ESCOs employees is highly contextual, tacit, and difficult to transfer from one site to another. This problem hinders the uptake of innovative projects—many rounds of information exchange are needed in order to establish facts and clarify perspectives.

Drawing on studies on communities of practice and learning spaces, we attempt to formulate a model to manage collaboration and promote learning among different stakeholders.

Brown and Duguid [17] presented a holistic view of the way we work, learn, and innovate through communities of practice. Communities of practice are formed by people who engage in a process of collective learning in a shared domain of human endeavor. Social scientists have used versions of CoP for a variety of analytical purpose. Wenger coined the term while studying apprenticeship as a learning model. The concept of CoP has found a number of practical applications in business, organizational design, government, education, professional associations, development projects, and civic life.

Since CoP is still an evolving concept, Li et al. [49] recommended focusing on optimizing specific characteristics of the concept, such as support for members interacting with each other, sharing knowledge, and building a sense of belonging within networks/team/groups.

CoPs are considered to be a type of learning community [16, 50, 51]. Community generally describes groups of people connected by a common interest and who define their identities by the roles they play and the relationships they share in the group's activity. A community can exist over time despite a change of participants. It develops its own culture and communication methods as it matures.

Lave and Wenger [50] suggested that most of the learning for practitioners occurs in social relationships at the workplace rather than in a training classroom setting, a concept known as situated learning. The central aspects of this concept are the interactions between novices and experts and the process by which newcomers create a professional identity. Much of the learning happened during informal gatherings where professionals interacted with each other and shared stories about their experience and where novices consulted openly with experts. Through this process, gaps in the practice were identified, and solutions were developed. The informal interactions eventually became the means for practitioners to improve practice and generate new ways to address recurrent problems. The journey from being a newcomer to becoming an expert is captured in the concept of "legitimate peripheral learning," in which newcomers are given opportunities to learn by engaging in simple tasks. In this context, CoPs can be viewed as a system for

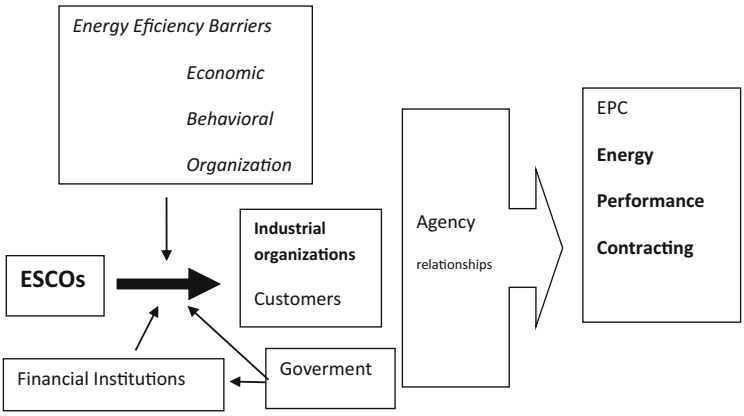

Fig. 2 Barriers and stakeholders in the communities of practices for improving EPC

people to acquire and polish existing skills rather than to create new ways to complete a task [52].

The view of "learning in the job" is supported by Brown and Duguid [17], but in a slightly different way. Brown and Duguid also focused on the close relationships among working, learning, and innovating for workers and stressed the importance of social environment in advancing practitioners' skills and knowledge in organizations. They encourage interaction of people across different communities, a concept known as "community of communities." Furthermore, communities may have different goals, cultures, and politics, all of which may pose challenges for individuals who attempt to balance their participation across different communities.

The new competitive environment brings new threats and opportunities that communities must confront through the redefinition of their context. Communities must seek mechanisms and interventions that support and encourage this process of adaptation between the organization and its environment (see Fig. 2).

The CoP model can provide opportunities to break down professional and organizational barriers and to support the learning of newcomers to the field. It can offer a way to translate and share tacit knowledge or "know how," which can be a valuable resource for capacity building and the implementation of evidence-based practices [53].

Within the field of EPC, collaborative and interdisciplinary actions are imperative for the development and implementations of proactive, holistic projects. They try to understand how knowledge sharing between different professional groups and practices may be facilitated. Specific focus has been on identifying mechanisms for interaction and knowledge sharing between actors that normally do not meet in their everyday practice [15]. The knowledge that a community possesses reflects its norms and preoccupations and, in the long run, limits its ability to develop new ideas.

3 Results and Findings

The focus of the agency theory lies on determining the most efficient contract governing the principal-agent relationship given assumptions about stakeholders (self-interest, bounded rationality, risk aversion, and goal conflict) and information. Specifically, the question becomes, if it is a behavior-oriented contract (positivist stream) more efficient than an outcome-oriented contract (principal-agent stream). Information systems also curb agent opportunism, because the information system inform the principal about what the agent is actually doing.

Using agency theory, we would be concerned with the design of contracts between stakeholders, especially between ESCOs and clients. The design of EPC is a crucial aspect in the promotion of ESCO industry.

We find two different streams in agency theory if we want to understand the evolutions of contracts and behaviors:

1. In the positivist stream, the common approach is to identify a policy or behavior in which principal and agent interests diverge and then to demonstrate that information system, mechanism, or incentive that coalign both behaviors and goals.
2. The principal-agent stream is more directly focused on the contract between the principal and the agent.

Whereas the positivist stream lays the foundation of the relationship, the principal-agent stream indicates the most efficient contract alternative in a given situation.

Palm and Thollander [8] showed that energy efficiency depends on social relationships, discussions, and negotiations. One consequence of this perspective is that energy-saving measures in one sociocultural domain may be useless in another. Focusing in social negotiations and agreements helps explain why energy-efficiency technologies are rejected or adopted in different sectors. According to that perspective, we find that the principal-agent stream allows to design the right contract in a given situation that specify the incentives that align both sides (principal and agent).

Jaffe and Stavins [1] found that market barrier related to the energy-efficiency gap, such as problems with information, justifies a public intervention to overcome them. There are also market failure issues that do not relate to the paradox but which are relevant to policy debates about energy gap, such as actual energy prices, environmental consequences of energy generation and use, and the level of discount rates. Uncertainty in contrast to imperfect information is not a source of market failure but contribute to the energy-efficiency paradox.

The government should consider the market barriers when dealing the agency relationship with ESCOs, industrial sectors, and end users. According to this perspective, we find that the government policy can foster general EPC contracts to regulate general behaviors but also allow the evolution of these general EPC to grasp the specificities of given situations. Government can enhance communication

among stakeholders with initiatives such as CoP that develop knowledge and reduce information asymmetry. Letting actors cross traditional communication boundaries and actively stimulating new social arrangements, involving actors from different sectors who can share their good practices with each other, should be an important policy.

Agency variables such as information system, outcome uncertainty, and risk should be considered in the evolution of the EPC. Critically, EPCs are without risk to the customer. Working with an experienced ESCO ensures that savings are measured, verified, and guaranteed. The guarantee, in effect, transfers all technical and operational risks to the ESCO. It also ensures that change happens. That's a lot of lost cost saving opportunity gone forever.

Many EPC projects involve guarantees made by the ESCO to the customer that the project energy savings will be sufficient to pay the full cost of the long-term project financing. The form of the guarantees varies between projects, because the guarantees are designed to fit the requirements of particular customers, as well as legislation and regulations.

There are two basic types of EPC contracts: shared savings and guaranteed savings. Each type of contract describes the relationship and risk allocations among the ESCO, customer, and lender/financing institution. Under a shared savings contract, the costs savings are split for a predetermined length of time in accordance with a prearranged percentage, and there is no "standard" split as this depends on the cost of the project, the length of the contract, and the risks taken by the ESCO and the customer. Under a guaranteed savings contract, the ESCO guarantees a certain level of energy savings and in this way shields the client from any performance risks.

An important difference to note between the guaranteed and shared saving models is that in the guaranteed model, the performance guarantee is the level of energy saved, while in the shared savings model it is the cost of energy saved (and credit risk taken on behalf of the ESCO).

There is a third type of EPC: energy supply contracting (ESC). Within this contract an energy supply service company (not an ESCO) supplies a set of energy services via the outsourcing of the central energy plant (primary energy conversion equipment) providing heating and/or cooling to the end-use equipment. The payment is at a fixed rate without any energy performance or efficiency requirements. The ESC may have incentives related to energy use reduction, but without assuming any risk in case the expected efficiency is not reached [54].

In Europe, most ESCOs prefer to use the guaranteed savings model. Under a guaranteed savings contract, the ESCO guarantees a certain level of energy consumption savings and in this way shields the client from any performance risk. The ESCO does this under a guaranteed savings contract by assuming the entire design, installation, and savings performance risks. However, the ESCO does not assume the credit risk of repayment programs costs by the customer.

In the developed EPC market in the USA, the guaranteed savings model evolved from the shared savings model in response to customer's desire to significantly reduce interest costs in exchange for accepting more risk due to their increased

comfort with energy savings technologies. This was dependent on a market that included experienced ESCOs able to demonstrate a depth of experience and success in the implementation of energy savings programs.

The ability to align the interest of diverse stakeholders is a critical factor for success in EPC. Understanding existing stakeholder networks is crucial for gaining access to the different parties whose participants and resources are needed for completion of change programs [36]. Understanding the user context is stressed in the literature on user involvement in design. The cases studied by Heiskanen revealed three topics to manage complex networks of interests in multi-stakeholder cooperation in energy-efficiency projects:

1. The importance of combining formal and informal observation. Surveys (formal knowledge) and informal discussions provide information. Much more was learned in informal interactions with users, at meetings organized by the project during small audits done at user building or industry.
2. The challenge of aligning diverse interests in projects. It is relevant to develop projects in flexible way. Users came up with many ideas and needs. The project managers had to make suggestions for fair and equitable solutions. The project changed greatly at this final stage.
3. The interpersonal skills needed to manage flexible, user-responsive projects. The accounts in the previous sections already suggest some of the emotional challenges for project managers in the flexible and user-responsive kinds of projects represented by ESCOs.

Knowledge sharing across communities of practices can be facilitated through participation in social networks, informal meetings, and workgroups. Furthermore, governing entities may act as enablers for knowledge sharing across community boundaries by mobilizing incentives for collaborative endeavors and mutual engagement to solve organizational problems.

A final practical implication concerns funding bodies, which often set the framework for projects promoting energy efficiency, on a local level. Funding for projects to change energy use should include time for research on the particular group of end users. Moreover, user involvement and co-design require flexibility in project planning. If founding bodies want their projects to really make a difference, they should allow time for understanding the end users' perspective and flexibility to change project plans.

Gluch et al. [15] conclude that although energy-efficiency and sustainable projects cannot be fully characterized as CoP, it did show a potential for facilitating knowledge sharing and learning. Social interaction around a special interest allows for learning among individuals with various backgrounds. Collaborative work in small-scale sociotechnical experiments allows to facilitate knowledge sharing and learning, what reduce information asymmetry problem in agency relationships. However, some handicaps needs to be overcome: e.g., power distance between the groups, different goals, agendas and discourses, and practices.

ESCOs managers and employees need better knowledge of human behavior and group dynamics as well as proactive design and business planning. They need to

interpret the information the different users and stakeholders provide in the local context.

Agency theory applied to energy-efficiency industry highlights the fundamentals of EPC to understand the interaction among different stakeholders when facing energy-efficiency barriers. EPC is a turnkey service, sometimes compared to design contracting which provides customers with a comprehensive set of energy-efficiency measures and often is accompanied with guarantees that the savings produced by a project will be sufficient to finance the full cost of the project.

Many EPC projects involve guarantees made by the ESCO to the customer that the project energy savings will be sufficient to pay the full cost of the long-term project financing. The form of the guarantees varies between projects, because the guarantees are designed to fit the requirements of particular customers, as well as legislation and regulations.

ESCOs, customers, utilities, and regulators learned several major lessons during this growth of the performance contracting business, including:

- The performance contracting business model could deliver large volumes of energy and demand savings, but the lack of a robust financing market and the elaborate monitoring and verification (M&V) protocols were severely limiting its growth.
- The technologies employed in most performance contract projects were not very risky, because the technologies had matured and most customers shied away from cutting-edge technologies.
- The financing of performance contracts was profitable and not very risky.
- The M&V protocols employed in earlier programs were overkill as they were expensive to implement and over measured technologies with fairly well-understood consumption patterns.

To accelerate industry growth, the ESCO industry would have to lead the development of a multi-stakeholder, standardized, and simplified M&V protocol that could be understood by bankers and other non-expert parties [40].

ESCOs are constantly adding new measures to their projects, in response to customer requests, but ESCOs should not be considered vehicles to push new technologies into the marketplace. ESCOs and their customers tend to be fairly conservative when selecting technologies for projects, because the total cost of most ESCO projects are paid from energy savings, often secured with financial guarantees. It is a vital aspect how the ESCOs define a clear *business plan* with the technology agreed with the client.

Despite the need for increased industrial energy efficiency, some studies indicate that cost-efficient energy conservation measures are not always implemented, explained by the existence of barriers to energy-efficiency measures.

Several factors are holding back the growth of the EPC market, including:

1. M&V Limitations—New systems are required to make the calculation of project energy savings more understandable to nontechnical clients.

2. Shortage of Skilled Personnel—ESCOs, utilities, state regulatory agencies, and customers are struggling to find the skilled engineering and technical personnel required to implement large-scale energy-efficiency and renewable energy programs and to operate and maintain energy-efficiency and renewable energy technologies.
3. Specific Market Barriers—Each of the major EPC market segments suffers from its own constraints as we have seen in previous sections (see, e.g., [8, 55]).

Energy-saving companies are facing the energy-efficiency barriers, through better communication the information that is included in EPC. Employees in these companies are being better skilled, not only when considering technical aspects but also marketing, consumer behavior, and contracting skills.

4 Conclusions

Despite the fact that the implementation of energy optimizing measures has been demonstrated as cost-effective, collectively, previous studies have identified a somewhat comprehensive list of barriers to adoption of energy efficiency in the industrial sector. However, there is no consensus on which barriers are the most relevant. Perhaps more importantly, it is unclear whether overcoming the most significant barriers will automatically lead to better energy adoption, specifically if the barriers are interconnected and highlighting that the main barrier lied on information problems.

It is more important to approach barriers from a new perspective, using nontraditional analytical tools that can contribute new understanding or questions as to why a particular barrier is perceived by other stakeholder. We identify as key stakeholder to ESCOs as they lead energy-efficiency programs through the evolution of EPC. The evolution of methodologies to assure the relationship among investors, ESCOs, and industrial customers in order to guarantee energy savings in the EPC is a result of the interaction of all stakeholders. We focus the interaction from the point of view of EPCs provider, that is, ESCOs.

Principal-agent models are supposed to be dynamic, not static. They characterize relationships that develop and evolve. Stakeholders (ESCOs, clients, government, financial institutions) learn over time about better implementation of EPC. This change in the pattern of information has the potential to move a relationship from traditional principal-agent model to another case. The introduction of information in some cases even may have the impact of changing goals. Agency theory provides an adequate and comprehensive theoretical framework to analyze the complex relation-based issue proposed.

The CoP approach, that is, understanding the context in which energy-efficiency measures are going to be introduced, facilitates the learning needed to improve energy-efficiency steps further by openly sharing the stakeholder's knowledge. This

is reinforced by the fact that energy-efficiency projects successfully implemented in one socioeconomic environment may be useless in another.

It is not only about overcoming energy-efficiency barriers but also improving the whole system by introducing innovations in the EPC. The EPC is the contract in these agency relationships developed in the ESCOs industry. Information and goal conflict are two important elements in agency relationships as we have reviewed in this chapter. Knowledge sharing in CoP reduces information asymmetry, and targeted incentives and policies from the government can make the energy-efficiency sector expand as goals are aligned. Gaining knowledge on ESCOs projects is important to intensively develop different EPC models through better comprehension of its elements: risk sharing, guarantees, and incentives.

References

1. Jaffe AB, Stavins RN (1994) The energy-efficiency gap. What does it mean? Energy Policy 22 (10):804–810
2. DeCanio SJ (1993) Barriers within firms to energy-efficient investments. Energy Policy 21:907–914
3. Weber L (1997) Some reflections on barriers to the efficient use of energy. Energy Policy 25 (10):833–835
4. DeCanio SJ (1998) The efficiency paradox: bureaucratic and organizational barriers to profitable energy-saving investments. Energy Policy 26(5):441–454
5. Thollander P, Karlsson M, Söderström M, Creutz D (2005) Reducing industrial energy costs through energy efficiency measures in a liberalized European electricity market-case study of Swedish iron foundry. Appl Energy 81(2):115–126
6. Rohdin P, Thollander P, Solding P (2007) Barriers to and drivers for energy efficiency in the Swedish foundry industry. Energy Policy 35:672–677
7. Wang G, Wang Y et al (2008) Analysis of interactions among the barriers to energy saving in China. Energy Policy 36(6):1879–1889
8. Palm J, Thollander P (2010) An interdisciplinary perspective on industrial energy efficiency. Appl Energy 87:3255–3261
9. Sardianou E (2007) Barriers to industrial energy efficiency investments in Greece. J Clean Prod 16:1416–1423
10. Sarkar A, Singh J (2010) Financing energy efficiency in developing countries – lessons learned and remaining challenges. Energy Policy 38:5560–5571
11. Chai KH, Yeo C (2012) Overcoming energy efficiency barriers through systems approach – a conceptual framework. Energy Policy 46:460–472
12. Ross S (1973) The economic theory of agency: the principal's problem. Am Econ Rev 63:135–151
13. Perrow C (1986) Complex organizations. Random House, New York
14. Vine E (2005) An international survey of the energy service company (ESCO) industry. Energy Policy 33(5):691–704
15. Gluch P, Johansson K, Räisänen C (2013) Knowledge sharing and learning across community boundaries in an arena for energy efficient buildings. J Clean Prod 48:232–240
16. Wenger E (1998) Communities of practice: learning, meaning and identity. University Press, New York/Cambridge

17. Brown JS, Duguid P (1991) Organizational learning and communities-of-practice: toward a unified view of working, learning, and innovation. Organ Sci 2(1):40–57, Special issue: organizational learning: papers in honor of James G
18. Owens S, Driffill L (2008) How to change attitudes and behaviors in the context of energy. Energy Policy 36(12):4412–4418
19. Stephenson J, Barton B et al (2010) Energy culture: a framework for understanding energy behaviours. Energy Policy 38(10):6120–6129
20. Adamides ED, Mouzakitis Y (2009) Industrial ecosystem as technological niches. J Clean Prod 17(2):172–180
21. Smith A, Voss JP et al (2010) Innovation studies and sustainability transitions: the allure of the multi-level perspective and its challenges. Res Policy 39(4):435–448
22. Jensen MC, Mecking WH (1976) Theory of the firm: managerial behaviour, agency costs and ownership structure. J Financ Econ 3:305–360
23. Zajac EJ, Westphal JD (2004) The social construction of market value: institutionalization and learning perspectives on stock market reactions. Annu Sociol Rev 69:233–257
24. Mitnick BM (1980) The political economy of regulation. Columbia University Press, New York
25. Shapiro SP (2005) Agency theory. Annu Rev Sociol 31:263–284
26. Eisenhardt KM (1989) Agency theory: an assessment and review. Acad Manag Rev 14(1):57–74
27. Sorrel S, O'Malley E, Schleich J, Scott S (2004) The economics of energy efficiency – barriers to cost effective investment. Edward Elgar, Cheltenham
28. Schleich J (2009) Barriers to energy efficiency: a comparison across the German commercial and service sector. Ecol Econ 68:2150–2159
29. Fleiter T, Worrel E, Eichhammer W (2011) Barriers to energy efficiency in industrial bottom-up energy demand models - a review. Renew Sustain Energy Rev 15:3099–3111
30. UNEP (2006) Barriers to energy efficiency in industry in Asia: United Nations environment program. http://www.energyefficiencyasia.org/docs/Barriers%20to%20Energy%20Efficiency%20review%20and%20policy%20guidance.pdf. Accessed 31 Mar 2014
31. Nagesha N, Balachandra P (2006) Barriers to energy efficiency in small industry clusters: multi-criteria-based priorization using the analytic hierarchy process. Energy 31(12):1969–1983
32. Geller H, Atali S (2005) The experience with energy efficiency policies and programmes in the IEA countries: learning from the critics. IEA, Paris
33. European Parliament (2010) Directive 2010/31/EU of the European Parliament and of the Council of 19 May 2010, on the energy performance of buildings. Official Journal of the European Union L 153/13
34. European Parliament (2012) Directive 2012/27/EU of the European Parliament and of the Council of 25 October 2012, on energy efficiency, amending Directives 2009/125/EC and 2010/30/EU and repealing Directives 2004/8/EC and 2006/32/EC. Official Journal of the European Union L 315/1
35. Geller H, Harrington P et al (2006) Policies for increasing energy efficiency: thirty years of experience in OECD countries. Energy Policy 34(5):556–573
36. Heiskanen E, Johnson M, Vadovics E (2013) Learning about and involving users in energy saving on the local level. J Clean Prod 48:241–248
37. Goldman CA, Hopper NC, Osborn JG (2005) Review of the US ESCO industry markets trends: an empirical analysis of project data. Energy Policy 33(3):387–405
38. Hopper NC, Goldman C, MCWilliams J et al (2005) Public and institutional markets for ESCO services: comparing programs, practices and performance, (LBNL-55002). Ernest Orlando Lawrence Berkeley National Laboratory, Berkeley
39. European Parliament (2006) Directive 2006/32/EC of the European Parliament and of the Council of 5 April 2006, on energy use-efficiency and energy services and repealing Council Directive 93/76/EEC. Official Journal of the European Union L 114/64. Accessed 27 Apr 2006

40. ICF International National Association of Energy Services Companies (2007) Introduction to energy performance contracting. http://www.energystar.gov/ia/partners/spp_res/Introduction_to_Performance_Contracting.pdf. Accessed 31 Mar 2014
41. Berger S, Schäfer M (2010) EESI-European energy service initiative: challenges and chances for energy performance contracting in Europe, short study, Berlin energy agency, intelligent energy-Europe, European energy service initiative, Berlin. http://www.european-energy-service-initiative.net/de/nachrichten/news/epcstudy.html. Accessed 21 Mar 2014
42. Satchwell A, Larsen P, Goldman C, Lawrence Berkeley National Laboratory (2011) Combining energy efficiency building retrofits and onsite generation: an emerging business model from the ESCO industry. ACEEE Summer Study Energy Effic Ind 1:132–145
43. Waterman RW, Meier KJ (1998) Principal-agent models: an expansion? J Public Adm Res Theory 8(2):173–202
44. Moe T (1987) An assessment of the positive theory of "congressional dominance". Legis Stud Q 12:475–520
45. Barnard C (1938) The functions of executive. Harvard University Press, Cambridge
46. March J, Simon H (1958) Organizations. Wiley, New York
47. Chandler A (1962) Strategy and structure. Doubleday, New York
48. Galbraith J (1973) Designing complex organizations. Addison Wesley, Reading
49. Li LC, Grimshaw JM et al (2009) Evolution of Wenger's concept of community of practice. Implement Sci 4(11):1–8. doi:10.1186/1748-5908-4-11
50. Lave J, Wenger E (1991) Legitimate peripheral participation in communities of practice: situated learning theory. Cambridge University Press, Cambridge
51. Wenger E, McDermott RA, Synder W (2002) Cultivating communities of practice. Harvard Business Press, Boston
52. Cox A (2005) What are communities of practice? A comparative review of four seminal works. J Inf Sci 31:527–540
53. McKellar KA, Pitzul KB, Yi JY, Cole DC (2014) Evaluating communities of practice and knowledge networks: a systematic scoping review of evaluation frameworks. Ecohealth 11:383–399
54. European Association of Energy Service Companies (EU.BAC-ESCO) (2011) Energy Performance Contracting in the European Union, Energy Solutions, Berlin Energy Agency. http://www.euesco.org/fileadmin/euesco_daten/pdfs/euESCO_response_concerning_EPC.pdf. Accessed 26 Nov 2014
55. Transparense (2013) European EPC market overview. Results of the EU-wide market survey. EU program "intelligent energy Europe", London, http://www.transparense.eu. Accessed 31 Mar 2014

Index

G. Lefebvre et al. (eds.), *Environment, Energy and Climate Change II: Energies from New Resources and the Climate Change*, Hdb Env Chem (2016) 34: 261–264,
DOI 10.1007/698_2014,